Modeling, Analysis, and Control of Biological Oscillators

Hadi Taghvafard

university of groningen

The research described in this dissertation has been carried out at the Faculty of Science and Engineering, University of Groningen, Groningen, The Netherlands.

disc

This dissertation has been completed in partial fulfillment of the requirements of the Dutch Institute of Systems and Control (DISC) for graduate study.

This dissertation has been supported by the European Research Council under grant ERC-StG-307207.

Printed by Ipskamp Drukkers
Enschede, The Netherlands

Cover design by the author; the primary sources of the cover are from freepik.com.

ISBN (book): 978-94-034-0714-2
ISBN (e-book): 978-94-034-0713-5

university of groningen

Modeling, Analysis, and Control of Biological Oscillators

PhD thesis

to obtain the degree of PhD at the
University of Groningen
on the authority of the
Rector Magnificus Prof. E. Sterken
and in accordance with
the decision by the College of Deans.

This thesis will be defended in public on

Friday 22 June 2018 at 14.30 hours

by

Hadi Taghvafard

born on 15 June 1982
in Shiraz, Iran

Promotores
Prof. M. Cao
Prof. J.M.A. Scherpen

Assessment committee
Prof. A.J. van der Schaft
Prof. R. Sepulchre
Prof. R. Middleton

To my family, in particular, my parents
and
to all my mentors

Acknowledgments

The material included in this thesis is related to the research I performed at the University of Groningen (UG). If I made any progress during my education and in particular in the past four years of my PhD, it would not have been accomplished by myself solely. I am greatly indebted to my family, in particular, my parents for their unconditional selfless support, and also my experienced mentors who guided me through obstacles; I sincerely dedicate this thesis to them.

Taking into account the past four years as the last part of my education, I am most indebted to my first advisor, Prof. Ming Cao, who taught me different aspects of scientific research and pointed out my shortcomings and mistakes. I highly appreciate his freedom in choosing research topics, his constructive comments on my drafts, and his career suggestions. I also do like to thank my second advisor, Prof. Jacquelien Scherpen, for all her supports and encouragements and also her management of both the department and the institute.

During my PhD, I mostly discussed and collaborated with[†] Dr. Hildeberto Jardón-Kojakhmetov (UG) and Dr. Anton Proskurnikov (UG & TU Delft). I greatly appreciate both of them for all the discussions and also for their time and effort in reading and providing invaluable comments on my drafts. In addition, I am very thankful to Dr. Rose Faghih (MIT & University of Houston) for all our discussions through email, leading to Chapter 3 of this thesis.

I do like to thank Prof. Peter Szmolyan (TU Wien) from whose constructive comments on Chapter 7 of this thesis I greatly benefited during my visit at TU Wien and also from our discussions through email.

I would like to thank my thesis committee members[†], Prof. Rick Middleton (University of Newcastle), Prof. Rodolphe Sepulchre (University of Cambridge), and Prof. Arjan van der Schaft (UG) for their time and effort in assessing this thesis and providing valuable comments.

[†] alphabetical order

I also want to point out my gratitude to† Prof. Brian D.O. Anderson (Australian National University), Prof. Henk Broer (UG), Dr. Yu Kawano (UG), Prof. Alexander Medvedev (Uppsala University), and Dr. Andreas Milias Argeitis (UG) for several discussions.

Lastly, I would like to thank all my former and current colleagues and friends at UG, and also those people who indirectly contributed to this thesis. In particular, I am grateful to† Alain Govaert and Dr. Qingkai Yang who will be my paranymphs on my defense day. Furthermore, thanks to Alain Govaert for translating the summary of this thesis into Dutch.

Hadi Taghvafard
Groningen, June 2018

†alphabetical order

Contents

1

Introduction

> *"This is a story about dynamics: about change, flow, and rhythm, mostly in things that are alive. (...)*
> *This is a story about dynamics, but not about all kinds of dynamics. It is mostly about processes that repeat themselves regularly. In living systems, as in much of mankind's energy-handling machinery, rhythmic return through a cycle of change is a ubiquitous principle of organization. So this book of temporal morphology is mostly about circles, in one guise after another. The word phase is used (...) to signify position on a circle, on a cycle of states. Phase provides us with a banner around which to rally a welter of diverse rhythmic (temporal) or periodic (spatial) patterns that lie close at hand all around us in the natural world. (...)*
> *We turn now to the simplest abstractions about* ***rhythms****,* ***cycles****, and* ***clocks****, with a few examples. Examples are merely mentioned here, pending their fuller description in later chapters, where the context is riper.*"
>
> - Arthur T. Winfree, *The Geometry of Biological Time*

Indeed, as emphasized in the beginning of the seminal book "The Geometry of Biological Time" [169], *rhythms* as ubiquitous principles of the real world as well as their abstractions as dynamical processes that evolve on a cycle of states are of great importance. In this regard, this thesis is devoted to the study of rhythms, so-called "oscillators". In particular, it deals with modeling, analysis, and control of biological oscillators. This thesis is divided into two parts, where Part I is concerned with the application of control theory to endocrinology, and Part II is devoted to the application of dynamical systems to microbiology.

1

This chapter starts with the research context in Section 1.1, followed by Section 1.2 to briefly introduce the problems that are studied in Parts I and II. Contributions and outline of the thesis are presented in Sections 1.3 and 1.4, respectively.

1.1 Research context

RECENT advances in technologies which significantly influence our lives are widely accelerating the pace of discovery in medicine and biology. However, such developments highly depend on an interdisciplinary approach that involves several other branches of science, such as mathematics, physics, chemistry, and in particular, dynamical systems and control theory. This interdisciplinary approach has led to not only a better understanding and more comprehensive analysis of the individual biological components but also the connections and the regulatory processes among them. This approach is known as "systems biology" where dynamical systems and control theory play crucial roles [1].

Oscillators are ubiquitous in different fields of science, such as biology [12, 44, 168], chemistry [28, 45, 46], neuroscience [65, 66, 74], and engineering [134, 135, 152]. Such periodic fluctuations occur with a variety of underlying mechanisms [47], and take place at all levels of biological organization over a wide range of periods ranging from milliseconds (e.g., neurons) to seconds (e.g., cardiac cells), minutes (e.g., oscillatory enzymes), hours and days (e.g., hormones), weeks and even years (e.g., epidemiological processes and predator-prey interactions in ecology) [47, 113, 117]. The main role of sustained oscillations is to control major physiological functions, while their dysfunction is related to a variety of physiological disorders [47].

In biological and biochemical oscillators, several concepts such as dynamics, stability, instability, interactions, signaling, regulation, tracking, robustness, identification, and sensitivity analysis are of great importance, and have counterparts in dynamical systems and control theory [123]. Therefore, tools from systems and control theory can be useful to gain better understanding of the dynamics and complex mechanisms underlying biological oscillators. Indeed, dynamical systems and control theory have been connected to biological systems since the 19th century as presented in the seminal work of the celebrated physiologist Claude Bernard on the *milieu interieur*[1] in 1859 [6], who noticed that the constancy of the internal environment is crucial for the survival and perpetuation of warm-blooded animals [38]. In 1929, Walter Cannon [9] expanded upon Claude Bernard's concept of *homeostasis*, which is a process that needs coordinated control over endocrine, behavioral and autonomic nervous system responses to the environment [38]. Next, through the development of cybernetics, Norbert Wiener connected homeostasis to

[1] "the internal environment".

more rigorous formalisms in feedback control in 1948 [166]. Then Fred Grondis *et al.*, in their influential paper [59] in 1954, studied human physiology where, using electric circuit analogs, they investigated the response of the respiratory system to CO_2 inhalation as a feedback regulator [72]. Subsequent works on physiological and living systems have followed by, e.g., Grodins [58] in 1963, Bayliss [5], Kalmus [78], Milhorn [108] in 1966, and so on[2].

In order to gain a better understanding of the functioning and dynamics of biological systems, only identifying and characterizing the individual components of a system is not sufficient. In addition, it is necessary to understand the interactions and regulatory processes among such components. To this end, mathematical models can yield insights into how biological systems act as "networks" in which individual components communicate with one another [39]. Owing to the fact that biological systems are very complex and incompletely understood [114], devising a mathematical model that describes all features of such systems is a challenging task. Therefore, to gain deeper insights into the complexity of biological systems through mathematical tools, a *modeling approach* is chosen, in which only the most essential components and interactions among them are taken into account [105].

Although in the modeling approach, mathematical models are not complete due to simplifying some details of biological systems, what they have in common is that they are "fully" explicit about the structure, and inclusion or exclusion of the assumptions in the model, while experimental systems typically do not have such characteristics. A mathematical model which is correctly built based on underlying biology allows us to investigate whether the structure and assumptions of the model can explain the observed, or desired, results. Moreover, by *in silico*[3] experimentation, such a model helps us to investigate some aspects of the underlying biological system that are *unethical* (e.g., knock out or modify a gene in human), *expensive* (e.g., change the expression level of different combination of genes), *difficult* (e.g., severely reduce nutrient input), or *impractical* to do *in vitro*[4] or *in vivo*[5]. Further, mathematical models can complement experiments: on one hand, experiments can identify parameter values, functions and interactions that are crucial for establishing the topology and kinetics of a model; on the other hand, mathematical models can suggest new experiments and reveal some hidden aspects of the underlying biological system that have never been observed *experimentally* [47, 114].

[2]Here we have referred to some works focused on physiological and living systems. Of course, there are some other works connecting systems and control theory to biological systems; for instance, the interested reader is referred to [168] and references therein.

[3]"performed on computer or via computer simulation".

[4]"within the glass".

[5]"within the living".

1

1.2 Applications

In this thesis, tools from dynamical systems and control theory are used to study several oscillatory processes. In general, it is divided into two parts, where Part I is concerned with the application of control theory to endocrinology, and Part II is devoted to the application of dynamical systems to microbiology. In this regard, the following subsections give a brief background on the problems that are investigated in Parts I and II.

1.2.1 Part I: Application of control theory to endocrinology

Endocrine axes

Hormones are chemical blood-borne substances produced by glands. The *endocrine system* is the collection of glands which secrete their products (hormones) into the blood *directly*. The operation of endocrine glands is triggered and controlled by the *hypothalamus* and the *pituitary* gland[6], both of which are located at the base of the brain, see Fig. 1.1. The most important function of the hypothalamus is to link the nervous system to the other endocrine glands via the pituitary gland. The hypothalamus, as well as the other neuroendocrine neural systems that are connected to it, plays a crucial role in regulating the homeostatic functions. The role of the pituitary gland is to control the endocrine glands, although its weight is just 0.5 grams in human [38].

Growth, blood pressure, reproduction, metabolism, stress, and feeding and drinking are some of the bodily functions that are controlled by the hypothalamus-pituitary (HP) "neurohormonal" axis [38, 133]. The *most essential* feedback and feedforward control mechanisms underlying the HP axes are as follows [133]. First, neural interactions in the hypothalamus secrete *releasing* hormones. Next, releasing hormones stimulate release of *tropic* hormones produced by the pituitary gland, which, in turn, induces a "target" gland/organ to release *effector* hormones. Lastly, the target gland/organ exerts negative feedback signals on the production of *both* releasing and tropic hormones, see Fig. 1.1. The four-tiered neuroendocrine systems are (i) the hypothalamic-pituitary-gonadal (HPG) axis, (ii) the hypothalamic-pituitary-adrenal (HPA) axis, (iii) the hypothalamic-pituitary-somatotropic[7] (HPS) axis, and the hypothalamic-pituitary-thyroid (HPT) axis.

Pulsatility of endocrine axes

In the neuroendocrine axes, hormones are secreted directly into the blood either in a continuous or *pulsatile* (burst-like or episodic) manner. The latter, recognized in

[6] Also known as *hypophysis*.
[7] Also known as *growth hormone*.

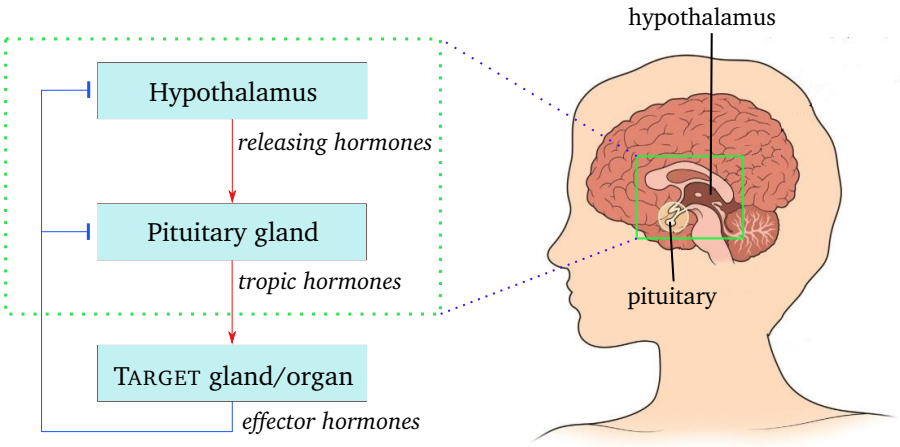

Figure 1.1: Structure of the hypothalamus-pituitary neurohormonal axis; feedforward and feedback control mechanisms are illustrated by ↓ and ⊣, respectively. (The right part of the figure is adapted from hormone.org)

the second half of the 20th century [29], is a fundamental property of the majority of hormone secretion patterns [157]. Pulsatility is the physiological way to increase hormone concentrations rapidly and send distinct signaling information to target cells [155]. It is believed that pulsatile signaling offers greater control, permits hormone concentrations to change rapidly, and is more energy efficient [164].

Owing to the fact that the hypothalamus is located in the base of the brain (see Fig. 1.1), its hormone secretion into the pituitary gland is pulsatile. Thus, it seems that the endocrine control mechanisms of the HP axes are *hybrid*, i.e., a mixture of continuous and intermittent signal exchange [157], and hence their corresponding mathematical models can be analyzed by tools and techniques developed for impulsive dynamical systems, see e.g. [41, 54, 62, 96].

Disorders of endocrine axes

Disorders of the HP axes are hypersecretion (hormone excess), hyposecretion (hormone deficiency), or tumors of the endocrine glands [30, 120]. For instance, disorders of the HPA axis are related to a number of psychiatric and metabolic diseases [171, 172]. In particular, adrenal deficiency is a disorder that might be due to impairment of the adrenal glands, the pituitary gland, or the hypothalamus [30]; Addison's disease is an example of such a disorder. Some of the diseases that can be caused by adrenal deficiency are, e.g., unexpected dehydration and weight loss in adults, hypoglycemia, and poor weight gain [147]. Another disorder of the HPA axis is adrenal excess; Cushing's syndrome, in which the cortisol level in blood is

high, is an example of such a disorder that may result in, e.g., muscle weakness, weight gain, fatigue, heart disease, and diabetes [120].

Disorders of the HP axes can be treated by tablets, injections or surgery. In the current medication protocols, the dosage (timing and amount) is not optimal and may cause other disorders. Therefore, it is of great importance to have a model in order to predict the dose-response, and also an optimal approach to treat hormonal disorders in order to minimize the side-effects of the medication [30]. All these motivate the development of mathematical models which describe the complex behavior of endocrine axes.

Mathematical modeling

The existence of many stimulatory (feedforward) and inhibitory (feedback) couplings between hormones motivates the study of interactions between glands as a dynamical system. This indicates that tools from systems and control theory may be useful for modeling, analysis, and control of the endocrine system.

Owing to the complexity of the underlying biological structure, obtaining a "global" mathematical model, describing the endocrine system in detail, is a challenge. However, in order to have a *sensible* and *tractable* mathematical model [79], usually HP axes that are responsible for different physiological functions are studied.

The main objective of Part I of this thesis is to develop mathematical models to provide deeper insights into the functioning and dynamics of the endocrine axes. A detailed literature review on the mathematical models that have been postulated to describe such axes is given in the introductions of Chapters 3, 4, and 5.

1.2.2 Part II: Application of dynamical systems to microbiology

Part II of this thesis establishes an approach to analyzing a class of oscillators. This part clearly shows how mathematical models complement experimental systems.

Biochemical oscillations often occur in several contexts including signaling, development, metabolism, and regulation of important physiological cell functions [115]. Part II studies a biochemical oscillator model that describes the developmental cycle of myxobacteria. Myxobacteria are multicellular organisms that are common in the topsoil [77], and characterized by social behavior and a complex developmental cycle [24]. The history of studying such bacteria goes back to the late 19th century when Ronald Thaxter recognized them as bacteria for the first time in 1892 [149]. For a complete review about the social and developmental biology of myxobacteria, the interested reader is referred to [24, 112, 159].

The developmental cycle of myxobacteria, which is illustrated in Fig. 1.2, is described as follows [77]. During vegetative growth, i.e. when food is ample, myxobacteria constitute small swarms by a mechanism called "gliding" [73]. In

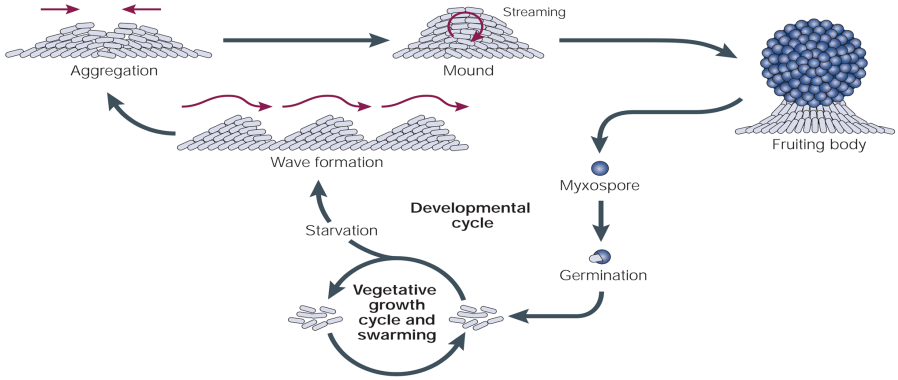

Figure 1.2: Schematic diagram of the developmental cycle of myxobacteria. (This figure is adapted by permission from Springer Customer Service Centre GmbH: Springer Nature, *Nature Reviews Microbiology*, D. Kaiser [77], Copyright 2003.)

contrast, under starvation circumstances, they aggregate and initiate a complex developmental cycle during which small swarms are transformed into a multicellular single body, known as "fruiting body", whose role is to produce spores for the next generation of bacteria [77]. During the aforementioned transition, myxobacteria pass through a developmental stage called the "ripple phase" [73, 77], characterized by complex patterns of waves that propagate within the whole colony.

Two genetically distinct molecular motors are concentrated at the cell poles of myxobacteria, allowing them to glide on surfaces; these two motors are called Adventurous (A-motility) and Social (S-motility) motors. The role of the former is to push the cells forward, while the role of the latter is to pull them together. So in order for a cell to reverse its direction, it has to alternatively activate its A-motility (push) and S-motility (pull) motors at opposite cell poles [73]. As a result, by forward and backward motion of myxobacteria, complex spatial wave patterns are created. In particular, wave patterns are produced by the coordination of motion of individual cells through a *direct end-to-end* contact signal, so-called the "C-signal". During the ripple phase of development, the C-signaling induces reversals, while suppressing them during the aggregation stage of development. Observations from experiments led to the proposal of a biochemical oscillator model in [73], which acts as a "clock" that controls reversals. This model, known as the Frzilator (or Frz model), will be further described in Chapter 6 from both biological and mathematical perspectives.

In [73], it is claimed that the Frz model has stable and robust oscillations over a wide range of parameters; however, such a range has not been explicitly given. Moreover, our observation from simulations shows that, for a range of

parameter values, solutions of the Frz converge to a unique limit cycle[8]. Further, from numerical simulations, we have observed that there are several "time scales" along the unique limit cycle which are related to the small parameters of the system. A complete analysis of such a model may provide a better understanding of the biochemical clock. To this end, Part II of this thesis is devoted to giving a detailed and rigorous analysis of all such claims and observations.

In order to analyze the Frz model, we use various tools from dynamical systems, such as regular perturbation theory, geometric singular perturbation theory, slow-fast systems, Fenichel theory, and blow-up method, which are briefly introduced in Chapter 2.

1.3 Contributions

We start with the main results in Chapter 3 where we present a minimal model of cortisol's diurnal patterns. In general, the contributions of this chapter are related to *modeling* and *control*, respectively. For the modeling, we develop a second-order impulsive differential equation model using the stochastic model presented in [7]. Unlike the stochastic model [7], in which the pulsatile input in the adrenal glands is assumed to be doubly stochastic with amplitudes in Gaussian distribution and inter-arrival times in gamma distribution, in the model presented in Chapter 3 the input is assumed to be an "abstraction" of hormone pulses, i.e., we explicitly assume that the system is impulsive. For the control, through an *analytical approach*, we design an impulsive controller to identify the number, timing, and amplitude of secretory events, while the blood cortisol levels are confined within a specific circadian range. Moreover, by presenting an algorithm and employing it into various examples, we show that the achieved cortisol levels lead to the circadian and ultradian rhythms which are in line with the known physiology of cortisol secretion. The main source of the material presented in this chapter is [141].

Chapter 4 develops a third-order ordinary differential equation model to describe the HP axes. As the Goodwin's model [52] is a "prototypical biological oscillator", and Goodwin-like models are still broadly used in endocrine regulation modeling, we first extend the Goodwin's model by introducing an additional *nonlinear feedback*, whose special case has been studied in [4] to describe the HPA axis. In contrast to the model investigated in [4], we do not restrict nonlinearities of our model, which are used to describe the two negative feedbacks, to be identical and the Hill-type [51]; this is an important extension since the actual chemical kinetics of hormone secretions are not entirely known. The model presented in Chapter 4 is new in the sense that, to the best of the author's knowledge, its general form has never been studied in the literature.

[8] A *limit cycle* is an isolated closed trajectory.

Another contribution of Chapter 4 is the mathematical analysis of the model, establishing the relation between its "local" behavior at the equilibrium point and "global" behavior, namely, the convergence of solutions to periodic orbits. Such an analysis is available *only* for *cyclic* Goodwin-like models, and endocrine regulation systems with multiple feedback loops have been studied *only* by standard *local* methods, such as linearization, and Hopf bifurcation theorem. In Chapter 4, the existence of periodic solutions is proven by Hopf bifurcation theory whose mathematically rigorous application is non-trivial, since a one-parameter family of systems has to be constructed. In addition, the convergence of solutions to periodic orbits is proven by the results of [101], while such results are not directly applicable to the extended Goodwin's model since their *fundamental* condition, i.e. "sign-symmetry" coupling among components, is violated. We show that in the case where the additional feedback satisfies a slope condition, a *special transformation exists* that removes this asymmetry, allowing thus to apply the results of [101]. To the best of the author's knowledge, for a system whose couplings among its components are *asymmetric*, no *global* results have been reported in the literature. The results presented in this chapter are published in [139, 145].

Chapter 5 develops a third-order impulsive differential equation for endocrine regulation. In particular, it extends the impulsive Goodwin's oscillator [15] by introducing an additional *affine* feedback. Although the introduction of such a feedback results in an affine system between two consecutive pulses and allows us to extend the theory developed in [15] for *non-cyclic* endocrine systems with two feedback loops, due to the fact that the affine system is governed by a non-Metzler matrix, some solutions may become negative at some time (i.e., the positive orthant is not an invariant set) and hence are not biologically feasible.

In Chapter 5, we prove the existence, uniqueness, and positivity of a type of periodic solution, called 1-cycle, having only one pulse in its smallest period. Our approach is based on a *special transformation of variables* under which the extended system is transformed into a system whose linear part is governed by a Metzler matrix. After establishing the existence, uniqueness and positivity of a 1-cycle solution for the transformed system, we demonstrate that, under some conditions, this solution is mapped to a positive and unique 1-cycle solution of the original system. The main source of the material presented in this chapter is [144]. A special case of the model, in which the additional feedback is described by a *linear* function, is studied in [140] from a *different approach*.

Part II of this thesis (i.e., Chapters 6 and 7) is concerned with the analysis of a biochemical oscillator model (the Frz model), describing the social-behavior transition phase of myxobacteria. It presents a rigorous and complete proof of claims made in [73], and of our observations from numerical simulations. In general, Part II provides two types of results, namely, *modeling* and *analysis*. The contributions of each chapter are as follows.

Chapter 6 develops a tool based on bifurcation analysis for parameter-robustness analysis for a class of oscillators, and in particular, studies the Frz model. Generally, our studies start from modeling to local analysis, followed by global analysis. For modeling, as the reactions in the Frz model possess the property of "zero-order ultrasensitivity" [73], we first identify some *small* parameters of the model, and then unify them by a single parameter ε. Identification of suitable parameters that can be unified is a crucial step in modeling, because there may exist other parameters (which do exist in the Frz model) that are small as well, but they cannot be unified with the other parameters, due to some biological reasons.

Owing to the fact that the Frz model with the unified parameter ε has a unique and hyperbolic equilibrium for the case $\varepsilon = 0$, using regular perturbation theory, we show that the uniqueness and hyperbolicity of the equilibrium can be preserved in certain parameter regimes, given explicitly. Next, we prove that the system has oscillatory behavior in such regimes, and then the equilibrium switches from being unstable to stable. In addition, we provide global results, meaning that (almost) all solutions converge to a finite number of periodic solutions, one of which is asymptotically stable. Lastly, we show that the reported convergence result is robust in the sense that any smooth, sufficiently small, and not necessarily symmetric change in the parameters, unified by ε, will lead to the same qualitative behavior of the solutions. The results of this chapter are published in [142].

Chapter 7 studies the Frz system from a completely different approach, namely, *geometric singular perturbation theory*. Our observations from numerical simulations show that (almost) all solutions of the system converge to a unique limit cycle, and more importantly, the system is a "relaxation" oscillator, meaning that there are *multiple time scales* along the orbit of the oscillator. Nevertheless, the Frz system is not in the *standard form* (i.e., without a global separation into slow and fast variables) of the multiple-time-scale dynamical systems, and hence poses several mathematical challenges.

The main contribution of Chapter 7 is to prove that, within certain parameter regimes, there exists a *strongly attracting periodic orbit* for the Frz system. In addition, the detailed description of the structure of such a periodic orbit is given. The methodology used to prove the result consists first on an appropriate rescaling of the original model, which leads to a slow-fast (or two time-scales) system. By taking the advantage of the two time-scales of the rescaled system, a geometric analysis through techniques of multiple-time-scale dynamical systems is developed. From an analytical point of view, the main difficulty of this analysis is the detailed description of a transition along two *non-hyperbolic lines*, where the *blow-up method* is used. The principal source of the material presented in this chapter is [143].

1.3.1 Related publications

The material presented in this thesis is in the most part based on the following papers.

Conference papers

- H. Taghvafard, A.V. Proskurnikov, and M. Cao. Stability properties of the Goodwin-Smith oscillator model with additional feedback. *IFAC-PapersOnLine*, 49(14):131–136, 2016.
- H. Taghvafard, A.V. Proskurnikov, and M. Cao. An impulsive model of endocrine regulation with two negative feedback loops. *IFAC-PapersOnLine*, 50(1):14717–14722, 2017.

Journal papers

- H. Taghvafard, H. Jardón-Kojakhmetov, and M. Cao. Parameter-robustness analysis for a biochemical oscillator model describing the social-behaviour transition phase of myxobacteria. *Proceedings of the Royal Society A – Mathematical, Physical and Engineering Sciences*, 474(2209):20170499, 2018.
- H. Taghvafard, A.V. Proskurnikov, and M. Cao. Local and global analysis of endocrine regulation as a non-cyclic feedback system. *Automatica*, 91:190–196, 2018.
- H. Taghvafard, M. Cao, Y. Kawano, and R.T. Faghih. Design of intermittent control for cortisol secretion under time-varying demand and holding cost constraints. *Submitted*, 2018.
- H. Taghvafard, H. Jardón-Kojakhmetov, P. Szmolyan, and M. Cao. Geometric analysis of oscillations in the Frzilator. *In preparation*, 2018.
- H. Taghvafard, A. Medvedev, A.V. Proskurnikov, and M. Cao. Impulsive model of endocrine regulation with a local continuous feedback. *In preparation*, 2018.

1.4 Outline of the thesis

The outline of the reminder of this book is as follows. Chapter 2 reviews some concepts and tools that are used in the following chapters. In particular, it starts with some concepts and basic definitions from dynamical systems theory, followed by regular and singular perturbation, bifurcation theory, slow-fast system, Fenichel theory, and lastly blow-up method.

Chapter 3 first develops a mathematical model describing the pulsatile release of cortisol. Next, it proposes a method and then an algorithm for calculating the timing and amplitude of secretory events. This chapter proceeds with the results, discussions, and conclusions.

Chapter 4 first extends the Goodwin's model by introducing an additional nonlinear feedback. Then, conditions for local stability analysis, existence of periodic solutions, and global stability of solutions are given. This chapter is followed by proofs of the results, numerical simulations, and lastly, concluding remarks.

Chapter 5 first extends the impulsive Goodwin's model by introducing an additional affine feedback. It proceeds with the main result as well as the approach by which the main result is proven. Concluding remarks close this chapter.

Chapter 6 first describes the Frz system in more details, from both biological and mathematical perspective. Next, local stability analysis is presented, followed by Hopf bifurcation analysis. Then it continues with convergence analysis of solutions, robustness of the bifurcation as well as concluding remarks.

Chapter 7 first gives a preliminary analysis on the Frz system, followed by the slow-fast analysis of an auxiliary system, which is equivalent to the Frz system. Next, the blow-up analysis of two non-hyperbolic lines is presented. This chapter proceeds with giving an explicit range of an independent parameter of the system in which the main result is valid.

Chapter 8 summarizes what has been accomplished in this thesis. In addition, some potential directions for future research are suggested.

2

Preliminaries

This chapter reviews some concepts and tools that are used in the following chapters. Section 2.1 recalls some basic definitions from the dynamical systems theory. Section 2.2 continues to briefly introduce bifurcation theory, followed by regular and singular perturbation theory in Section 2.3. Slow-fast systems and Fenichel theory are presented in Sections 2.4 and 2.5, respectively. Finally, blow-up method is introduced in Section 2.6 through a simple example. The material presented in this chapter is based on [10, 53, 76, 86, 92].

2.1 Basic definitions

Let $U \subseteq \mathbb{R}^n$ and $V \subseteq \mathbb{R}^k$ (for $n, k \in \mathbb{N}$) be open subsets, and $f : U \times V \to \mathbb{R}^n$ be a smooth function. Here the term "smooth" means that the function f is continuously differentiable (i.e., $f \in C^\infty$). An *Ordinary Differential Equation* (ODE) is an equation of the form

$$\dot{x} = f(x, \lambda), \tag{2.1}$$

where "dot" denotes differentiation with respect to t (i.e., $\dot{} = \frac{d}{dt}$), x is a vector of the state variables, and λ is a vector of parameters. In particular, when we are concerned with the components of a vector differential equation, we say that (2.1) is a *system of differential equations*. Moreover, if we are interested in changes with respect to parameters, we call (2.1) a *family of differential equations*.

As ODEs are used to describe the evolution of a state variable for a dynamical process, we are interested in determining the future values of the state variable from its initial value. Then the mathematical model corresponding to such a

dynamical process is given by

$$\dot{x} = f(x, \lambda),$$
$$x(t_0) = x_0,$$

where the second equation is called an *initial condition*.

When $\lambda \in \mathbb{R}^k$ is fixed, it is more convenient to represent (2.1) as follows

$$\dot{x} = f(x), \qquad x \in \mathbb{R}^n. \tag{2.2}$$

We say that the *vector field* f generates a *flow* $\phi_t(\cdot) : U \to \mathbb{R}^n$, where $\phi_t(x) = \phi(t, x)$ is a smooth function defined for all $x \in U$ and $t \in I$ where I is an open subset of $\mathbb{R}$, and ϕ satisfies (2.2) in the sense that

$$\frac{d\phi(t,x)}{dt}\Big|_{t=\tau} = f(\phi(\tau, x)), \qquad \forall x \in U, \quad \tau \in I. \tag{2.3}$$

Systems of the form (2.2), in which the vector field does not contain the time explicitly, are called *autonomous*.

Given an initial condition $x(t_0) = x_0$, we look for a solution $\phi(t, x_0)$ such that $\phi(t_0, x_0) = x_0$. In this case, $\phi(\cdot, x_0) : I \to \mathbb{R}^n$ defines a *solution* of the differential equation (2.2) *through the point* x_0. Although the word "trajectory" is also used to refer to solutions of the differential equations, here we define a term that refers to the *image* of a solution in $\mathbb{R}^n$. So we define the *orbit* of the solution ϕ through the point x_0 to be

$$O(x_0) := \{\phi \in \mathbb{R}^n \,|\, \phi = \phi(t, x_0),\, t \in I\}. \tag{2.4}$$

A geometric picture of all the orbits is called its *phase portrait*.

Equation (2.2) may have the following special types of orbits:

1. *Equilibrium point*[1]: if there exists a point $x_0 \in \mathbb{R}^n$ such that $f(x_0) = 0$, then x_0 is called an *equilibrium point*. Further, if the Jacobian matrix $D_x(f)\big|_{x=x_0}$ has all its eigenvalues off the imaginary axis, then we say that x_0 is *hyperbolic*; otherwise, is *non-hyperbolic*. A hyperbolic equilibrium point x_0 is called *saddle* if the Jacobian matrix $D_x(f)\big|_{x=x_0}$ has at least one eigenvalue with positive real part and one eigenvalue with negative real part.

2. *Periodic orbit*: if equation (2.2) has a closed orbit and $t \mapsto \phi(t, x_0)$ is a solution with the initial value x_0 on this orbit, then there exists $T > 0$ such that $\phi(T, x_0) = \phi(t_0, x_0)$. In such a case, the solution is called T-periodic; i.e., $\phi(t + T, x_0) = \phi(t, x_0)$ for all $t \in \mathbb{R}$. Such closed orbits are also called *periodic orbits*. The *smallest* $T > 0$ that satisfies $\phi(t + T, x_0) = \phi(t, x_0)$ for all $t \in \mathbb{R}$ is called the *period* of the periodic orbit through x_0.

[1] This point is also called a *steady state*, or a *critical point*.

Although equilibria and periodic orbits correspond to very special solutions of (2.2), they are the most important orbits in applications, and hence their stability is of great importance. In this regard, we first define the stability of an equilibrium.

Remark 2.1. Throughout this thesis, the Euclidean norm of $x \in \mathbb{R}^n$ is denoted by $\|x\|$.

Definition 2.2. [10, Definiton 1.38] An equilibrium point x_0 of the differential equation (2.2) is *stable* (in the sense of Lyapunov) if for each $\epsilon > 0$, there exists a number $\delta > 0$ such that $\|\phi(t, x) - x_0\| < \epsilon$ for all $t \geqslant 0$ whenever $\|x - x_0\| < \delta$.

Definition 2.2 only defines the stability of an equilibrium point, which is a special solution. In the following, we extend this definition and define the stability of any arbitrary solution of (2.2).

Definition 2.3. [10, Definiton 1.39] Suppose that x_0 is in the domain of definition of the differential equation (2.2). The solution $t \mapsto \phi(t, x_0)$ of (2.2) is called *stable* (in the sense of Lyapunov) if for each $\epsilon > 0$, there exists $\delta > 0$ such that $\|\phi(t, x) - \phi(t, x_0)\| < \epsilon$ for all $t \geqslant 0$ whenever $\|x - x_0\| < \delta$.

A solution which is not stable is called *unstable*.

Definition 2.4. [10, Definiton 1.40] A solution $t \mapsto \phi(t, x_0)$ of (2.2) is called *asymptotically stable* if it is stable and there is a constant $a > 0$ such that $\lim_{t\to\infty} \|\phi(t, x) - \phi(t, x_0)\| = 0$ whenever $\|x - x_0\| < a$.

So far, we have defined the concept of stability for solutions for a *given initial condition*. The notion of stability for periodic orbits is different, which is given as follows.

Definition 2.5. [10, Definiton 1.41] A periodic orbit Γ of the differential equation (2.2) is *orbitally stable* if for each open set $V \subseteq \mathbb{R}^n$ that contains Γ, there is an open set $W \subseteq V$ such that every solution, starting at a point in W at $t = 0$, stays in V for all $t \geqslant 0$. The periodic orbit is called *orbitally asymptotically stable* if , in addition, there is a subset $X \subseteq W$ such that every solution starting in X is asymptotic to Γ as $t \to \infty$.

Dealing with mathematical models, it is of great interest to know the long-term behavior of solutions of a dynamical system. In this regard, we present the following definition, which precisely describes the limiting behavior of an arbitrary orbit.

Definition 2.6. [10, Definiton 1.165] Suppsoe that $\phi(t, \cdot)$ is a flow on $\mathbb{R}^n$ and $p \in \mathbb{R}^n$. A point x in $\mathbb{R}^n$ is called an *omega limit point* (ω-limit point) of the orbit through p if there is a sequence of numbers $t_1 \leqslant t_2 \leqslant t_3 \leqslant \cdots$ such that $\lim_{i\to\infty} t_i = \infty$ and $\lim_{i\to\infty} \phi(t_i, p) = x$. The collection of all such omega limit

points is denoted by $\omega(p)$ and called the *omega limit set* (ω-limit set) of p. Similarly, the α-limit set $\alpha(p)$ is defined to be the set of all limits $\lim_{i\to\infty}\phi(t_i,p)=x$ where $t_1 \geqslant t_2 \geqslant t_3 \geqslant \cdots$ and $\lim_{i\to\infty} t_i = -\infty$

We are now ready to define the concept of limit cycle, which is widely used in this thesis.

Definition 2.7. [10, Definiton 1.178] A *limit cycle* Γ is a periodic orbit that is either the ω-limit set or the α-limit set of some point that is in the phase space but not in Γ.

Besides limit cycles, a dynamical system may have other types of orbits, such as *homoclinic* and *heteroclinic* orbits. To define such orbits, first let us define a *saddle connection* to be an orbit whose α- and ω-limit sets are hyperbolic saddle points [10].

Definition 2.8. [10] A saddle connection is called a *homoclinic orbit* if its α- and ω-limit sets coincide. On the other hand, the saddle connection is called a *heteroclinic orbit* if its α-limit set is disjoint form its ω-limit set.

2.2 Bifurcation theory

Dynamical processes that are described by ODEs can have several parameters, and a small change in a parameter may lead to a significant change on the solutions of the ODEs. As mentioned in the previous section, equilibria and periodic orbits are the most important orbits in applications. So it is of great interest to know how equilibria and periodic orbits can be continued with respect to the variation of a parameter, and also how qualitative changes in the behavior of solutions can be predicted with respect to such a parameter variation. The answer to such questions is given by *bifurcation theory*.

Let us consider a family of ODEs of the form

$$\dot{x} = f(x,\lambda), \tag{2.5}$$

where $x \in \mathbb{R}^n$ is the state variable, and $\lambda \in \mathbb{R}^k$ is the parameter. Bifurcation theory deals with the behavior of solutions of (2.5) under variations of the parameter λ.

Assume that λ_0 is a particular value of λ. Then for values of λ near λ_0, the system (2.5) is called an *unfolding* of

$$\dot{x} = f(x,\lambda_0). \tag{2.6}$$

In a region in the state space, if the phase portraits of (2.5) are qualitatively the same as those of (2.6) when $\|\lambda-\lambda_0\|$ is sufficiently small, then (2.6) is *structurally*

stable. Values of λ_0 for which (2.6) is not structurally stable are called *bifurcation values* [53].

The simplest solutions to (2.5) are the equilibria, which are the solutions to the equation

$$f(x, \lambda) = 0. \tag{2.7}$$

Let us consider (2.5) with $\lambda \in \mathbb{R}$, and assume that $f(x_0, \lambda_0) = 0$. The eigenvalues of the Jacobian matrix $D_x(f)\big|_{(x_0,\lambda_0)}$ can be one of the followings [53]:

- A simple zero eigenvalue; this case is called a *fold* point, where a change in the stability of the solutions occurs under parameter perturbations.
- A conjugate pair of pure imaginary eigenvalues, i.e., $\pm i\beta$ where $\beta > 0$; this case is called a *Hopf* point, where the change in the stability leads to the emergence of another type of solution, namely, periodic orbits.

A non-trivial application of Hopf bifurcation is presented in Chapters 4, 6, and 7.

2.3 Regular versus singular perturbation

Most of ODEs describing dynamical processes cannot be solved exactly, due to their complexity. Nevertheless, it may be the case that a small parameter, namely ε, can be identified such that the solution is available (for instance, it is linear or exactly solvable) for $\varepsilon = 0$. Then, it is of great interest to know how the behavior of such a solution will change for *non-zero but small* variation of the parameter ε. The answer to his question is given by *perturbation theory*.

Let us consider a family of ODEs of the form

$$\dot{x} = f(x, \varepsilon), \tag{2.8}$$

where the state variable $x \in \mathbb{R}^n$, $\varepsilon > 0$ is a small parameter, and f is a continuous function in a domain $\mathcal{D} \subseteq \mathbb{R}^{n+1}$. Setting $\varepsilon = 0$ in (2.8) defines the *unperturbed system*

$$\dot{x} = f(x, 0). \tag{2.9}$$

Let $x_\varepsilon(t)$ and $x_0(t)$ denote, respectively, solutions of (2.8) and (2.9) with initial conditions $x_\varepsilon(t_0) = x_0(t_0) = x_0$ when $t \in [t_0, \bar{T}]$ and $(x_0, \varepsilon) \in \mathcal{D}$. As f is continuous in the domain $\mathcal{D}$, then for a sufficiently small $\varepsilon > 0$, the solution $x_\varepsilon(t)$ when $t \in [t_0, \bar{T}]$ can be represented as

$$x_\varepsilon(t) = x_0(t) + R_0(t, \varepsilon), \tag{2.10}$$

where $R_0(t, \varepsilon) \to 0$ as $\varepsilon \to 0$ uniformly with respect to t where $t \in [t_0, \bar{T}]$.

In the case when f is continuously differentiable $k \geqslant 1$ times with respect to both x and ε (i.e. $f \in C^k(\mathcal{D})$), for a sufficiently small $\varepsilon > 0$, the solution $x_\varepsilon(t)$ can be represented as

$$x_\varepsilon(t) = x_0(t) + \varepsilon x_1(t) + \varepsilon^2 x_2(t) + \cdots + \varepsilon^{k-1} x_{k-1}(t) + R_k(t, \varepsilon), \tag{2.11}$$

where $R_k(t, \varepsilon) \to 0$ as $\varepsilon \to 0$ uniformly with respect to t where $t \in [t_0, \bar{T}]$. Further, if $f \in C^\infty(\mathcal{D})$, then the solution $x_\varepsilon(t)$ can be represented as

$$x_\varepsilon(t) = x_0(t) + \sum_{k=1}^{\infty} \varepsilon^k x_k(t), \tag{2.12}$$

which converges uniformly with respect to t where $t \in [t_0, \bar{T}]$.

From (2.10), (2.11), and (2.12), it is clear that $x_\varepsilon(t) \to x_0(t)$ as $\varepsilon \to 0$. Such problems in which the solution of the general problem (2.8) converges to the solution of the unperturbed problem (2.9), as the parameter approaches the limit value (i.e., $\varepsilon \to 0$), are called *regular perturbation* problems. In contrast, those problems in which the solutions of the unperturbed problem are different in character from the limit of the general problem are called *singular perturbation* problems. In fact, the structure of the asymptotic expansions of the singular perturbation problems is both complicated and unexpected, and may have expansion terms such as $(\ln \varepsilon)^{-k}$, $\varepsilon^k (\ln \varepsilon)^\ell$, or even $\varepsilon^k (\ln |\ln \varepsilon|)^{-\ell}$ where $k, \ell \in \mathbb{N}$ [119]. The existence of such terms in an asymptotic expansion does not allow us to analyze its corresponding system via regular perturbation theory, and hence tools beyond such a theory are required.

To overcome such issues, geometric methods from dynamical systems theory, namely, *blow-up method* [22] is useful. Blow-up is a complicated rescaling of the time which allows us to analyze the dynamics near a singularity. In Chapter 7 of this thesis, concepts from singular perturbation theory based on the blow-up method are used to analyze a biochemical oscillator model, which evolves on *different time scales*, i.e., the dynamics of some variables are faster than the dynamics of other variables. In this regard, *slow-fast systems* are introduced in the following section.

2.4 Slow-fast systems

Some dynamical processes in nature can be modeled by differential equations of the form

$$\begin{aligned} \varepsilon \dot{x} &= f(x, y, \varepsilon), \\ \dot{y} &= g(x, y, \varepsilon), \end{aligned} \tag{2.13}$$

where $\dot{} = \frac{d}{dt}$, $(x, y) \in \mathbb{R}^m \times \mathbb{R}^n$ for $m, n \in \mathbb{N}$, functions f and g are smooth in all three arguments (x, y, ε), and $\varepsilon > 0$ is a small parameter (i.e., $0 < \varepsilon \ll 1$). Setting $\tau = \frac{t}{\varepsilon}$, system (2.14) is represented by

$$\begin{aligned} x' &= f(x, y, \varepsilon), \\ y' &= \varepsilon g(x, y, \varepsilon), \end{aligned} \tag{2.14}$$

where $' = \frac{d}{d\tau}$. As long as $\varepsilon \neq 0$, the time scale given by t is said to be slow, whereas that for τ is fast. Therefore, we call (2.13) the *slow system*, and (2.14) the *fast system*. A slow-fast system is in the *standard form* if the separation into slow and fast variables (i.e., in the form of either (2.13) or (2.14)) is given a priori, while is in the *non-standard form* if such a separation is not given.

For $\varepsilon > 0$, systems (2.13) and (2.14) are equivalent in the sense that they have the same phase portrait, while they have different speed of propagation along their orbits. Further, they have distinguished limits as $\varepsilon \to 0$.

To study slow and fast processes *separately* but *simultaneously*, we study the dynamics of (2.13) and (2.14) as $\varepsilon \to 0$. Setting $\varepsilon = 0$ in (2.13), we obtain

$$\begin{aligned} 0 &= f(x, y, 0), \\ \dot{y} &= g(x, y, 0), \end{aligned} \tag{2.15}$$

which is called the *reduced problem*. Now by setting $\varepsilon = 0$ in (2.14), we obtain

$$\begin{aligned} x' &= f(x, y, 0), \\ y' &= 0, \end{aligned} \tag{2.16}$$

which is called the *layer problem*. As observed in (2.16), the variable x will change with respect to τ, while y will remain constant.

Note that (2.15) is not only an ODE, but an ODE with the algebraic constraint $f(x, y, 0) = 0$. Therefore (2.15) is a Differential-Algebraic Equation (DAE). The set

$$S := \{(x, y) \in \mathbb{R}^{m+n} \mid f(x, y, 0) = 0\}, \tag{2.17}$$

is called the *critical manifold* or the *critical set*. In contrast to (2.15), in the analysis of the layer problem (2.16) we study the dynamics of the fast variable x, while y is constant. Note that the critical manifold S is the set of the equilibria of the layer problem (2.16), and hence is related to the fast dynamics as well.

If $f(x, y, 0) = 0$, then the flow is trivial for (2.16). However, the flow of (2.15) is non-trivial on the set S, but is not defined outside S. The main goal of the *Geometric Singular Perturbation Theory* (GSPT) is to realize both these aspects (i.e., slow and fast) simultaneously. This contradictory goal will be done within the phase space of (2.13) (or, equivalently, (2.14)) for ε *non-zero but small* [76].

The following reasons explain why GSPT is a powerful tool for analyzing high-dimensional systems [76]:

1. In many applications, quantities change on different time scales, and hence are modeled in the from of (2.13) (or, equivalently, (2.14)).

2. Equations (2.14) can be reduced to the lower-dimensional systems (2.15) and (2.16).

An important property that a critical manifold may posses is normal hyperbolicity, which is defined as follows.

Definition 2.9. [92, Definition 3.1.1] A subset $S_0 \subset S$ is called *normally hyperbolic* if the $m \times m$ matrix $(D_x f)(p, 0)$ of the first partial derivatives with respect to the fast variable has no eigenvalues with zero real part for all $p \in S_0$.

The type of equilibria for the fast subsystem that lies in S_0 determines whether S_0 is stable or unstable. In this regard, we have the following definition.

Definition 2.10. [92, Definition 3.1.3] A normally hyperbolic subset $S_0 \subset S$ is called *attracting* if all eigenvalues of $(D_x f)(p, 0)$ have negative real parts for $p \in S_0$; similarly, S_0 is called *repelling* if all eigenvalues have positive real parts. If S_0 is normally hyperbolic and neither attracting not repelling, it is of the *saddle type*.

Remark 2.11. In a neighborhood of a point in the critical manifold S whose Jacobian is non-singular, using implicit function theorem, the equation $f(x, y, 0) = 0$ can be solved for $x = h_0(y)$, and hence the reduced problem (2.15) is described by $\dot{y} = g(h_0(y), y, 0)$.

As mentioned, the critical manifold S, which is a manifold of equilibria of the layer problem (2.16), may have normally hyperbolic and non-hyperbolic points, respectively. In order to analyze the system at such points, we use Fenichel theory for the former, while blow-up method for the latter. In this regard, a brief introduction to these tools are given in the following sections.

2.5 Fenichel theory

In the seminal paper [37], Fenichel showed that normally hyperbolic points of the critical manifold S perturb *smoothly* to locally invariant *slow manifolds*, for sufficiently small ε, see Fig. 2.1. As Fenichel theory plays a crucial role in our analysis in Chapter 7, this section is devoted to such a theory, before which we recall the following definitions.

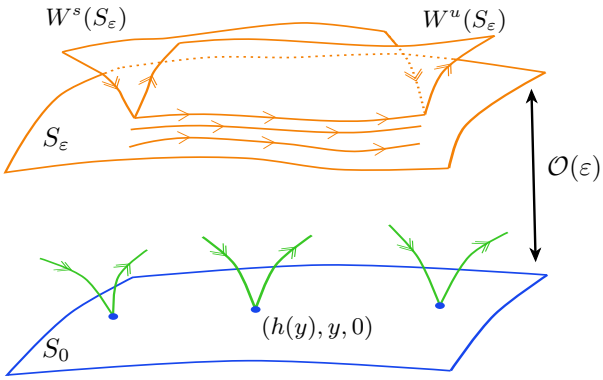

Figure 2.1: Perturbation of a normally hyperbolic submanifold S_0 to a slow manifold S_ε by the Fenichel's theorem.

Definition 2.12. [92] The *Hausdorff distance* between two nonempty sets $U, V \subset \mathbb{R}^{m+n}$ is defined by

$$d_{\mathrm{H}}(U,V) := \max\left\{ \sup_{u\in U}\inf_{v\in V}\|u-v\|, \sup_{v\in V}\inf_{u\in U}\|u-v\| \right\}.$$

Definition 2.13. Let $f, g : \mathbb{R}\setminus\{0\} \to \mathbb{R}$ be real functions. We say that $f = \mathcal{O}(g)$ as $x \to 0$ if there exist constants $C, r > 0$ such that

$$|f(x)| \leqslant C|g(x)|, \qquad 0 < |x| < r.$$

We are now ready to present the Fenichel's theorem.

Theorem 2.14. *[92, Theorem 3.1.4]**(Fenichel's theorem)** Assume that S_0 is a compact normally hyperbolic submanifold of the critical manifold S, and that $f, g \in C^r$ $(r < \infty)$. Then for $\varepsilon > 0$ sufficiently small, the following statements hold:*

(F1) There exists a locally invariant manifold S_ε diffeomorphic to S_0. Local invariance means that trajectories can enter or leave S_ε only through its boundaries.

(F2) S_ε has the Hausdorff distance $\mathcal{O}(\varepsilon)$ as $\varepsilon \to 0$ from S_0.

(F3) The flow on S_ε converges to the slow flow as $\varepsilon \to 0$.

(F4) S_ε is C^r-smooth.

(F5) S_ε is normally hyperbolic and has the same stability properties with respect to the fast variables as S_0 (attracting, repelling, or of saddle type).

(F6) *S_ε is usually not unique. In regions that remain at the fixed distance from ∂S_ε, all manifolds satisfying items (F1)-(F5) lie at a Hausdorff distance $\mathcal{O}(\exp(-K/\varepsilon))$ from each other for some $K > 0$, $K = \mathcal{O}(1)$.*

Note that all asymptotic notation refers to $\varepsilon \to 0$. The same conclusions as for S_0 hold locally for its stable and unstable manifolds:

$$W^{\mathrm{s}}_{loc}(S_0) = \bigcup_{p\in S_0} W^{\mathrm{s}}_{loc}(p), \qquad W^{\mathrm{u}}_{loc}(S_0) = \bigcup_{p\in S_0} W^{\mathrm{u}}_{loc}(p),$$

where we view points $p \in S_0$ as equilibria of the fast subsystem. These manifolds also persist for $\varepsilon > 0$ sufficiently small: there exist local stable and unstable manifolds $W^{\mathrm{s}}_{loc}(S_\varepsilon)$ and $W^{\mathrm{u}}_{loc}(S_\varepsilon)$, respectively for which conclusions (F1)-(F6) hold if we replace S_ε and S_0 by $W^{\mathrm{s}}_{loc}(S_\varepsilon)$ and $W^{\mathrm{s}}_{loc}(S_0)$ (or similarly by $W^{\mathrm{u}}_{loc}(S_\varepsilon)$ and $W^{\mathrm{u}}_{loc}(S_0)$).

Definition 2.15. [92, Definiton 3.1.5] A manifold S_ε, as obtained in the conclusion of Theorem 2.14, is called a *slow manifold*.

2.6 Blow-up method

As mentioned in the previous section, Fenichel theory is solely applicable to hyperbolic points of the critical manifold S, while for the *fold* points and *non-hyperbolic* points of S such a theory fails. Therefore, more advanced tools and techniques are required to analyze the dynamics at these points. One of such techniques is the *blow-up method*, introduced in the seminal work by Dumortier and Roussarie [22]. Using the blow-up method, singularities (i.e., fold and non-hyperbolic points) at which slow and fast directions intersect can be transformed into partially hyperbolic problems. This geometric method has been successfully applied to many problems, see e.g. [23, 86, 88, 92, 109, 137], and can be regarded as a complement of Fenichel theory for singular points.

To introduce and clearly show the blow-up technique in multiple-time-scale dynamics, we consider a concrete low-dimensional example. In this regard, let us consider the planar singularly perturbed system

$$\begin{aligned} x' &= f(x, y, \varepsilon), \\ y' &= \varepsilon g(x, y, \varepsilon), \end{aligned} \tag{2.18}$$

where $(x, y) \in \mathbb{R}^2$ and

$$f(0, 0, 0) = 0, \qquad f_x(0, 0, 0) = 0. \tag{2.19}$$

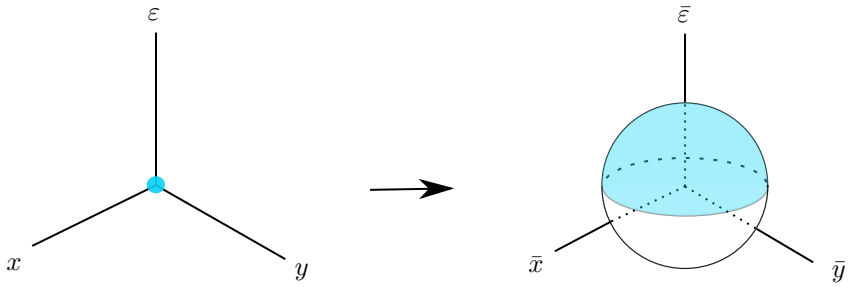

Figure 2.2: Blow-up of a point to a sphere.

Now, we add a trivial equation $\varepsilon' = 0$ to (2.18), which results in the system

$$\begin{aligned} x' &= f(x, y, \varepsilon), \\ y' &= \varepsilon g(x, y, \varepsilon), \\ \varepsilon' &= 0. \end{aligned} \tag{2.20}$$

As is clear from (2.19), the linearization of (2.20) at $(0, 0, 0)$ has triple zero eigenvalues; in other words, $(0, 0, 0)$ is a *degenerate* equilibrium for (2.20). To overcome such a degeneracy, we use the blow-up technique by which the degenerate equilibrium is blown-up to a sphere (see Fig. 2.2) by a suitably weighted spherical coordinates transformation, which is defined by the mapping

$$\begin{aligned} &\Phi : \mathbb{S}^2 \times [0, r_0] \to \mathbb{R}^3, \\ &(\bar{x}, \bar{y}, \bar{\varepsilon}) \longmapsto (x, y, \varepsilon), \end{aligned}$$

such that

$$x = r^\alpha \bar{x}, \qquad y = r^\beta \bar{y}, \qquad \varepsilon = r^\gamma \bar{\varepsilon}, \tag{2.21}$$

where $\mathbb{S}^2 := \{(\bar{x}, \bar{y}, \bar{\varepsilon}) \,|\, \bar{x}^2 + \bar{y}^2 + \bar{\varepsilon}^2 = 1\}$, $r_0 > 0$, and the suitable weights $(\alpha, \beta, \gamma) \in \mathbb{Z}^3$. Denoting X as the vector field of (2.20), the map Φ induces a blown-up vector field, namely $\bar{X}$, such that the diagram

$$\begin{array}{ccc} B_0 & \xrightarrow{\Phi} & \mathbb{R}^3 \\ \bar{X} \downarrow & & \downarrow X \\ TB_0 & \xrightarrow[\Phi_*]{} & T\mathbb{R}^3 \end{array}$$

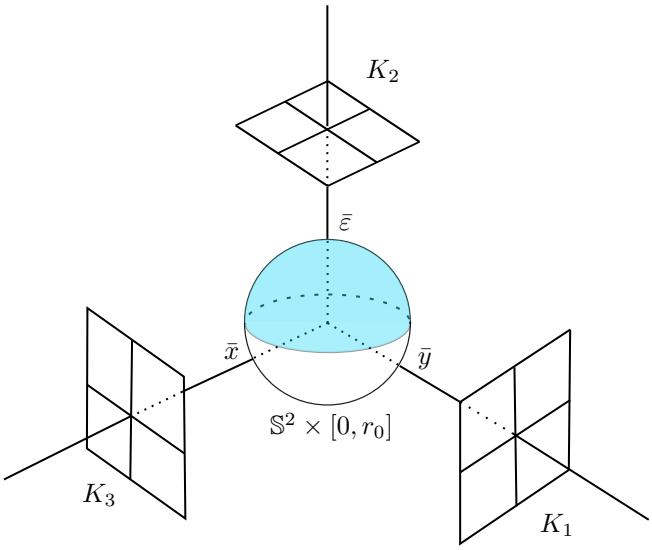

Figure 2.3: Coordinate charts for blow-up method.

commutes, where $B_0 := \mathbb{S}^2 \times [0, r_0]$, and TB_0 denotes the tangent bundle[2] of B_0. Owing to the fact that a degenerate equilibrium is blown-up to a sphere, the blown-up vector field $\bar{X}$ vanishes on the sphere. To overcome such a problem, a suitable power of the radial variable r is divided out such that the flow on the sphere is not degenerate anymore and allows us to analyze the blown-up vector field on the sphere.

The blown-up vector field is analyzed in local charts. The idea for finding such charts is that in the transformation (2.21), one blown-up variable on $\mathbb{S}^2$ is set to be equal to ± 1, while keeping the others unchanged. In doing so, the whole sphere is covered by several planar charts, which are perpendicular to the axes, see Fig. 2.3. Among all charts, the most important one, so-called the *central* chart, corresponds to the case where $\bar{\varepsilon} = 1$ in (2.21). In fact, the central chart is an ε-rescaling of the original variables x and y, since setting $\bar{\varepsilon} = 1$ in (2.21) implies that $r = \varepsilon^{-\gamma}$. In the central chart, the variable r acts as a parameter since $\varepsilon' = 0$ implies that $r' = 0$, while in the other charts this variable is dynamic. The additional charts are useful for the analysis of the blown-up dynamics on the *unbounded* domains of the central chart.

In this section, we have briefly presented how a singular point is blown-up to a sphere; for a more complete and detailed analysis, the interested reader is refereed to [90, 93]. A non-trivial application of the blow-up method is presented in Chapter 7, where a non-hyperbolic line is blown-up to a cylinder.

[2]The *tangent bundle* of B_0 is the union of all tangent spaces of B_0.

Part I

Application of Control Theory to Endocrinology

3

Design of intermittent control for cortisol secretion

In this chapter we take the release of stress hormone cortisol as a part of an intermittent control feedback system as opposed to a continuous one. By modeling cortisol secretion as an impulsive system, we design an impulsive controller for adjusting cortisol levels while maintaining the blood cortisol levels within levels that satisfy circadian demand and cost constraints. Following an analytical approach, both the timing and amplitude of the control are identified. We use various examples to illustrate that the proposed approach achieves impulsive control and that the obtained blood cortisol levels show the circadian rhythm and the ultradian rhythm that are consistent with the known physiology of cortisol secretion.

This chapter starts with an introduction, followed by Section 3.2 where we develop a mathematical model, and propose an algorithm. The results are given in Section 3.3. Lastly, discussions and concluding remarks are given in Sections 3.4 and 3.5, respectively.

3.1 Introduction

HORMONES are signaling substances that regulate many vital bodily functions, such as growth, stress, and metabolism. In the endocrine system, glands communicate with remote target cells through a combination of continuous and intermittent (pulsatile) signal exchanges [157]. Continuous signaling permits hormone concentrations to vary slowly, while pulsatile signaling allows them to have instantaneous adjustment [157]. In fact, pulsatility is a physiological mechanism through which hormone concentrations can increase rapidly and send distinct signaling information to target cells [155]. Compared with continuous

signaling, pulsatile signaling is more energy efficient, permits more rapid changes in hormone concentrations, and offers greater control flexibility [164]. On one hand, it is widely known that several hormones, such as gonadal steroid, growth, insulin and cortisol, are released in a pulsatile manner [15, 124, 153, 155, 156, 163]; on the other hand, pulsatile signaling is significantly different from continuous signaling [132]. Therefore, it is crucial to understand the physiology underlying the pulsatile hormone release [34].

The hypothalamic-pituitary-adrenal (HPA) axis is one of the most important endocrine systems, which controls intermittent release of cortisol. Cortisol is a steroid hormone that is mainly responsible for regulating metabolism and the body's reaction to stress and inflammation [7]. The HPA axis includes several direct influences and feedback interactions among the hypothalamus, the pituitary gland, and the adrenal glands. It is known that the mechanisms of the HPA axis are governed not only by a circadian rhythm, but also by an ultradian pattern of pulsatile release of cortisol [7, 32, 34, 157, 163, 164]. The pulsatile release of cortisol from the adrenal glands is controlled by the pulsatile release of adrenocorticotropic hormone (ACTH) from the anterior pituitary, which is induced by the corticotropin-releasing hormone (CRH), produced in the hypothalamus [7]. Cortisol in turn exerts negative feedback effect on the release of CRH and ACTH, produced respectively in the hypothalamus and the pituitary gland [7, 82]. Dysregulation of cortisol pulsatility is related to a number of psychiatric and metabolic diseases [171, 172]; however, due to ethical reasons, direct measurement of endocrine glands (e.g., CRH) is impossible in healthy humans [157]. Therefore, it is crucial to understand the sophisticated control mechanisms, which involves (i) determining the number, timing, and amplitude of cortisol pulses to better understand the physiology, effects of drugs, and other interventions [31, 33]; (ii) designing intermittent controllers to optimally control cortisol levels in disorders linked to cortisol pulsatility [31, 34].

Due to the fact that the hypothalamus, the pituitary gland, and the adrenal glands are interacting in the HPA axis, in order to investigate pathological conditions related to cortisol, and design optimal treatment strategies, one may build a mathematical model based on the physiology underlying the HPA axis, and then develop signal processing and control algorithms for diagnostic and treatment purposes. Besides the interactions among the three hormones in the HPA axis, a complete mathematical model of the diurnal cortisol variation should also include the effects of the exogenous factors such as stress, meals, and sleep [7, 98, 130]. However, in order to have a tractable mathematical model [154], an alternative approach is to define a minimal model based on the known physiology of the HPA axis which captures only known essential characteristics of the observed diurnal patterns [7].

Although the three hormones in the HPA axis are interacting, it is believed [165] that the pulsatile secretion of CRH is not the main factor to control the pulsatile

ultradian patterns. Instead the oscillatory behavior exists at a sub-hypothalamic level, i.e., the pituitary-adrenal system. It has been further observed [165] that the pituitary-adrenal system can generate pulsatile oscillatory patterns of both ACTH and cortisol levels with a physiological ultradian frequency even in presence of constant CRH levels. Moreover, studies in sheep indicate that surgical disconnection of the hypothalamus from the pituitary still maintains the pulsatile patterns of cortisol [163]. Therefore, it seems that the pulsatile release of cortisol is controlled by the dynamics in the anterior pituitary. This motivates us to study the control mechanisms of the pulsatile cortisol release in the pituitary-adrenal system.

Although mathematically, recovering the number, timing and amplitude of hormone pulses can lead to an ill-posed problem mainly due to existence of multiple solutions [31, 32], by using the characteristic of the sparsity of hormone pulses and taking into account more constraints, several methods have been presented to estimate such quantities [32, 33, 75, 83, 157, 160, 162]. In some recent work [31, 34], an optimization approach based on a deterministic model has been proposed to design impulsive inputs (i.e. determine the timing, amplitude, and number of secretory events) to achieve pulsatile dynamics in the pituitary-adrenal system in presence of circadian amplitude constraints on the cortisol levels. However, since this optimization problem is solved by the ℓ_1-norm minimization algorithm presented in [8, 36], it can lead to finding suboptimal solutions. In this work, we present a parsimonious mathematical model describing the pulsatile cortisol release in the pituitary-adrenal system. We postulate that there exists an "impulsive" controller in the anterior pituitary which allows the state of the system to have instantaneous changes, and controls the cortisol secretion and the ultradian rhythm of the pulses. In addition, we propose an *analytical approach* to design an intermittent controller (i.e. calculate the number, timing, and amplitude of impulsive control input) in presence of circadian demand and holding cost constraints on the blood cortisol level, which are assumed to be two-harmonic time-varying circadian functions with periods of 12 and 24 hours [34]. We illustrate several examples to show the efficiency and accuracy of our methods. One direct application of our intermittent control design is determining the timing and dosage of hydrocortisone (i.e. synthetic cortisol) injections in Addisonian patients given desired circadian demand and holding cost constraints on the blood cortisol levels and the patients' metabolic rate.

3.2 Methods

We propose an impulsive differential equation model using the stochastic differential equation model of diurnal cortisol patterns presented in [7], which is based on the first-order kinetics for cortisol synthesis in the adrenal glands, cortisol infusion

to the blood, and cortisol clearance by the liver [7, 30, 32, 34]. In the stochastic model presented in [7], the “pulsatile" input in the adrenal glands is supposed to be doubly stochastic with amplitudes in Gaussian and inter-arrival times in gamma distributions respectively. However, in the model presented here, the input is considered to be an “abstraction” of hormone pulses which results in cortisol secretion. We make the following physiologically plausible assumptions for the proposed model:

1. Cortisol levels can be described by the first-order kinetics for cortisol synthesis in the adrenal glands, cortisol infusion to the blood, and cortisol clearance by the liver [7].

2. There is a time-varying circadian holding function $H(t)$ on the cortisol level which is the highest cortisol level that the body should produce in order to have a normal cortisol profile [34].

3. There is a time-varying cortisol demand $D(t)$ that should be satisfied throughout the day, which is a function of the circadian rhythm [34].

4. The input $u(t)$ is non-negative since it is a hormone secretory event.

In view of these assumptions, we propose the following model to control the secretion of cortisol:

$$\begin{aligned} \frac{dx_1(t)}{dt} &= -\lambda x_1(t) + u(t), \\ \frac{dx_2(t)}{dt} &= \lambda x_1(t) - \gamma x_2(t), \end{aligned} \tag{3.1}$$

where

$$D(t) \leqslant x_2(t) \leqslant H(t), \tag{3.2}$$

and

$$u(t) = \sum_{k=1}^{\infty} u_k \delta(t - t_k). \tag{3.3}$$

In equations (3.1), $x_1(t)$ is the concentration of cortisol in the adrenal glands, and $x_2(t)$ is the serum cortisol concentration at time t. Following [7, 32], we denote $\lambda > 0$ as the infusion constant governing the rate at which cortisol enters the blood from the adrenal gland, and $\gamma > 0$ as the clearance parameter describing the rate at which cortisol is cleared from the blood by the liver. In equation (3.3), $\delta(t)$ denotes the Dirac delta-function, and u_k represents the amount of the hormone’s input at time t_k, which is known as the secretory (firing) time. In other words, u_k is zero if a hormone pulse is not fired at time t_k.

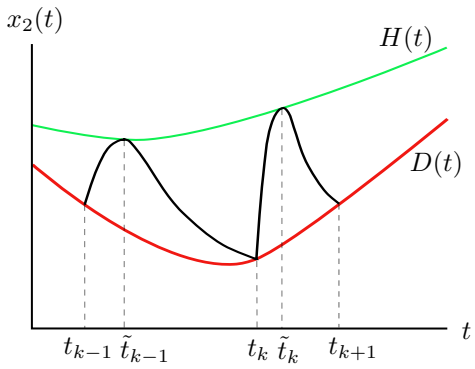

Figure 3.1: Schematic representation of the trajectory $x_2(t)$ for the time interval $(t_{k-1}, t_{k+1}]$.

In view of the known physiology of *de novo* cortisol synthesis, i.e., no cortisol is stored in the adrenal gland, we assume that the initial condition of the cortisol level in the adrenal gland is zero, i.e. $x_1(t_0) = 0$ [7, 75].

Equations (3.1) and (3.3) can be represented equivalently as follows:

$$\begin{aligned} \frac{dx(t)}{dt} &= Ax(t), & t \neq t_k, \\ x(t_k^+) &= x(t_k^-) + Bu_k, & t = t_k, \end{aligned} \tag{3.4}$$

where $t_{k+1} > t_k (\forall k \geqslant 0)$, and

$$x(t) = \begin{bmatrix} x_1(t) \\ x_2(t) \end{bmatrix}, \qquad A = \begin{bmatrix} -\lambda & 0 \\ \lambda & -\gamma \end{bmatrix}, \qquad B = \begin{bmatrix} 1 \\ 0 \end{bmatrix}.$$

The notations $x(t_k^-)$ and $x(t_k^+)$ in (3.4) denote, respectively, the left- and right-hand sided limits of $x(t)$ at time t_k.

Mathematically, equations (3.4) are treated as follows. At time t_k, a pulse is fired, corresponding to the concentration of cortisol in the adrenal gland, which is described by the jump of its concentration, i.e. $x_1(t_k^+) = x_1(t_k^-) + u_k$, while it does not affect the serum cortisol concentration, i.e. $x_2(t_k^+) = x_2(t_k^-)$. In this work, $x_1(t)$ is considered to be left-continuous, i.e., $x_1(t_k^-) = x_1(t_k)$.

In view of system (3.1)-(3.3), our goal hereafter is to present an algorithm for the computation of

(a) the secretory time t_k at which $x_2(t_k) = D(t_k)$, and

(b) the input u_k at the secretory time t_k such that $x_2(t)$ reaches the upper bound $H(t)$ from $D(t_k)$,

when $k > 0$ (see Fig. 3.1). The objective (a) gives time t_k at which $x_2(t)$ reaches the lower bound $D(t)$ from the upper bound $H(t)$. This time needs to be calculated in order to know when the next secretory event should occur. The objective (b) gives the amount of the input u_k so that after some time, $x_2(t)$ reaches the upper bound $H(t)$ from the lower bound $D(t)$. More precisely, when the input u_k is implemented into system (3.1) at time t_k, there exists $\tilde{t}_k > t_k$ ($k > 0$) such that $x_2(\tilde{t}_k) = H(\tilde{t}_k)$, see Fig. 3.1.

Remark 3.1. As $D(t)$ and $H(t)$ are, respectively, the lower and upper bounds on the cortisol level, we are only interested in secretion times t_k and inputs u_k such that $x_2(t)$ remains within these bounds (see Fig. 3.1).

Remark 3.2. We do not restrict the state $x_2(t)$ to start from the upper bound $H(t)$ at time t_0. In other words, we choose a random number, namely x_2^0, within the upper and lower bounds as the initial condition of $x_2(t)$ at time t_0, i.e., $D(t_0) < x_2^0 \leqslant H(t_0)$.

In the rest of this section, we present a method on how to calculate t_k and u_k *analytically*. To this end, let us assume that $x_2(t)$ is at the upper bound at time $\tilde{t}_{k-1}$ ($k > 1$), see Fig. 3.1. For the case $k = 1$, we set $\tilde{t}_0 = t_0$. Our approach for the computation of t_k and u_k are as follows:

(a) *Calculation of* t_k : At time $\tilde{t}_{k-1}$ we have $x_2(\tilde{t}_{k-1}) = H(\tilde{t}_{k-1})$. The goal is to calculate t_k such that $x_2(t_k) = D(t_k)$ where $t_k > \tilde{t}_{k-1}$ ($k > 0$), see Fig. 3.1. From (3.4) we know that between two consecutive pulses, equations (3.1) and (3.3) are described by the linear system

$$\frac{dx(t)}{dt} = Ax(t), \qquad t_{k-1} < t < t_k,$$

whose solution is given by

$$x(t) = e^{A(t-t_{k-1})}x(t_{k-1}^+), \qquad t_{k-1} < t < t_k. \tag{3.5}$$

Owing to the fact that $\tilde{t}_{k-1} > t_{k-1}$ ($k > 1$), using (3.5) with the initial time $\tilde{t}_{k-1}$, the trajectory $x_2(t)$ when $t \in [\tilde{t}_{k-1}, t_k)$ is given by

$$x_2^L(t) := \frac{\lambda}{\lambda - \gamma}\left(e^{-\gamma(t-\tilde{t}_{k-1})} - e^{-\lambda(t-\tilde{t}_{k-1})}\right)x_1(\tilde{t}_{k-1}) + e^{-\gamma(t-\tilde{t}_{k-1})}x_2(\tilde{t}_{k-1}), \tag{3.6}$$

where $x_1(\tilde{t}_{k-1})$ and $x_2(\tilde{t}_{k-1})$ are computed by (3.5). Since our goal is to calculate t_k such that $x_2^L(t_k) = D(t_k)$, solving

$$x_2^L(t) - D(t) = 0, \tag{3.7}$$

with respect to t gives t_k.

Remark 3.3. Due to the fact that matrix A is Hurwitz, there exists at least one solution to (3.7) when $t > \tilde{t}_{k-1}$.

Remark 3.4. In order to guarantee that $x_2^L(t)$ does not cross the lower bound $D(t)$, we only consider the minimum root of (3.7) which is greater than $\tilde{t}_{k-1}$.

In view of Remarks 3.3 and 3.4, the secretory time t_k exists and is calculated by

$$t_k = \min\{t^* \mid x_2^L(t^*) - D(t^*) = 0,\ t^* > \tilde{t}_{k-1}\}. \tag{3.8}$$

Once t_k is computed in (3.8), we can plot the dynamics on the interval $[\tilde{t}_{k-1}, t_k]$ by (3.5).

(b) *Calculation of* u_k : At time t_k, the trajectory $x_2(t)$ is at the lower bound, i.e., $x_2(t_k) = D(t_k)$, see Fig. 3.1. Our goal is to calculate u_k such that $x_2(t)$ reaches exactly the upper bound $H(t)$ at time $\tilde{t}_k > t_k$ ($k > 0$), while does not crossing it, see Fig. 3.1.

From (3.4), the trajectory $x_2(t)$ when $t \in [t_k, \tilde{t}_k]$ is given by

$$x_2^J(t; u_k) := \frac{\lambda}{\lambda - \gamma}\left(e^{-\gamma(t-t_k)} - e^{-\lambda(t-t_k)}\right)(x_1(t_k) + u_k) + e^{-\gamma(t-t_k)}x_2(t_k). \tag{3.9}$$

By implementing the input u_k at time t_k, the trajectory $x_2^J(t; u_k)$ has to reach the upper bound $H(t)$ at time $\tilde{t}_k$ (i.e., $x_2(\tilde{t}_k) = H(\tilde{t}_k)$), and it should not cross it. The former implies that $x_2^J(\tilde{t}_k; u_k) = H(\tilde{t}_k)$, and the latter implies that $x_2^J(t; u_k)$ has to be tangent to $H(t)$ at $\tilde{t}_k$. So solving the system of equations

$$\begin{cases} x_2^J(t; u_k) - H(t) = 0, \\ \dfrac{d}{dt}\left(x_2^J(t; u_k) - H(t)\right) = 0, \end{cases} \qquad t > t_k, \tag{3.10}$$

with respect to t and u_k gives the time $\tilde{t}_k$ and the input u_k.

Remark 3.5. For both $\lambda > \gamma$ and $\lambda < \gamma$, $x_2^J(t; u_k)$ is always strictly increasing with respect to u_k. Therefore, the existence of at least one pair $(\tilde{t}_k, u_k)$ for (3.10) is ensured.

Remark 3.6. System of equations (3.10) may have more than one pair of solutions. We hypothesize that the controller $u(t)$ in the anterior pituitary minimizes the number of secretory events [34]. Moreover, we are interested in inputs u_k such that the trajectory $x_2(t)$ does not cross the upper bound $H(t)$ (see Remark 3.1). Therefore, in the case when (3.10) has multiple pairs of solutions, we select the pair $(\tilde{t}_k, u_k)$ among which $\tilde{t}_k$ is the greatest whose corresponding input u_k keeps the trajectory $x_2(t)$ within the bounds.

Once $(\tilde{t}_k, u_k)$ are computed by (3.10), one can obtain the dynamics on the

interval $[t_k, \tilde{t}_k]$ by the following equations:

$$\begin{bmatrix} x_1(t) \\ x_2(t) \end{bmatrix} = e^{A(t-t_k)} \begin{bmatrix} x_1(t_k) + u_k \\ x_2(t_k) \end{bmatrix}, \qquad t_k \leqslant t \leqslant \tilde{t}_k. \tag{3.11}$$

Now we are ready to present our algorithm to calculate the number N, timing t_k and the amplitude u_k $(k > 0)$ on the time interval $[t_0, t_f]$, where t_f is our desired final time.

Algorithm 1: Calculating the number, timing and amplitude of the secretory events.

Input : λ, γ, t_0, t_f, x_2^0, $D(t)$, $H(t)$
$x_1(t_0) := 0$
$x_2(t_0) := x_2^0$
$\tilde{t}_0 := t_0$
$k := 1$
$N := 0$
repeat
  Calculate t_k from (3.8)
  Calculate $x(t_k)$ from (3.5)
  Calculate $(\tilde{t}_k, u_k)$ from (3.10) in view of Remark 3.6
  Calculate $x(\tilde{t}_k)$ from (3.11)
  $N := k$
  $k := k + 1$
until $\tilde{t}_k < t_f$;
Output : N, t_k, u_k, $\tilde{t}_k$

Assume that we have run Algorithm 1 for N iterations to compute t_k, u_k and $\tilde{t}_k$ $(k = 1, 2, ..., N)$ on the time interval $[t_0, t_f]$. By having such information, we can obtain $x_1(t)$ and $x_2(t)$ on $[t_0, t_f]$ from the following equation

$$x(t) = e^{A(t-t_k)} \left(x(t_k) + Bu_k \right), \qquad t \in (t_k, t_{k+1}], \qquad k = 1, 2, ..., N. \tag{3.12}$$

3.3 Results

In this section, we present three examples to show the efficiency and accuracy of both the model and algorithm presented in Section 3.2. In the first and second examples, which correspond to healthy subjects, the obtained secretory times and the cortisol level are in agreement with physiologically plausible profiles in healthy human data. In the third example, although the number of pulses is not within a physiologically plausible range reported for healthy subjects [7, 156], the cortisol level is still within the desired bounds.

Example	λ (min^{-1})	γ (min^{-1})
1, 2	0.0585	0.0122
3	0.1248	0.0061

Table 3.1: Model Parameters for Examples 1-3 [34]

For our examples, we use the parameters λ and γ, given in Table 3.1, which respectively represent the infusion rate of cortisol into the circulation from the adrenal glands, and the clearance rate of cortisol by the liver. In addition, we use the lower and upper bounds given, respectively, in Tables 3.2 and 3.3.

Example	$D(t)$ $\left(\frac{\text{ug}}{\text{dl}}\right)$
1	$3.2478 - 0.7813\sin(\frac{2\pi t}{1440}) - 2.8144\cos(\frac{2\pi t}{1440})$ $-0.2927\sin(\frac{2\pi t}{720}) + 1.3063\cos(\frac{2\pi t}{720})$
2, 3	$5.5065 + 1.5544\sin(\frac{2\pi t}{1440}) - 4.3112\cos(\frac{2\pi t}{1440})$ $-1.6355\sin(\frac{2\pi t}{720}) - 0.9565\cos(\frac{2\pi t}{720})$

Table 3.2: Lower Bounds on the Cortisol Level for Examples 1-3 [34]

Example	$H(t)$ $\left(\frac{\text{ug}}{\text{dl}}\right)$
1	$5.3782 + 0.3939\sin(\frac{2\pi t}{1440}) - 3.5550\cos(\frac{2\pi t}{1440})$ $-0.5492\sin(\frac{2\pi t}{720}) + 1.0148\cos(\frac{2\pi t}{720})$
2, 3	$8.6051 + 3.0306\sin(\frac{2\pi t}{1440}) - 5.0931\cos(\frac{2\pi t}{1440})$ $-1.8151\sin(\frac{2\pi t}{720}) - 1.6570\cos(\frac{2\pi t}{720})$

Table 3.3: Upper Bounds on the Cortisol Level for Examples 1-3 [34]

3.3.1 Example 1

Using Algorithm 1 with the parameters given in Table 3.1, and the lower and upper bounds given respectively in Tables 3.2 and 3.3 for Example 1, we have calculated the timing and the amplitude of secretory events, and hence using (3.12) we have

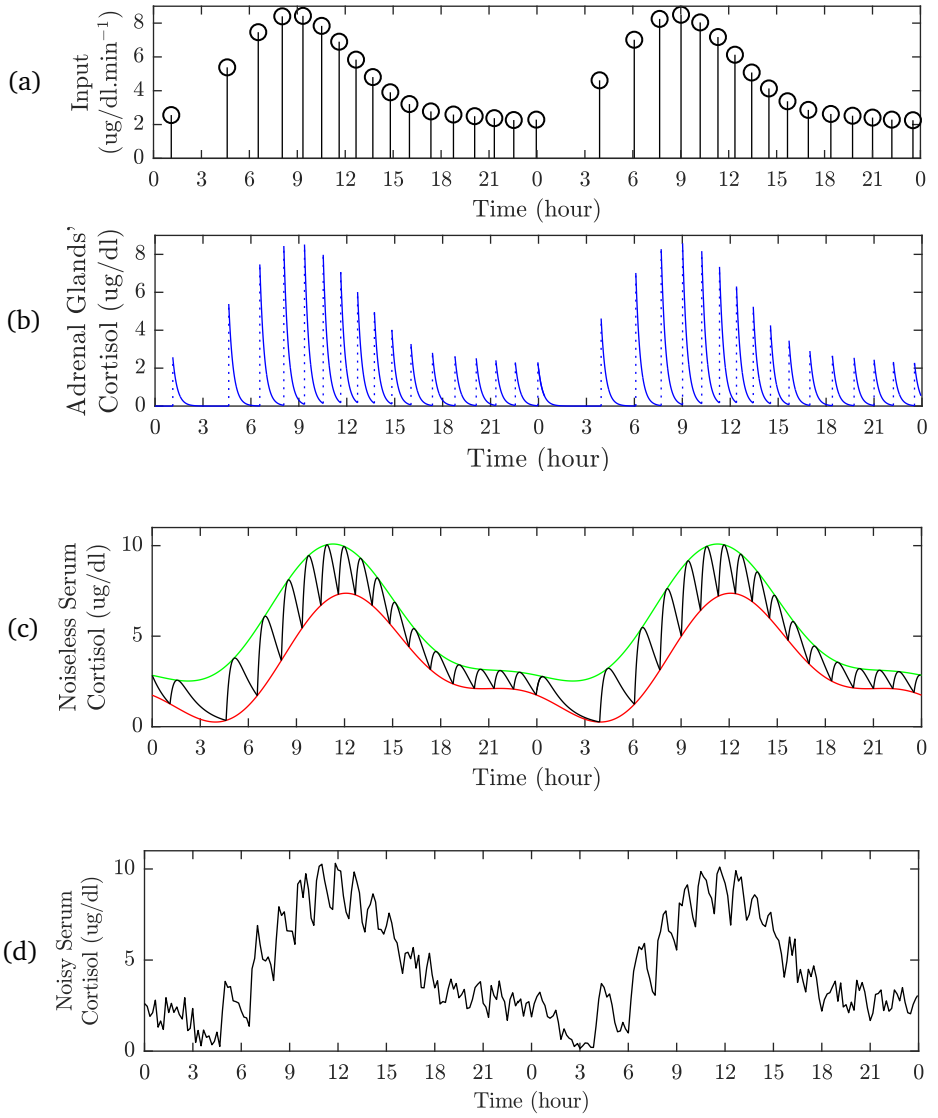

Figure 3.2: Obtained cortisol level and control inputs for Example 1. We have used the parameters, and the lower and upper bounds, respectively, given in Tables 3.1- 3.3 for Example 1. The initial conditions are $(x_1(0), x_2(0)) = (0, H(0))$, and all panels (a)-(d) are plotted over 48 h. Panel (a) displays 16 impulses over 24 h which control cortisol to remain within upper and lower bounds. In panel (b), solid curves display the state $x_1(t)$, while the dashed lines show the jumps in this state. Panel (c) shows the optimal cortisol profile (black curve), restricted by the lower bound (red curve) and the upper bound (green curve). Panel (d) illustrates the optimal cortisol profile obtained by recording the cortisol level every 10 min, and adding a zero Gaussian measurement error with a standard deviation of $\sigma = 0.45$ to each simulated data point.

plotted the intermittent input/control in panel (a), $x_1(t)$ in panel (b), $x_2(t)$ in panel (c), and the noisy observed $x_2(t)$ in panel (d) of Fig. 3.2. In this example, the initial conditions are $(x_1(0), x_2(0)) = (0, H(0))$, i.e., $x_2(t)$ starts from the upper bound $H(t)$. This figure shows that the state $x_2(t)$ and the calculated control inputs are optimal in the sense that $x_2(t)$ starts at the upper bound and decreases until it reaches the lower bound at which point the obtained input implements a jump into the system and hence $x_2(t)$ reaches exactly the upper bound, and this process is repeated until $x_2(t)$ reaches our desired final time.

As illustrated in panel (a), there are 16 pulses over the 24-hour period which is within the physiologically plausible range of 15-22 pulses [7, 156]. Furthermore, our observation from panel (a) is that the amplitudes are lower and less frequent during the night than the day. Panel (b) clearly shows pulsatility of the state x_1 along with its jumps.

It is widely known that in healthy humans, the cortisol level has regular periodic time-varying patterns which consists of pulsatile release of secretory events with different timings and amplitudes in a regular circadian rhythm. As is observed in panel (c), the cortisol level is pretty low during the night, while it increases around 5 AM and reaches its higher amplitude around 12 PM. Afterwards, it decreases slowly until the midnight. This example indicates that the mathematical model (3.1)-(3.3) can describe the pulsatile cortisol secretion that have physiologically plausible profiles similar to those observed in healthy human data.

Similar to measurement noise and sampling interval of cortisol data in human subjects [32], we have recorded the cortisol level every 10 minutes, added a zero mean Gaussian measurement error with a standard deviation of $\sigma = 0.45$ to each simulated data point, and hence plotted panel (d) in Fig. 3.2 which resembles cortisol human data presented in [32].

3.3.2 Example 2

In this example, we use the same parameters λ and γ as those in Example 1, while the lower and upper bounds are different, see Tables 3.1-3.3. Using (3.12) and Algorithm 1 with the initial conditions $(x_1(0), x_2(0)) = (0, 1)$, in Fig. 3.3 we have plotted the intermittent input/control, $x_1(t)$, $x_2(t)$, and the noisy observed $x_2(t)$ in panels (a), (b), (c), and (d), respectively. This figure demonstrates that the obtained cortisol level and the inputs are again optimal during the whole 48 h. In this example, the initial condition $x_2(0) = 1$ shows that Algorithm 1 can produce optimal solutions even if the state $x_2(t)$ is not initiated from the upper bound $H(t)$.

Panel (a) illustrates that 16 pulses are fired over 24 h, which is within the physiologically range of 15 - 22 pulses [7, 156]. The impulses are low at night, while they are higher and more frequent between 4 AM to 12 PM. Panel (b) displays pulsatility of the state x_1 along with its jumps.

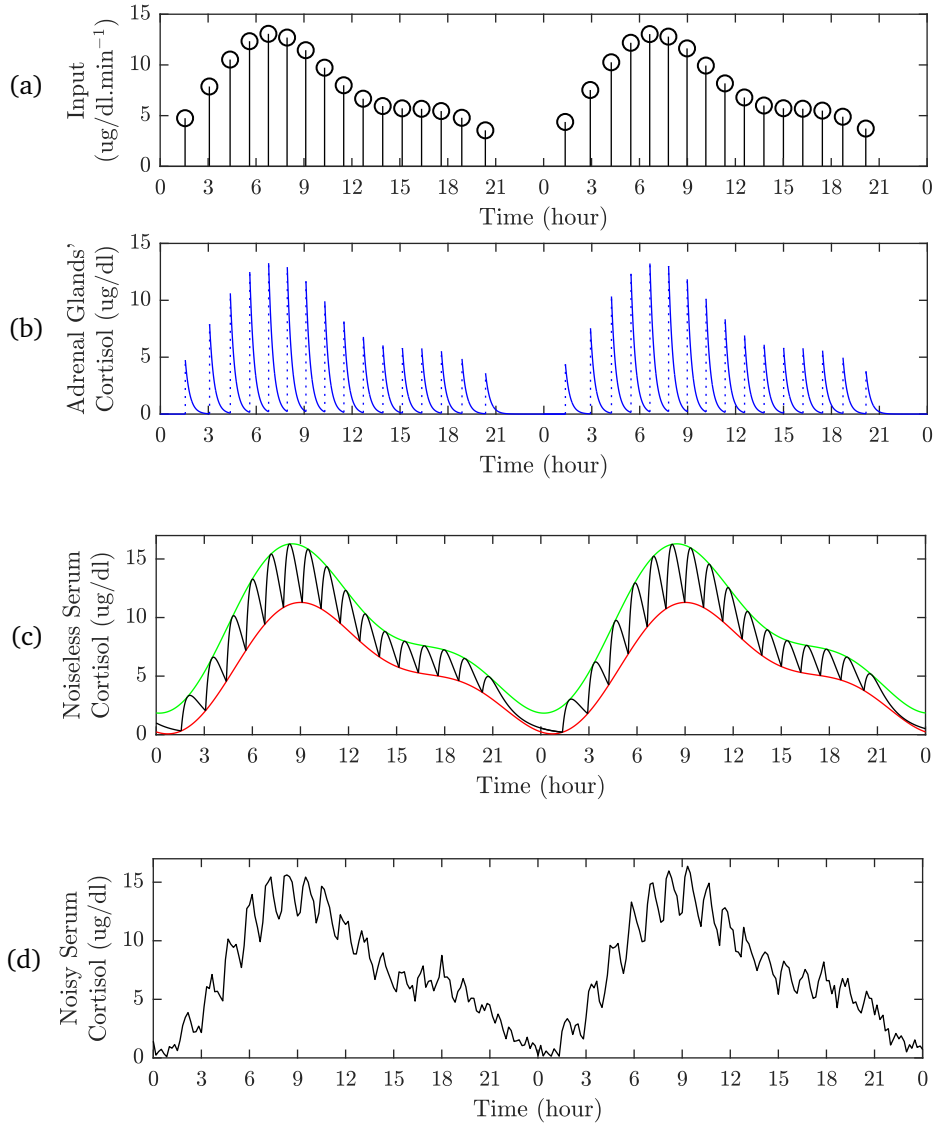

Figure 3.3: **Obtained cortisol level and control inputs for Example 2.** We have used the parameters, and the lower and upper bounds, respectively, given in Tables 3.1- 3.3 for Example 2. The initial conditions are $(x_1(0), x_2(0)) = (0, 1)$, and all panels (a)-(d) are plotted over 48 h. Panel (a) displays 16 impulses over 24 h which control cortisol to remain within upper and lower bounds. In panel (b), solid curves display the state $x_1(t)$, while the dashed lines show the jumps in this state. Panel (c) shows the optimal cortisol profile (black curve), restricted by the lower bound (red curve) and the upper bound (green curve). Panel (d) illustrates the optimal cortisol profile obtained by recording the cortisol level every 10 min, and adding a zero Gaussian measurement error with a standard deviation of $\sigma = 0.45$ to each simulated data point.

The cortisol level increases from midnight to 9 AM, while it decays gradually from 9 AM to midnight such that it reaches its lowest level at midnight. This example again shows that both the model and approach presented in Section 3.2 can describe the pulsatile cortisol secretion that have physiologically plausible profiles similar to those observed in healthy human data.

Similar to measurement noise and sampling interval of cortisol data in human subjects [32], we have recorded the cortisol level ever 10 minutes, added a zero mean Gaussian measurement error with a standard deviation of $\sigma = 0.45$ to each simulated data point, and then plotted panel (d) which resembles cortisol human data presented in [32].

3.3.3 Example 3

In this example, we use the same upper and lower bounds as those in Example 2, while using different parameters γ and λ which, respectively, result in higher infusion rate of cortisol, and lower clearance rate of cortisol, see Tables 3.1-3.3. Using Algorithm 1 and equation (3.12) with the initial conditions $(x_1(0), x_2(0)) = (0, 1.5)$ we have plotted panels (a), (b), (c), and (d) in Fig. 3.4 for 48 h.

Panel (a) shows that 12 pulses are fired over 24 h. Panel (b) illustrates pulsatility of $x_1(t)$ along with its jumps. Panel (c) shows that the cortisol level is low at midnight. Then it increases gradually until it reaches its higher value around 9 AM. Afterwards, it decreases slowly such that it obtains its lowest value at midnight. Observations from panel (c) demonstrate that the cortisol level and the inputs are optimal over 48 h. Comparing panels (c) of Fig. 3.3 and Fig. 3.4, one concludes that the impulses in panel (c) of Fig. 3.3 have higher amplitudes and are more frequent than the corresponding ones in panel (c) of Fig. 3.4.

Although in this example the cortisol level and the obtained impulses are optimal, the number of pulses are not within the physiologically range of 15-22 pulses, reported for healthy subjects [7, 156]; this may indicate a case of cortisol deficiency. Compared to Example 2, the peak values of the cortisol levels have been changed in Example 3, and on average have lower values, which could indicate a case of cortisol deficiency. We have recorded the cortisol level ever 10 minutes, added a zero mean Gaussian measurement error with a standard deviation of $\sigma = 0.45$ to each simulated data point, and hence plotted panel (d) which resembles cortisol human data presented in [32]. Panel (d) of Fig. 3.4 shows that the number of pulses has decreased compared to the corresponding one in Fig. 3.3, which was expected as cortisol has a lower clearance rate in Example 3.

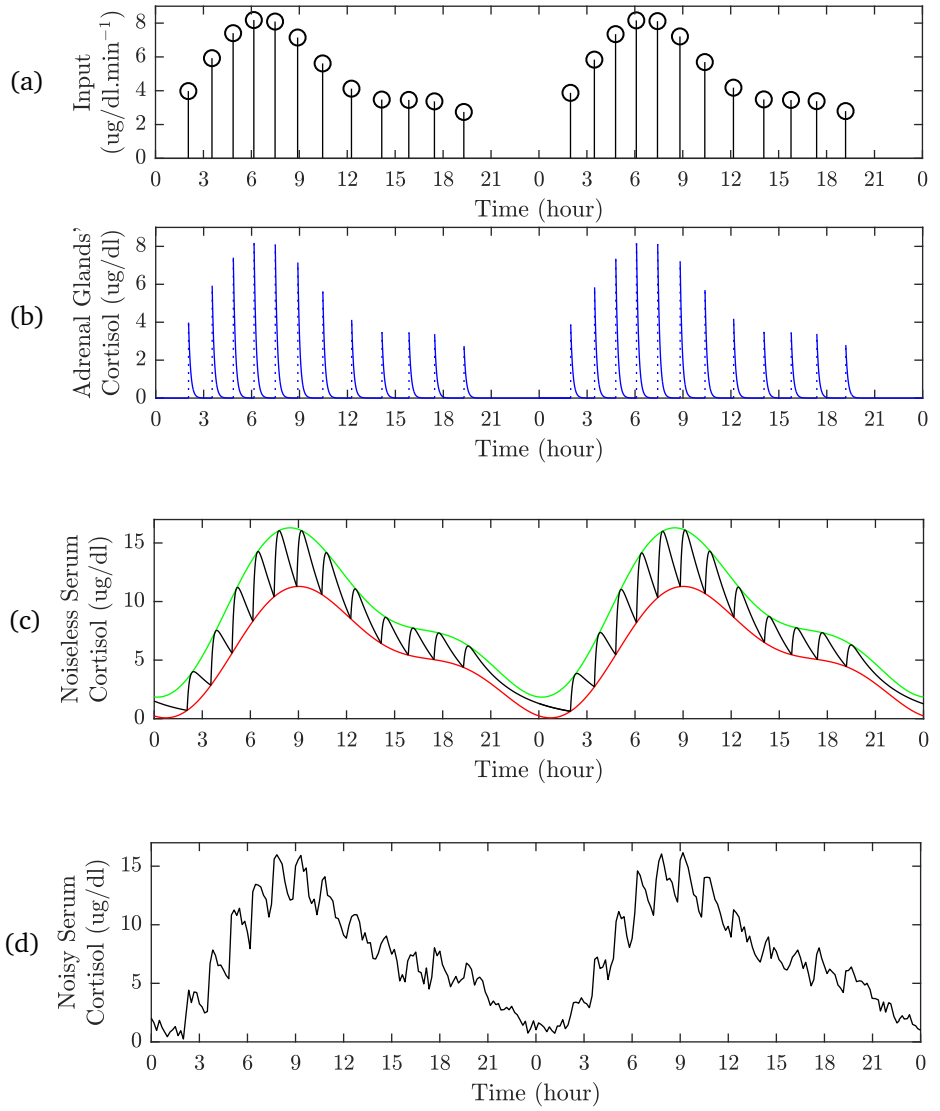

Figure 3.4: Obtained cortisol level and control inputs for Example 3. We have used the parameters, and the lower and upper bounds, respectively, given in Tables 3.1- 3.3 for Example 3. The initial conditions are $(x_1(0), x_2(0)) = (0, 1.5)$, and all panels (a)-(d) are plotted over 48 h. Panel (a) displays 12 impulses over 24 h which control cortisol to remain within upper and lower bounds. In panel (b), solid curves display the state $x_1(t)$, while the dashed lines show the jumps in this state. Panel (c) shows the optimal cortisol profile (black curve), restricted by the lower bound (red curve) and the upper bound (green curve). Panel (d) illustrates the optimal cortisol profile obtained by recording the cortisol level every 10 min, and adding a zero Gaussian measurement error with a standard deviation of $\sigma = 0.45$ to each simulated data point.

3.4 Discussion

Many dynamical processes, such as pharmacokinetics systems, optimal control problems in economics, biological phenomena involving thresholds, and bursting rhythm models in medicine and biology, are characterized by the fact that they experience a rapid change in their states at certain moments of time. In such processes, there exist short-term perturbations whose duration with respect to the duration of the entire evolution is negligible [96]. Therefore, one can mathematically formulate such perturbations in the form of impulses.

It is widely known that several hormones such as cortisol, insulin, growth, and testosterone are released in pulses. Moreover, changes in the pulsatility of such hormones are related to, e.g., obesity, aging, and metabolic and psychiatric diseases [116, 154, 171, 172]. Therefore, understanding the pulsatile secretion mechanisms and the modeling underlying such systems are of great interest.

Motivated by the applications of analyzing pulsatile release of hormones, our goal in this work has been to study the impulsive control mechanisms underlying the HPA axis. In this regard, we have proposed a minimal model which describes the pituitary-adrenal system whose interactions are as follows: cortisol is released in pulses in response to the pulses of ACTH, while in return, exerts a negative feedback on the release of ACTH. More precisely, we model the pituitary-adrenal system based on the first-order kinetics for cortisol infusion and clearance, and explicitly assume that the system is impulsive, due to the pulses in ACTH. We have assumed that the circadian rhythms on the cortisol level are two-harmonic time-varying functions with periods of 12 and 24 h, which are the most important periods in the cortisol release. Although various deterministic and stochastic models have been postulated to describe the pituitary-adrenal system [7, 32, 34, 97], in this work we have presented an *analytical approach* for calculating the number, timing, and amplitude of the secretory events in presence of circadian demand and holding cost constraints.

Illustrated by various examples, we have shown that the proposed model and approach yield the optimal solution in the sense that the cortisol level, started at the upper bound, decreases until it reaches the lower bound at which point the obtained inputs exert jumps into the system and as a result, the cortisol level arrives exactly at the upper bound again; this process is repeated for the desired time. Furthermore, the achieved number, timing, and amplitude of the recovered secretory events are physiologically plausible, and the obtained cortisol levels are in agreement with the circadian rhythm which has been observed in healthy human data, i.e., there are 15-22 pulses with varying amplitudes in a regular circadian rhythm; the cortisol profile gets its lowest amplitude between 8 PM and 2 AM, while increases throughout the late night, reaches its maximum between 8 AM and 10 AM, and afterwards declines throughout the course of the day into the

evening [7]. We emphasize that for all the three examples presented in Section 3.3, our approach gives the optimal solution, even for Example 3 in which the number of pulses is not within a physiologically plausible range of 15-22 pulses, reported for healthy subjects [7, 156].

In order to validate the model by experiments, one can first calculate the infusion and clearance rates from a rat model, and also obtain the upper and lower bounds on cortisol levels from a healthy rat. Second, by making the adrenal glands of the rat malfunctional, the rat can become Addisonian such that it cannot secret cortisol anymore. Lastly, by designing an intermittent controller using the algorithm provided in this study, one can obtain a time-varying cortisol level which remains within the upper and lower bounds that had been found when the rat was healthy [34].

Now, we compare our model and results with those in [34]: (i) The main difference between the model presented in this chapter and the one in [34] is that in the latter, the model is continuous, i.e., without explicitly assuming the system is impulsive, the goal was to obtain impulse control. However, in the former, based on the physiology underlying the HPA axis, we have explicitly assumed that the nature of the system is impulsive, and the goal has been to design a controller for calculating the number, timing, and amplitude of the secretory events. (ii) The optimization formulation in [34] is mainly an ℓ_0-norm problem; however, since such problems are NP-hard, an alternative approach (considering ℓ_1-norm as a relaxation of the ℓ_0-norm) was used to solve the problem. Next, using the iterative algorithm proposed in [8], the ℓ_1-norm optimization problem was solved to find the optimal solution. The iterative algorithm in [8, 34] does not always find the optimal solution and can lead to finding suboptimal solutions. In this study, we have presented an analytical approach to find the secretory events, by which the solution is always optimal. For instance, in Example 2, cortisol level, obtained by our algorithm, gives optimal solutions over 24 h, while the corresponding one presented in [34] gives optimal solutions for the first 20 h and suboptimal solutions for the last 4 h. Moreover, comparing Example 3 with the corresponding one in [34], one observes that the obtained cortisol level and inputs are optimal over the whole 24 h, while the corresponding one in [34] gives optimal cortisol level over the first 19 h, while suboptimal for the last 5 h.

Although we have presented a simple impulsive model to describe the pulsatile cortisol release in the pituitary-adrenal system, there are some other scenarios under which the system can obtain the impulse control. We have assumed that the infusion and clearance rates are constant. However, these parameters can change after every jump, and hence the problem can be formulated as a switched system, i.e., matrix A in (3.4) is not fixed anymore and might vary after every jumps. Instantaneous changes in one or both of the infusion and clearance rates may lead to impulse control [34]. First, assume that the clearance rate is fixed, while the

infusion rate of cortisol starts from a constant level at wake, and decreases suddenly to a new constant level. In order to compensate such a degradation, a large level of cortisol should be produced in a short time such that the desired cortisol level can be obtained [34]. Second, let us consider the case when the infusion rate is fixed, while the clearance rate of cortisol starts from a constant level at wake, and increases instantaneously to another constant level; then, in a short time, a large level of cortisol should be produced such that the desired cortisol level can be achieved [34]. Lastly, assume that both the clearance and infusion rates start from a constant level and change abruptly to different levels periodically. As a result, the overall effect on cortisol is that it gets infused to the blood more slowly, or gets cleared from the blood faster [34]. In such a case, as long as there is no upper bound on control variable, the impulse control can be obtained. For an example with a time-varying rate which obtains the impulse control, the interested reader is refereed to [125], where the "maximum principle" is used to find the optimal solution. Another possibility for obtaining the impulse control for neurohormone systems is to explicitly assume that the system is impulsive, and the timing and amplitude of the secretory events are functions of the states; such a mathematical model for testosterone regulation is presented in [15].

In this work, as a prototype, we have focused on the HPA axis, and proposed a physiological plausible model for cortisol secretion in the pituitary-adrenal system. However, as the control mechanism of the pulsatile feedback in cortisol is similar to the other neuroendocrine hormones such as gonadal hormone, growth hormone, insulin hormone and thyroid hormone [82, 105], a similar approach can be used to study the pulsatile release of such hormones. As pulsatile secretion is considerably different form basal (continuous) secretion, and some hormonal disorders are associated with hormone pulsatility, one can obtain insight into some hormonal disorders and pathological neuroendocrine states through mathematical models. For instance, one of the disorders which is caused by the adrenal deficiency is Addison's disease. A patient suffering from this disease takes cortisone one or twice a day in order to control their cortisol deficiency which does not seem optimal, because there are 15-22 secretory events in a healthy subject over 24 h. Using the methods presented in this study, it is possible to personalize the medications and use an impulsive controller to control the the cortisol levels optimally.

3.5 Concluding remarks

This chapter has developed a second-oder impulsive differential equation model to describe the pulsatile release of cortisol secretion in presence of circadian demand and holding cost constraints on the blood cortisol level. By proposing an analytical approach, the number, timing, and amplitude of the impulsive control

are calculated. This type of bio-inspired intermittent controllers has the great potential to be employed for designing non-continuous controllers in treating different disorders using biofeedback and brain-machine interface design.

The model presented in this chapter describes a subsystem of the HPA axis, i.e., the pituitary-adrenal system. A third-order ordinary differential equation model that generally describes the oscillatory behavior of the HP axes is studied in the next chapter.

4

Endocrine regulation as a non-cyclic feedback system

To understand the sophisticated control mechanisms of the human's endocrine system is a challenging task that is a crucial step towards precise medical treatment of many dysfunctions and diseases. Although mathematical models describing the endocrine system as a whole are still elusive, recently some substantial progress has been made in analyzing theoretically its subsystems (or *axes*) that regulate the production of specific hormones. Secretion of many vital hormones, responsible for growth, reproduction and metabolism, is orchestrated by feedback mechanisms that are similar in structure to the model of simple genetic oscillators, proposed first by B.C. Goodwin [52]. Unlike the celebrated Goodwin's model, the endocrine regulation mechanisms are in fact known to have *non-cyclic* structures and involve multiple feedbacks; a Goodwin-type model thus represents only a part of such a complicated mechanism.

This chapter studies a non-cyclic feedback system of hormonal regulation, obtained from the classical Goodwin's oscillator by introducing an additional negative feedback. It starts with an introduction, followed by Section 7.2 that introduces the model in question, whose local stability properties are examined in Section 4.3. Section 4.4 presents the main results, which are concerned with global properties of the system. Section 4.5 illustrates the model in question by numerical simulations. Proofs of the results and concluding remarks are given in Sections 4.6 and 4.7, respectively.

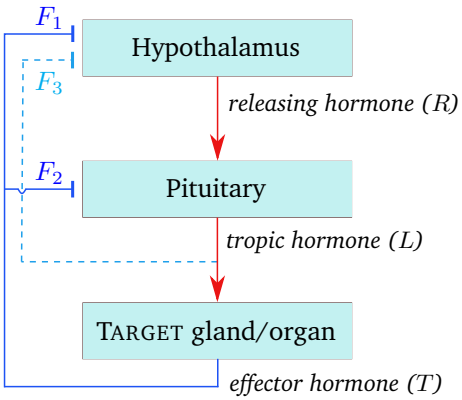

Figure 4.1: Structure of a hypothalamic-pituitary axis [133]; feedforward and feedback control mechanisms are illustrated respectively by ↓ and ⊣.

4

4.1 Introduction

HORMONES are signaling molecules that are secreted by glands and involved in many vital bodily functions. Sophisticated mechanisms of interactions between glands and hormones couple them into the *endocrine system*, whose mathematical modeling remains a challenging problem. At the same time, visible progress has been made in modeling some of its subsystems (*axes*), which are responsible for the secretion of specific hormones. Many processes in the body, including growth, metabolism, reproduction and stress resistance, are controlled by the hypothalamic-pituitary (HP) neurohormonal axes. In the seminal work [133] the feedback and feedforward *control* mechanisms, lying in the heart of the HP axes functioning, have been revealed; the first mathematical models had been proposed even earlier, see e.g. [17, 122] and references therein. Regulatory centers in the hypothalamus release special neurohormones, called *releasing hormones* or *releasing factors* [133]. Each of these hormones stimulates the secretion of the corresponding *tropic* hormone by the pituitary gland, which, in turn, stimulates some "target" gland/organ to release the *effector* hormone (Fig. 4.1). Besides its direct signaling functions, the effector hormone inhibits the production of the corresponding releasing and tropic hormones. These negative feedback loops maintain the concentrations of all three hormones within certain limits.

Understanding of endocrine regulation mechanisms may add insight into the possibilities of efficient diagnosing and treatment of endocrine dysfunctions and diseases caused by them, such as reproductive failures and prostate cancer [29], obesity and aging [154], disorders of the central nervous system [4], and effects on the cardiovascular system [120]. All these motivate the development of mathe-

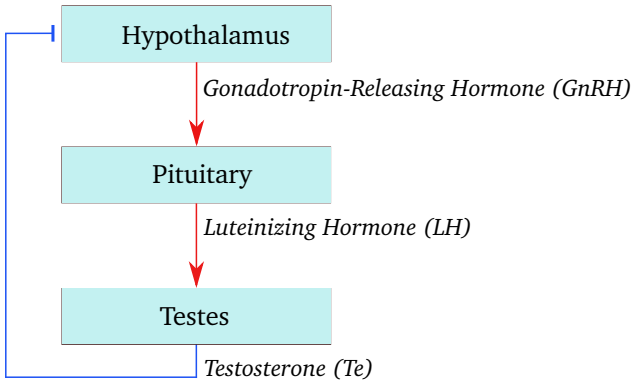

Figure 4.2: The cyclic structure of testosterone regulation [15, 128]; feedforward and feedback control mechanisms are illustrated by ↓ and ⊣, respectively.

matical models, portraying the complex behavior of endocrine axes.

As many other biochemical systems, the states of the endocrine systems do not convergence to stable equilibria: the blood levels of hormones oscillate, exhibiting both circadian (24-hour) and ultradian (short-period) oscillations [81, 161]. This oscillatory behavior resembles the dynamics of the celebrated *Goodwin's* model with three variables [52], considered as a "prototypical biological oscillator" [51]. Originally proposed for a genetic intracellular oscillator [52], Goodwin-like models have been extensively used to describe the dynamics of HP axes, in particular, the regulation of thyroid [17] and testosterone [128] hormones. For Goodwin's oscillator and more general *cyclic* feedback systems, profound mathematical results have been established, ensuring the existence of periodic orbits [64, 67] in the case where the (only) system's equilibrium is unstable. For the classical model from [52] such an instability appears to be a restrictive condition; for example, the feedback is described by the conventional Hill function [51] with the corresponding Hill constant being required to be greater than 8 [128, 150]. This restriction can be substantially relaxed (yet not completely discarded [26]), taking into account the delays in hormone transporting [18, 129]. Other factors leading to oscillations are *pulsatile* secretion of neurohormones [15, 16, 80] and stochastic noises [80, 81].

Although relatively well studied, Goodwin-type models are restrictive in assuming the presence of only one negative feedback loop from the effector hormone to the hypothalamus (F_1 in Fig. 4.1). This is illustrated by the models of testosterone regulation in males, examined in [15, 18, 128, 129] and illustrated in Fig. 4.2. At the same time, the complete mechanism of an HP axis involves multiple feedback loops [133]; the effector hormones inhibit the secretion of *both* releasing and tropic hormones, closing thus the *long* negative feedback loops (see F_1, F_2 in Fig. 4.1). Besides them, the *short* feedback loop (F_3) may also exist, whose effect,

however, is ignored by most of the existing mathematical models of endocrine regulation [3, 4, 55, 80, 99, 131, 161]. Being much weaker than the long feedbacks and "most vulnerable" [133] among the three types of feedback mechanisms, the short feedback loops still lack experimental studies that can validate their ubiquity and reveal their role in endocrine regulation [133].

Mathematical models, taking the existence of multiple feedback loops into account, have been recently proposed for the testosterone regulation in males [55, 99, 146] and cortisol regulation [4, 131, 161]. Similar models with multiple feedback loops have been reported to describe the dynamics of some metabolic pathways [43, 126]. Unlike the classical Goodwin's oscillators, these models do not have the cyclic structure, which makes the relevant results, ensuring the existence or absence of periodic solutions [27, 64, 67, 68, 150], inapplicable; the mathematical analysis is limited to examination of local stability of equilibrium points and the bifurcation analysis via Andronov-Hopf techniques, ensuring the existence of periodic orbits only for *some* values of the system's parameters.

In this chapter, we examine a model of hormonal regulation with two negative feedbacks, which has been originally proposed in [4] to describe the mechanism of cortisol regulation in the hypothalamus-pituitary-adrenal (HPA) axis; our simulations (Section 4.5) shows that it can also be applied to testosterone regulation modeling. The model is similar in structure to the classical Goodwin's oscillator, but involves two nonlinearities, standing for respectively the negative feedbacks from the effector hormone to the releasing and tropic hormones (F_1, F_2 in Fig. 4.1). Unlike the original model in [4], we do not restrict these nonlinearities to be identical or Hill functions. To keep the analysis concise, in this work we neglect the transport delays, discontinuities, describing the pulsatile secretion of neurohormones, and the effects of stochastic noises. For the model in question, we develop the "global" theory, showing that its properties, in spite of the non-cyclic structure, are similar to those of the Goodwin's oscillator. In particular, under some assumptions, the *local* instability of the equilibrium implies the existence of periodic orbits, and furthermore, the convergence of *almost all* solutions to such an orbit. The latter statement, observed in simulations, have not been proved even for the classical Goodwin's model.

4.2 Goodwin's model and its extension

We start with the conventional Goodwin's model [52], describing a self-regulating system of three chemicals, whose concentrations are denoted by R, L, and T, and

evolve in accordance with the following equations

$$\begin{aligned} \dot{R} &= -b_1 R + f(T), \\ \dot{L} &= g_1 R - b_2 L, \\ \dot{T} &= g_2 L - b_3 T. \end{aligned} \tag{4.1}$$

The model (4.1) was originally used by B.C. Goodwin for modeling oscillations in a single self-repressing gene [52]. Our notation follows [128], where Goodwin's oscillator was proposed for modeling of the gonadal axis in male (Fig. 4.2) and R, L, and T stood, respectively, for the blood levels of the gonadotropin-releasing hormone (GnRH), luteinizing hormone (LH), and testosterone (Te).

The constants $b_i > 0$ (where $i = 1, 2, 3$) stand for the clearing rates of the corresponding chemicals, whereas the constants $g_1, g_2 > 0$ and the *decreasing* function $f : [0; \infty) \to (0; \infty)$ determine their production rates. Often $f(T)$ stands for the nonlinear *Hill function* [51]

$$f(T) = \frac{K}{1 + \beta T^n}, \tag{4.2}$$

where $K, \beta, n > 0$ are constants. The releasing factor (R) drives the production of the tropic hormone (L), which in turn stimulates the secretion of the effector hormone (T); the positive constants g_1, g_2 stand for the corresponding *feedforward* control gains. The effector hormone *inhibits* the production of the releasing factor: as f is a decreasing function, an increase in T reduces the production rate $\dot{R}$, and vice versa. The nonlinearity $f(T)$ characterizes thus the negative *feedback loop*.

In this chapter, we consider a generalization of Goodwin's oscillator (4.1), including *two* negative feedbacks

$$\begin{aligned} \dot{R} &= -b_1 R + f_1(T), \\ \dot{L} &= g_1 R - b_2 L + f_2(T), \\ \dot{T} &= g_2 L - b_3 T. \end{aligned} \tag{4.3}$$

A special case of (4.3), where f_1, f_2 stand for the Hill nonlinearities with the same Hill constants n, yet different gains K_1, K_2, has been proposed in [4] to describe the dynamics of the HPA axis: R, L, T stand, respectively, for the levels of corticotropin-releasing hormone (CRH), adrenocorticotropic hormone (ACTH) and cortisol. The nonlinearities f_1, f_2 describe, respectively, the negative feedbacks F_1, F_2 in Fig. 4.1; the effect of short negative feedback (F_3) is neglected. Unlike [4], in this work we do not consider the effects of transport delays; at the same time, we substantially relax the assumptions imposed in [4] on f_1 and f_2. These nonlinear maps are *not necessarily* identical or Hill functions. As discussed in the work [161],

dealing with a similar model of cortisol regulation, the natural assumptions on these functions are their non-negativity (which prevents the solutions from leaving the domain where $R, L, T \geq 0$). Moreover, it is natural to assume that $f_1(T) > 0$ since "the feedbacks must not shut down hormone production completely" [161]. Similar to Goodwin's model, two feedbacks are inhibitory, which implies that f_1 and f_2 are non-increasing. We thus adopt the following assumption.

Assumption 4.1. The functions $f_1 : [0; \infty) \to (0; \infty)$ and $f_2 : [0; \infty) \to [0; \infty)$ are continuously differentiable and non-increasing, i.e. $f_1'(T), f_2'(T) \leq 0$ for any $T \geq 0$. The parameters $b_1, b_2, b_3, g_1, g_2 > 0$ are constant.

Notice that we allow that $f_2(T) \equiv 0$; all of the results, obtained below, are thus applicable to the classical Goodwin's oscillator (4.1). However, we are mainly interested in the case where $f_2 \not\equiv 0$, which leads to the *non-cyclic* structure of the system and makes it impossible to use mathematical tools developed for cyclic systems, such as criteria for global stability and the existence of periodic solutions existence [64, 67, 68, 150]. Unlike the existing works on multi-feedback models of hormonal regulation [4, 55, 99, 131, 146, 161], our examination of the model (4.3) is not limited to establishing only local stability criteria and bifurcation analysis. In this chapter, we are interested in the *interplay* between local and global properties, revealed for the classical Goodwin's oscillator, namely, the existence of oscillatory solutions, provided that the (only) equilibrium of the system is unstable.

4.3 Equilibria and local stability properties

As R, L, and T stand for the chemical concentrations, one is interested in the solutions, starting in the positive octant $R(0), L(0), T(0) \geq 0$; this requires, due to Assumption 4.1, that $R(t), L(t), T(t) > 0$ for any $t > 0$. Since $f_i(T) \leq f_i(0)$, for all $T > 0$, every solution is bounded. In particular, all the solutions are prolongable up to ∞. Similar to (4.1), the extended model has a unique equilibrium in the positive octant, found as follows.

Lemma 4.2. *System* (4.3) *has the unique equilibrium point* $E^0 := (R^0, L^0, T^0)$ *in the positive octant. Here* T^0 *is the only positive solution to the nonlinear equation*

$$\frac{b_1 b_2 b_3}{g_1 g_2} T^0 - \left(f_1(T^0) + \frac{b_1}{g_1} f_2(T^0) \right) = 0, \tag{4.4}$$

and the remaining coordinates are as follows

$$R^0 = \frac{1}{b_1} f_1(T^0), \qquad L_0 = \left(\frac{b_3}{g_2} \right) T^0. \tag{4.5}$$

Lemma 4.2 will be proven in Section 4.6. The local stability condition of the equilibrium E^0 is immediate from the Routh-Hurwitz criterion. Linearizing the system (4.3) at E^0, one obtains the system

$$\begin{aligned} \dot{z}_1 &= -b_1 z_1 + f_1'(T^0) z_3, \\ \dot{z}_2 &= g_1 z_1 - b_2 z_2 + f_2'(T^0) z_3, \\ \dot{z}_3 &= g_2 z_2 - b_3 z_3, \end{aligned} \tag{4.6}$$

which, in the matrix form, is rewritten as $\dot{z} = Az$ where

$$z = \begin{bmatrix} z_1 \\ z_2 \\ z_3 \end{bmatrix}, \qquad A = \begin{bmatrix} -b_1 & 0 & f_1'(T^0) \\ g_1 & -b_2 & f_2'(T^0) \\ 0 & g_2 & -b_3 \end{bmatrix}. \tag{4.7}$$

The steady state is stable when all the roots of the characteristic equation of matrix A have negative real parts, and is (strictly) unstable when at least one root has a positive real part. In the following lemma, which will be proven in Section 4.6, we present the local stability properties of the equilibrium E^0. In this regard, let us denote

$$\Theta_0 := a_3 - a_1 a_2 + g_2 \left[(b_2 + b_3) f_2'(T^0) - g_1 f_1'(T^0) \right], \tag{4.8}$$

where

$$a_1 := b_1 + b_2 + b_3, \qquad a_2 := b_1 b_2 + b_1 b_3 + b_2 b_3, \qquad a_3 := b_1 b_2 b_3. \tag{4.9}$$

Lemma 4.3. *In both cases of $\Theta_0 < 0$ and $\Theta_0 > 0$, the equilibrium E^0 is hyperbolic. If $\Theta_0 = 0$, then the two eigenvalues are complex-conjugated imaginary numbers.*

In general, biochemical systems may have locally stable equilibria, whose existence does not exclude the possibility of periodic rhythms. At the same time, for Goodwin's oscillator (4.1) the well-known "secant condition" [150], being necessary and sufficient for local stability of the equilibrium, is in fact very close to the sufficient conditions of *global* stability [2]. In spite of some gap between the conditions of local and global stability, for Goodwin's models the equilibrium's instability is considered as the requirement of the biological feasibility; it is known, for instance, that Goodwin's oscillators and more general cyclic systems with unstable equilibria have periodic orbits [64, 67]. After the publication of the seminal Goodwin's paper [52], it was noticed [57, 128, 150] that for the Hill nonlinearity (4.2) the equilibrium can be unstable (for some choice of the parameters b_i, g_i) if and only if $n > 8$. The following theorem extends the latter result to the generalized system (4.3) and arbitrary decreasing functions $f_1(T), f_2(T)$. We introduce an

auxiliary function

$$M(T) := -Tf_1'(T)/f_1(T) > 0, \qquad \forall T > 0. \tag{4.10}$$

Theorem 4.4. *Let the functions f_1, f_2 satisfy Assumption 4.1. Then the following statements hold:*

1. *if $M(T) < 8\,\forall T > 0$ then $\Theta_0 < 0$ for any choice of $b_i, g_i > 0$: the equilibrium of (4.3) is stable;*
2. *if $M(T) \le 8\,\forall T > 0$ then $\Theta_0 \le 0$ for any $b_i, g_i > 0$; the inequality is strict if $f_2(T) > 0$ for any $T > 0$;*
3. *if $M(T) > 8$ for some $T > 0$ then there exist parameters b_i, g_i such that the equilibrium is unstable ($\Theta_0 > 0$) and, furthermore, the system has at least one non-constant periodic solution.*

Theorem 4.4 will be proven in Section 4.6; for the usual Goodwin-Smith model (4.1), it has been established in [128]. The existence of periodic solutions in statement 3 of Theorem 4.4 is based on the Hopf bifurcation theorem [118]. However, the proof substantially differs from most of the existing results on the Hopf bifurcation analysis in *delayed* biological oscillators [55, 70, 136], proving the bifurcations at the "critical" delay values, under which the equilibrium loses its stability. To construct a one-parameter family of systems (4.3), satisfying the conditions of the Hopf bifurcation theorem, is not a trivial task (unlike the delayed case, where the delay is a natural parameter). One of such parameterizations has been proposed in [128] for the model (4.1); however, the complete and rigorous proof of the Hopf bifurcation existence has remained elusive.

Remark 4.5. While the necessary condition for instability is independent of the function $f_2(\cdot)$, the set of parameters b_i, g_i, for which the equilibrium is unstable, depends on it.

Remark 4.6. Theorem 4.4 does not imply that a periodic solution exists, *whenever* the equilibrium in unstable. The corresponding strong result holds for the Goodwin-Smith model (4.1) and more general cyclic systems [64, 67]; in Section 4.4 we extend this result to a broad class of systems (4.3), where the nonlinearity $f_2(T)$ satisfies a special slope restriction, whose relaxation remains a non-trivial open problem. At the same time, as discussed in Section 4.4, the equilibrium's instability implies oscillatory behavior of the system (4.3) in a weaker sense.

Remark 4.7. Although the conditions ensuring the equilibrium's global attractivity in the positive octant are close to the local stability [2], the existence of (non-constant) periodic solutions in the case where $M(T) \le 8$ seems to be an open problem even for the Goodwin's model (4.1). Furthermore, the Hopf bifurcation

analysis in Section 4.6 shows that in the case where $M(T) > 8$, there always exists a set of parameters b_i and g_i, for which a periodic orbit coexists with the locally *stable* equilibrium.

Applying Theorem 4.4 to the case where $f_1(T)$ is the Hill function (4.2), one has

$$M(T) = -\frac{Tf_1'(T)}{f_1(T)} = n\frac{\beta T^n}{1+\beta T^n}$$

and the condition $M(T) > 8$ reduces to the well-known condition $n > 8$. One arrives at the following.

Corollary 4.8. *Suppose that $f_1(T)$ is the Hill function* (4.2)*, and f_2 satisfies Assumption 4.1. Then the equilibrium of* (4.3) *is stable whenever $n \leq 8$. If $n > 8$, then for some choice of $b_i, g_i > 0$ the system has the unstable equilibrium, and at least one periodic solution.*

It should be noticed that although the Hill functions (4.2) with exponents $n > 4$ are often considered to be non-realistic, Goodwin's models with $n > 8$ adequately describe some metabolic reactions (see [51] and references therein). More important, Goodwin-type oscillators with large Hill exponents n naturally arise from *model reduction* procedures [51], approximating a long chain of chemical reactions by a lower-dimensional system.

4.4 Oscillatory properties of solutions

As one can notice, Theorem 4.4 does not establish any properties of system (4.3) with some specific parameters b_i, g_i. As discussed in Remark 4.6, it does not answer a natural question whether the equilibrium's instability $\Theta_0 > 0$ implies any oscillatory properties of the system. In the case of the classical Goodwin-Smith system (4.1) ($f_2 \equiv 0$), it is widely known that the local instability implies the existence of at least one periodic trajectory. A general result from [64] establishes this for a general *cyclic* system (with a sufficiently smooth right-hand side). The cyclic structure of the system and the equilibrium's instability imply the existence of an *invariant toroidal domain* [64], and closed orbits in it correspond to fixed points of the Poincaré map. This result, however, is not applicable to system (4.3). Another approach, used in [67, 68, 85] to examine oscillations in gene-protein regulatory circuits, employs elegant results by Mallet-Paret [101, 103], extending the Poincaré-Bendixson theory to Goodwin-type systems. As discussed in Subsect. 4.4.2, these results can be applied to system (4.3) only if some additional restriction holds.

At the same time, when $\Theta_0 > 0$, one is able to prove an oscillatory property of the solutions, which was introduced by V.A. Yakubovich [151, 170] and states that the solution is bounded, yet does not converge to an equilibrium. In the next subsection it is shown that, in fact, almost all solutions are oscillatory in this sense.

4.4.1 Yakubovich-oscillatory solutions

Following [117], we introduce the following definition.

Lemma 4.9. *A scalar bounded function $\varrho : [0;\infty) \to \mathbb{R}$ is called Yakubovich-oscillatory, or Y-*oscillation*, if $\liminf\limits_{t\to\infty} \varrho(t) < \limsup\limits_{t\to\infty} \varrho(t)$. A vector-valued function $x : [0;\infty) \to \mathbb{R}^m$ is called Y-oscillation if at least one of its elements $x_i(\cdot)$ is Y-oscillation.*

In other words, Y-oscillation is a bounded function, having no limit as $t \to \infty$. Our next result shows that system (4.3) with an unstable equilibrium has Y-oscillations; moreover, almost every solution is Y-oscillation.

Lemma 4.10. *Suppose that system* (4.3) *has an unstable equilibrium ($\Theta_0 > 0$). Then for any initial condition $(R(0), L(0), T(0))$, except for the points from some set of zero Lebesgue measure, the corresponding solution $(R(t), L(t), T(t))$ is Yakubovich-oscillatory as $t \to \infty$.*

Obviously, any periodic solution is Yakubovich-oscillatory, and the same holds for solutions converging to periodic orbits. In general, a dynamical system can have other Y-oscillations, e.g. showing "strange" (chaotic) behavior. It is known, however, that solutions of the conventional Goodwin-Smith model (4.1) and many other cyclic feedback systems [67, 68, 85] in fact exhibit a very regular behavior, similar to that of planar (two-dimensional) systems. The corresponding elegant result has been established in the papers by Mallet-Paret [101, 103]. A natural question, addressed in the next subsection, is the applicability of the Mallet-Paret's theory to the extended Goodwin-Smith model (4.3).

4.4.2 The structure of ω-limit set

The well-known Poincaré-Bendixson theory for planar autonomous (time-invariant) systems states that the ω-limit set of a bounded solution can be a closed orbit, an equilibrium point, or union of several equilibria and heteroclinic orbits, converging to them (it is possible that ω-limit set is a union of an equilibrium and homoclinic orbit, converging to it). Although this result is not applicable to the systems of order three or higher, it remains valid for *cyclic* systems [103], including the classical Goodwin's oscillator (4.1) and similar models [67, 68]. In the more recent papers [25, 101, 102] the Poincaré-Bendixson theory has been extended to tridiagonal systems (the result from [101] is applicable to even more general case of the delayed tridiagonal system). For the reader's convenience, we formulate the corresponding result below.

Consider the dynamical system of order $N+1$, where $N \geq 2$, described by the

equations

$$\begin{aligned}\dot{x}_0 &= h_0(x_0, x_1)\\ \dot{x}_i &= h_i(x_{i-1}, x_i, x_{i+1}), \qquad i = 1, \dots, N-1\\ \dot{x}_N &= h_N(x_{N-1}, x_N, x_0),\end{aligned} \tag{4.11}$$

Here the functions $h_0(\xi, \zeta)$ and $h_i(\eta, \xi, \zeta)$, $(i = 1, \dots, N)$, are C^1-smooth. It is assumed that all of them are *strictly* monotone in ζ; the functions $h_i(\eta, \xi, \zeta)$ for $i = 1, \dots, N$ are also non-strictly monotone in η. That is, the ith chemical (where $i = 1, \dots, N$) influences the production rate of the $(i-1)$th one, positively or negatively, and the 0th chemical influences the production of the Nth one. At the same time, chemical i (where $i = 0, \dots, N-1$) may influence the production of chemical $(i+1)$; however, such an influence is not necessary: it is allowed that $\frac{\partial h_{i+1}}{\partial x_i} \equiv 0$. The central assumption is that if the "adjacent" components influence each other, then the corresponding influences are *equally signed* (being either both stimulatory or inhibitory)

$$\frac{\partial h_{i+1}}{\partial x_i}\frac{\partial h_i}{\partial x_{i+1}} \geq 0, \qquad \forall i = 0, \dots, N-1. \tag{4.12}$$

Applying a simple change of variables, one may assume, without loss of generality [101, 102] that

$$\frac{\partial h_i(\eta, \xi, \zeta)}{\partial \eta} \geq 0, \qquad \delta_i \frac{\partial h_i(\eta, \xi, \zeta)}{\partial \zeta} > 0, \tag{4.13}$$

where

$$\delta_i = \begin{cases} 1, & i < N,\\ \pm 1, & i = N.\end{cases}$$

In this work, we are interested in tridiagonal systems (4.11) with a single equilibrium, for which the result of [101, Theorem 2.1] reduces[1] to the following simpler lemma.

Lemma 4.11. *[68] Let the C^1-smooth nonlinearities h_i in* (4.11) *satisfy the conditions* (4.12) *and the system has only one equilibrium. Then the ω-limit set of any* bounded *solution can have one of the following structural types: (a) closed orbit; (b) union of the equilibrium point and a homoclinic orbit; (c) the equilibrium point (singleton).*

Note that the "sign-symmetry" assumption (4.12) plays an essential role in Lemma 4.11. However, this assumption is violated in system (4.3): recall that the

[1] Formally, the paper [101] deals with delay systems, explicitly assuming that the delay is non-zero. The results are, however, valid for tridiagonal systems (4.11) without delays; as mentioned in [101, p. 442], the corresponding result (under some additional restrictions) has been established in [25].

effector hormone's (T) production is driven by the tropic hormone (L) and, at the same time, inhibits the secretion of L (Fig. 4.1). So Lemma 4.11 cannot be *directly* applied to system (4.3). To overcome this problem, we show that there exists a one-to-one mapping $(R, L, T) \to (x_0, x_1, x_2)$ which transforms system (4.3) into the "canonical" form (4.13) with $N = 3$ and $\delta_N = -1$. The corresponding extension is our main result.

Theorem 4.12. *Suppose that Assumption 4.1 holds and*

$$\sup_{T \geq 0} |f_2'(T)| \leqslant \frac{(b_3 - b_2)^2}{4g_2}. \tag{4.14}$$

Then any solution of (4.3) *has the ω-limit set of one of the three types, listed in Lemma 4.11. If the equilibrium is unstable, then almost any solution converges to either a periodic orbit or a homoclinic orbit.*

It should be noticed that (4.14) automatically holds for the classical Goodwin's oscillator (4.1) (and, more generally, when f_2 is constant). Furthermore, if the equilibrium is unstable, the system (4.1) has in fact no homoclinic orbits [67]. This leads to the following corollary.

Corollary 4.13. *If the system* (4.1) *has an unstable equilibrium, then it also has a (non-trivial) periodic orbit. Moreover, almost any solution converges to such an orbit.*

Whereas the first statement of Corollary 4.13 has been established for a very broad class of cyclic systems [64] and in fact does not rely on Mallet-Paret's theory, the second statement, confirmed numerical simulations, has not yet been proven mathematically. For the general system (4.3), the inequality (4.14) restricts the slope of the nonlinear function $f_2(\cdot)$. Our numerical simulations in Section 4.5 show that this condition is only sufficient, and the solutions' convergence to the periodic orbit may take place even if it is violated.

4.5 Numerical simulation

In this section, we give a numerical simulation, which allows to compare the behaviors of systems (4.1) and (4.3). The model parameters $b_1 = 0.1$ min^{-1}, $b_2 = 0.015$ min^{-1}, $b_3 = 0.023$ min^{-1}, $g_1 = 5$ min^{-1} and $g_2 = 0.01$ min^{-1} are chosen to comply with the existing experimental data reported in [11, 18], dealing with testosterone regulation (Fig 4.2).

The functions $f_1(T), f_2(T)$ were chosen of the Hill-type as follows:

$$f_1(T) = \frac{K_1}{1 + \beta_1 T^n}, \qquad f_2(T) = \frac{K_2}{1 + \beta_2 T^m}. \tag{4.15}$$

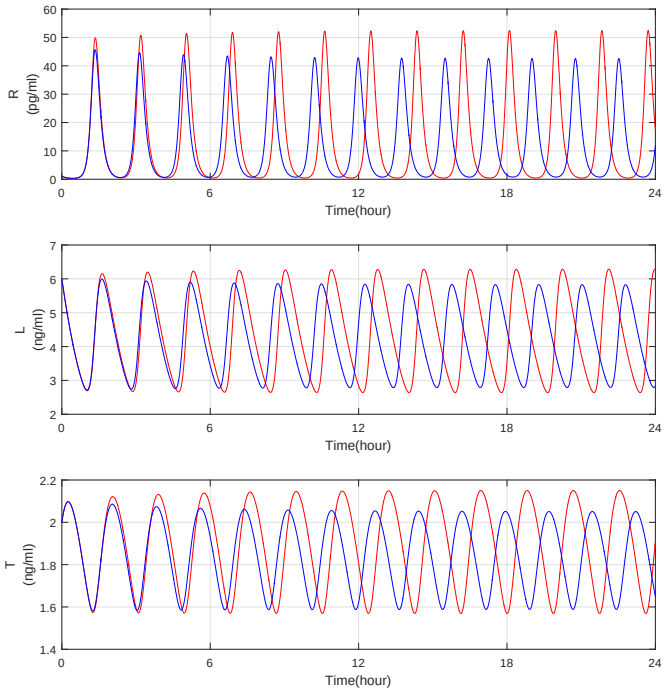

Figure 4.3: Red and blue plots show numerical simulations of systems (4.1) and (4.3), respectively, with the same initial conditions and parameter values.

As discussed in [51, 161], Hill's kinetics naturally arises in many biochemical and pharmacological systems. Following [18], the parameters of f_1 are considered to be $K_1 = \beta_1 = n = 20$. To show the effect of the additional feedback f_2 on the oscillations of hormones, its parameters are chosen to be $K_2 = m = 20$ and $\beta_2 = 10$. A straightforward calculation shows that the equilibria of systems (4.1) and (4.3) are respectively given by

$$E^{GS} = (0.0098,\ 3.2529,\ 1.4143), \qquad E^{New} = (0.0094,\ 3.2589,\ 1.4169),$$

Moreover, the quantity Θ_0, defined in (4.8), for systems (4.1) and (4.3) is given by

$$\Theta_0^{GS} = 1.5207 \times 10^{-4}, \qquad \Theta_0^{New} = 1.1590 \times 10^{-4},$$

confirming the instability of equilibria. Both systems (4.1) and (4.3) are plotted in Fig. 4.3 for a time period of 24 hours with the same parameters and initial conditions

$$R(0) = 1 \text{ pg/ml}, \qquad L(0) = 6 \text{ ng/ml}, \qquad T(0) = 2 \text{ ng/ml}.$$

Although nonlinearity f_2 considered in the example does not satisfy condition (4.14), system (4.3) still has oscillatory behavior for parameters b_i and g_i considered above.

As is seen in Fig. 4.3, after some time, both amplitude and period of the oscillations of R, L, and T in system (4.3) become less than the corresponding ones in system (4.1). The amplitudes of oscillation for systems (4.1) and (4.3), calculated numerically, are respectively given by

$$A^{GS} \approx (52.00 \text{ pg/ml},\ 3.64 \text{ ng/ml},\ 0.58 \text{ ng/ml}),$$
$$A^{New} \approx (41.75 \text{ pg/ml},\ 3.04 \text{ ng/ml},\ 0.46 \text{ ng/ml}).$$

Furthermore, the periods of oscillation for systems (4.1) and (4.3) are given by $P^{GS} \approx 1.870$ and $P^{New} \approx 1.755$. So the feedback $f_2(\cdot)$ influences both the amplitude and period of oscillations.

4

4.6 Proof of the results

We start with the proof of Lemma 4.2, which gives the existence and uniqueness of the equilibrium of system (4.3).

Proof of Lemma 4.2. By definition, the point $E^0 = (R^0,\ L^0,\ T^0)$ is an equilibrium of system (4.3) if and only if

$$\begin{aligned} -b_1 R^0 + f_1(T^0) &= 0, \\ g_1 R^0 - b_2 L^0 + f_2(T^0) &= 0, \\ g_2 L^0 - b_3 T^0 &= 0. \end{aligned}$$

Thus, the point E^0 is an equilibrium if and only if (4.4) and (4.5) hold. In view of Assumption 4.1, since $f_1(\cdot)$ and $f_2(\cdot)$ are positive and decreasing, the equation (4.4) has the only positive solution T^0, and hence E^0 is unique. □

We now prove Lemma 4.3, presenting the local stability properties of the equilibrium.

Proof of Lemma 4.3. A straightforward computation shows that the characteristic polynomial corresponding to matrix A, defined in (4.7), is

$$P(\lambda) = \lambda^3 + a_1\lambda^2 + (a_2 - g_2 f_2'(T^0))\lambda + a_3 - g_2\left(g_1 f_1'(T^0) + b_1 f_2'(T^0)\right). \quad (4.16)$$

As $f_1(\cdot)$ and $f_2(\cdot)$ are decreasing, the coefficients of $P(\lambda)$ are positive; it has a real negative root, and the two remaining roots are complex-conjugated.

Based on the Routh-Hurwitz criterion, the steady state is stable if and only if

$$\det \begin{bmatrix} 1 & a_2 - g_2 f_2'(T^0) \\ a_1 & a_3 - g_2\left(g_1 f_1'(T^0) + b_1 f_2'(T^0)\right) \end{bmatrix} = \Theta_0,$$

is negative, and unstable if and only if it is positive.

We now show that if $\Theta_0 = 0$, then the two eigenvalues are complex-conjugated imaginary numbers. To this end, without loss of generality, assume that $\lambda_1, \lambda_2, \lambda_3$ are roots of $P(\lambda)$ where $\lambda_1 \in \mathbb{R}$, $\lambda_2 = \alpha + i\beta$ and $\lambda_3 = \alpha - i\beta$. According to the Vieta's formulas, the following relations among such zeros hold:

$$\begin{aligned} &\lambda_1 + \lambda_2 + \lambda_3 = -a_1, \\ &\lambda_1\lambda_2 + \lambda_2\lambda_3 + \lambda_1\lambda_3 = a_2 - g_2 f_2'(T), \\ &\lambda_1\lambda_2\lambda_3 = -a_3 + g_2\left(g_1 f_1'(T) + b_1 f_2'(T)\right). \end{aligned} \tag{4.17}$$

Now, in view of (4.17), one can rewrite (4.8) as follows

$$\begin{aligned} \Theta_0 &= a_3 - g_2(b_1 f_2'(T) + g_1 f_1'(T)) - a_1\left(a_2 - g_2 f_2'(T)\right) \\ &= -\lambda_1\lambda_2\lambda_3 + (\lambda_1 + 2\alpha)(a_2 - g_2 f_2'(T)) \\ &= -\lambda_1(\lambda_2\lambda_3 - (a_2 - g_2 f_2'(T))) + 2\alpha(a_2 - g_2 f_2'(T)) \\ &= (a_1 + 2\alpha)(\lambda_2\lambda_3 - (a_2 - g_2 f_2'(T))) + 2\alpha(a_2 - g_2 f_2'(T))) \\ &= (a_1 + 2\alpha)[2\alpha(a_1 + 2\alpha) + 2\alpha(a_2 - g_2 f_2'(T)) \\ &= 2\alpha\left((a_1 + 2\alpha)^2 + a_2 - g_2 f_2'(T)\right). \end{aligned}$$

Thus,

$$\Theta_0 = 2\alpha\left((a_1 + 2\alpha)^2 + a_2 - g_2 f_2'(T)\right). \tag{4.18}$$

Owing to the fact that $\left((a_1 + 2\alpha)^2 + a_2 - g_2 f_2'(T)\right) > 0$, the condition $\Theta_0 = 0$ implies that $\alpha = 0$, and hence λ_2 and λ_3 are complex-conjugated imaginary numbers. □

We now turn to prove Theorem 4.4, extending the proofs from [57] and [128]. The proof employs the widely known McLaurin's inequality [63] for the case of three variables

$$\frac{1}{3}(b_1 + b_2 + b_3) \geqslant \left(\frac{1}{3}\left(b_1b_2 + b_1b_3 + b_2b_3\right)\right)^{\frac{1}{2}} \geqslant (b_1b_2b_3)^{\frac{1}{3}},$$

which holds for any $b_1, b_2, b_3 > 0$; both inequalities are strict unless $b_1 = b_2 = b_3$. It implies, in particular, that

$$\frac{(b_1 + b_2 + b_3)(b_1b_2 + b_1b_3 + b_2b_3)}{b_1b_2b_3} \geq 9. \tag{4.19}$$

Another result, used in the proof, is the Hopf bifurcation theorem [118]. This theorem deals with a one-parameter family of dynamical systems

$$\dot{x} = F(x, \mu), \qquad \mu \in (-\varepsilon; \varepsilon). \tag{4.20}$$

It is assumed that for $\mu = 0$, the system has an equilibrium at x_0, for which $F(x, \mu)$ is C^1-smooth in the vicinity of $(x_0, 0)$, and the Jacobian matrix $D_x F(x_0, 0)$ has a pair of simple imaginary eigenvalues $\pm i\omega_0$ (where $\omega_0 \neq 0$) and all other eigenvalues have non-zero real parts; in particular, $D_x F(x_0, 0)$ is invertible. The implicit function theorem implies that for $\mu \approx 0$ there exists an equilibrium point $x(\mu)$ of system (4.20) (that is, $F(x(\mu), \mu)$), such that $x(0) = x_0$. The corresponding Jacobian $D_x F(x(\mu), \mu)$ has a pair of complex-conjugated eigenvalues $\alpha(\mu) \pm i\omega(\mu)$, smooth for $\mu \approx 0$; here $\alpha(0) = 0$ and $\omega(0) = \omega_0$. The Hopf bifurcation theorem is as follows [118, Theorem 2.3].

Theorem 4.14. *If $\alpha'(0) \neq 0$, the dynamical system* (4.20) *undergoes the Hopf bifurcation at $\mu = 0$, that is, there exist $\varepsilon_0 > 0$ such that for any $\mu \in (-\varepsilon_0, \varepsilon_0) \setminus \{0\}$ system* (4.20) *has a non-trivial periodic solution.*

Proof of Theorem 4.4. Assuming that (R^0, L^0, T^0) is an equilibrium of (4.3) for some choice $b_i, g_i > 0$ and applying (4.4), one obtains

$$g_2 = \frac{b_1 b_2 b_3 T^0}{g_1 f_1(T^0) + b_1 f_2(T^0)}. \tag{4.21}$$

Substituting (4.21) into (4.8) and dividing by $(b_1 b_2 b_3)$, the inequality (4.19) and Assumption 4.1 imply that

$$\begin{aligned} \frac{\Theta_0}{b_1 b_2 b_3} = &\underbrace{\frac{T^0(b_2 + b_3) f_2'(T^0)}{g_1 f_1(T^0) + b_1 f_2(T^0)}}_{\leq 0} + \underbrace{\frac{g_1(-T^0 f_1'(T^0))}{g_1 f_1(T^0) + b_1 f_2(T^0)}}_{\leq M(T^0)} \\ &- \frac{(b_1 + b_2 + b_3)(b_1 b_2 + b_1 b_3 + b_2 b_3)}{b_1 b_2 b_3} + 1 \leq M(T^0) - 8. \end{aligned} \tag{4.22}$$

The inequality (4.22) is strict unless $b_1 = b_2 = b_3$ and $f_2(T^0) = f_2'(T^0) = 0$, implying thus statements 1 and 2.

We are now going to prove statement 3. Supposing that $M(T^0) > 8$ for some $T^0 > 0$, let $R^0 = \frac{1}{b_1} f_1(T^0)$ and $L^0 = \frac{b_3}{g_2} T^0$. It can be easily noticed from (4.4) that any system (4.3), whose parameters satisfy the condition (4.21), has the equilibrium at (R^0, L^0, T^0). We are now going to design a one-parameter family of the systems (4.3) with this equilibrium, switching from stability to instability through a Hopf bifurcation. To do this, we fix $b_1 = b_2 = b_3 = b$ (where $b > 0$ is chosen arbitrarily) and determine g_2 from (4.21), leaving the parameter $g_1 > 0$ free. It can be easily noticed from (4.22) that $\Theta_0 = \Theta_0(g_1)$ is a smooth and strict increasing function of g_1, $\lim\limits_{g_1 \to 0} \Theta_0(g_1) < 0$ and $\lim\limits_{g_1 \to \infty} \Theta_0(g_1) = M(T^0) - 8 > 0$. Thus for sufficiently large $g_1 > 0$ the system has unstable equilibrium point. Furthermore, for $\varepsilon > 0$ sufficiently small, the image of $\Theta_0(\cdot)$ contains the interval $(-\varepsilon; \varepsilon)$; therefore, one can define the smooth inverse function $g_1 = g_1(\mu)$ in such a way

that $\Theta_0(g_1(\mu)) = \mu$ for any $\mu = (-\varepsilon; \varepsilon)$.

We now claim that the one-parameter family of systems (4.3) with $b_1 = b_2 = b_3 = b > 0$, $g_1 = g_1(\mu)$ and $g_2 = g_2(\mu)$ determined by (4.21) satisfies the conditions of Hopf bifurcation theorem (Theorem 4.14). By definition, the Routh-Hurwitz discriminant (4.8), corresponding to a specific μ, equals $\Theta_0(g_1(\mu)) = \mu$; by Lemma 4.3 the system with $\mu = 0$ has a pair of pure imaginary eigenvalues. Considering the extension of these eigenvalues $\alpha(\mu) \pm i\omega(\mu)$ for $\mu \approx 0$, it is shown (see (4.18)) that

$$2\alpha(\mu)\left[(a_1 + 2\alpha(\mu))^2 + (a_2 - g_2(\mu)f_2'(T^0))\right] = \mu, \tag{4.23}$$

(here a_i are defined by (4.9)). Differentiating (4.23) at $\mu = 0$ and recalling that $\alpha(0) = 0$, one arrives at

$$\alpha'(0) = \frac{1}{2\left[a_1^2 + (a_2 - g_2(0)f_2'(T^0)\right]} > 0.$$

Therefore, for $\mu \in (0; \varepsilon_0)$ (where $\varepsilon_0 > 0$) system (4.3) with the aforementioned type has an unstable equilibrium at (R^0, L^0, T^0), and at least one periodic solution. Notice, however, that for $\mu \in (-\varepsilon_0; 0)$ the system also has a periodic solution in spite of the equilibrium's local stability (see Remark 4.7). □

Proof of Lemma 4.10. This Lemma is immediate from [117, Theorem 1] since system (4.3) (a) has the only equilibrium; (b) if $\Theta_0 > 0$ then this equilibrium is *hyperbolic* (there are no imaginary eigenvalues); (c) all solutions are uniformly ultimately bounded, that is, $C > 0$ exists such that

$$\limsup_{t\to\infty}(|R(t)| + |L(t)| + |T(t)|) \le C, \qquad \forall R(0), L(0), T(0) > 0.$$

The properties (a) and (b) follow from Lemma 4.3; to prove (c), it suffices to notice that (4.3) is decomposable as

$$\dot{X}(t) = \bar{A}X(t) + F(X(t)), \qquad X(t) = (R(t), L(t), T(t))^\top,$$

where $\bar{A}$ is a Hurwitz matrix and $F(\cdot)$ is bounded. □

Proof of Theorem 4.12. The restriction (4.14) entails the existence of a one-to-one linear change of variables $(R, L, T) \mapsto (x_0, x_1, x_2)$, transforming (4.3) into the general system (4.11), satisfying (4.13) with $\delta_N = -1$, $N = 2$. Indeed, let

$$x_0 := T, \qquad x_1 := L + aT, \qquad x_2 := R, \tag{4.24}$$

where $a \in \mathbb{R}$ is a parameter to be specified later. First, let us consider the first equation of (4.3), i.e., $\dot{R} = -b_1 R + f_1(T)$. In view of (4.24), we have

$$\dot{x}_2 = -b_1 x_2 + f_1(x_0).$$

Denoting $h_2(x_1, x_2, x_0) := -b_1 x_2 + f_1(x_0)$, we have achieved the third equation of (4.11) with $N = 2$, satisfying the conditions (4.13), i.e.,

$$\frac{\partial h_2(x_1, x_2, x_0)}{\partial x_1} = 0 \geqslant 0, \qquad \frac{\partial h_2(x_1, x_2, x_0)}{\partial x_0} = \delta_2 \frac{\partial f}{\partial x_0} > 0, \qquad \delta_2 = -1.$$

Now, let us consider the third equation of (4.3), i.e., $\dot{T} = g_2 L - b_3 T$. As $x_0 = T$ and $x_1 = L + aT$, one has

$$\dot{x}_0 = g_2(x_1 - a x_0) - b_3 x_0. \tag{4.25}$$

Denoting $h_0(x_0, x_1) := g_2 x_1 - (g_2 a + b_3) x_0$, we have obtained the first equation of (4.11) satisfying the conditions (4.13), i.e.,

$$\frac{\partial h_0(x_0, x_1)}{\partial x_2} = 0 \geqslant 0, \qquad \frac{\partial h_0(x_0, x_1)}{\partial x_1} = g_2 > 0.$$

Finally, let us consider the third equation of (4.3), i.e., $\dot{L} = g_1 R - b_2 L + f_2(T)$. Equations (4.24) imply that $L = x_1 - a x_0$, and hence

$$\dot{L} = \dot{x}_1 - a \dot{x}_0. \tag{4.26}$$

As $\dot{L} = g_1 R - b_2 L + f_2(T)$, in view of (4.24) and (4.26), one has

$$\dot{x}_1 - a \dot{x}_0 = g_1 x_2 - b_2(x_1 - a x_0) + f_2(x_0), \tag{4.27}$$

or, equivalently,

$$\dot{x}_1 = \left(a(b_2 - b_3) - g_2 a^2\right) x_0 + (a g_2 - b_2) x_1 + g_1 x_2 + f_2(x_0). \tag{4.28}$$

Denoting

$$h_1(x_0, x_1, x_2) := \left(a(b_2 - b_3) - g_2 a^2\right) x_0 + (a g_2 - b_2) x_1 + g_1 x_2 + f_2(x_0),$$

and owing to the fact that $g_1, g_2 > 0$, the conditions (4.13) hold provided that

$$\frac{\partial h_1}{\partial x_0} \geq a(b_2 - b_3) - g_2 a^2 - \sup |f_2'(T)| \geq 0,$$

which always can be provided under the assumption (4.14) by choosing appropriate $a \in \mathbb{R}$. Theorem 4.12 now follows from Lemmas 4.10 and 4.11: if the equilibrium is unstable, then almost all solutions do not converge. □

4.7 Concluding remarks

In this chapter, a mathematical model for endocrine regulation has been examined. The model extends the conventional Goodwin's model by introducing an additional negative feedback. We have studied the local properties of the extended model and their relations to global properties, showing that the (locally) unstable equilibrium implies that almost all solutions oscillate and (under some conditions) converge to periodic orbits. The results are based on the general criterion of oscillation existence [151] and the Mallet-Paret's theory [101]; they can be extended to many other models, e.g. the model from [161].

In this chapter, the pulsatility of the feedback from effector hormones (T) to releasing hormones (R) is not taken into account. This issue is treated in next chapter, while the feedback from effector hormones (T) to tropic hormones (L) is assumed to be an *affine function*.

5

Impulsive model of endocrine regulation with a local continuous feedback

This chapter develops an impulsive model of endocrine regulation. In particular, it extends the impulsive Goodwin's model [15] by introducing an additional affine feedback. This local continuous feedback allows us to apply the theory, developed in [15], to our model to prove that, under some conditions on the parameters of the affine feedback, the extended model has a positive and unique 1-cycle solution.

This chapter starts with an introduction, followed by Section 5.2 where the model in question is introduced. The main result is presented in Section 5.3. It proceeds with Section 5.4 where we first present our approach for the proof of the main result, and then give the proofs of the results. This chapter ends with concluding remarks in Section 5.5.

5.1 Introduction

Hormones are products of glands, playing essential roles in vital bodily functions such as metabolism, reproduction and growth. This motivates the study of interactions between glands, consisting of many stimulatory (feedforward) and inhibitory (feedback) signals. The operation of endocrine glands is orchestrated by the brain, in particular, the hypothalamus and the pituitary gland. The former produces bursts of so-called release hormones that communicate control information to the glands through pulse amplitude and frequency. Thus the neuroendocrine control loop incorporating the hypothalamus and the involved endocrine glands is in fact hybrid, i.e., combining continuous and discrete dynamics. Due to the complexity of the resulting system, presenting a somewhat complete mathematical model of the endocrine system is a challenging problem. To obtain a tractable mathematical

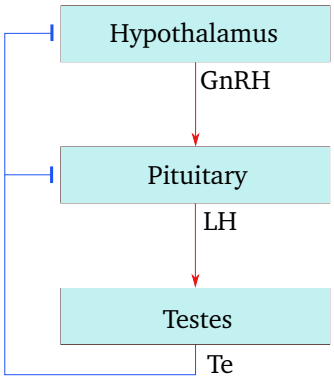

Figure 5.1: Structure of the hypothalamic-pituitary-gonadal axis with two negative feedbacks; feedforward and feedback control mechanisms are shown, respectively, by ↓ and ⊣.

model [80], such a complex system is usually decoupled into subsystems (or axes), capturing only known essential characteristics and interactions [129].

One of the most mathematically studied endocrine subsystems, the GnRH-LH-Te axis, regulates the production of testosterone (Te) in the male, where the Gonadotropin-Releasing Hormone (GnRH) and the Luteinizing Hormone (LH) play crucial roles. GnRH, produced in the hypothalamus, stimulates the pituitary gland that responds by the secretion of LH that, in its turn, stimulates the production of Te in the testes. This cascade of stimulations from GnRH to Te is then closed by two negative feedback loops from Te to *both* GnRH and LH, i.e., Te inhibits the secretion of GnRH and LH *directly* [80, 154], see Fig. 5.1. Although this chapter deals with a model for testosterone regulation, the construct serves as a "benchmark" in mathematical modeling of endocrine regulation, because much of the structure is widely applicable to some other *neuroendocrine* regulatory circuits (see e.g. [100, 121, 161]), controlled by the brain regulatory centers (hypothalamus) and the pituitary gland [82, 133].

Several mathematical models have been postulated to describe the regulation of testosterone in the male. One of the relatively simple models, suggested by Smith [128], is a direct application on the Goodwin's oscillator [52], introduced in Chapter 4. This model describes the cascade of stimulations from GnRH to Te controlled by a negative feedback from Te to GnRH, while the feedback from Te to LH is neglected. As the feedback from Te to GnRH is parametrized by a Hill function nonlinearity [51] in the Goodwin's oscillator, the periodic solutions exist only for the Hill functions of order greater than 8. Although oscillatory solutions arise in the Goodwin's model with delays for Hill functions of smaller than 8 [18, 128], the domain of feasible parameters is still quite small.

In fact, it is known that the feedback mechanism from Te to GnRH is not continuous but *pulsatile* (burst-like or episodic), see e.g. [80, 82, 89, 155] and the references therein. Pulsatility is the physiological mechanism to increase rapidly hormone concentrations and transport distinct signal information to the selected target tissues [155]. In [15], pulsatility of the feedback from Te to GnRH in the Goodwin's model has been described by amplitude and frequency pulse modulation [42]. The pulse-modulated model for testosterone regulation studied in [15] has been more recently validated on experimental data [104, 105]. Note that the structure and function of the pulsatile feedback mechanism from testosterone to GnRH is similar to the function of some other releasing hormones such as cortisol, growth, adrenal, and parathyroid hormones [105].

Despite its utility, the *cyclic* structure of the minimal model of the GnRH-LH-Te axis in [15] is a simplification since *only* the negative feedback from Te to GnRH is considered. A more complete model of the axis involves two more feedback loops [133], one *long* negative feedback from Te to LH, and one *short* negative feedback from LH to GnRH. The latter, which is very short in comparison with the other two feedbacks, is the *most vulnerable* one, and is not firmly established [133]. However, the former was reported in literature and strongly supported by experiments, see [80, 82, 154, 158] and the references therein. Several mathematical models with multiple feedbacks have been studied in literature, while most of them employ continuous dynamics [4, 55, 139, 146, 161]. Exceptions are the most complete stochastic models presented in [80, 82], while a rigorous analysis of these models is still lacking.

In spite of the existence of multiple feedback loops for neuroendocrine regulatory circuits [4, 80, 82, 133, 155, 161], there is no consensus on the mathematical description of the respective feedback controls. In this chapter, an *affine function* is introduced into the previously developed mathematical model in [15] to describe the feedback from Te to LH. Although one possibility is to describe such a feedback by a Hill function, several reasons [40] justify why this feedback may not be parametrized by a Hill nonlinearity. First, from any set of the experimental or simulated data, the feedback is commonly not observed in its full domain of definition, that may challenge the involved numerical methods. Second, as identification methods basically deal with systems whose dynamics depend *linearly* on unknown parameters, we can use the advantage of an affine function than a nonlinear Hill function. Lastly, by implementing an affine function into the mathematical model developed in [15], we can preserve the important property of the model studied in [15], i.e., representing the extended mathematical model in the Lure's form with the pulsatile feedback from Te to GnRH. In view of such an affine function, we introduce two unknown parameters into the previously developed model [15], making it possible to suggest an identification procedure analogous to the one presented in [104, 105]. Although by introducing an affine feedback into the model

studied in [15] the dynamics between two consecutive pulses is linear, it poses the problem of solution feasibility since some solutions may escape from the positive octant and hence lose biological interpretation.

Owing to the fact that endocrine regulation processes exhibit self-sustained oscillations, in this chapter we are primarily interested in *periodic solutions*. Dealing with testosterone regulation, as discussed in [15], clinical experiments reveal that such solutions are usually featured by the existence of one or two pulses over *one period* (called respectively 1-cycle and 2-cycle). For the cyclic model presented in [15], the existence and uniqueness of 1-cycle solutions along with their local stability are discussed. In this work, we extend such results to a system with an additional feedback. Note that the positivity of 1-cycle solutions of the cyclic model [15] is automatically held, while it is not true for the extended system. So another contribution of this chapter is to give conditions under which the positivity of 1-cycle solutions of the extended system is guaranteed. We start with the extended model in the next section.

5

5.2 Extended mathematical model

Consider the following model of endocrine regulation

$$\begin{aligned} \dot{R} &= -b_1 R + f(T), \\ \dot{L} &= g_1 R - b_2 L - kT + \mu, \\ \dot{T} &= g_2 L - b_3 T, \end{aligned} \tag{5.1}$$

where R, L and T stand for the concentrations of three hormones interacting in a closed loop. In testosterone regulation, these variables represent serum concentrations of GnRH, LH and Te, respectively. The constants $b_i > 0$ $(i = 1, 2, 3)$ are the clearing rates of the corresponding hormones, while the constants $k, g_i > 0$ $(i = 1, 2)$ and the decreasing function $f(\cdot) > 0$ represent the secretion rates of the corresponding hormones. Unlike the classical Goodwin-Smith model [52, 128], the model (5.1) involves an *additional* negative feedback loop from T to L, described by the *affine* function "$-kT + \mu$" where $\mu \in \mathbb{R}$; the cyclic model in [128] corresponds to the case when $k = \mu = 0$.

In the model (5.1), the nonlinear function $f(T)$ describes the negative feedback from T to R. To capture the pulsatility of the neural feedback, following [15], we replace the nonlinear function $f(T)$ by a pulse modulation mechanism [42]. Implementing such a pulsatile feedback and rewriting system (5.1) in a vector

form, we obtain the system

$$\begin{aligned} \dot{x} &= Ax + B\xi(t) + D, \\ y &= Cx, \end{aligned} \tag{5.2}$$

where

$$\begin{aligned} x = \begin{bmatrix} R \\ L \\ T \end{bmatrix}, \qquad A = \begin{bmatrix} -b_1 & 0 & 0 \\ g_1 & -b_2 & -k \\ 0 & g_2 & -b_3 \end{bmatrix}, \\ B = \begin{bmatrix} 1 \\ 0 \\ 0 \end{bmatrix}, \qquad C^\top = \begin{bmatrix} 0 \\ 0 \\ 1 \end{bmatrix}, \qquad D = \begin{bmatrix} 0 \\ \mu \\ 0 \end{bmatrix}, \end{aligned} \tag{5.3}$$

and

$$\xi(t) = \sum_{n=0}^{\infty} \lambda_n \delta(t - t_n). \tag{5.4}$$

Here $\delta(t)$ is the Dirac delta-function, and T and R are the modulating and the modulated signals, respectively. In testosterone regulation, the function $\xi(t)$ is determined by the times t_n at which GnRH pulses are fired with the weights λ_n.

Suppose that the firing times t_n and the weights λ_n are given by

$$\begin{gathered} t_{n+1} = t_n + \tau_n, \qquad \tau_n = \Phi(y(t_n)), \qquad \lambda_n = \Psi(y(t_n)), \\ t_0 = 0, \qquad y(0^-) = y(0), \end{gathered} \tag{5.5}$$

where $\Phi(\cdot)$ and $\Psi(\cdot)$ stand, respectively, for the frequency and amplitude modulation characteristics [42]. Hereafter $y(t_n^-)$ and $y(t_n^+)$ denote, respectively, the left- and right-side limits of $y(t)$ at time t_n. Due to the fact that an increase in the concentration of Te results in sparser pulses of GnRH of lower amplitude [154], we assume that $\Phi(y)$ and $\Psi(y)$ are respectively, non-decreasing and non-increasing for $y \geqslant 0$; these functions are also positive and uniformly bounded, that is,

$$\Phi : [0, \infty) \longrightarrow [\Phi_1, \Phi_2], \qquad \Psi : [0, \infty) \longrightarrow [\Psi_1, \Psi_2], \tag{5.6}$$

where $\Phi_i, \Psi_i > 0$ are some constants.

Mathematically, the continuous part of system (5.2) is treated as follows. A pulse, corresponding to the release of GnRH, is fired at time t_n and corresponds to a jump of the hormone concentration $R(t_n^+) = R(t_n^-) + \lambda_n$ while it does not immediately affect the two remaining concentrations $L(t_n^-) = L(t_n^+)$ and $T(t_n^-) = T(t_n^+)$. Equivalently, in the vector form, we have

$$x(t_n^+) = x(t_n^-) + \lambda_n B. \tag{5.7}$$

Here, the jump weight λ_n and the interval between two consecutive firing times τ_n depend on the output $y(t_n)$, i.e. the concentration T. Between the consecutive instants t_n and t_{n+1}, the dynamics of (5.2) are described by the affine system

$$\dot{x} = Ax + D, \qquad t_n < t < t_{n+1}. \tag{5.8}$$

It is emphasized that the closed-loop dynamics of (5.2)-(5.5) are hybrid and the state vector of the model comprises both the continuous states in $x(t)$ and the discrete state t_n.

As the elements of $x(t)$ stand for hormonal concentrations, only *non-negative* and *bounded* solutions of closed-loop system (5.2) are meaningful. For $k = 0$ [15], the solution starting in the positive orthant remains there as the matrix A is Metzler[1], and thus neither the linear dynamics in (5.8) nor the jumps in (5.7) result in solutions outside the positive orthant. This, however, does not hold when $k > 0$ since the matrix A is not Metzler anymore, and when the second element of vector D, i.e. μ, is negative. The very presence of the vector D makes the continuous part of the model non-autonomous because the component μ enters the regulation loop as an exogenous signal. The state vector $x(t)$, obeying (5.8), may escape from the positive orthant between two consecutive pulses. Boundedness of the solutions to (5.2) follows due to the fact that the matrix A is Hurwitz stable, and the functions $\Phi(y)$ and $\Psi(y)$ are bounded.

The matter of positivity arises due to the nature of the mathematical tools selected to capture the system dynamics. In fact, the process of synthesis and clearing of hormone molecules is essentially discrete and the number of molecules in blood is countable. When the last molecule clears out and no more new ones are synthesized, the number of molecules stays at zero. Yet, when hormone concentrations are chosen as the state variables of the model, the discrete nature of the process is lost in the description by differential equations. Thus, special attention has to be paid to the model structure in order to maintain positivity of the solutions.

Owing to the fact that hormones' concentrations fluctuate periodically, in this chapter we show that, under some conditions, the closed-loop system (5.2) has positive periodic solutions with only one discontinuity point t_n over the *smallest* period, so-called "1-cycle" solutions [173].

5.3 Main result

By definition, we call a solution *τ-periodic*, where $\tau > 0$, if $x(t) = x(t + \tau)$ for any $t \geqslant 0$. System (5.2) may have one or more pulses in its smallest period; however,

[1]Matrix $A = (a_{ij})$ is called Metzler if all its off-diagonal components are nonnegative, i.e., $a_{ij} \geqslant 0, i \neq j$.

according to (5.5) and (5.6), the number of pulses are *finite*, because the time between two consecutive pulses is not less than $\Phi_1 > 0$ and hence Zeno behavior is not possible. A periodic solution of (5.2) is called m-cycle if exactly m pulses are fired over the smallest period [173].

As demonstrated in [15], system (5.2) with $k = \mu = 0$ has a unique 1-cycle solution. By using an efficient numerical procedures, such a solution can be found and tested for local stability. Although (i) when $k > 0$, matrix A is not Metzler anymore, and (ii) when $\mu < 0$, some solutions of the affine system (5.8) may become negative at some time $t > 0$, we show that the existence, uniqueness, and positivity of 1-cycle solutions remain valid if the parameter k satisfies the conditions

$$k < k^* := \frac{(b_3 - b_2)^2}{4g_2}, \qquad k \neq k^0 := \frac{(b_3 - b_1)(b_1 - b_2)}{g_2}, \tag{5.9}$$

and the parameter μ remains within some bounds (see Theorem 5.2 for explicit bounds).

Before stating the main results, we introduce some notations as follows:

$$\alpha := \frac{b_2 + b_3}{2}, \qquad \beta := \frac{\sqrt{(b_3 - b_2)^2 - 4kg_2}}{2}, \tag{5.10}$$

$$\eta_1 := b_1, \qquad \eta_2 := \alpha + \beta, \qquad \eta_3 := \alpha - \beta, \qquad \zeta_j := \Pi_{\substack{i=1 \\ i \neq j}}^{3} \frac{1}{(\eta_j - \eta_i)}, \tag{5.11}$$

$$\rho^0 := \frac{(b_2 - b_3) - 2\beta}{2g_2}, \tag{5.12}$$

$$V_1 := \frac{\Psi_1}{e^{b_1 \Phi_2} - 1}, \qquad U_1 := \frac{\Psi_2}{1 - e^{-b_1 \Phi_1}}, \tag{5.13}$$

$$\gamma := b_2 - \frac{V_1 + U_1}{U_1 - V_1} b_3. \tag{5.14}$$

Remark 5.1. The quantity k^0, defined in (5.9), is positive when either $b_1 \in (b_3, b_2)$ or $b_1 \in (b_2, b_3)$, while is negative for the other cases. The assumption $k \neq k^0$ in (5.9) ensures that $\eta_j \neq \eta_i$ $(i, j = 1, 2, 3,\ i \neq j)$ and hence ζ_j are well-defined when $b_1 \in (b_3, b_2)$ or $b_1 \in (b_2, b_3)$. Further, owing to the fact that all the involved hormones have different clearing rates [154], we have $b_i \neq b_j$ $(i \neq j)$, and hence $k^0 \neq 0$.

Theorem 5.2. *In view of* (5.9)*, assume that one of the following conditions holds:*

1. $b_3 > b_2$ *and* $\mu \geqslant -g_1 V_1$*, or*
2. $b_2 > b_3$*,* $\mu \geqslant \frac{g_1}{b_3}(\gamma - 2\beta)$ *and one of the following holds:*
   (a) $\gamma \leqslant 0$*, or*

(b) $\gamma > 0$, *and* $k < \frac{(b_3-b_2)^2-\gamma^2}{4g_2}$.

Then system (5.2) *has a positive and unique 1-cycle solution with the initial condition* $x^0 = (R^0, L^0 - \rho^0 T^0, T^0)$ *where* T^0 *is calculated from the system of transcendental equations*

$$T^0 = \frac{\mu g_2}{\eta_2 \eta_3} + \lambda_0 g_1 g_2 \sum_{j=1}^{3} \frac{\zeta_j}{e^{\eta_j \tau_0} - 1}, \qquad \lambda_0 = \Psi(T^0), \qquad \tau_0 = \Phi(T^0), \tag{5.15}$$

and

$$R^0 = \frac{\lambda_0}{e^{\eta_1 \tau_0} - 1}, \qquad L^0 = \frac{\mu}{\eta_2} + \frac{\lambda_0 g_1}{(\eta_1 - \eta_2)} \left(\frac{1}{e^{\eta_2 \tau_0} - 1} - \frac{1}{e^{\eta_1 \tau_0} - 1} \right). \tag{5.16}$$

5.4 Methods

This section is devoted to the proof of Theorem 5.2. Our approach, presented in Subsections 5.4.1 – 5.4.3, is as follows. Under the conditions given in Theorem 5.2, (i) in Subsection 5.4.1 we use a one-to-one linear change of variables to transform system (5.2) to a system whose linear part is Metzler; (ii) in Subsection 5.4.2, we prove that the transformed system has a unique and positive 1-cycle solution; (iii) in Subsection 5.4.3, we show that any positive 1-cycle solution of (5.2) is such a solution of the transformed system and vice versa. The proof of Theorem 5.2 is presented in Subsection 5.4.4. We start with the linear transformation of (5.2) in the following subsection.

5.4.1 Transformation of the system

The goal of this subsection is to use a one-to-one linear change of variables to transform system (5.2) to a system whose linear part is Metzler. To this end, we propose the linear mapping

$$\begin{aligned} &\mathscr{M} : (R,\, L,\, T) \longmapsto (z_1,\, z_2,\, z_3), \\ &z_1 := R, \qquad z_2 := L + \rho T, \qquad z_3 := T, \qquad \rho \in \mathbb{R}, \end{aligned} \tag{5.17}$$

where the parameter ρ will be determined later. In view of the mapping $\mathscr{M}$, system (5.2) is transformed to the equations

$$\begin{aligned} \dot{z}_1 &= -b_1 z_1 + \xi(t), \\ \dot{z}_2 &= g_1 z_1 - (b_2 - \rho g_2) z_2 + g_3 z_3 + \mu, \\ \dot{z}_3 &= g_2 z_2 - (b_3 + \rho g_2) z_3, \end{aligned} \tag{5.18}$$

where the parameters b_1, b_2, b_3, g_1, g_2 and μ are the same as those given in (5.3), and

$$g_3 := -g_2\rho^2 + (b_2 - b_3)\rho - k, \qquad \rho \in \mathbb{R}. \tag{5.19}$$

As $g_1, g_2 > 0$, one possibility for the linear part of (5.18) to be Metzler is to find conditions under which $g_3 = 0$. Considering g_3 as a quadratic function of ρ, a sufficient condition to have $g_3 = 0$ is that $k < k^* = \frac{(b_3-b_2)^2}{4g_2}$, which is one of the assumptions in (5.9). In view of $k < k^*$, the quantity ρ^0, defined in (5.12), is a zero of (5.19). Thus, $k < k^*$ and $\rho = \rho^0$ implies that $g_3 = 0$, and hence the linear part of (5.18) is Metzler.

Although $k < k^*$ and $\rho = \rho^0$ imply that $g_3 = 0$ and hence the linear part of system (5.18) is Metzler, in the case that $\mu < 0$, yet some of its solutions may escape from the positive orthant even if they start from there, i.e., the positive orthant is not an invariant set. Once it occurs, the output of the system may become negative, and hence the functions $\Phi(\cdot)$ and $\Psi(\cdot)$ are not well-defined for $y < 0$, see (5.5) and (5.6). In this regard, we expand $\Phi(\cdot)$ and $\Psi(\cdot)$ on $(-\infty, \infty)$ as follows

$$\tilde{\Phi}(y) = \begin{cases} \Phi(y) & y \geqslant 0, \\ \Phi_1 & y < 0, \end{cases} \qquad \tilde{\Psi}(y) = \begin{cases} \Psi(y) & y \geqslant 0, \\ \Psi_2 & y < 0, \end{cases} \tag{5.20}$$

where Φ_1 and Ψ_2 are, respectively, the lower and upper bounds of functions $\Phi(\cdot)$ and $\Psi(\cdot)$, introduced in (5.6).

Remark 5.3. The extended functions $\tilde{\Phi}(\cdot)$ and $\tilde{\Psi}(\cdot)$ are non-decreasing and non-increasing, respectively, and for any $y \in \mathbb{R}$, they are within the bounds, given in (5.6). Further, $\tilde{\Phi}(y) = \Phi(y)$ and $\tilde{\Psi}(y) = \Psi(y)$, for any $y \geqslant 0$.

It is verified that $b_2 - g_2\rho^0 = \eta_2$ and $b_3 + g_2\rho^0 = \eta_3$, where η_2 and η_3 are defined in (5.11). In view of $k < k^*$ and $\rho = \rho^0$, the equations (5.18) lead to the system

$$\begin{cases} \dot{z} = \tilde{A}z + B\tilde{\xi}(t) + D, \\ \tilde{y} = Cz, \end{cases} \tag{5.21}$$

where

$$z = \begin{bmatrix} z_1 \\ z_2 \\ z_3 \end{bmatrix}, \qquad \tilde{A} = \begin{bmatrix} -\eta_1 & 0 & 0 \\ g_1 & -\eta_2 & 0 \\ 0 & g_2 & -\eta_3 \end{bmatrix}, \tag{5.22}$$

B, C, D are the same as those introduced in (5.3), and $\tilde{\xi}(t)$ is denoted by

$$\tilde{\xi}(t) = \sum_{n=0}^{\infty} \tilde{\lambda}_n \delta(t - t_n), \tag{5.23}$$

where

$$t_{n+1} - t_n = \tilde{\tau}_n, \qquad \tilde{\tau}_n = \tilde{\Phi}(\tilde{y}(t_n)), \qquad \tilde{\lambda}_n = \tilde{\Psi}(\tilde{y}(t_n)). \tag{5.24}$$

Between the consecutive instants t_n and t_{n+1}, system (5.21) is represented by the affine system

$$\dot{z} = \tilde{A}z + D, \qquad t_n < t < t_{n+1}, \tag{5.25}$$

with

$$z(t_n^+) = z(t_n^-) + \tilde{\lambda}_n B. \tag{5.26}$$

Remark 5.4. The inequalities $\alpha > \beta > 0$ and $b_1 > 0$ implies that the eigenvalues of $\tilde{A}$ are negative, and hence it is Hurwitz stable. On the other hand, functions $\tilde{\Phi}(\cdot)$ and $\tilde{\Psi}(\cdot)$ are bounded. Therefore solutions of (5.21) are bounded.

As mentioned, some solutions of system (5.21) may become negative at some time when $\mu < 0$. So our goal in the rest of this subsection is to find conditions on μ such that *periodic solutions* of (5.21) remain positive. Since such solutions stay between the asymptotic bounds of (5.21) for any $t \geqslant 0$, it suffices to find conditions on μ such that the lower asymptotic bounds of (5.21) are non-negative. In the following proposition, such asymptotic bounds are given.

Proposition 5.5. *Solutions of system* (5.21) *have the asymptotic bounds*

$$V_i \leqslant \liminf_{t\to\infty} z_i(t) \leqslant \limsup_{t\to\infty} z_i(t) \leqslant U_i, \qquad i = 1, 2, 3,$$

where V_1 and U_1 are defined in (5.13)*, and*

$$\begin{aligned} V_2 &:= \frac{g_1 V_1 + \mu}{\eta_2}, & U_2 &:= \frac{g_1 U_1 + \mu}{\eta_2}, \\ V_3 &:= \frac{(g_1 V_1 + \mu) g_2}{\eta_2 \eta_3}, & U_3 &:= \frac{(g_1 U_1 + \mu) g_2}{\eta_2 \eta_3}. \end{aligned} \tag{5.27}$$

Moreover, the asymptotic bounds are non-negative if $\mu \geqslant -g_1 V_1$.

5.4.2 Periodic solutions

In this subsection, we study periodic solutions of system (5.21). More precisely, we show that system (5.21) has a unique and positive 1-cycle solution, i.e., there exist $\tilde{\lambda}_0, \tilde{\tau}_0, \tilde{y}^0 > 0$ such that $t_{n+1} - t_n = \tilde{\tau}_0$, $\tilde{y}(t_n^-) = \tilde{y}^0$ and $\tilde{\lambda}_n = \tilde{\lambda}_0$, for any $n \geqslant 0$. To this end, let us denote $z^n := z(t_n^-)$ where $z(t)$ is a solution of (5.21). Then one from (5.24), (5.25) and (5.26) obtains

$$z^{n+1} = e^{\tilde{A}(t_{n+1}-t_n)}[z^n + \tilde{\lambda}_n B] + \int_{t_n}^{t_{n+1}} e^{\tilde{A}(t_{n+1}-s)} D ds. \tag{5.28}$$

In view of $t_{n+1} - t_n = \tilde{\tau}_n$, we denote

$$E(\tilde{\tau}_n) := \int_{t_n}^{t_{n+1}} e^{\tilde{A}(t_{n+1}-s)} D ds.$$

Then from (5.28) we have

$$\begin{aligned} z^{n+1} &= e^{\tilde{A}(t_{n+1}-t_n)}[z^n + \tilde{\lambda}_n B] + E(\tilde{\tau}_n) \\ &= e^{\tilde{A}\tau_n}[z^n + \tilde{\lambda}_n B] + E(\tilde{\tau}_n) \\ &= e^{\tilde{A}\tilde{\Phi}(Cz^n)}[z^n + \tilde{\Psi}(Cz^n)B] + E(\tilde{\Phi}(Cz^n)). \end{aligned}$$

So the states z^n are described by the discrete map

$$z^{n+1} = P(z^n), \qquad \forall n \geqslant 0, \tag{5.29}$$

where

$$P(z) := e^{\tilde{A}\tilde{\Phi}(Cz)}[z + \tilde{\Psi}(Cz)B] + E(\tilde{\Phi}(Cz)). \tag{5.30}$$

As we mentioned above, for a 1-cycle solution we have $t_{n+1} - t_n = \tilde{\tau}_0 > 0$ with the jump $\tilde{\lambda}_n = \tilde{\lambda}_0 > 0$ for all $n \geqslant 0$. So 1-cycle, starting at $z^0 := z(0^-)$, corresponds to a *fixed point* of $P(z)$. Indeed, $z^1 = z^0$ and thus

$$P(z^0) = z^0. \tag{5.31}$$

On the other hand, suppose that (5.31) has a solution z^0. Denoting $\tilde{\tau}_0, t_1, \tilde{\lambda}_0$ from (5.24) with $n = 0$ and defining the function $z(t)$ on $(t_0; t_1)$, the initial condition $z(t_0^+) = z^0 + \tilde{\lambda}_0 B$ and the affine system (5.25) imply that $z(t_1^-) \overset{(5.29)}{=} P(z^0) = z^0$. Denoting $t_2 := t_1 + \tilde{\tau}_0$ and $z(t_1^+) = z^0 + \tilde{\lambda}_0 B$, one can extend the function $z(t)$ to $(t_1; t_2)$ and shows that $z(t_2^-) = z^0$, and so on; so one may formally construct a $\tilde{\tau}_0$-periodic 1-cycle. The following theorem gives sufficient conditions for the existence, uniqueness and also positivity of a 1-cycle solution of system (5.21) along with its parameters (i.e. $\tilde{\tau}_0, \tilde{\lambda}_0$ and $\tilde{y}^0$).

Theorem 5.6. *In view of assumptions* (5.9)*, the equation* (5.31) *has a unique solution z^0, and this solution corresponds to a unique 1-cycle solution of* (5.21)*; if $\mu \geqslant -g_1 V_1$, then the solution is positive. Furthermore, the point z^0 can be calculated from the system of equations*

$$\tilde{y}^0 = CQ(\tilde{y}^0), \tag{5.32}$$

$$z^0 = Q(\tilde{y}^0), \tag{5.33}$$

where

$$Q(\tilde{y}^0) := (e^{-\tilde{A}\tilde{\Phi}(\tilde{y}^0)} - I)^{-1}\left[\tilde{\Psi}(\tilde{y}^0)B + e^{-\tilde{A}\tilde{\Phi}(\tilde{y}^0)}E(\tilde{\Phi}(\tilde{y}^0))\right].$$

5.4.3 One-to-one correspondence between 1-cycle solutions

Under the conditions given in Theorem 5.6, system (5.21) has a unique and positive 1-cycle solution. However, we are interested in positive 1-cycle solutions of (5.2). So the goal of this subsection is to map back the 1-cycle solution of (5.21) to the corresponding one of (5.2) so that its positivity is preserved. In view of the mapping $\mathscr{M}$, defined in (5.17), the inverse mapping is defined by

$$\begin{aligned} &\mathscr{M}^{-1} : (z_1,\, z_2,\, z_3) \longmapsto (R,\, L,\, T), \\ &R = z_1, \qquad L = z_2 - \rho z_3, \qquad T = z_3, \qquad \rho \in \mathbb{R}. \end{aligned} \tag{5.34}$$

Note that in order to map back the 1-cycle solution of (5.21) to the corresponding one of (5.2), we set $\rho = \rho^0$ in (5.34). Now we show that, under some conditions, there exists a one-to-one correspondence between positive 1-cycle solutions of (5.2) and (5.21), i.e., any positive 1-cycle solution of (5.2) is such a solution of (5.21) and vice versa. Note that the sign of ρ^0, which plays a crucial role in the positivity of solutions in both mapping $\mathscr{M}$ and $\mathscr{M}^{-1}$, depends on the sign of $(b_3 - b_2)$. So we have the following lemmas.

Lemma 5.7. *If $b_3 > b_2$, $\mu \geqslant -g_1V_1$ and assumptions* (5.9) *hold, then any positive 1-cycle solution of* (5.2) *corresponds to such a solution of* (5.21) *and vice versa.*

Lemma 5.8. *If $b_2 > b_3$ and assumptions* (5.9) *hold, then any positive 1-cycle solution of* (5.2) *corresponds to such a solution of* (5.21) *and vice versa, provided that one of the following conditions is satisfied:*

1. *$\gamma \leqslant 0$, or*
2. *$\gamma > 0$ and $k < \frac{(b_3-b_2)^2-\gamma^2}{4g_2}$,*

where γ is defined in (5.14).

5.4.4 Proof of the results

Proof of Proposition 5.5. We rewrite $\dot{z} = \tilde{A}z + B\tilde{\xi}(t) + D$, defined in (5.21), as follows:

$$\begin{aligned} \dot{z}_1 &= -\eta_1 z_1 + \tilde{\xi}(t), \\ \dot{z}_2 &= g_1 z_1 - \eta_2 z_2 + \mu, \\ \dot{z}_3 &= g_2 z_2 - \eta_3 z_3. \end{aligned}$$

The asymptotic bounds of z_1 are [15]

$$V_1 = \frac{\Psi_1}{e^{\eta_1 \Phi_2} - 1} \leqslant \liminf_{t\to\infty} z_1(t) \leqslant \limsup_{t\to\infty} z_1(t) \leqslant \frac{\Psi_2}{1 - e^{-\eta_1 \Phi_1}} = U_1. \tag{5.35}$$

Given the initial condition $z_2(0)$, the solution to $\dot{z}_2 = g_1 z_1 - \eta_2 z_2 + \mu$ is

$$z_2(t) = e^{-\eta_2 t} z_2(0) + \int_0^t e^{-\eta_2 (t-s)} (g_1 z_1(s) + \mu) ds. \tag{5.36}$$

In order to calculate the asymptotic bounds of (5.36), it suffices to find the asymptotic bounds of its integral part as $\lim_{t\to\infty} e^{-\eta_2 t} z_2(0) = 0$. To this end, in view of (5.35), one obtains

$$\begin{aligned}
\limsup_{t\to\infty} z_2(t) &= \limsup_{t\to\infty} \int_0^t e^{-\eta_2 (t-s)} (g_1 z_1(s) + \mu) ds \\
&\leqslant (g_1 U_1 + \mu) \limsup_{t\to\infty} \int_0^t e^{-\eta_2 (t-s)} ds \\
&= (g_1 U_1 + \mu) \limsup_{t\to\infty} \frac{1}{\eta_2} (1 - e^{-\eta_2 t}) \\
&= \frac{g_1 U_1 + \mu}{\eta_2} = U_2.
\end{aligned}$$

Analogously, it is proven that $\liminf_{t\to\infty} z_2(t) \geqslant \frac{g_1 V_1 + \mu}{\eta_2} = V_2$, and z_3 has the asymptotic bounds, given in (5.27). Positivity of the asymptotic bounds (5.27) is immediate if $\mu \geqslant -g_1 V_1$. □

Proof of Theorem 5.6. We present the proof in 3 steps. In Step 1 we show that the equation (5.31) is equivalent to (5.32) and (5.33), followed by Step 2 to prove that there exists a unique solution to the nonlinear equation (5.32). In Step 3 we show that the 1-cycle solution is positive if $\mu \geqslant -g_1 V_1$.

Step 1. To prove that the equation (5.31) is equivalent to the equations (5.32) and (5.33), first let us assume that z^0 is a solution to (5.31). Denoting $\tilde{y}^0 = C z^0$, the pair $\tilde{y}^0, z^0$ is a solution to (5.32) and (5.33). On the other hand, if $\tilde{y}^0$ and z^0 solve (5.32) and (5.33), respectively, then a straightforward calculation shows that $\tilde{y}^0 = C z^0$. Substituting $\tilde{y}^0$ into (5.33), one obtains $P(z^0) = z^0$. So the existence of a fixed point for (5.31) is equivalent to find a solution to (5.32).

Step 2. The goal of this step is to find a unique solution to (5.32). To this end, we show that the right-hand side of (5.32) is bounded and non-increasing in the positive quadrant. We rewrite the function $CQ(\tilde{y}^0)$ as follows

$$CQ(\tilde{y}^0) = \tilde{\Psi}(\tilde{y}^0) F(\tilde{\Phi}(\tilde{y}^0)) + G(\tilde{\Phi}(\tilde{y}^0)), \tag{5.37}$$

where

$$F(\tilde{y}) := C(e^{-\tilde{y}\tilde{A}} - I)^{-1}B, \qquad G(\tilde{y}) := C(e^{-\tilde{y}\tilde{A}} - I)^{-1}e^{-\tilde{y}\tilde{A}}E(\tilde{y}).$$

As $\tilde{\Psi}$ is non-increasing and $\tilde{\Phi}$ is non-decreasing, both being uniformly positive and bounded, it suffices to prove that both $F(\tilde{y})$ and $G(\tilde{y})$ are non-increasing and positive as $\tilde{y} \geqslant 0$. A straightforward calculation shows that $G(\tilde{y}) = \dfrac{\mu g_2}{\eta_2\eta_3}$, which is either a positive or a negative constant, according to μ.

Following [15, Theorem 1], we prove that $F(\tilde{y})$ is positive, non-increasing, and $\lim_{\tilde{y}\to\infty} F(\tilde{y}) = 0$. It can be readily seen that

$$F'(\tilde{y}) = g_1 g_2 \sum_{j=1}^{3}(-\zeta_j)\psi_{\tilde{y}}(\eta_j), \qquad \psi_{\tilde{y}}(\eta) := \frac{\eta e^{\eta\tilde{y}}}{(e^{\eta\tilde{y}} - 1)^2}, \tag{5.38}$$

where η_j and ζ_j are defined in (5.11). As $\zeta_j = \Pi_{\substack{i=1\\ i\neq j}}^{3} \frac{1}{(\eta_j - \eta_i)}$, the sign of ζ_j depends on the sign of $(\eta_i - \eta_j)$ for $i \neq j$. The equations (5.11) imply that

$$\eta_1 - \eta_2 = b_1 - \alpha - \beta, \qquad \eta_1 - \eta_3 = b_1 - \alpha + \beta, \qquad \eta_2 - \eta_3 = 2\beta. \tag{5.39}$$

It is clear from (5.39) that the signs of $\eta_1 - \eta_2$ and $\eta_1 - \eta_3$ can change with respect to the variation of parameter b_1. Thus, three cases including (i) $b_1 > \alpha + \beta$, (ii) $\alpha - \beta < b_1 < \alpha + \beta$, and (iii) $b_1 < \alpha - \beta$ may occur. Note that since $k \neq k^0$, one concludes that $b_1 \notin \{\alpha - \beta, \alpha + \beta\}$. In the following, only the proof of case (i) is given. The proof of other cases follow the same line of reasoning as case (i), and are omitted for brevity.

Let us assume that $b_1 > \alpha + \beta$. It follows from (5.39) that $\zeta_1, \zeta_3 > 0$ and $\zeta_2 < 0$. Then $F'(\tilde{y}) \leqslant 0$ if the inequality

$$-\zeta_2\psi_{\tilde{y}}(\eta_2) \leqslant \zeta_1\psi_{\tilde{y}}(\eta_1) + \zeta_3\psi_{\tilde{y}}(\eta_3), \tag{5.40}$$

holds. Owing to the fact that $\zeta_1 + \zeta_2 + \zeta_3 = 0$, and denoting $\theta := -\frac{\zeta_1}{\zeta_2}$, one concludes that $0 < \theta < 1$ and $(1 - \theta) = -\frac{\zeta_3}{\zeta_2}$. Moreover, it can be readily seen that $\eta_2 = \theta\eta_1 + (1 - \theta)\eta_3$. So the inequality (5.40) can be rewritten as

$$\psi_{\tilde{y}}(\theta\eta_1 + (1 - \theta)\eta_3) \leqslant \theta\psi_{\tilde{y}}(\eta_1) + (1 - \theta)\psi_{\tilde{y}}(\eta_3). \tag{5.41}$$

It is verified that for any $\tilde{y} > 0$, the second derivative of $\psi_{\tilde{y}}(\eta)$ with respect to η is positive and hence $\psi_{\tilde{y}}(\eta)$ is a convex function with respect to η for any $\tilde{y} > 0$. Therefore, the inequality (5.41) holds and hence $F'(\tilde{y}) \leqslant 0$.

Now we show that $F(\tilde{y}) \geqslant 0$ for any $\tilde{y} \geqslant 0$. The function $F(\tilde{y})$ can be written as

follows:

$$F(\tilde{y}) = C(e^{-\tilde{y}\tilde{A}} - I)^{-1}B = C(I - e^{\tilde{y}\tilde{A}})^{-1}e^{\tilde{y}\tilde{A}}B.$$

Due to the fact that matrix $\tilde{A}$ is Hurwitz, one concludes that $\lim_{\tilde{y}\to\infty} F(\tilde{y}) = 0$. As F is positive and non-increasing for any $y > 0$ and $\lim_{y\to\infty} F(y) = 0$, the unique solution $\tilde{y}^0$ which is computed via the transcendental equations

$$\tilde{y}^0 = \frac{\mu g_2}{\eta_2\eta_3} + \tilde{\lambda}_0 g_1 g_2 \sum_{j=1}^{3} \frac{\zeta_j}{e^{\eta_j \tilde{\tau}_0} - 1}, \qquad \tilde{\lambda}_0 = \tilde{\Psi}(\tilde{y}^0), \qquad \tilde{\tau}_0 = \tilde{\Phi}(\tilde{y}^0), \tag{5.42}$$

solves (5.32), that is $CQ(\tilde{y}^0) = \tilde{y}^0$.

After calculating $\tilde{y}^0$, $\tilde{\lambda}_0$ and $\tilde{\tau}_0$ from the equations (5.42), one can calculate the fixed point z^0 from (5.33). The third element of z^0 is $\tilde{y}^0$, which is calculated from equations (5.42), and its first and second elements are

$$z_1^0 = \frac{\tilde{\lambda}_0}{e^{\eta_1\tilde{\tau}_0} - 1}, \qquad z_2^0 = \frac{\mu}{\eta_2} + \frac{\tilde{\lambda}_0 g_1}{(\eta_1 - \eta_2)}\left[\frac{1}{e^{\eta_2\tilde{\tau}_0} - 1} - \frac{1}{e^{\eta_1\tilde{\tau}_0} - 1}\right]. \tag{5.43}$$

Step 3. In this step we show that the entire 1-cycle, generated from z^0, is positive if $\mu \geqslant -g_1V_1$. On one hand, every periodic solution of system (5.21) remains between its asymptotic bounds. On the other hand, in view of $\mu \geqslant -g_1V_1$, Proposition 5.5 ensures that the asymptotic bounds of system (5.21) are positive. Therefore, the entire 1-cycle is positive for any $t \geqslant 0$. This completes the proof of Theorem 5.6. □

Proof of Lemma 5.7. From $b_3 > b_2$ and assumptions (5.9), one concludes that $\rho^0 < 0$. First assume that $z = \begin{bmatrix} z_1 & z_2 & z_3 \end{bmatrix}^\top \geqslant 0$ is a 1-cycle solution of system (5.21). As $\rho^0 < 0$, the corresponding solution under mapping $\mathscr{M}^{-1}$ with $\rho = \rho^0$, given by

$$x = \begin{bmatrix} R & L & T \end{bmatrix}^\top \overset{(5.34)}{=} \begin{bmatrix} z_1 & z_2 - \rho^0 z_3 & z_3 \end{bmatrix}^\top,$$

is positive.

Now assume that $x = \begin{bmatrix} R & L & T \end{bmatrix}^\top \geqslant 0$ is a 1-cycle solution of system (5.2). The corresponding one under mapping $\mathscr{M}$ with $\rho = \rho^0$ is given by

$$z = \begin{bmatrix} z_1 & z_2 & z_3 \end{bmatrix}^\top \overset{(5.17)}{=} \begin{bmatrix} R & L + \rho^0 T & T \end{bmatrix}^\top.$$

Although $\rho^0 < 0$, we claim that $z_2 = L + \rho^0 T$ is positive. On one hand, $z(t)$ is a periodic solution of (5.21). On the other hand, Proposition 5.5 with $\mu \geqslant -g_1V_1$ implies that z_i $(i = 1, 2, 3)$ has positive asymptotic bounds. Therefore, $z \geqslant 0$ as it must remain between its asymptotic bounds. □

Proof of Lemma 5.8. Assumptions (5.9) and $b_2 > b_3$ imply that $\rho^0 > 0$. First let us assume that $x = \begin{bmatrix} R & L & T \end{bmatrix}^\top \geqslant 0$ is a 1-cycle solution of (5.2). The corresponding one under mapping $\mathscr{M}$ with $\rho = \rho^0$ is

$$z = \begin{bmatrix} z_1 & z_2 & z_3 \end{bmatrix}^\top \overset{(5.17)}{=} \begin{bmatrix} R & L + \rho^0 T & T \end{bmatrix}^\top,$$

which is positive.

Now assume that $z = \begin{bmatrix} z_1 & z_2 & z_3 \end{bmatrix}^\top \geqslant 0$ is a 1-cycle solution of system (5.21). Then the corresponding solution under mapping $\mathscr{M}^{-1}$ with $\rho = \rho^0$ is

$$x = \begin{bmatrix} R & L & T \end{bmatrix}^\top \overset{(5.34)}{=} \begin{bmatrix} z_1 & z_2 - \rho^0 z_3 & z_3 \end{bmatrix}^\top.$$

As $\rho^0 > 0$, the positivity of $L = z_2 - \rho^0 z_3$ is not ensured, and hence some periodic solutions of system (5.21) may be potentially mapped to infeasible solutions of system (5.2).

We know that the 1-cycle solution $z(t)$ of (5.21) stays between its asymptotic bounds for any $t \geqslant 0$. As $\rho^0 > 0$, the minimum value of $L = z_2 - \rho^0 z_3$ occurs when z_2 is in its lower asymptotic bound (i.e., V_2), and z_3 is in its upper asymptotic bound (i.e., U_3). So if $V_2 - \rho^0 U_3 \geqslant 0$, then $L \geqslant 0$. Substituting V_2 and U_3 from (5.27) result in

$$\begin{aligned} V_2 - \rho^0 U_3 &= \frac{(g_1 V_1 + \mu)\eta_3 - (g_1 U_1 + \mu)\rho^0 g_2}{\eta_2 \eta_3} \\ &= \frac{g_1(\eta_3 V_1 - \rho^0 g_2 U_1) + \mu b_3}{\eta_2 \eta_3}, \end{aligned}$$

which is positive if and only if

$$\mu \geqslant \frac{g_1}{b_3}\Xi, \qquad \Xi := \rho^0 g_2 U_1 - \eta_3 V_1.$$

It can be readily seen that $\rho^0 \to 0$ and $\eta_3 \to b_3$ as $k \to 0$. Therefore, $\frac{g_1}{b_3}\Xi \to -g_1 V_1$ as $k \to 0$, and hence the parameter μ can be chosen to be negative for a sufficiently small $k > 0$.

It is verified that $\Xi < 0$ if and only if

$$\gamma < 2\beta, \tag{5.44}$$

where γ is defined in (5.14). If $\gamma \leqslant 0$, then the inequality (5.44) automatically holds and the periodic solution $z(t)$ is positive when $\mu \geqslant \frac{g_1}{b_3}\Xi = \frac{g_1}{b_3}(\gamma - 2\beta)$ and $k < \frac{(b_3 - b_2)^2}{4g_2}$. However if $\gamma > 0$, one from (5.44) concludes that if $k < \frac{(b_3 - b_2)^2 - \gamma^2}{4g_2}$, then the periodic solution $z(t)$ is positive when $\mu \geqslant \frac{g_1}{b_3}\Xi$. Therefore, under the conditions given in Lemma 5.8, the periodic solution $z(t)$ is positive, and hence

there exists a one-to-one correspondence between 1-cycle solutions of systems (5.2) and (5.21). □

Now we use Theorem 5.6 and Lemmas 5.7 and 5.8 to prove Theorem 5.2.

Proof of Theorem 5.2. Assume that conditions (5.9) hold. Then under mapping $\mathscr{M}$ with $\rho = \rho^0$ defined in (5.12), system (5.2) is transformed to system (5.21), as described in Section 5.4.1. In view of Theorem 5.6, there exists a unique 1-cycle solution $z(t)$ to (5.21).

Now we turn to prove that, under the conditions given in Theorem 5.2, $z(t)$ is mapped to a positive solution $x(t)$ of (5.2). First let us assume that $b_3 > b_2$. In view of $\mu \geqslant -g_1 V_1$, any 1-cycle solution of (5.21) is positive, and there exists a one-to-one correspondence between periodic solutions of systems (5.2) and (5.21). Therefore, under mapping $\mathscr{M}^{-1}$ with $\rho = \rho^0$, the unique and positive 1-cycle solution $z(t)$ of (5.21) is mapped to a unique and positive 1-cycle solution $x(t)$ of (5.2) with the initial point $x^0 = (z_1^0, z_2^0 - \rho^0 \tilde{y}^0, \tilde{y}^0)$ where z_1^0, z_2^0 are computed by solving the equation (5.33), and $\tilde{y}^0$ is calculated by solving the transcendental equations (5.42).

Now assume that $b_2 > b_3$. The condition $\mu \geqslant -g_1 V_1$ implies that any 1-cycle solution of system (5.21) is positive. On the other hand, from Lemma 5.8, both statements 1 and 2 of Theorem 5.2 ensure that there exists a one-to-one correspondence between periodic solutions of (5.2) and (5.21). Therefore, the mapping $\mathscr{M}^{-1}$ with $\rho = \rho^0$ maps the unique and positive 1-cycle solution $z(t)$ of (5.21) to a unique and positive 1-cycle solution $x(t)$ of (5.2) with the initial point $x^0 = (z_1^0, z_2^0 - \rho^0 \tilde{y}^0, \tilde{y}^0)$ where z_1^0, z_2^0 are given in (5.43), and $\tilde{y}^0$ is obtained by solving (5.42). In view of Remark 5.3, the statements of Theorem 5.2 are immediate. □

5.5 Concluding remarks

We have studied a pulse-modulated model of endocrine regulation, which is derived from the impulsive Goodwin's oscillator [15]. In this model, the feedback from Te to GnRH is described by pulse-amplitude-frequency modulation, while the feedback from Te to LH is described by an affine function.

Introduction of an affine feedback into the impulsive Goodwin's model allows us to use the theory developed in [15] for our non-cyclic endocrine system and investigate 1-cycle solutions of the system. Moreover, it allows us to suggest an identification procedure similar to [104, 105], because the affine feedback introduces two uncertain parameters, compared to the model in [15].

Although the dynamics of the extended system, similar to the one in [15], is linear between consecutive pulses, it is not, however, governed by a Metzler matrix, allowing thus some solutions to leave the positive orthant. Nevertheless,

we have proven that, for the extended system, the results of [15] (i.e. the existence, uniqueness and positivity of 1-cycle solutions) are still valid , under some conditions on the parameters of the affine feedback.

Part II

Application of Dynamical Systems to Microbiology

6

Parameter-robustness analysis from regular-perturbation perspective

We develop a tool based on bifurcation analysis for parameter-robustness analysis for a class of oscillators, and in particular, examine a biochemical oscillator model that describes the transition phase between social behaviors of myxobacteria. We provide a detailed analysis of such an oscillator and show that there exists some interval in parameter space where the behavior of the system is robust, i.e., the system behaves similarly for all parameter values. In more mathematical terms, we show the existence and convergence of trajectories to a limit cycle, and provide estimates of the parameter regimes under which such a behavior occurs. Further, we show that the reported convergence result is robust, in the sense that any small change in the parameters leads to the same qualitative behavior of the solution.

This chapter starts with an introduction, followed by the system description in Section 6.2. Local analysis and Hopf bifurcation analysis are presented in Sections 6.3 and 6.4, respectively. Global analysis, and the robustness of bifurcation with respect to parameter changes are carried out in Sections 6.5 and 6.6, respectively. This chapter ends with concluding remarks in Section 6.7.

6.1 Introduction

OSCILLATORS as theoretical models capture various oscillating behaviors in dynamical processes that have been studied in engineering [152], biology [168], neuroscience [65], medicine [52], biochemistry [45, 46], and other scientific fields. In this chapter, we investigate a biochemical oscillator that describes the behavior of *myxobacteria* during their development of a multicellular structure [73]. Myxobacteria are a particular group of soil bacteria that have two dogmatically different

types of social behavior: when food is abundant they live fairly isolated forming swarms, but when food is scarce, they aggregate into a multicellular organism. In the transition between the two types of behaviors, spatial wave patterns are produced, which is generally believed to be regulated by a certain "clock" that controls the direction of myxobacteria's motion. This clock has been suggested in [73] in the form of a biochemical oscillator model.

This oscillator is described by a three-dimensional ordinary differential equation, which will be further described in Section 6.2. From observations based on numerical simulations, it has been argued that the model is robust [73]. In particular, it has been argued that the overall behavior of the oscillator remains the same upon small variation of parameters. Correspondingly, the main contribution of this chapter is to formalize the above claims by means of rigorous mathematical bifurcation analysis. More precisely, we prove that there exists an open set of parameter values, under which the model is robust, and more importantly, we provide an estimate of such an interval. Furthermore, we show that for almost all initial conditions, and a certain range of parameter values, the trajectories converge to a finite number of periodic solutions, at least one of which is asymptotically stable. With these results we rule out the existence of chaotic and homoclinic solutions for the identified parameter interval. We emphasize that the methods and techniques used in this chapter are not confined to the analysis of the particular myxobacteria model, but rather applicable to a wide range of systems having oscillatory behavior.

6.2 System description

We study a mathematical model that describes several important properties of myxobacteria during development [73]. This model, known as the Frz system, is based on a negative feedback loop. The Frz system includes a methyltransferase (FrzF), the cytoplasmic methyl-accepting protein (FrzCD), and a protein kinase (FrzE). When two cells of myxobacteria collide with each by *direct end-to-end* contacts, a C-signal is produced. After the C-signal transmission, a protein called FruA is phosphorylated. The signal from phosphorylated FruA (FruA-P) activates the Frz proteins as follows [73]:

- the methyltransferase FrzF (FrzF*) is activated by the protein FruA-P;
- in response to FrzF*, the protein FrzCD is methylated (FrzCD-M);
- the phosphorylation of FrzE (FrzE-P) is activated by the methylated form of FrzCD;
- FrzF* is inhibited by the phosphorylated form of FrzE.

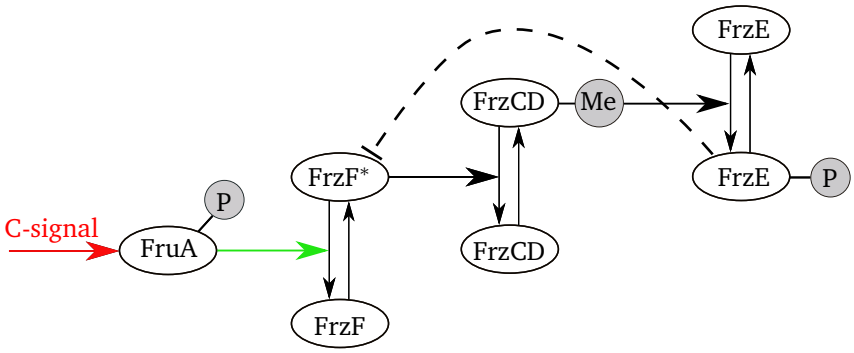

Figure 6.1: Essential components of the Frz system

A schematic representation of the Frz system is shown in Figure 6.1. For a more detailed explanation of the model and its biological background, see [73]. Denote f, c and e as the fraction of activated FrzF, methylated FrzCD, and phosphorylated FrzE, respectively. These fractions are given by [73]

$$f := \frac{[\text{FrzF}^*]}{[\text{FrzF}^*] + [\text{FrzF}]}, \quad c := \frac{[\text{FrzCD-M}]}{[\text{FrzCD}] + [\text{FrzCD-M}]}, \quad e := \frac{[\text{FrzE-P}]}{[\text{FrzE}] + [\text{FrzE-P}]}.$$

The interaction between the Frz proteins is modeled by Michaelis-Menten kinetics, and hence leads to the dynamical system

$$\begin{aligned} \frac{df}{dt} &= k_{\text{a}}(1-f) - k_{\text{d}} f e, \\ \frac{dc}{dt} &= k_{\text{m}}(1-c) f - k_{\text{dm}} c, \\ \frac{de}{dt} &= k_{\text{p}}(1-e) c - k_{\text{dp}} e, \end{aligned} \tag{6.1}$$

where

$$\begin{aligned} k_{\text{a}} &:= \frac{k_{\text{a}}^{\max}}{K_{\text{a}} + (1-f)}, & k_{\text{d}} &:= \frac{k_{\text{d}}^{\max}}{K_{\text{d}} + f}, \\ k_{\text{m}} &:= \frac{k_{\text{m}}^{\max}}{K_{\text{m}} + (1-c)}, & k_{\text{dm}} &:= \frac{k_{\text{dm}}^{\max}}{K_{\text{dm}} + c}, \\ k_{\text{p}} &:= \frac{k_{\text{p}}^{\max}}{K_{\text{p}} + (1-e)}, & k_{\text{dp}} &:= \frac{k_{\text{dp}}^{\max}}{K_{\text{dp}} + e}. \end{aligned} \tag{6.2}$$

The presence of variable e on the right-hand side in the first equation of (6.1) indicates the negative feedback exerted on the accumulation of the active form of FrzF by FrzE-P [73]. In (6.2), k_* and K_* denote, respectively, the maximum

effective rates and the Michaelis-Menten constants for each of the components involved in the Frz system.

In [73], the choices of the parameter values are as follows. First, the C-signal, denoted by $k_{\mathrm{a}}^{\max}$, is assumed to be constant. Next, the following parameter values are given

$$\begin{aligned} k_{\mathrm{d}}^{\max} &= 1 \text{ min}^{-1}, & k_{\mathrm{a}}^{\max} &= 0.08 \text{ min}^{-1}, \\ k_{\mathrm{m}}^{\max} &= k_{\mathrm{p}}^{\max} = 4 \text{ min}^{-1}, & k_{\mathrm{dm}}^{\max} &= k_{\mathrm{dp}}^{\max} = 2 \text{ min}^{-1}, \end{aligned}$$

and

$$K_{\mathrm{a}} = 10^{-2}, \qquad K_{\mathrm{d}} = K_{\mathrm{m}} = K_{\mathrm{dm}} = K_{\mathrm{p}} = K_{\mathrm{dp}} = 5 \times 10^{-3}. \tag{6.3}$$

It is observed *numerically* in [73] that under these parameter values, system (6.1) exhibits oscillatory behavior. Note that the reaction possesses the property of "zero-order ultrasensitivity"[73], meaning that the Michaelis-Menten constants (6.3) have to be *small* [48]. Since $K_{\mathrm{a}}, K_{\mathrm{d}}, K_{\mathrm{m}}, K_{\mathrm{dm}}, K_{\mathrm{p}}$ and K_{dp} are dimensionless Michaelis-Menten constants, we propose to set

$$\varepsilon := K_{\mathrm{a}} = 2K_{\mathrm{d}} = 2K_{\mathrm{m}} = 2K_{\mathrm{dm}} = 2K_{\mathrm{p}} = 2K_{\mathrm{dp}}.$$

We remark, however, that although $k_{\mathrm{a}}^{\max}$ is small as well, its unit is "min^{-1}" which cannot be unified with the Michaelis-Menten constants.

Substituting (6.2) in (6.1), and taking care of the previous considerations, we obtain the following dynamical system

$$\begin{aligned} \dot{f} &= \frac{0.08(1-f)}{\varepsilon + (1-f)} - \frac{2fe}{\varepsilon + 2f}, \\ \dot{c} &= \frac{8(1-c)f}{\varepsilon + 2(1-c)} - \frac{4c}{\varepsilon + 2c}, \\ \dot{e} &= \frac{8(1-e)c}{\varepsilon + 2(1-e)} - \frac{4e}{\varepsilon + 2e}. \end{aligned} \tag{6.4}$$

For the sake of brevity, we denote system (6.4) by

$$\dot{x} = G(x, \varepsilon), \tag{6.5}$$

where

$$x := \begin{bmatrix} f, & c, & e \end{bmatrix}^{\top}, \qquad G(x,\varepsilon) := \begin{bmatrix} G_1(x,\varepsilon), & G_2(x,\varepsilon), & G_3(x,\varepsilon) \end{bmatrix}^{\top},$$

and $G_1(x,\varepsilon)$, $G_2(x,\varepsilon)$, and $G_3(x,\varepsilon)$ are the right-hand sides of $\dot{f}$, $\dot{c}$, and $\dot{e}$, respectively.

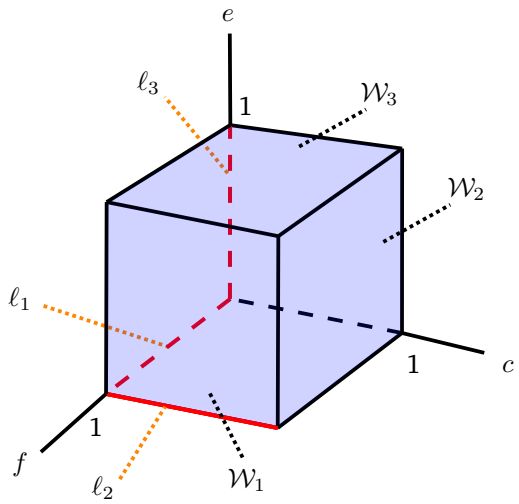

Figure 6.2: The unit cube $\mathcal{C}$, the walls $\mathcal{W}_j$, and the lines ℓ_j, $j = 1, 2, 3$.

Remark 6.1. From a biochemical point of view, the variables f, c, e of system (6.4) stand for fractions of activated protein concentrations. Therefore, their values are restricted to $[0, 1]$. Thus, from now on, we confine our analysis to the unit cube (see Figure 6.2), defined by

$$\mathcal{C} := \left\{ x \in \mathbb{R}^3 \,|\, x \in [0,1] \times [0,1] \times [0,1] \right\}.$$

Our numerical simulations (see Figure 6.3) show that system (6.4) has the following characteristics:

- the trajectories are contained in the unit cube $\mathcal{C}$ provided that they start within,
- for the particular value $\bar{\varepsilon} = 0.01$ used in [73], and in general, for a *sufficiently small* perturbation of $\bar{\varepsilon}$, the solutions are periodic,
- the solutions converge to a limit cycle.

Due to the fact that these three properties are highly interesting, because of their biological implications for understanding the developmental stage of maxobacteria, it is of great importance to provide rigorous mathematical analysis in addition to the simulation results reported so far. More precisely, since the Michaelis-Menten constants have not been experimentally identified [73], it is crucial to be able to predict the range of parameters under which the model produces the anticipated oscillatory behavior for which it has been designed. Towards this goal, we start our analysis of (6.4) by investigating its local properties in the next section.

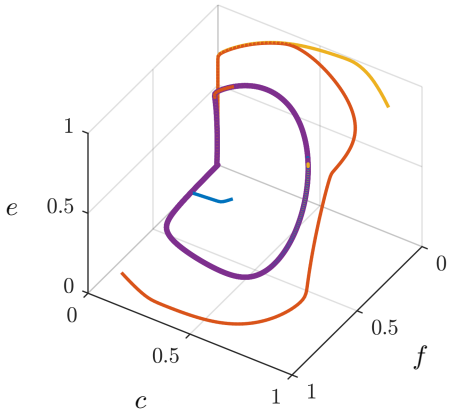

Figure 6.3: Trajectories of (6.4) for $\varepsilon = 0.01$ with three different initial conditions.

6.3 Local analysis

Some of the arguments that we use in this chapter are of a "regular perturbation" nature. Therefore, before providing any details, we show that the *local* properties around a unique equilibrium point of the vector field $\dot{x} = G(x, \varepsilon)$ can be regarded as a regular perturbation problem of $\dot{x} = G(x, 0)$ for "sufficiently small" $\varepsilon > 0$. More specifically, we show that $\dot{x} = G(x, 0)$ is structurally stable near its equilibrium point.

Hereafter, the interior and the boundary of a set $\mathcal{S} \subset \mathbb{R}^n$ are respectively denoted by $\mathring{\mathcal{S}}$ and $\partial\mathcal{S}$. We denote the boundary of the cube $\mathcal{C}$ by $\partial\mathcal{C} := \bigcup_{i=1}^{6} \mathcal{W}_i$ where (see Figure 6.2)

$$\begin{aligned} \mathcal{W}_1 &:= \{x \in \mathcal{C} \,|\, f = 1\}, & \mathcal{W}_2 &:= \{x \in \mathcal{C} \,|\, c = 1\}, \\ \mathcal{W}_3 &:= \{x \in \mathcal{C} \,|\, e = 1\}, & \mathcal{W}_4 &:= \{x \in \mathcal{C} \,|\, f = 0\}, \\ \mathcal{W}_5 &:= \{x \in \mathcal{C} \,|\, c = 0\}, & \mathcal{W}_6 &:= \{x \in \mathcal{C} \,|\, e = 0\}. \end{aligned} \tag{6.6}$$

The following lemma shows that for any $\varepsilon > 0$, the equation $G(x, \varepsilon) = 0$ does not have any solution on the boundary of $\mathcal{C}$.

Lemma 6.2. *For any $\varepsilon > 0$, the boundary of the cube $\mathcal{C}$ does not contain any equilibria of system* (6.4).

Proof. Let us show only one case on the wall $\mathcal{W}_1 = \{x \in \mathcal{C} \,|\, f = 1\}$, which exemplifies the situation for the rest of the walls. Restricted to $\mathcal{W}_1$, system $\dot{x} = G(x, \varepsilon)$

reads as

$$\dot{f} = -\frac{2e}{\varepsilon + 2} \tag{6.7a}$$

$$\dot{c} = \frac{8(1-c)}{\varepsilon + 2(1-c)} - \frac{4c}{\varepsilon + 2c} \tag{6.7b}$$

$$\dot{e} = \frac{8(1-e)c}{\varepsilon + 2(1-e)} - \frac{4e}{\varepsilon + 2e}. \tag{6.7c}$$

If $(1, c^*, e^*)$ is an equilibrium point of (6.7) then, from (6.7a) we have that necessarily $e^* = 0$. In turn, the latter implies in (6.7c) that $c^* = 0$. However, (6.7b) does not vanish at $(1, 0, 0)$. Therefore, $(1, 0, 0)$ is not an equilibrium. The claim is proven by following similar arguments on the rest of the walls defined in (6.6). □

It follows from Lemma 6.2 that if $\dot{x} = G(x, \varepsilon)$ has an equilibrium point for $\varepsilon > 0$, then it is necessarily located in the interior of $\mathcal{C}$. Another property of the cube $\mathcal{C}$ is that it is forward invariant under the flow generated by (6.4). Before proving this statement, we give the definition of a forward invariant set.

Definition 6.3. Let F be a smooth vector field on $\mathbb{R}^n$, and denote by $\phi(t, z) : \mathbb{R} \times \mathbb{R}^n \to \mathbb{R}^n$ the flow generated by F. We say that a set $S \subset \mathbb{R}^n$ is forward invariant if $s \in S$ implies $\phi(t, s) \in S$ for all $t \geqslant t_0 \in \mathbb{R}$.

Lemma 6.4. *For $\varepsilon > 0$, the cube $\mathcal{C}$ is forward invariant under the flow generated by* (6.4). *Moreover, every trajectory with the initial condition in the boundary of $\mathcal{C}$ evolves towards the interior of $\mathcal{C}$ in forward time.*

Proof. To prove that the cube $\mathcal{C}$ is forward invariant, we need to check the sign of the vector field $G(x, \varepsilon)$ defined by (6.4) restricted to the walls $\mathcal{W}_i$ given in (6.6). It can be readily seen that

$$\begin{aligned}
&\dot{f}|_{\mathcal{W}_1} = -\frac{2e}{\varepsilon + 2} \leqslant 0, && \dot{c}|_{\mathcal{W}_2} = -\frac{4}{\varepsilon + 2} < 0, && \dot{e}|_{\mathcal{W}_3} = -\frac{4}{\varepsilon + 2} < 0, \\
&\dot{f}|_{\mathcal{W}_4} = \frac{0.08}{\varepsilon + 1} > 0, && \dot{c}|_{\mathcal{W}_5} = \frac{8f}{\varepsilon + 2} \geqslant 0, && \dot{e}|_{\mathcal{W}_6} = \frac{8c}{\varepsilon + 2} \geqslant 0.
\end{aligned} \tag{6.8}$$

From (6.8) it follows that trajectories of (6.4) cannot leave the cube $\mathcal{C}$, which implies that $\mathcal{C}$ is forward invariant under the flow generated by $G(x, \varepsilon)$. Next, to show our second claim, note that there are three lines (see Figure 6.2) where the derivatives in (6.8) may vanish, namely,

$$\begin{aligned}
\ell_1 &:= \{x \in \mathcal{C} \,|\, x = (f, 0, 0)\}, \\
\ell_2 &:= \{x \in \mathcal{C} \,|\, x = (1, c, 0)\}, \\
\ell_3 &:= \{x \in \mathcal{C} \,|\, x = (0, 0, e)\}.
\end{aligned}$$

Let $\phi(t,x) : [t_0,\infty) \times \mathcal{C} \to \mathcal{C}$ denote the forward-flow generated by (6.4). So far, we have shown that for all initial conditions $\phi(t_0,x_0) = x_0 \in \Omega$, where $\Omega := \partial\mathcal{C}\backslash(\ell_1 \cup \ell_2 \cup \ell_3)$, the trajectory $\phi(t,x_0) \in \mathring{\mathcal{C}}$ for all $t > t_0$. Then, we need to check the behavior of the trajectories with those initial conditions on the lines ℓ_1, ℓ_2, and ℓ_3. So we proceed as follows. The vector field restricted to a line, say ℓ_1, is given by

$$\begin{aligned} \dot{f} &= \frac{0.08(1-f)}{\varepsilon + 1 - f} \\ \dot{c} &= \frac{8f}{\varepsilon + 2} \\ \dot{e} &= 0. \end{aligned} \tag{6.9}$$

From (6.9) we observe that $\dot{e} = 0$, and $\dot{c} > 0$ for $f \in (0,1)$. These two facts imply that (6.9) is transversal to the line $\ell_1|_{f\in(0,1)}$. Thus, we conclude that a trajectory with an initial condition in $\ell_1|_{f\in(0,1)}$ leaves such a line, and hence reaches Ω. Next, consider a trajectory with an initial condition in $\ell_1|_{f=0}$. In view of (6.9) one has that $\dot{f} > 0$ and hence the trajectory is tangent to ℓ_1. This implies that the trajectory reaches the line $\ell_1|_{f\in(0,1)}$, which we have discussed above. Similar arguments follow for the lines ℓ_2 and ℓ_3. This completes the proof. □

We now turn to the analysis of the equilibria of (6.4) inside the cube $\mathcal{C}$, i.e., when $x \in \mathring{\mathcal{C}}$. For the case $\varepsilon = 0$, the following lemma is given, whose proof follows from straightforward and standard computations.

Lemma 6.5. *Consider the vector field $\dot{x} = G(x,\varepsilon)$ defined by (6.4) with $\varepsilon = 0$. Then the following properties hold:*

1. *Let $x \in \mathring{\mathcal{C}}$. Then, the linear algebraic equation $G(x,0) = 0$ has the unique solution $x^0 = (0.5, 0.5, 0.08)$.*

2. *The equilibrium point x^0 is hyperbolic, that is, the Jacobian $D_xG(x,0)|_{x=x^0}$ has eigenvalues with nonzero real parts. Moreover, such eigenvalues satisfy $\lambda_1^0 < 0$ and $\lambda_{2,3}^0 = \alpha^0 \pm i\beta^0$, where $\alpha^0, \beta^0 > 0$.*

Now, assume that $x(\varepsilon) = \left(f^\varepsilon, c^\varepsilon, e^\varepsilon\right)$ is an equilibrium point of (6.4) such that $x(0) = x^0$, where x^0 is the equilibrium point of $\dot{x} = G(x,0)$ when $x \in \mathring{\mathcal{C}}$. Linearizing (6.4) at $x(\varepsilon)$ results in $\dot{x} = D_xG(x(\varepsilon),\varepsilon)x$ where $D_xG(x(\varepsilon),\varepsilon)$, which denotes the Jacobian matrix calculated at $x(\varepsilon)$, is given by

$$D_xG(x(\varepsilon),\varepsilon) := \begin{bmatrix} \eta_1^\varepsilon & 0 & \theta_1^\varepsilon \\ \theta_2^\varepsilon & \eta_2^\varepsilon & 0 \\ 0 & \theta_3^\varepsilon & \eta_3^\varepsilon \end{bmatrix}, \tag{6.10}$$

where

$$\begin{aligned}
\eta_1^\varepsilon &:= \frac{\partial G_1}{\partial f}\Big|_{x=x(\varepsilon)} = -\frac{2\varepsilon e^\varepsilon}{(\varepsilon+2f^\varepsilon)^2} - \frac{0.08\varepsilon}{(\varepsilon+1-f^\varepsilon)^2},\\
\eta_2^\varepsilon &:= \frac{\partial G_2}{\partial c}\Big|_{x=x(\varepsilon)} = -\frac{4\varepsilon}{(\varepsilon+2c^\varepsilon)^2} - \frac{8\varepsilon f^\varepsilon}{(\varepsilon+2(1-c^\varepsilon))^2},\\
\eta_3^\varepsilon &:= \frac{\partial G_3}{\partial e}\Big|_{x=x(\varepsilon)} = -\frac{4\varepsilon}{(\varepsilon+2e^\varepsilon)^2} - \frac{8\varepsilon c^\varepsilon}{(\varepsilon+2(1-e^\varepsilon))^2},
\end{aligned} \tag{6.11}$$

$$\begin{aligned}
\theta_1^\varepsilon &:= \frac{\partial G_1}{\partial e}\Big|_{x=x(\varepsilon)} = \frac{-2f^\varepsilon}{\varepsilon+2f^\varepsilon},\\
\theta_2^\varepsilon &:= \frac{\partial G_2}{\partial f}\Big|_{x=x(\varepsilon)} = \frac{8(1-c^\varepsilon)}{\varepsilon+2(1-c^\varepsilon)},\\
\theta_3^\varepsilon &:= \frac{\partial G_3}{\partial c}\Big|_{x=x(\varepsilon)} = \frac{8(1-e^\varepsilon)}{\varepsilon+2(1-e^\varepsilon)}.
\end{aligned} \tag{6.12}$$

Remark 6.6. In order to compute the equilibrium point $x(\varepsilon)$ of (6.4) when $\varepsilon > 0$, one needs to solve simultaneously the equations $G_i(x,\varepsilon) = 0$, $i = 1,2,3$, which results in

$$0.04(1-f)(\varepsilon+2f) - (\varepsilon+1-f)fe = 0, \tag{6.13a}$$
$$2(1-c)(\varepsilon+2c)f - (\varepsilon+2(1-c))c = 0, \tag{6.13b}$$
$$2(1-e)(\varepsilon+2e)c - (\varepsilon+2(1-e))e = 0, \tag{6.13c}$$

each of which is a polynomial of degree 3. If, for example, we solve e from (6.13a) and substitute it in (6.13c), the obtained equation can then be solved for c. This solution in turn is substituted in (6.13b), leading to a 9th-degree polynomial of f with ε-dependent coefficients. Since it is not easy (or might be impossible) to analytically find the roots of this 9th-degree polynomial when $\varepsilon > 0$, we use regular perturbation arguments to study (6.4).

From Lemma 6.5 we know that the equilibrium point of $\dot{x} = G(x,0)$, when $x \in \mathring{\mathcal{C}}$, is unique and hyperbolic. The following lemma shows that all the *local* properties of x^0 persist under sufficiently small perturbations of ε. That is $\dot{x} = G(x,0)$ is structurally stable around x^0, see [95, Theorem 2.2].

Lemma 6.7. *The vector field $\dot{x} = G(x,\varepsilon)$ defined by* (6.4) *has the following properties:*

1. *The Jacobian $D_x G(x,\varepsilon)$ is a smooth function of ε for all $x \in \mathring{\mathcal{C}}$.*
2. *For sufficiently small $\varepsilon > 0$, the equilibrium x^0 perturbs to the unique equilibrium $x(\varepsilon) = x^0 + \mathcal{O}(\varepsilon)$, which has the same local stability properties as x^0.*

Proof. The nonzero entries of the Jacobian $D_x G(x,\varepsilon)$, defined in (6.10), can be rewritten as an additive combination of terms of the form

$$Q(x,\varepsilon) := \frac{A(x,\varepsilon)}{B(x,\varepsilon)+C(x)}, \tag{6.14}$$

where $A(x,\varepsilon), B(x,\varepsilon)$ and $C(x)$ are polynomials satisfying: i) $B(x,\varepsilon)+C(x)>0$ for all $x\in\mathcal{C}$ and $\varepsilon>0$, ii) $B(x,0)=0$, iii) $C(x)>0$ for all $x\in\mathring{\mathcal{C}}$, and iv) $C(x)=0$ if $x\in\partial\mathcal{C}$, that is, $C(x)$ vanishes only in the boundary of $\mathcal{C}$. Thus, to show the first property holds, it suffices to show that (6.14) is a smooth function of ε in $\mathring{\mathcal{C}}$. It is clear that the only point where the k-th derivatives of $Q(x,\varepsilon)$ with respect to ε, i.e. $D^k_\varepsilon Q(x,\varepsilon)$, $k=0,1,\ldots$, are undefined is whenever $B(x,\varepsilon)+C(x)=0$. From the above properties $B(x,\varepsilon)+C(x)$ may vanish only when $\varepsilon=0$. Thus, to ensure that $D^k_\varepsilon Q(x,\varepsilon)$ is well-defined for $\varepsilon\geqslant 0$, we just need $x\in\mathring{\mathcal{C}}$. Next, the first part of the second property follows from Lemma 6.5, and the implicit function theorem. For the stability properties of $x(\varepsilon)$, it follows from the fact that the eigenvalues of a matrix, depending smoothly on a parameter, vary continuously with respect to such a parameter [95]. □

The characteristic polynomial corresponding to the Jacobian matrix $D_x G(x(\varepsilon),\varepsilon)$, defined in (6.10), is given by

$$P(\lambda,\varepsilon) = \lambda^3 + k_1^\varepsilon\lambda^2 + k_2^\varepsilon\lambda + k_3^\varepsilon,$$

where

$$\begin{aligned} k_1^\varepsilon &:= -(\eta_1^\varepsilon+\eta_2^\varepsilon+\eta_3^\varepsilon),\\ k_2^\varepsilon &:= \eta_1^\varepsilon\eta_2^\varepsilon+\eta_1^\varepsilon\eta_3^\varepsilon+\eta_2^\varepsilon\eta_3^\varepsilon,\\ k_3^\varepsilon &:= -(\eta_1^\varepsilon\eta_2^\varepsilon\eta_3^\varepsilon+\theta_1^\varepsilon\theta_2^\varepsilon\theta_3^\varepsilon). \end{aligned} \tag{6.15}$$

Remark 6.8. For any $\varepsilon>0$, it follows from Lemmas 6.4 and 6.7, and equations (6.11) and (6.12) that $\eta_i^\varepsilon<0$ $(i=1,2,3)$, $\theta_1^\varepsilon<0$, and $\theta_2^\varepsilon,\theta_3^\varepsilon>0$. Hence, $k_i^\varepsilon>0$.

The equilibrium $x(\varepsilon)$ is stable when all roots of $P(\lambda,\varepsilon)$ have negative real parts, and unstable if *at least one* of the roots has a positive real part. Applying the Routh-Hurwitz criterion and denoting

$$\Gamma(\varepsilon) := k_1^\varepsilon k_2^\varepsilon - k_3^\varepsilon, \tag{6.16}$$

the following proposition is given for the stability of $x(\varepsilon)$.

Proposition 6.9. *For any $\varepsilon>0$, the equilibrium point $x(\varepsilon)$ is stable if $\Gamma(\varepsilon)>0$, and is unstable if $\Gamma(\varepsilon)<0$.*

Proof. According to the Routh-Hurwitz criterion, the equilibrium point $x(\varepsilon)$ is stable if $k_1^\varepsilon, k_3^\varepsilon, \Gamma(\varepsilon) > 0$, and it is unstable if at least one of these conditions is violated. We know from Remark 6.8 that $k_1^\varepsilon,\ k_3^\varepsilon > 0$. So, the only quantity that can change the stability of the equilibrium point is $\Gamma(\varepsilon)$. Thus, based on the Routh-Hurwitz criterion, the equilibrium point is stable if $\Gamma(\varepsilon)$ is positive, and it is unstable if it is negative. □

Remark 6.10. From Remark 6.8 we know that the coefficients of the characteristic polynomial $P(\lambda, \varepsilon)$ are positive ($k_i^\varepsilon > 0$) when $\varepsilon > 0$. Therefore, due to the fact that $\det(D_x G(x(\varepsilon), \varepsilon)) < 0$, one of its roots is negative and the other two are either real of the same sign or complex-conjugated. However, we know from Lemma 6.7 that the eigenvalues of $D_x G(x^0, 0)$ satisfy $\lambda_1^0 < 0$ and $\lambda_{2,3}^0 = \alpha^0 \pm i\beta^0$, where $\alpha^0, \beta^0 > 0$. Moreover, from the structural stability of $\dot{x} = G(x, 0)$ we know that for sufficiently small $\varepsilon > 0$, the eigenvalues of $D_x G(x(\varepsilon), \varepsilon)$ satisfy $\lambda_1(\varepsilon) < 0$ and $\lambda_{2,3}(\varepsilon) = \alpha(\varepsilon) \pm i\beta(\varepsilon)$ with $\alpha(\varepsilon), \beta(\varepsilon) > 0$, where $\lambda_i(0) = \lambda_i^0$, $\alpha(0) = \alpha^0$, and $\beta(0) = \beta^0$.

What we have studied so far are the local stability properties of the equilibrium point of (6.4) and the forward invariance of $\mathcal{C}$. However, since we are investigating a biochemical oscillator model, one of the most important questions is about the existence of periodic solutions. In particular, it is necessary to describe the relationship between the parameter ε and the existence of and the convergence to such solutions. Furthermore, from Remark 6.10 we know that the equilibrium point $x(\varepsilon)$ has a pair of associated complex-conjugated eigenvalues. This motivates the further analysis via Hopf bifurcation theory, presented in the following section.

6.4 Hopf bifurcation analysis

In this section we give sufficient conditions for the existence of periodic solutions of (6.4). In principle, the existence of such solutions depends on the parameter ε. We know from Remark 6.10 that $\lambda_1(\varepsilon) < 0$ and $\lambda_{2,3}(\varepsilon) = \alpha(\varepsilon) \pm i\beta(\varepsilon)$, with $\alpha(\varepsilon),\ \beta(\varepsilon) > 0$, for sufficiently small $\varepsilon > 0$. Therefore, upon variation of ε, the eigenvalues $\lambda_{2,3}(\varepsilon)$ may cross transversally the imaginary axis. This would allow us to apply the Hopf bifurcation theorem to prove the existence of periodic solutions. The first step is then to further study the behavior of $\alpha(\varepsilon)$.

Lemma 6.11. *For any $\varepsilon \geqslant 0$, the real part of $\lambda_{2,3}(\varepsilon)$ satisfies the equation*

$$\Gamma(\varepsilon) = -2\alpha(\varepsilon)[(k_1^\varepsilon + 2\alpha(\varepsilon))^2 + k_2^\varepsilon], \tag{6.17}$$

where $\Gamma(\varepsilon)$ is defined in (6.16).

Proof. Since $P(\lambda,\varepsilon)$ is a cubic function with respect to λ, we may assume without loss of generality that its zeros are $\lambda_1(\varepsilon)\in\mathbb{R}$ and $\lambda_{2,3}(\varepsilon)=\alpha(\varepsilon)\pm i\beta(\varepsilon)$. Based on the Vieta's formulas, the following relations among such zeros hold:

$$\begin{aligned}
&\lambda_1^\varepsilon+\lambda_2^\varepsilon+\lambda_3^\varepsilon=-k_1^\varepsilon,\\
&\lambda_1^\varepsilon\lambda_2^\varepsilon+\lambda_1^\varepsilon\lambda_3^\varepsilon+\lambda_2^\varepsilon\lambda_3^\varepsilon=k_2^\varepsilon,\\
&\lambda_1^\varepsilon\lambda_2^\varepsilon\lambda_3^\varepsilon=-k_3^\varepsilon,
\end{aligned}\tag{6.18}$$

where k_i^ε are defined in (6.15). Then

$$\begin{aligned}
\Gamma(\varepsilon)&=k_1^\varepsilon k_2^\varepsilon-k_3^\varepsilon\\
&=-(\lambda_1^\varepsilon+\lambda_2^\varepsilon+\lambda_3^\varepsilon)k_2^\varepsilon+\lambda_1^\varepsilon\lambda_2^\varepsilon\lambda_3^\varepsilon\\
&=-\lambda_1^\varepsilon(k_2^\varepsilon-\lambda_2^\varepsilon\lambda_3^\varepsilon)-(\lambda_2^\varepsilon+\lambda_3^\varepsilon)k_2^\varepsilon\\
&=-\lambda_1^\varepsilon[2\alpha(\varepsilon)\lambda_1^\varepsilon]-2\alpha(\varepsilon)k_2^\varepsilon\\
&=-2\alpha(\varepsilon)[(\lambda_1^\varepsilon)^2+k_2^\varepsilon]\\
&=-2\alpha(\varepsilon)[(k_1^\varepsilon+2\alpha(\varepsilon))^2+k_2^\varepsilon].
\end{aligned}$$

□

From Lemma 6.11 and the fact that $k_2^\varepsilon>0$ (Remark 6.8) we have $\operatorname{sign}(\Gamma(\varepsilon))=-\operatorname{sign}(\alpha(\varepsilon))$ for any $\varepsilon\geqslant 0$. So, one concludes that if there exists ε^0 such that $\Gamma(\varepsilon^0)=0$, then the real part of the eigenvalues is zero at ε^0, i.e. $\alpha(\varepsilon^0)=0$. Therefore ε^0 is the bifurcation point at which the equilibrium point switches from being instable to stable. This change of stability is an important factor towards showing the existence of periodic solutions by means of the Hopf bifurcation theorem [118].

Theorem 6.12 (Hopf bifurcation theorem)**.** *Assume that system $\dot{z}=F(z,\mu)$, with $(z,\mu)\in\mathbb{R}^n\times\mathbb{R}$, has the equilibrium point $(z(\mu^0),\mu^0)$ where the vector field F is sufficiently smooth on a sufficiently large open set containing $(z(\mu^0),\mu^0)$. Assume that the following properties hold:*

1. *The Jacobian $D_zF\big|_{(z(\mu^0),\mu^0)}$ has a simple pair of pure imaginary eigenvalues $\lambda(\mu^0)$ and $\overline{\lambda(\mu^0)}$, and the real parts of the other eigenvalues are not zero,*
2. $\dfrac{d}{d\mu}(Re\lambda(\mu))\big|_{\mu=\mu^0}\neq 0.$

Then the dynamics $\dot{z}=F(z,\mu)$ undergo a Hopf bifurcation at $(z(\mu^0),\mu^0)$, that is, in a sufficiently small neighborhood of $(z(\mu^0),\mu^0)$, a family of periodic solutions exists.

The following lemma demonstrates the existence of periodic solutions for (6.4) with $\varepsilon>0$.

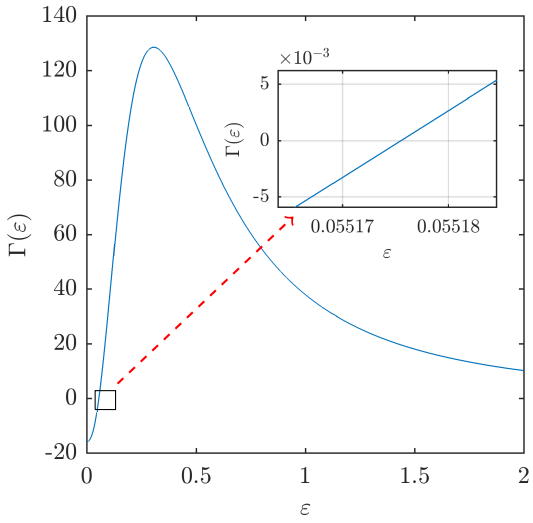

Figure 6.4: The curve Γ with respect to ε, and the zoom-in of Γ near the bifurcation value $\varepsilon = \varepsilon^0$.

Lemma 6.13. *For system* (6.4) *parametrized by* $\varepsilon > 0$*, there exists* $\varepsilon^0 > 0$ *such that the dynamics* $\dot{x} = G(x, \varepsilon)$ *undergo a Hopf bifurcation at* $(x(\varepsilon^0), \varepsilon^0)$.

Proof. Recall from Remark 6.10 that for sufficiently small $\varepsilon > 0$, we have $\lambda_1(\varepsilon) < 0$, and the other two eigenvalues are in the form of $\lambda_{2,3}(\varepsilon) = \alpha(\varepsilon) + i\beta(\varepsilon)$. On one hand, it follows from Lemma 6.7 that $\Gamma(\varepsilon)$ is a smooth function of ε. On the other hand, $\Gamma(0) < 0$ and $\Gamma(1) > 0$ (which is computed numerically from Remark 6.6). Therefore, there exists $0 < \varepsilon^0 < 1$ such that $\Gamma(\varepsilon^0) = 0$, which means that the eigenvalues $\lambda_{2,3}(\varepsilon)$ cross the imaginary axis. In Figure 6.4 we observe that $\Gamma'(\varepsilon^0) > 0$. Due to the latter fact, there exists a neighborhood $\mathcal{N} = (\varepsilon^0 - \delta, \varepsilon^0 + \delta)$, with $\delta > 0$, such that $\Gamma'(\varepsilon) > 0$ for all $\varepsilon \in \mathcal{N}$. In view of Lemma 6.11, one concludes that $\alpha(\varepsilon^0) = 0$. Therefore, $D_x G(x(\varepsilon^0), \varepsilon^0)$ has a pair of pure imaginary eigenvalues $\pm i\beta(\varepsilon^0)$, and the other eigenvalue is negative (i.e. $\lambda_1(\varepsilon^0) < 0$, Remark 6.10), satisfying assumption 1 of Theorem 6.12.

In addition, the differentiation of (6.17) with respect to ε gives

$$\Gamma'(\varepsilon) = -2\left(\alpha'(\varepsilon)\left[(k_1^\varepsilon + 2\alpha(\varepsilon))^2 + k_2^\varepsilon\right] + \alpha(\varepsilon)\frac{d}{d\varepsilon}\left[(k_1^\varepsilon + 2\alpha(\varepsilon))^2 + k_2^\varepsilon\right]\right). \quad (6.19)$$

Now, due to the fact that $\alpha(\varepsilon^0) = 0$, evaluating (6.19) at $\varepsilon = \varepsilon^0$ results in

$$\Gamma'(\varepsilon^0) = -2\alpha'(\varepsilon^0)\left[(k_1^{\varepsilon^0})^2 + k_2^{\varepsilon^0}\right], \quad (6.20)$$

and hence

$$\alpha'(\varepsilon^0) = \frac{\Gamma'(\varepsilon^0)}{-2\left[(k_1^{\varepsilon^0})^2 + k_2^{\varepsilon^0}\right]}. \tag{6.21}$$

Note that from Remark 6.8 we know that $k_1^{\varepsilon^0}, k_2^{\varepsilon^0} > 0$, and hence (6.21) is well-defined. Recalling $\Gamma'(\varepsilon^0) > 0$, one concludes that $\alpha'(\varepsilon^0) < 0$, and hence the second assumption of Theorem 6.12 is satisfied. Therefore, the dynamics $\dot{x} = G(x, \varepsilon)$ undergo a Hopf bifurcation at $(x(\varepsilon^0), \varepsilon^0)$. □

From Lemma 6.13 we know that system (6.4) undergoes a Hopf bifurcation at $(x(\varepsilon^0), \varepsilon^0)$. The numerical continuation software MATCONT [21] is used to track such a bifurcation. The value of the bifurcation parameter, computed by MATCONT, is $\varepsilon^0 \simeq 0.05517665$. The equilibrium point corresponding to ε^0 is

$$x(\varepsilon^0) = (0.48668602,\ 0.37822906,\ 0.07633009).$$

The bifurcation diagrams of f, c, and e with respect to ε, and their zoom-ins around the Hopf bifurcation point "H" are presented in Figures 6.5(a), 6.5(b) and 6.5(c), respectively. In Figure 6.5, the black curves depict the position of the equilibrium point $x(\varepsilon)$; the dashed black curve corresponds to the case when $x(\varepsilon)$ is unstable, while the solid one represents the case when $x(\varepsilon)$ is stable. On the other hand, the red and blue curves correspond to periodic solutions; the solid blue curve indicates that the periodic solution is stable, while the dashed red one shows that the periodic solution is unstable. For each fixed ε, these curves provide the maximum and the minimum values of each variable along the corresponding periodic solution. Moreover, in Figures 6.5(a), 6.5(b) and 6.5(c) in the zoom-ins around the Hopf bifurcation point "H", we observe that for a range of ε started from ε^0, both stable and unstable periodic solutions exist simultaneously.

In this section we have shown the existence of periodic solutions in (6.4) for $\varepsilon \in (0, \varepsilon^0)$. However, the presented results do not consider the stability of the periodic solutions. Furthermore, the number of periodic solutions is still unknown. These issues are treated in next section.

6.5 Global behavior of solutions

The local analysis performed in the previous section does not fully capture the behavior of the solutions of (6.4). For example, we cannot conclude directly from the previous results whether the trajectories are oscillatory or they evolve in some unexpected way, e.g. chaotically. In this section, we show that when the equilibrium point $x(\varepsilon)$ of (6.4) is unstable, *almost all* trajectories converge to periodic solutions, ruling out chaotic behavior and the existence of homoclinic solutions. To this end, we study the structure of the ω-limit set of (6.4).

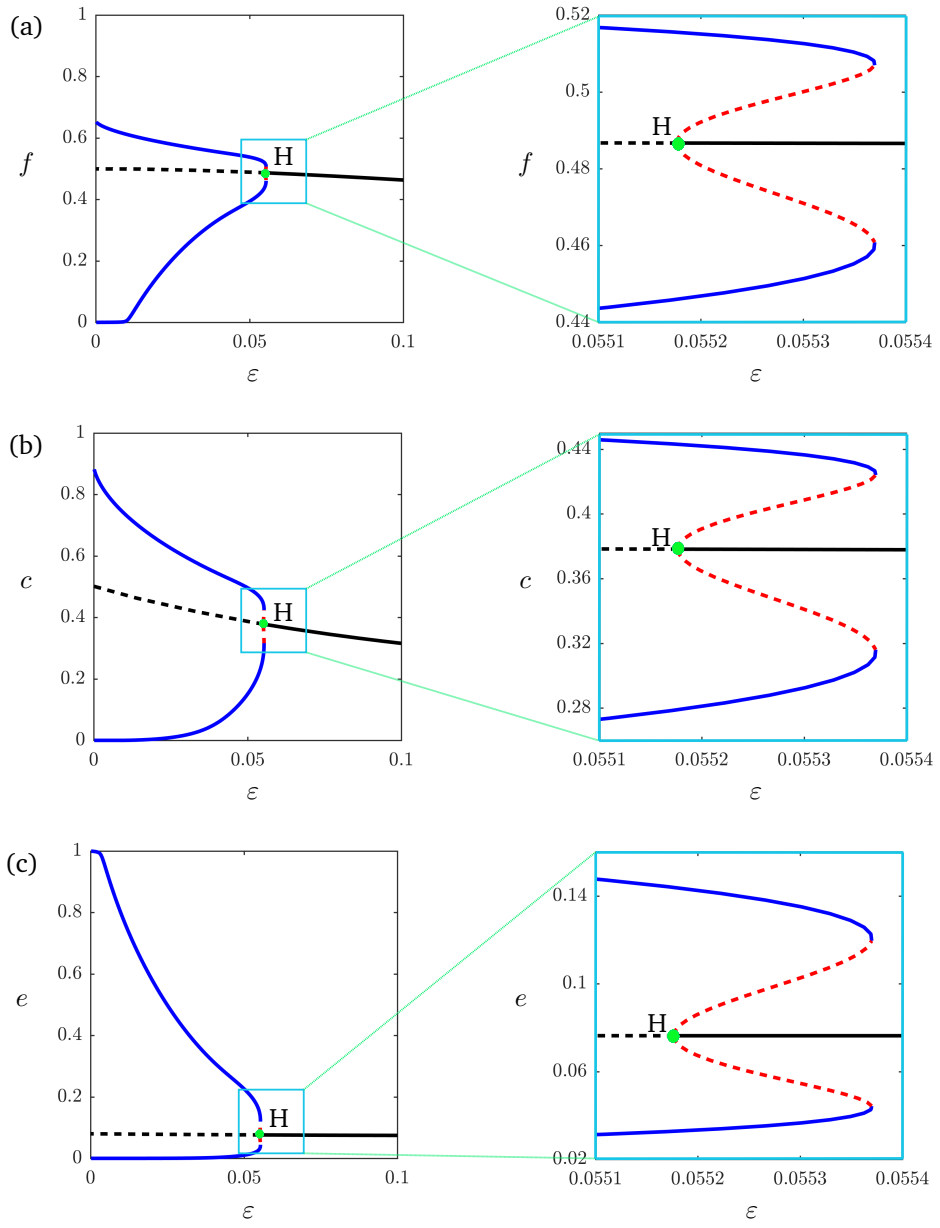

Figure 6.5: In the left-side of Figures (a), (b), and (c), the bifurcation diagrams of f, c and e with respect to ε is given, whose zoom-ins around the Hopf bifurcation point, denoted by "H", are given on the right-side. The black curve depicts the position of the unique equilibrium point $x(\varepsilon)$; the dashed (resp. solid) section of this curve represents the interval within which $x(\varepsilon)$ is unstable (resp. stable). The solid blue and the dashed red curves describe the amplitude of oscillation for each of the variables. The solid blue curve corresponds to a stable periodic solution, while the dashed red curve indicates an unstable one.

In general, an ω-limit set can be empty. However, if a solution is *bounded*, then its ω-limit set is nonempty, closed and connected [167]. In the context of system (6.4), the ω-limit set of a trajectory with an initial condition in $\mathcal{C}$ is non-empty due to the forward invariance of $\mathcal{C}$ (see Lemma 6.4).

For *planar* autonomous dynamical systems, the structure of the ω-limit set of solutions is given by the celebrated Poincaré-Bendixson theorem. This theorem states that the ω-limit set of a bounded solution is either (i) an equilibrium point, (ii) a closed trajectory, or (iii) the union of equilibria and the trajectories connecting them [60]. The latter are referred to as *heteroclinic* solutions when they connect distinct points, and *homoclinic* solutions when they connect a point to itself. Although the Poincaré-Bendixson theorem is not applicable to systems of dimensions higher than 2, it holds for *monotone* cyclic feedback systems [103]. For the reader's convenience, we formulate the results of [103] on the positively invariant domain $\mathbb{R}^n_+ := [0,\infty)^n$ with bounded solutions as follows.

Consider a system of the form

$$\dot{y}_i = h_i(y_{i-1}, y_i), \qquad i = 1, 2, ..., n, \tag{6.22}$$

where y_0 is interpreted as y_n, and the nonlinearity $h = (h_1, h_2, ..., h_n)$ is assumed to be C^1-smooth on $\mathbb{R}^n_+$. Systems of the form (6.22) are called cyclic. The *fundamental* assumption on (6.22) is that the variable y_{i-1} influences h_i *monotonically*. So, it is assumed that for some $\delta_j \in \{-1, 1\}$, the conditions

$$\delta_i \frac{\partial h_i(y_{i-1}, y_i)}{\partial y_{i-1}} > 0, \qquad i = 1, 2, ..., n, \tag{6.23}$$

hold, meaning that the functions h_i are *strictly* monotone in y_{i-1}. Moreover, δ_i describes whether the role of y_{i-1} is to reduce ($\delta_i = -1$) the growth of y_i, or to augment ($\delta_i = 1$) it. The product

$$\Delta := \prod_{i=1}^{n} \delta_i \tag{6.24}$$

describes whether the entire system has positive feedback ($\Delta = 1$) or negative feedback ($\Delta = -1$). A cyclic system (6.22) that satisfies conditions (6.23) is called a *monotone cyclic feedback system*, and it is shown in [103] that they have the Poincaré-Bendixson properties. We recall this important result in Theorem 6.16. Before that, we give the following definitions.

Definition 6.14. The distance between two sets $S_1, S_2 \subset \mathbb{R}^n$ is denoted and defined by

$$d(S_1, S_2) := \inf\{\|s_1 - s_2\| \ : \ s_1 \in S_1, s_2 \in S_2\}, \tag{6.25}$$

where $\|\cdot\|$ is an arbitrary norm in $\mathbb{R}^n$.

Definition 6.15. [127] Let F be a smooth vector field on $\mathbb{R}^n$ and denote by $\phi(t,z):\mathbb{R}\times\mathbb{R}^n\to\mathbb{R}^n$ the flow generated by F.

- A set $K\subset\mathbb{R}^n$ is said to *attract* a set $M\subset\mathbb{R}^n$, if $K\neq\varnothing$ and $d(K,\phi(t,M))\to 0$ as $t\to\infty$. We also say that M is attracted by K.
- A set K is called an *attractor* of M, if K is invariant and attracts M. In this situation, we also say that M has the attractor K. The set K is called a *compact attractor* of M if, in addition, K is compact.

Next, for brevity, we recall the relevant results of Theorems 4.1 and 4.3 of [103] as follows.

Theorem 6.16. *Let the cyclic system* (6.22) *satisfy conditions* (6.23) *in* $\mathbb{R}^n_+$. *Then the following statements hold.*

1. *Assume that* $\mathbb{R}^n_+$ *is forward invariant for* (6.22)*, and that it contains a unique equilibrium point* y^*. *Then the structure of the* ω*-limit set of any bounded solution of the system is either*
   (a) *the equilibrium point* y^*,
   (b) *a nonconstant periodic solution, or*
   (c) *the equilibrium point* y^* *together with a collection of solutions homoclinic to* y^*. *This case does not occur if*
   $$\Delta\det(-D_yh(y^*))<0, \tag{6.26}$$
   where $D_yh(y^*)$ *denotes the Jacobian matrix of system* (6.22) *at* y^*.
2. *Suppose that* (6.22) *satisfies* $\Delta=-1$*, and possesses a compact attractor* $K\subset\mathring{\mathbb{R}}^n_+$. *Assume that* K *contains a unique equilibrium point* y^**, and that* $D_yh(y^*)$ *satisfies* (6.26) *and has at least two eigenvalues with positive real parts. Then* (6.22) *has at least one, but no more than a finite number of nontrivial periodic solutions. Moreover, at least one of such solutions is orbitally asymptotically stable.*

Remark 6.17. [103] In Theorem 6.16, $\mathbb{R}^n_+$ can be replaced by any other forward invariant closed *convex* domain Ω containing a single equilibrium point.

The following theorem describes the global behavior of solutions of system (6.4).

Theorem 6.18. *For sufficiently small $\varepsilon > 0$, and for almost all initial conditions $x_0 \in \mathcal{C}$, the trajectories $\phi(t, x_0)$ of (6.4) converge to a finite number of non constant periodic solutions. Moreover, at least one of such solutions is orbitally asymptotically stable.*

Proof. First of all, to show that (6.4) is cyclic, note that it can be written as

$$\begin{aligned} \dot{f} &= G_1^\varepsilon(e, f), \\ \dot{c} &= G_2^\varepsilon(f, c), \\ \dot{e} &= G_3^\varepsilon(c, e), \end{aligned} \tag{6.27}$$

where $G_1^\varepsilon(e, f)$, $G_2^\varepsilon(f, c)$, and $G_3^\varepsilon(c, e)$ denote the right-hand sides of $\dot{f}$, $\dot{c}$, and $\dot{e}$, respectively, presented in (6.4). Thus, system (6.4) is cyclic for any ε. Next, recalling Remark 6.8, we have that $\frac{\partial G_1^\varepsilon}{\partial e} < 0$, $\frac{\partial G_2^\varepsilon}{\partial f} > 0$, and $\frac{\partial G_3^\varepsilon}{\partial c} > 0$, which implies that, according to (6.23) and (6.24), $\delta_1 = -1$, $\delta_2 = \delta_3 = 1$ and hence $\Delta = -1$. This means that (6.4) is a monotone cyclic negative feedback system. In view of $\det(D_x G(x(\varepsilon), \varepsilon)) < 0$ (Remark 6.10), we conclude that (6.4) satisfies (6.26). Therefore, from statement 1 of Theorem 6.16, the ω-limit set of any trajectory of (6.4) with the initial condition $x_0 \in \mathcal{C}$ is either an equilibrium point or a non-constant periodic solutions. Then, recall from our local analysis results in Lemma 6.7 that for sufficiently small $\varepsilon > 0$, the equilibrium point $x(\varepsilon)$ is associated with a 1-dimensional stable and a 2-dimensional unstable manifolds. This means that the only trajectories that converge to the equilibrium point $x(\varepsilon)$ are those with the initial conditions along the stable manifold, while all the other trajectories, due to the above arguments, converge to some non-constant periodic solution. Note that the set of initial conditions contained in the stable manifold is negligible[1] with respect to all other initial conditions in $\mathcal{C}$.

Next, due to the fact that the cube $\mathcal{C}$ is forward invariant for any $\varepsilon > 0$ (Lemma 6.4), system (6.4) possesses a compact attractor $K \subset \mathring{\mathcal{C}}$ [103]. Moreover, for sufficiently small $\varepsilon > 0$ and from Lemmas 6.5 and 6.7, we know that the equilibrium point $x(\varepsilon)$ is unique, the Jacobian matrix $D_x G(x(\varepsilon), \varepsilon)$ has two eigenvalues with positive real parts, and $\Delta \det(-D_x G(x(\varepsilon), \varepsilon)) < 0$. Therefore, system (6.4) satisfies all the assumptions of the statement 2 of Theorem 6.16, and hence (6.4) has a finite number of non-constant periodic solutions, at least one of which is orbitally asymptotically stable. □

Remark 6.19. From the bifurcation analysis performed in Section 6.4, it is clear that by "for sufficiently small $\varepsilon > 0$" in Theorem 6.18 we mean $\varepsilon \in (0, \varepsilon^0)$.

[1] A subset of Euclidean space is called negligible if its Lebesgue measure is zero.

6.6 On the robustness of bifurcation with respect to parameter changes

This section is devoted to investigate how robust our bifurcation analysis and qualitative results are under small but not necessarily symmetric changes in the parameters of system (6.4). Note that our bifurcation analysis is based only on the scalar parameter ε, because, as discussed in Section 6.2, we have unified all the Michaelis-Menten constants by ε, i.e., $K_{\mathrm{a}} = 2K_{\mathrm{d}} = 2K_{\mathrm{m}} = 2K_{\mathrm{dm}} = 2K_{\mathrm{p}} = 2K_{\mathrm{dp}} = \varepsilon$. Now, we are interested in understanding how the conclusion of the bifurcation analysis may change if there is a small "asymmetry" in parameter values. In other words, we want to know how system (6.4) behaves if the perturbation of the parameters is no longer restricted to the scalar parameter ε, but depends on a 6-dimensional parameter vector according to the Michaelis-Menten constants.

Claim 6.20. *The bifurcation analysis result for $G(x, \varepsilon) = 0$, given by* (6.5)*, is robust in the sense that any (smooth, sufficiently small, and not necessarily symmetric) change in the parameters will lead to the same qualitative behavior of the solutions as that already described in this chapter.*

To provide a formal proof of Claim 6.20 (see Proposition 6.26 below) we follow [50]. To avoid making this section inconveniently long, we adopt the same terminology and notation as in [50] and recall just the essential definitions and results. For more details on the concepts being used below, and a brief introduction to algebraic geometry and singularity theory, the interested reader is referred to [50] and [49] respectively.

Let G be a (germ of a) function in $n+1$ variables near 0, that is $G : (\mathbb{R}^n \times \mathbb{R}, 0) \to (\mathbb{R}^m, 0)$.

Definition 6.21. [50, Definition 2.1a] An ℓ-parameter unfolding of G is a C^∞ map $F : (\mathbb{R}^n \times \mathbb{R} \times \mathbb{R}^\ell, 0) \to (\mathbb{R}^m, 0)$ such that $F(x, \lambda, 0) = G(x, \lambda)$ for all $(x, \lambda) \in \mathbb{R}^n \times \mathbb{R}$.

Definition 6.22. [50, Definition 2.1c] F is a universal unfolding of G if every unfolding of G factors through F.

In some sense, a bifurcation problem defined by $F = 0$ contains all the qualitative behavior present in $G = 0$. Moreover, any other unfolding of G does not contain new information or behavior already given by F. Thus, the goal is, given a bifurcation problem $G = 0$, to know if a universal unfolding F exists, and if it does, to compute it.

In order to address the aforementioned issue, let us first introduce some notations: we denote an ℓ-parameter unfolding of G by F_α with some fixed $\alpha \in \mathbb{R}^\ell$. We denote by $\mathcal{E}_{n+1}$ the ring of germs of (smooth) functions in n-variables and 1-parameter $(x, \lambda) \in \mathbb{R}^n \times \mathbb{R}$, and regard $\mathcal{E}_{n+1}^m$, the space of m-tuples, as a module

over $\mathcal{E}_{n+1}$ with component-wise multiplication. Moreover, we denote by $\mathcal{E}_{n+1}\left\{\frac{\partial G}{\partial x}\right\}$ the submodule of $\mathcal{E}_{n+1}^m$ generated by $\partial G/\partial x_1, \partial G/\partial x_2, ..., \partial G/\partial x_n$ over the ring $\mathcal{E}_{n+1}$, the ideal $\langle G\rangle = \langle G_1, G_2, ..., G_m\rangle$ in $\mathcal{E}_{n+1}$ generated by the m components of G, and $\mathcal{E}_\lambda\left\{\frac{\partial G}{\partial \lambda}\right\} := \left\{\phi(\lambda)\frac{\partial G}{\partial \lambda} \mid \phi \in \mathcal{E}_\lambda\right\}$, where $\phi \in \mathcal{E}_\lambda$ stands for $\phi \in \mathcal{E}_{n+1}$ when ϕ is just a function of λ and does not depend on x.

Remark 6.23. Recall from Lemma 6.13 that the bifurcation point of (6.5) is $(x(\varepsilon^0), \varepsilon^0)$. Therefore, for the particular bifurcation problem given by (6.5), the ring of germs $\mathcal{E}_{n+1}$ is defined around $x(\varepsilon^0)$ and $\lambda = \varepsilon - \varepsilon^0$ with $n = 3$, $m = 3$.

Definition 6.24. [50, Definition 2.3]

(i) Let $\tilde{TG} = \langle G\rangle^m + \mathcal{E}_{n+1}\left\{\frac{\partial G}{\partial x}\right\}$ and let $TG = \tilde{TG} + \mathcal{E}_\lambda\left\{\frac{\partial G}{\partial \lambda}\right\}$.

(ii) G has finite codimension if $\dim\left(\mathcal{E}_{n+1}^m/\tilde{TG}\right) < \infty$.

(iii) The codimension of G equals $\dim\left(\mathcal{E}_{n+1}^m/TG\right)$ and is denoted by $\operatorname{codim} G$.

Now, we are ready to present the main result of [50].

Theorem 6.25. *[50, Theorem 2.4] Suppose G has finite codimension, and let F_α be an ℓ-parameter unfolding of G. F_α is a universal unfolding of G if and only if TG plus the ℓ-vectors $\partial F/\partial\alpha_1|_{\alpha=0}, \cdots, \partial F/\partial\alpha_\ell|_{\alpha=0}$ together span $\mathcal{E}_{n+1}^m$ (over the reals). The minimum number of unfolding parameters in any universal unfolding is the codimension of G.*

6

In words, Theorem 6.25 states that given a bifurcation problem G of a certain codimension, say p, we need to add p parameters to the idealized problem $G = 0$ to obtain a robust bifurcation problem $F_\alpha = 0$. Then, any smooth perturbation whatsoever of the idealized problem $G = 0$ will give a qualitative behavior already presented for $F_\alpha = 0$.

Now we turn to check whether the bifurcation problem G given in (6.5) is robust.

Proposition 6.26. *The bifurcation problem G in* (6.5) *has codimension zero, i.e.* $\operatorname{codim} G = 0$.

Proof. First of all, note that up to relabeling of the variables (f, c, e), the equations $G_i(x, \varepsilon) = 0$, $i = 1, 2, 3$, are all equivalent, where $G_i(x, \varepsilon)$ are the right-hand sides of (6.4). Thus, without loss of generality, we can study, for instance, a bifurcation problem defined by $F = 0$, where $F(f, c, e, \varepsilon) : \mathbb{R}^3 \times \mathbb{R} \to \mathbb{R}$ is given by

$$F(f, c, e, \varepsilon) = \kappa_1\varepsilon + \kappa_2 f + \kappa_3\varepsilon f + \kappa_4 c^2 + \kappa_5 fe\varepsilon + \kappa_6 fc + \kappa_7 f^2 e, \tag{6.28}$$

which is the numerator of $G_1(x, \varepsilon)$ where κ_j $(j = 1, 2, ..., 7)$ are non-zero real constants, and we set $m = 1$.

Due to the dimension order $0 \leqslant \dim\left(\mathcal{E}_{n+1}/TF\right) \leqslant \dim\left(\mathcal{E}_{n+1}/\tilde{T}F\right)$, it suffices to show that $\dim\left(\mathcal{E}_{n+1}/\tilde{T}F\right) = 0$. The quotient space $\dim\left(\mathcal{E}_{n+1}/\tilde{T}F\right)$, its base, and its dimension are computable by hand. However, to simplify such tasks we have used the software "SINGULAR" [56] with which we can automate the necessary computations. By doing so we obtain

$$\dim\left(\mathcal{E}_{n+1}/\tilde{T}F\right) = 0. \tag{6.29}$$

Due to the dimension order $0 \leqslant \dim\left(\mathcal{E}_{n+1}/TF\right) \leqslant \dim\left(\mathcal{E}_{n+1}/\tilde{T}F\right)$, we conclude that $\dim\left(\mathcal{E}_{n+1}/TG_1\right) = \dim\left(\mathcal{E}_{n+1}/TF\right) = 0$. As mentioned above, the same claim holds for G_2 and G_3, that is $\dim\left(\mathcal{E}_{n+1}/TG_2\right) = \dim\left(\mathcal{E}_{n+1}/TG_3\right) = 0$. Thus, from the definition of $\mathcal{E}^m_{n+1}$ it follows that $\dim\left(\mathcal{E}^3_{n+1}/TG\right) = 0$. Therefore $\operatorname{codim} G = 0$. □

Remark 6.27. The proof of claim 6.20 follows from Theorem 6.26 and Proposition 6.25. As a consequence, the convergence result presented in Theorem 6.18 is robust, in the sense that any small change in the parameters leads to the same qualitative behavior of the solutions.

6.7 Concluding remarks

In this chapter, we have developed a tool based on bifurcation analysis for parameter-robustness analysis for a class of oscillators, and in particular, examined the Frz model. Our studies have started from the local behavior of the biochemical oscillator and concluded with a global description. First of all, we have identified some parameters of the model, and hence unified them using a single ε. Next, we have developed local analysis through which we have found a unique hyperbolic equilibrium point associated with the oscillator. Since such a point is hyperbolic, it turns out that the system is structurally stable in a small neighborhood of it, motivating us to further investigate the robustness of the system. However, up to this stage, oscillatory behavior cannot yet be explained. So we have used Hopf bifurcation theory to give sufficient conditions for the existence of periodic solutions. From bifurcation analysis we have been able to provide numerical estimates of the range of parameter under which periodic solutions exist. However, the results from the Hopf bifurcation analysis do not provide information on the cardinality of and convergence to periodic solutions. In this regards, we have performed global analysis to show that the number of possible limiting periodic solutions is finite and that trajectories converge to at least one of such solutions. At the end, we have shown that the bifurcation results are robust in the sense that any smooth,

sufficiently small, and not necessarily symmetric change in the parameters will lead to the same qualitative behavior of the solutions as the one that has been already described. All these results have led us to conclude that the biochemical oscillator proposed in [73] is indeed robust under sufficiently small C^1-perturbations of the parameter.

Theorem 6.18 proves the convergence of (almost) all trajectories to a finite number of periodic solutions. However, our observation from simulations shows that (almost) all trajectories actually converge to a unique limit cycle. In addition, from our numerical simulations, it appears that there are several "time scales" along the unique limit cycle, which are related to the small parameter ε. A thorough analysis of such time scales and their influences on the dynamics may provide a better understanding of their role in the biochemical clock. However, these issues cannot be analyzed by tools used in this chapter, and hence we need more advanced techniques to present a rigorous analysis of such issues. The subject of next chapter is to prove that the exists a *strongly attracting limit cycle*, and investigate the time scales along such a limit cycle.

7

Relaxation oscillations in a slow-fast system beyond the standard form

This chapter deals with the Frz system, studied in the previous chapter, from a different perspective. More precisely, in this chapter we use geometric singular perturbation theory and the blow-up method to prove the existence of a strongly attracting limit cycle. This limit cycle corresponds to a relaxation oscillation of an auxiliary system, whose singular perturbation nature originates from the small Michaelis-Menten constants of the Frz system, and has the same orbit as the original model. In addition, we give a detailed description of the structure of this limit cycle, and the time scales along it.

This chapter starts with an introduction, followed by Section 7.2 where a preliminary analysis on the system is presented. Section 7.3 gives the slow-fast analysis of the auxiliary system, followed by Section 7.4 where blow-up analysis of two non-hyperbolic lines is presented. The range of an independent parameter of the system in which the main result is valid as well as concluding remarks are given in Sections 7.5 and 7.6.

7.1 Introduction

OSCILLATORS are ubiquitous in different fields of science [12, 28, 44, 152, 168], and in particular, are of great importance in biological systems [46, 113]. One of the most important types of periodic fluctuations are *relaxation oscillations* [91, 92, 110, 138], which are characterized by repeated switching of slow and fast motions (i.e., multiple-time-scale dynamics). Relaxation oscillations involve a large class of nonlinear dynamical systems, and occur in biology, chemistry, mechanics, and engineering, see e.g., [74, 111, 148, 152]. Particularly, relaxation

oscillators describe some important biological phenomena, such as population cycles of predator-prey type [69], gene regulatory process [106], neuronal activity [74], and heartbeat [152].

Mathematical models have been useful to gain deeper insights into the complex mechanisms of oscillatory multiple-time-scale processes. Some of these phenomena have been modeled by the slow-fast systems of the form (2.13) (or equivalently (2.14)), which are in the standard form, i.e., the slow and fast variables are *explicitly* given. However, some others (see e.g., [20, 61, 71, 86, 87, 88]) are in the non-standard form, in which separation into slow and fast variables are not given a priori.

Our observations from numerical simulations show that (almost) all solutions of the Frz system, studied in Chapter 6, converge to a *unique* limit cycle, and further, this cycle has *multiple time scales*; in other words, the Frz system is a *relaxation oscillator*. Note that as the system is not in the standard form of slow-fast systems, the slow and fast variables are hidden, posing some mathematical challenges. In this chapter, using geometric singular perturbation theory and the blow-up method, we prove that, within certain parameter regimes, there exists a *strongly attracting* periodic orbit for the Frz system; moreover, we give the detailed description of the structure of such a periodic orbit, and the time scales along it.

7.2 Preliminary analysis

In this section we provide a preliminary analysis on the Frz system. In Subsection 7.2.1, we describe the behavior of the solutions for the parameters given in [73]. In Subsection 7.2.2, we present a two-parameter bifurcation analysis where we clarify the nature and the role of two distinct parameters of the system.

7.2.1 Basic properties and sustained oscillations

Let us recall the Frz system with the unified parameters that we studied in the previous chapter, i.e.,

$$\begin{aligned}
\frac{df}{d\tau} &= \frac{\gamma(1-f)}{\varepsilon+(1-f)} - \frac{2fe}{\varepsilon+2f},\\
\frac{dc}{d\tau} &= \frac{8(1-c)f}{\varepsilon+2(1-c)} - \frac{4c}{\varepsilon+2c},\\
\frac{de}{d\tau} &= \frac{8(1-e)c}{\varepsilon+2(1-e)} - \frac{4e}{\varepsilon+2e},
\end{aligned} \tag{7.1}$$

where γ is the C-signal, which is produced when a cell collides with other cells. In Chapter 6, we have assumed that $\gamma = 0.08$, as reported in [73] (see system (6.4)).

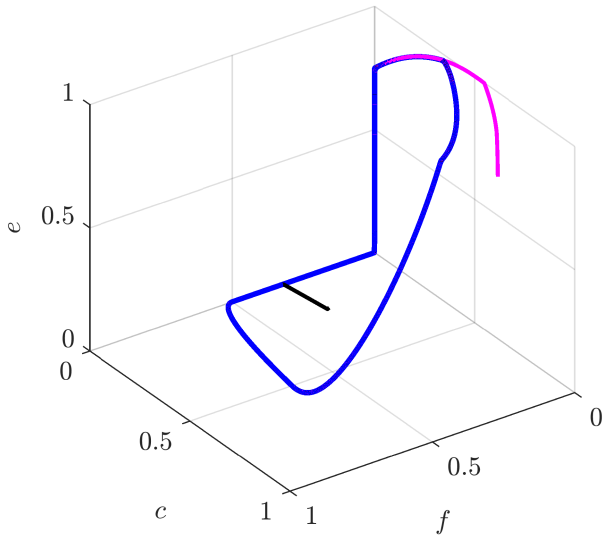

Figure 7.1: Numerically computed attracting limit cycle of system (7.1) for $\varepsilon = 10^{-3}$ and $\gamma = 0.08$ with three different initial conditions.

Figures 7.1 and 7.2 show, respectively, a numerically computed attracting limit cycle of system (7.1) and the corresponding time evolution for $\varepsilon = 10^{-3}$ and $\gamma = 0.08$. Provided $\varepsilon \ll 1$, the following switching behavior occurs (see Fig. 7.2). Initially, all protein ratios f, c and e are close to zero. Under the dynamics (7.1), the variable f increases (due to the action of the C-signal), while c and e stay close to zero. Once the variable f passes the activation threshold $f^* := 0.5$, the variable c increases rapidly. Next, as soon as the variable c passes the threshold $c^* := 0.5$, the variable e is activated and hence increases rapidly until it reaches its maximum value, i.e., $e = 1$. Due to the fact that there is a negative feedback from e to f, the increase in e results in the degradation of variable f. Once f reaches the threshold f^*, variable c decreases, and once c reaches the threshold c^*, the variable e decreases vary fast. As a result, the variables f and c reach their lowest values (i.e. very close to zero), while the variable e reaches the threshold $e^* := \gamma$. As soon as the variable e drops below the threshold e^*, the variable f is activated and increases. This behavior is repeated in a periodic manner, and hence a limit cycle is formed (see Figure 7.1).

Remark 7.1. We have plotted Figures 7.1 and 7.2 for $\gamma = 0.08$, reported in [73]. Later we show that the parameter $\gamma = 0.08$ can be relaxed to some extent such that the corresponding limit cycle has the same qualitative behavior; see Remark 7.3

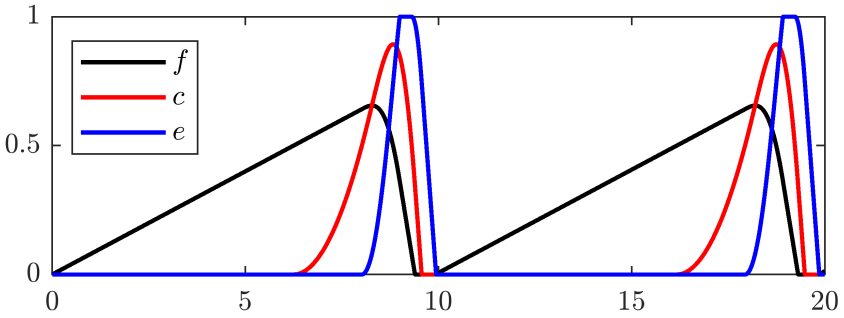

Figure 7.2: Numerically computed time evolution of system (7.1) for $\varepsilon = 10^{-3}$ and $\gamma = 0.08$.

and Section 7.5.

Remark 7.2. Owing to the fact that f, c and e represent fractions of protein concentrations, their values are restricted to $[0, 1]$. Thus, we restrict our analysis to the unit cube

$$\mathcal{C} := \left\{(f, c, e) \in \mathbb{R}^3 \,|\, f \in [0, 1],\, c \in [0, 1],\, e \in [0, 1]\right\}.$$

In Chapter 6, we have presented a parameter-robustness analysis for system (7.1) with respect to the parameter ε and for fixed $\gamma = 0.08$. More precisely, using bifurcation analysis, we have shown that the system is robust under the variation of ε for $\varepsilon \in (0, \varepsilon^*)$ with $\varepsilon^* := 0.05517665$. In this chapter, we analytically prove the existence of a strongly attracting limit cycle which explains the numerically computed periodic orbit in Fig. 7.1, for sufficiently small $\varepsilon > 0$. Similar mechanisms, leading to an attracting limit cycle, occur in the Goldbeter minimal model [45], which has been studied in [88].

7

7.2.2 Two-parameter bifurcation analysis

This subsection is devoted to the two-parameter bifurcation analysis of (7.1). In particular, we analyze the behavior of system (7.1) under the variation of parameters (ε, γ). To this end, we rewrite (7.1) in the form of

$$\frac{dx}{d\tau} = G(x; \varepsilon, \gamma), \tag{7.2}$$

where $x = \begin{bmatrix} f & c & e \end{bmatrix}^\top$, and $G(x; \varepsilon, \gamma)$ denotes the right-hand side of (7.1). We have used the numerical continuation software MATCONT [21] to compute the two-parameter bifurcation diagram of (7.2) with respect to (ε, γ), presented in Fig. 7.3; in this figure, the vertical and horizontal axes show the variations of ε and γ, respectively. The blue curve indicates that for any $0 < \gamma < 1$ and any ε

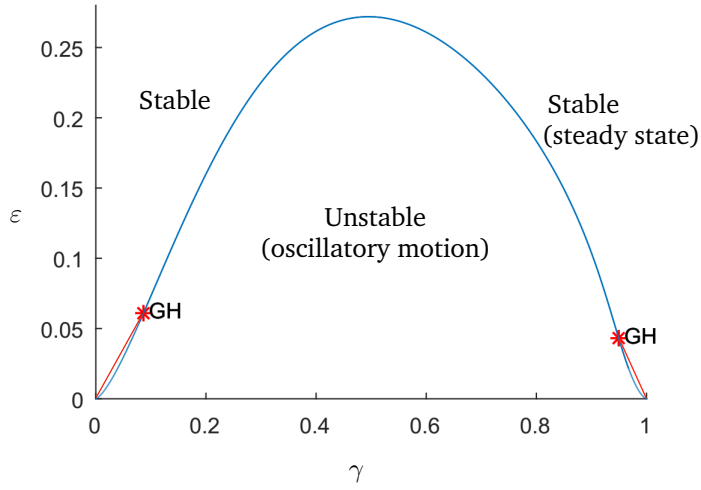

Figure 7.3: Two-parameter bifurcation analysis of (7.1) with respect to (ε, γ).

below the curve, the system has unstable equilibria and hence exhibits oscillatory behavior. For those values of ε which are above the blue curve, the equilibrium point is stable, and hence the system is not oscillatory anymore. In fact, the blue curve is the curve of Hopf bifurcations where the equilibria of the system switches from being stable to unstable: with fixed $0 < \gamma < 1$, as ε passes through the curve from above to below, a limit cycle is generated.

As illustrated in Fig. 7.3, there are two points, denoted by "GH", which are generalized Hopf (or Bautin) Bifurcation points. At these points, the equilibria of (7.2) have a pair of pure imaginary eigenvalues at which the first Lyapunov exponent coefficient of the Hopf bifurcation vanishes [95]. Computed by MATCONT, the values of (ε, γ) at "GH" points are as follows:

$$(\varepsilon_1, \gamma_1) = (0.060907128, 0.086423772), \qquad (\varepsilon_2, \gamma_2) = (0.043172692, 0.949470320).$$

In Fig. 7.3, the red curves are the curves of *limit points* (or saddle-node bifurcation) of cycles. For parameter values (ε, γ) between the blue and red curves, at least two limit cycles exist simultaneously, i.e., for $\gamma \in (0, \gamma_1)$ and $\gamma \in (\gamma_2, 1)$ with a suitable $0 < \varepsilon \ll 1$, at least one stable and one unstable limit cycle coexist.

Remark 7.3. As mentioned in Chapter 6, due to the property of "zero-order ultra-sensitivity", the Michaelis-Menten constants, unified by ε, have to be small. Our observation from numerical simulations shows that, for sufficiently small ε, system (7.1) has similar mechanisms when γ belongs to certain bounds which are close to 0 and 1. In this regard, we emphasize that although the position of the limit

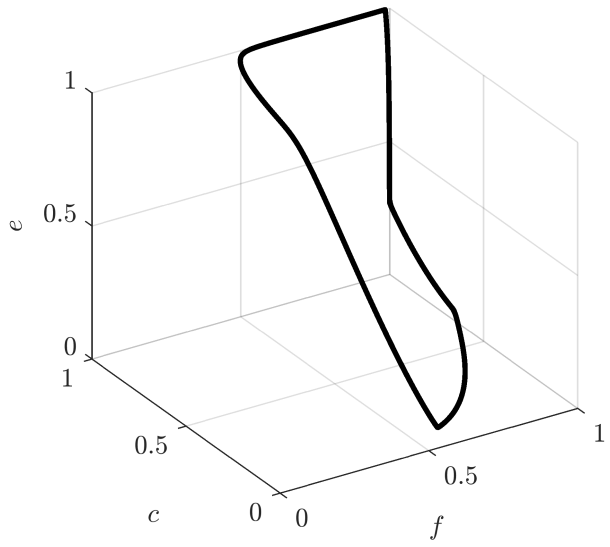

Figure 7.4: Numerically computed attracting limit cycle of system (7.1) for $\varepsilon = 10^{-3}$ and $\gamma = 0.9$.

cycle changes when γ is close to 1 (see, e.g., Fig. 7.4), the geometric analysis of the corresponding dynamics is the same as the case that γ is close to 0, for sufficiently small ε, see Section 7.5.

Remark 7.4. In system (7.1), we have unified all the Michaelis-Menten constants of the original Frz system, reported in [73], by the parameter ε. Although γ has similar size as the Michaelis-Menten constants, we have not unified it with them. One reason is that the unit of γ is "min^{-1}", while the Michaelis-Menten constants are unitless. The other reason is that the simultaneous limit $(\varepsilon, \gamma) \to (0, 0)$ is very singular because a certain point $(0, 0, \gamma)$, playing crucial role in our analysis (see Section 7.4), approaches $(0, 0, 0)$ which is the intersection of three critical manifolds $f = 0$, $c = 0$, and $e = 0$. It would be interesting to study this limit further, which could explain the coalescence of the Hopf curve and the saddle-node curve at $(0, 0)$, see Fig. 7.3; Similar remark holds as $(\varepsilon, \gamma) \to (0, 1)$.

7.3 Geometric singular perturbation analysis

Our goal is to understand the dynamics of (7.1) in the limit $\varepsilon \to 0$. However, as is seen in (7.1), when the variables f, c and e are very close to the boundary of $\mathcal{C}$, the limiting behavior is different from the case that they are away from the boundary.

To resolve this problem, one possibility is to consider an *auxiliary system* which is smoothly equivalent to (7.1). To this end, let us define

$$H^\varepsilon(f,c,e) := H_1^\varepsilon(f)H_2^\varepsilon(c)H_3^\varepsilon(e),$$

where

$$\begin{aligned} H_1^\varepsilon(f) &:= (\varepsilon+1-f)(\varepsilon+2f),\\ H_2^\varepsilon(c) &:= (\varepsilon+2-2c)(\varepsilon+2c),\\ H_3^\varepsilon(e) &:= (\varepsilon+2-2e)(\varepsilon+2e). \end{aligned} \tag{7.3}$$

Note that $H^\varepsilon(f,c,e) > 0$ for any $\varepsilon > 0$ and any $(f,c,e) \in \mathcal{C}$. Therefore, we can reparametrize the time of system (7.1) by multiplying both sides of (7.1) in $H^\varepsilon(f,c,e)$, which leads to the dynamical system

$$\begin{aligned} \frac{df}{d\tau} &= \left(\frac{\gamma(1-f)}{\varepsilon+(1-f)} - \frac{2fe}{\varepsilon+2f}\right) H^\varepsilon(f,c,e),\\ \frac{dc}{d\tau} &= \left(\frac{8(1-c)f}{\varepsilon+2(1-c)} - \frac{4c}{\varepsilon+2c}\right) H^\varepsilon(f,c,e),\\ \frac{de}{d\tau} &= \left(\frac{8(1-e)c}{\varepsilon+2(1-e)} - \frac{4e}{\varepsilon+2e}\right) H^\varepsilon(f,c,e), \end{aligned} \tag{7.4}$$

where, for simplicity, we recycle τ to denote the reparametrized time. One can rewrite (7.4) as follows

$$X_\varepsilon : \begin{cases} \dfrac{df}{d\tau} = [\gamma(1-f)(\varepsilon+2f) - 2fe(\varepsilon+1-f)]\, H_2^\varepsilon(c)H_3^\varepsilon(e),\\ \dfrac{dc}{d\tau} = [8(1-c)f(\varepsilon+2c) - 4c(\varepsilon+2-2c)]\, H_1^\varepsilon(f)H_3^\varepsilon(e),\\ \dfrac{de}{d\tau} = [8(1-e)c(\varepsilon+2e) - 4e(\varepsilon+2-2e)]\, H_1^\varepsilon(f)H_2^\varepsilon(c). \end{cases} \tag{7.5}$$

The vector field (7.5) is smoothly equivalent to (7.1) for $\varepsilon > 0$ [13], which from now on is the object of study. The main reason to rewrite system (7.1) into the form of system (7.5) is that the latter is a singularly perturbed ODE which allows us to analyze the system using geometric methods. Moreover, note that in contrast to (7.1), system (7.5) is in a polynomial form, which is another advantage of (7.5). The goal of this section is to give the detailed analysis of the slow-fast structure of the auxiliary system (7.5). We start our analysis in the following subsection with the layer problem of (7.5).

7.3.1 Layer problem and critical manifold

Setting $\varepsilon = 0$ in (7.5) results in the layer problem

$$\begin{aligned} \frac{df}{d\tau} &= (\gamma - e)\, H^0(f,c,e), \\ \frac{dc}{d\tau} &= 2\,(2f-1)\, H^0(f,c,e), \\ \frac{de}{d\tau} &= 2(2c-1) H^0(f,c,e), \end{aligned} \tag{7.6}$$

where

$$H^0(f,c,e) := 32fce(1-f)(1-c)(1-e).$$

Apart form the isolated equilibrium point $P := (0.5, 0.5, \gamma)$ which is inside the cube $\mathcal{C}$, the boundary of $\mathcal{C}$, consisting of six planes, is the equilibria set of the layer problem (7.6). We denote each plane of equilibria by S^i $(i = 1, 2, ..., 6)$ as follows:

$$\begin{aligned} S^1 &:= \{(f,c,e) \in \mathcal{C} \,|\, f = 0\}, & S^2 &:= \{(f,c,e) \in \mathcal{C} \,|\, c = 0\}, \\ S^3 &:= \{(f,c,e) \in \mathcal{C} \,|\, e = 0\}, & S^4 &:= \{(f,c,e) \in \mathcal{C} \,|\, f = 1\}, \\ S^5 &:= \{(f,c,e) \in \mathcal{C} \,|\, c = 1\}, & S^6 &:= \{(f,c,e) \in \mathcal{C} \,|\, e = 1\}. \end{aligned} \tag{7.7}$$

Thus, $S := \bigcup_{i=1}^{6} S^i$ is the critical manifold. The stability of system (7.5) changes at lines $\ell_f \in S^1, \ell^f \in S^4$ (given by $f = f^*$), $\ell_c \in S^2, \ell^c \in S^5$ (given by $c = c^*$), and $\ell_e \in S^3, \ell^e \in S^6$ (given by $e = e^*$). Moreover, the 12 edges of the unit cube, where the 6 planes S^i intersect, are non-hyperbolic lines as well. However, for our analysis, only the lines $\ell_1 = S^1 \cap S^2$ and $\ell_2 = S^2 \cap S^3$ are crucial (see Figure 7.5).

The stability of points in S is summarized in the following lemma.

Lemma 7.5. *The critical manifold S of the layer problem* (7.6) *has the following properties:*

- *S^1 is attracting for $e > e^*$ and repelling for $e < e^*$.*
- *S^2 is attracting for $f < f^*$ and repelling for $f > f^*$.*
- *S^3 is attracting for $c < c^*$ and repelling for $c > c^*$.*
- *S^4 is attracting for $e < e^*$ and repelling for $e > e^*$.*
- *S^5 is attracting for $f > f^*$ and repelling for $f < f^*$.*
- *S^6 is attracting for $c > c^*$ and repelling for $c < c^*$.*
- *The equilibrium $P = (0.5, 0.5, \gamma)$ is a saddle-focus point.*

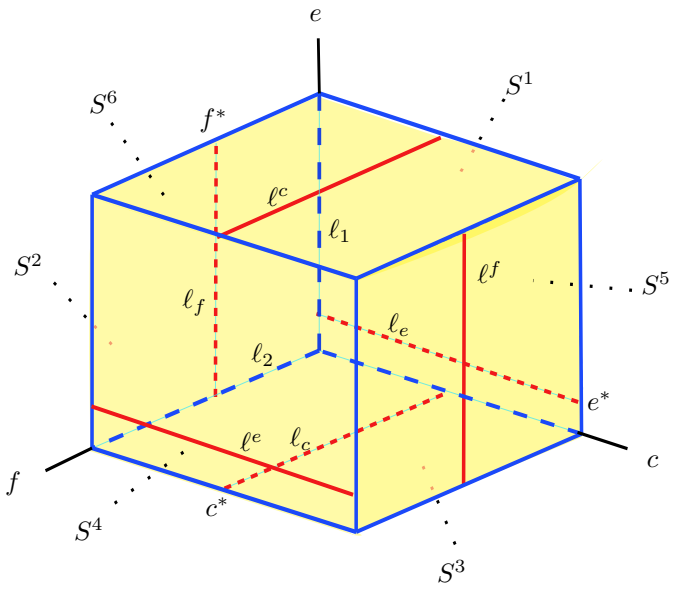

Figure 7.5: The critical manifold $S = \bigcup_{i=1}^{6} S^i$, non-hyperbolic lines ℓ_f, ℓ_c, ℓ_e, ℓ^f, ℓ^c, ℓ^e in red, all 12 non-hyperbolic edges in blue, and in particular, two non-hyperbolic edges ℓ_1 and ℓ_2.

- *The lines $\ell_f \in S^1, \ell_c \in S^2, \ell_e \in S^3, \ell^f \in S^4, \ell^c \in S^5, \ell^e \in S^6$, all 12 edges of the unit cube, and in particular, the edges $\ell_1 = S^1 \cap S^2$ and $\ell_2 = S^2 \cap S^3$ are non-hyperbolic.*

Proof. The eigenvalues of the linearization of system (7.6) at points, e.g., in the plane S^1 are given by

$$\lambda_1 = \lambda_2 = 0, \qquad \lambda_3 = -32ce(c-1)(e-1)(e-\gamma).$$

It is clear that λ_3 is zero at the boundary of S^1, and also along the line l_e given by $e = e^*$. Therefore, S^1 is attracting for $e > e^*$ and it is repelling for $e < e^*$. The proof of the other cases is given analogously, and is omitted for brevity. □

We denote the interior of the cube $\mathcal{C}$ by $\mathring{\mathcal{C}}$. Note that when $(f, c, e) \in \mathring{\mathcal{C}}$, the layer problem (7.6) can be divided by the positive term $H^0(f, c, e) = 32fce(1-f)(1-c)(1-e)$. Therefore away from the critical manifold S, all the variables evolve on the fast time scale τ and the orbits of the layer problem (7.6) are identical to the

orbits of the linear system

$$\begin{aligned} \frac{df}{d\tau} &= \gamma - e, \\ \frac{dc}{d\tau} &= 2(2f-1), \\ \frac{de}{d\tau} &= 2(2c-1). \end{aligned} \tag{7.8}$$

Remark 7.6. For $(f, c, e) \in \mathring{\mathcal{C}}$, system (7.8) is the limit of system (7.1) as $\varepsilon \to 0$.

7.3.2 Reduced problem, slow manifolds, and slow dynamics

From Subsection 7.3.1, we know that S is the critical manifold. Any compact subset of S that does not contain any non-hyperbolic point is normally hyperbolic, and hence Fenichel theory [37] is applicable. Fenichel theory implies that the normally hyperbolic parts of $\mathcal{C}$ perturb to slow manifolds, which lie within a distance of order $\mathcal{O}(\varepsilon)$ of the critical manifold S. In the following, we compute the slow manifolds and analyze the reduced flows in the planes, S^1, S^2, S^3, and S^6 which are essential for our analysis.

Lemma 7.7. *For sufficiently small $\delta > 0$, there exist $\varepsilon_0 > 0$ and a smooth function $h^1_\varepsilon(c, e)$ defined on $I^1_a = [\delta,\ 1-\delta] \times [\gamma + \delta,\ 1-\delta]$ such that the manifold*

$$S^1_{a,\varepsilon} = \left\{ (f, c, e) \in \mathcal{C} \mid f = h^1_\varepsilon(c, e),\ (c, e) \in I^1_a \right\}, \tag{7.9}$$

is a locally invariant attracting manifold of (7.5) *for $\varepsilon \in (0, \varepsilon_0]$. The function $h^1_\varepsilon(c, e)$ has the expansion*

$$h^1_\varepsilon(c, e) = \frac{\gamma}{2(e-\gamma)}\varepsilon + \mathcal{O}(\varepsilon^2). \tag{7.10}$$

Proof. As the set I^1_a is hyperbolic, Fenichel theory implies that there exists a sufficiently small $\varepsilon_0 > 0$ such that the function $h^1_\varepsilon(c, e)$ has the expansion $h^1_\varepsilon(c, e) = \eta(c, e)\varepsilon + \mathcal{O}(\varepsilon^2)$ for all $\varepsilon \in (0, \varepsilon_0]$. Due to invariance, we can substitute $h^1_\varepsilon(c, e)$ into the equation of $\frac{df}{d\tau}$ in (7.5) and identify coefficients of ε. After doing so, we obtain

$$\eta(c, e) = \frac{\gamma}{2(e-\gamma)}. \tag{7.11}$$

Note that (7.11) reflects the fact that the manifold $S^1_{a,\varepsilon}$ is not well-defined when $e = \gamma$. Thus, the invariant manifold $S^1_{a,\varepsilon}$ is given as stated in the lemma, which completes the proof. □

For the sake of brevity, we summarize our analysis in the planes S^2, S^3, and S^6 in the following lemmas, whose proofs follow the same line of reasoning as the one of Lemma 7.7.

Lemma 7.8. *For sufficiently small $\delta > 0$, there exist $\varepsilon_0 > 0$ and a smooth function $h^2_\varepsilon(f, e)$ defined on $I^2_a = \left[\delta,\ \frac{1}{2} - \delta\right] \times [\delta,\ 1 - \delta]$ such that the manifold*

$$S^2_{a,\varepsilon} = \left\{(f, c, e) \in \mathcal{C} \,|\, c = h^2_\varepsilon(f, e),\ (f, e) \in I^2_a\right\}, \tag{7.12}$$

is a locally invariant attracting manifold of (7.5) *for $\varepsilon \in (0, \varepsilon_0]$. The function $h^2_\varepsilon(f, e)$ has the expansion*

$$h^2_\varepsilon(f, e) = \frac{f}{1 - 2f}\varepsilon + \mathcal{O}(\varepsilon^2). \tag{7.13}$$

Lemma 7.9. *For sufficiently small $\delta > 0$, there exist $\varepsilon_0 > 0$ and a smooth function $h^3_\varepsilon(f, c)$ defined on $I^3_a = [\delta,\ 1 - \delta] \times \left[\delta,\ \frac{1}{2} - \delta\right]$ such that the manifold*

$$S^3_{a,\varepsilon} = \left\{(f, c, e) \in \mathcal{C} \,|\, e = h^3_\varepsilon(f, c),\ (f, c) \in I^3_a\right\}, \tag{7.14}$$

is a locally invariant attracting manifold of (7.5) *for $\varepsilon \in (0, \varepsilon_0]$. The function $h^3_\varepsilon(f, c)$ has the expansion*

$$h^3_\varepsilon(f, c) = \frac{c}{1 - 2c}\varepsilon + \mathcal{O}(\varepsilon^2) \tag{7.15}$$

Lemma 7.10. *For sufficiently small $\delta > 0$, there exist $\varepsilon_0 > 0$ and a smooth function $h^6_\varepsilon(f, c)$ defined on $I^6_a = [\delta,\ 1 - \delta] \times \left[\frac{1}{2} + \delta, 1 - \delta\right]$ such that the manifold*

$$S^6_{a,\varepsilon} = \left\{(f, c, e) \in \mathcal{C} \,|\, e = 1 + h^6_\varepsilon(f, c),\ (f, c) \in I^6_a\right\}, \tag{7.16}$$

is a locally invariant attracting manifold of (7.5) *for $\varepsilon \in (0, \varepsilon_0]$. The function $h^6_\varepsilon(f, c)$ has the expansion*

$$h^6_\varepsilon(f, c) = \frac{1}{2(1 - 2c)}\varepsilon + \mathcal{O}(\varepsilon^2), \tag{7.17}$$

Remark 7.11. Similar results can be obtained for the "repelling" parts $S^i_{r,\varepsilon}$, $i = 1, 2, ..., 6$. However, these are not needed in our analysis.

Remark 7.12. The expansions of the functions $h^i_\varepsilon(\cdot, \cdot)$, $i = 1, 2, 3, 6$, also explain why it is necessary to restrict the domain of definition of the slow manifolds to I^i_a to exclude their singularities.

We now turn to the analysis of the reduced flows in the planes S^1, S^2, S^3, and S^6 which respectively means the planes $f = 0, c = 0, e = 0$ and $e = 1$. We know that system (7.5) has the fast time scale τ. By substituting the functions h^i_ε, $i = 1, 2, 3, 6$, into (7.5), transforming the fast time variable to the slow one by $t = \varepsilon\tau$, and setting $\varepsilon = 0$, the equations governing the slow dynamics on the critical manifold S^i_a are computed. In the following, we give the analysis in the plane S^1.

After substituting h^1_ε into system (7.5), the dynamics of the reduced system in

S^1, i.e. in the plane $f = 0$, is governed by

$$\begin{aligned} c' &= \frac{-32ce^2(c-1)(e-1)}{e-\gamma}\varepsilon + \mathcal{O}(\varepsilon^2), \\ e' &= \frac{32ce^2(c-1)(e-1)(2c-1)}{e-\gamma}\varepsilon + \mathcal{O}(\varepsilon^2), \end{aligned} \tag{7.18}$$

where "prime" denotes the differentiation with respect to τ. Now by dividing out a factor of ε, which corresponds to switching from the fast time variable to the slow one, we have

$$\begin{aligned} \dot{c} &= \frac{-32ce^2(c-1)(e-1)}{e-\gamma} + \mathcal{O}(\varepsilon), \\ \dot{e} &= \frac{32ce^2(c-1)(e-1)(2c-1)}{e-\gamma} + \mathcal{O}(\varepsilon), \end{aligned} \tag{7.19}$$

where "dot" represents differentiation with respect to $t = \varepsilon\tau$. Now, by setting $\varepsilon = 0$ in (7.19), the reduced flow on S^1_a is given by

$$\begin{aligned} \dot{c} &= \frac{-32ce^2(c-1)(e-1)}{e-\gamma}, \\ \dot{e} &= \frac{32ce^2(c-1)(e-1)(2c-1)}{e-\gamma}. \end{aligned} \tag{7.20}$$

As is clear, the vector field (7.20) is singular at the line ℓ_e, given by $e = e^*$. In other words, the flow (7.20) is not defined on the line ℓ_e. The lines $c = 0$, $e = 0$, $c = 1$, and $e = 1$, shown in Figure 7.6, are lines of equilibria. The line $c = 0$ is attracting for $e > e^*$ and repelling for $e < e^*$, while the line $c = 1$ is attracting for $e < e^*$ and repelling for $e > e^*$.

By dividing out the factor $\frac{32ce^2(c-1)(e-1)}{e-\gamma}$ in (7.20), the orbits of the reduced flow can be derived from the desingularized system

$$\begin{aligned} \dot{c} &= -1, \\ \dot{e} &= 2c - 1, \end{aligned} \tag{7.21}$$

which can be integrated *explicitly*.

Remark 7.13. For $e > e^*$, systems (7.20) and (7.21) have qualitatively the same dynamics when $c, e \in (0, 1)$. In particular, the vector field (7.21) is C^∞-equivalent but not C^∞-conjugate to the vector field (7.20). For the case that $e < e^*$, the direction of the vector field (7.20) is not preserved in the vector field (7.21). However, for our analysis, it suffices to study the flow of system (7.20) when $e > e^*$.

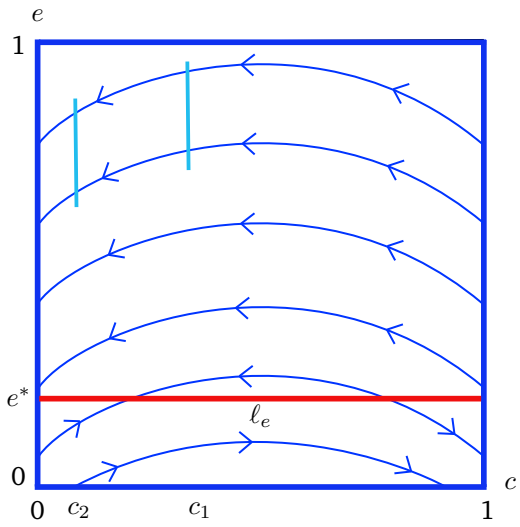

Figure 7.6: Flow of the slow vector field on S^1_a, the non-hyperbolic line ℓ_e in red, and sections c_1, c_2 in cyan.

From system (7.21), the following lemma is immediate.

Lemma 7.14. *For $e > e^*$, the reduced flow* (7.20) *on S^1, and hence the slow flow* (7.19) *on $S^1_{a,\varepsilon}$ map section $c = c_1$ to $c = c_2$, when $0 < c_2 < c_1 < \frac{1}{2}$; this map is well-defined with the derivatives close to one, see Fig. 7.6.*

In order to obtain the equations governing the slow flow on $S^2_{a,\varepsilon}, S^3_{a,\varepsilon}$ and $S^6_{a,\varepsilon}$, a similar analysis can be done by substituting the functions $h^2_\varepsilon, h^3_\varepsilon$ and h^6_ε into (7.5) and dividing out a factor of ε, which corresponds to switching to the slow time scale $t = \varepsilon\tau$. Next, by setting $\varepsilon = 0$ one obtains the reduced flow on the critical manifolds S^2_a, S^3_a and S^6_a. For the sake of brevity, we summarize the slow flows on S^2, S^3 and S^6 in Lemmas 7.15, 7.18 and 7.20, which are crucial for our analysis.

Lemma 7.15. *The reduced flow along S^2_a, defined as $X^2_a = \lim_{\varepsilon\to 0} \frac{1}{\varepsilon} X_\varepsilon|_{S^2_a}$, is given by*

$$\begin{aligned} \dot{f} &= \frac{16ef(e-1)(f-1)(e-\gamma)}{2f-1}, \\ \dot{e} &= \frac{32ef(e-1)(f-1)}{2f-1}. \end{aligned} \tag{7.22}$$

The phase portrait of (7.22) *is shown in Fig. 7.7.*

The vector field (7.22) is singular at the line $f = f^*$. This line is repelling for $e \in (\gamma, 1)$ while attracting for $e \in (0, \gamma)$, see Figure 7.7. The blue lines $f = 0$, $e = 0$,

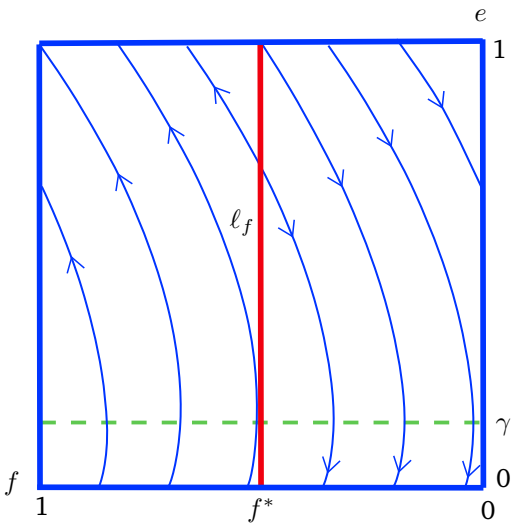

Figure 7.7: Flow of the slow vector field (7.22) on S_a^2, and the non-hyperbolic line ℓ_f in red.

$f = 1$, and $e = 1$ are lines of equilibria. The line $f = 1$ is attracting for $e \in (\gamma, 1)$ while repelling for $e \in (0, \gamma)$. However, the line $f = 0$ is attracting for $e > \gamma$ but repelling for $e < \gamma$. The line $e = 0$ is attracting for $f < f^*$, while repelling for $f > f^*$. Nevertheless, the line $e = 1$ is repelling for $f < f^*$ but attracting for $f > f^*$, see Fig. 7.7. By dividing out the factor $\frac{-16ef(e-1)(f-1)}{2f-1}$ in (7.22), the orbits of the reduced flow is derived from the desingularized system

$$\begin{aligned} \dot{f} &= \gamma - e, \\ \dot{e} &= -2. \end{aligned} \tag{7.23}$$

We directly have the following lemma from system (7.23).

Lemma 7.16. *For $f < f^*$ and $e < e^*$, the reduced flow (7.22) on S_a^2 and the corresponding slow flow on $S_{a,\varepsilon}^2$ are contracting in variable e, i.e., the induced map between sections $f = f_1$ and $f = f_2$ with $0 < f_1 < f_2 < f^*$ contracts the variable e, see Fig. 7.8.*

Remark 7.17. As is observed in Fig. 7.8, the variable f is tangent to the line $f = 0$ at $e = e^*$ in both vector fields (7.22) and (7.23). Moreover, the line $f = 0$ is repelling for $e < \gamma$. The point $e = \gamma$ in S_a^2 plays a crucial role in our analysis, see Section 7.4.

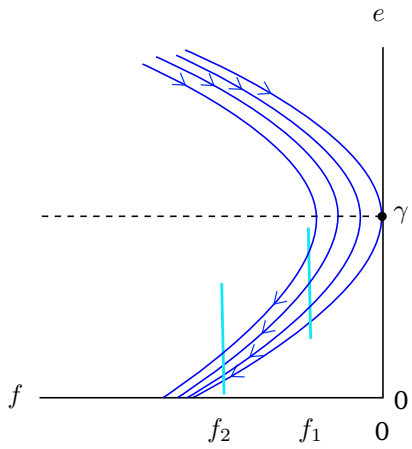

Figure 7.8: Slow flow of vector field (7.23) on S_a^2 around $e = e^*$ as well as the sections f_1, f_2 in cyan close to zero.

Lemma 7.18. *The slow flow along S_a^3, defined as $X_a^3 = \lim_{\varepsilon\to 0} \frac{1}{\varepsilon} X_\varepsilon|_{S_a^3}$, is given by*

$$\begin{aligned} \dot{f} &= \frac{-16\gamma c f(c-1)(f-1)}{2c-1}, \\ \dot{c} &= \frac{32 c f(c-1)(f-1)(1-2f)}{2c-1}. \end{aligned} \tag{7.24}$$

The phase portrait of (7.24) *is shown in Fig. 7.9.*

The vector field (7.24) is singular at the line $c = c^*$. By dividing out the factor $\frac{-16cf(c-1)(f-1)}{2c-1}$ in (7.24), the orbits of the reduced flow can be derived from the desingularized system

$$\begin{aligned} \dot{f} &= \gamma, \\ \dot{c} &= 2(2f-1). \end{aligned} \tag{7.25}$$

The following lemma is immediate from system (7.25).

Lemma 7.19. *For $c < c^*$, the reduced flow* (7.24) *on S_a^3 has the following properties:*

1. *For $f > f^*$ the reduced flow is directed towards the line $c = c^*$, and the solutions of the reduced flow on this part reaches the line $c = c^*$ in finite time.*

2. *For $f > f^*$ the reduced flow* (7.24) *on S_a^3 and the corresponding slow flow on $S_{a,\varepsilon}^3$ are contracting in f, i.e., the induced map between sections $c = c_1$ and $c = c_2$ with $0 < c_1 < c_2 < c^*$ contracts the variable f, (see Fig. 7.9).*

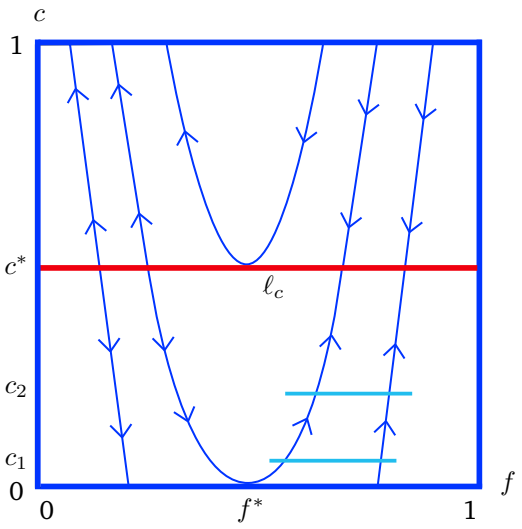

Figure 7.9: Flow of the slow vector field (7.24) on S_a^3, the non-hyperbolic line ℓ_c in red, and sections c_1, c_2 in cyan.

The same procedure applies to the critical manifold S_a^6, summarized in the following lemma.

Lemma 7.20. *The slow flow along S_a^6, defined as $X_a^6 = \lim_{\varepsilon\to 0} \frac{1}{\varepsilon} X_\varepsilon|_{S_a^6}$ is given as*

$$\begin{aligned} \dot{f} &= \frac{32(\gamma-1)fc^2(c-1)(f-1)}{2c-1}, \\ \dot{c} &= \frac{64fc^2(c-1)(f-1)(2f-1)}{2c-1}. \end{aligned} \tag{7.26}$$

The phase portrait of (7.26) *is shown in Fig. 7.10.*

By dividing out the factor $\frac{32fc^2(c-1)(f-1)}{2c-1}$ in (7.26), the orbits of the reduced flow is derived from the desingularized system

$$\begin{aligned} \dot{f} &= \gamma - 1, \\ \dot{c} &= 2(2f-1). \end{aligned} \tag{7.27}$$

From system (7.27), we obtain the following lemma.

Lemma 7.21. *For $c > c^*$, the reduced flow* (7.26) *on S_a^6 has the following properties:*

1. *For $f < f^*$, the reduced flow is directed towards the line $c = c^*$, and the solutions of the reduced flow on this part reaches the line $c = c^*$ in finite time.*

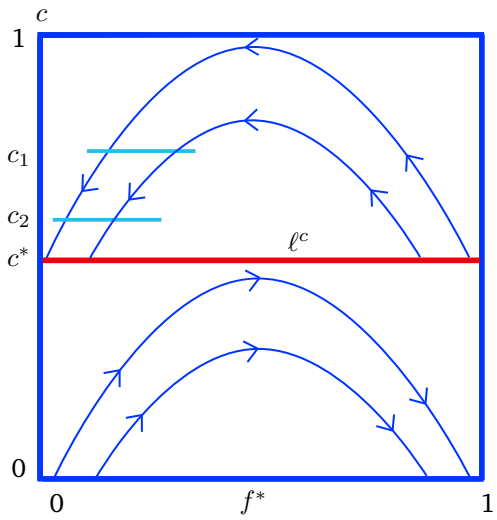

Figure 7.10: Flow of the slow vector field (7.26) on S_a^6, the non-hyperbolic line ℓ^c in red, and the sections c_1, c_2 in cyan.

2. *For $f < f^*$, the reduced flow* (7.26) *on S_a^6 and the corresponding slow flow on $S_{a,\varepsilon}^6$ are contracting in f, i.e., the induced map between sections $c = c_1$ and $c = c_2$ with $c^* < c_2 < c_1 < 1$ contracts the variable f, (see Fig. 7.10).*

Remark 7.22. For each of systems (7.22), (7.24), (7.26), and their corresponding desingularized system, a remark similar to Remark 7.13 holds, which is omitted for brevity.

7.3.3 Singular cycle

In this subsection, we present the overall behavior of the singular cycle, which is a closed curve consisting of alternating segments of the orbits of the layer problem, and the critical manifold S. By the information that we have so far from the critical manifold and the layer problem, we cannot, however, "fully" describe the singular cycle close to the non-hyperbolic lines ℓ_1 and ℓ_2. A full description of the singular cycle for those parts that cannot be derived from the critical manifold and the layer problem is presented in Section 7.4 by the blow-up method.

The construction of the singular cycle Γ_0 starts at the point $p^f := (0.5, 0, 0)$, see Fig. 7.11. This point is connected to the point $p_1 := \left(\frac{1+\sqrt{\gamma}}{2}, 0.5, 0\right) \in \ell_c$ through the orbit ω_1 of the reduced flow (7.25). Starting at p_1, the layer problem (7.8) intersects the attracting part of the plane S_a^6 in a point, denoted by p_2. This point, through the orbit ω_3 of the reduced flow (7.27), is connected to a point, denoted by $q^e \in \ell^c$. Starting at q^e, through the layer problem (7.8), the orbit ω_4 intersects

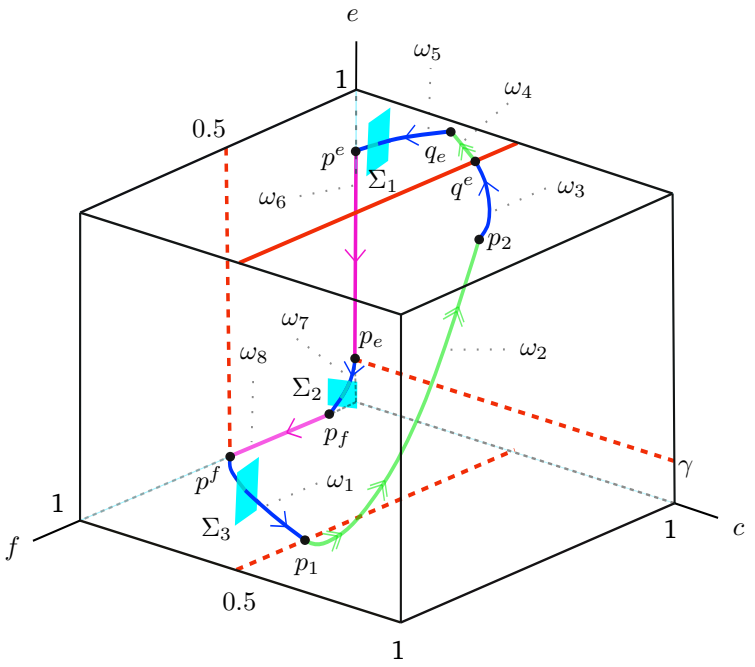

Figure 7.11: Schematic diagram of the singular cycle Γ_0.

the plane S_a^1 at a point, denoted by q_e. The orbit ω_5 of the reduced flow (7.18) connects q_e to a point, denoted by $p^e \in \ell_1$, which is the intersection of S_a^1 and S_a^2; p^e is connected to the point $p_e := (0, 0, \gamma)$ by a segment on the line ℓ_1, denoted by ω_6. The orbit ω_7 of the reduced flow (7.23) connects p_e to the point $p_f := (\frac{\gamma^2}{4}, 0, 0)$; Finally, p_f is connected to p^f by a segment on the line ℓ_2, denoted by ω_8. Hence, the singular cycle $\Gamma_0 \in \mathbb{R}^3$ of system (7.5) for $\varepsilon = 0$ is defined as follows (see Fig. 7.11):

$$\Gamma_0 := \omega_1 \cup \omega_2 \cup \omega_3 \cup \omega_4 \cup \omega_5 \cup \omega_6 \cup \omega_7 \cup \omega_8. \tag{7.28}$$

Remark 7.23. All the orbits ω_j $(j = 1, 2, ..., 8)$ are known analytically.

Owing to the fact that the layer problem is linear, all the points that connect ω_j to ω_{j+1} are explicitly known. For the particular quantity $\gamma = 0.08$, we have

$$p^f = (0.5, 0, 0), \quad p_e = (0, 0, 0.08), \quad p_f = (0.0016, 0, 0),$$
$$p_1 \approx (0.6414, 0.5, 0), \quad p_2 \approx (0.3638, 0.8485, 1), \quad q^e \approx (0.0771, 0.5, 1),$$
$$p^e \approx (0, 0, 0.7487), \quad q_e \approx (0, 0.3438, 0.9743).$$

Remark 7.24. There is a *very slow drift* from p_e to p_f, which is subtle in numerical

simulations, see Fig. 7.1. However, in order to clearly show the orbit ω_7, this part in Fig. 7.11 is illustrated larger.

Remark 7.25. At the singular level, there is no visible flow on the segments ω_6 and ω_8. The blow-up analysis, carried out in Section 7.4, will reveal a hidden flow for such segments.

7.3.4 Main result

In view of the singular cycle Γ^0, introduced in the previous subsection, we are now ready to present the main result.

Theorem 7.26. *Assume that Γ_0 is the singular cycle described in Subsection 7.3.3. Then, for sufficiently small $\varepsilon > 0$, there exists a strongly attracting periodic orbit Γ_ε of the auxiliary system* (7.5)*, and hence of the equivalent system* (7.1)*, which tends to the singular cycle Γ_0 as $\varepsilon \to 0$.*

To prove Theorem 7.26, we need to define the following sections

$$\begin{aligned}
\Sigma_1 &:= \{(f, c, e) \in \mathcal{C} \mid (f,\ e) \in R_1,\ c = \delta_1\},\\
\Sigma_2 &:= \{(f, c, e) \in \mathcal{C} \mid (c,\ e) \in R_2,\ f = \delta_2\},\\
\Sigma_3 &:= \{(f, c, e) \in \mathcal{C} \mid (f,\ e) \in R_3,\ c = \delta_3\},
\end{aligned} \tag{7.29}$$

where R_j $(j = 1, 2, 3)$ are suitable small rectangles, and δ_j are chosen sufficiently small. Note that Σ_1 is transversal to ω_5, Σ_2 is transversal to ω_7, and Σ_3 is transversal to ω_1, see Fig. 7.11.

In view of the sections Σ_j, introduced in (7.29), we define the following Poincaré maps for the flow of the system (7.5):

$$\begin{aligned}
&\pi_1 : \Sigma_1 \to \Sigma_2,\\
&\pi_2 : \Sigma_2 \to \Sigma_3,\\
&\pi_3 : \Sigma_3 \to \Sigma_1.
\end{aligned} \tag{7.30}$$

The map π_1 describes the passage from Σ_1 to Σ_2 along the non-hyperbolic line ℓ_1, the map π_2 describes the passage from Σ_2 to Σ_3 along the non-hyperbolic line ℓ_2, and the map π_3 describes the passage from Σ_3 to Σ_1; the map π_3 consists of slow flow along $S^3_{a,\varepsilon}$, followed by the fast dynamics from a neighborhood of p_1 to a neighborhood of p_2, followed by the slow flow along $S^6_{a,\varepsilon}$ to a neighborhood of q^e. Through the fast dynamics, this neighborhood is mapped to a neighborhood of q_e, followed by the slow flow along $S^1_{a,\varepsilon}$ to Σ_1.

We summarize the properties of the above maps in the following lemmas.

Lemma 7.27. *If the section Σ_1 is chosen sufficiently small, there exists $\varepsilon_0 > 0$ such that the map*

$$\pi_1 : \Sigma_1 \to \Sigma_2, \qquad (f, e) \mapsto (\pi_1^c(f, e, \varepsilon), \pi_1^e(f, e, \varepsilon)), \tag{7.31}$$

is well-defined for $\varepsilon \in [0, \varepsilon_0]$ and smooth for $\varepsilon \in (0, \varepsilon_0]$. The map π_1 is a strong contraction with contraction rate $\exp(-K/\varepsilon)$ for some $K > 0$. The image of Σ_1 is a two-dimensional domain of exponentially small size, which converges to the point $q_2 := \Sigma_2 \cap \omega_7$ as $\varepsilon \to 0$.

Lemma 7.28. *If the section Σ_2 is chosen sufficiently small, there exists $\varepsilon_0 > 0$ such that the map*

$$\pi_2 : \Sigma_2 \to \Sigma_3, \qquad (c, e) \mapsto (\pi_2^f(c, e, \varepsilon), \pi_2^e(c, e, \varepsilon)), \tag{7.32}$$

is well-defined for $\varepsilon \in [0, \varepsilon_0]$ and smooth for $\varepsilon \in (0, \varepsilon_0]$. The map π_2 is a strong contraction with contraction rate $\exp(-K/\varepsilon)$ for some $K > 0$. The image of Σ_2 is a two-dimensional domain of exponentially small size, which converges to the point $q_3 := \Sigma_3 \cap \omega_1$ as $\varepsilon \to 0$.

The proofs of Lemmas 7.27 and 7.28 are based on the blow-up analysis of the non-hyperbolic lines ℓ_1 and ℓ_2, respectively, which are presented in Subsections 7.4.1 and 7.4.2.

Remark 7.29. The points on the line ℓ_c when $0.5 < f < 1$, and on the line ℓ^c when $0 < f < 0.5$ are jump points, i.e., the trajectory switches from the slow dynamics to the fast dynamics. It is shown [138] that this behavior is very similar to the behavior of standard slow-fast systems with two slow variables and one fast variable near a generic "fold" line, studied in [138] based on the blow-up method. The critical manifolds S^3 and S^6 of system (7.5) can be viewed as a standard folded critical manifold, which has been straightened out by a suitable diffeomorphism. This leads to the curved fibers of the layer problem (7.6). Therefore, we can use the results of [138] to understand the behavior of (7.5) close to the non-hyperbolic lines ℓ_c and ℓ^c.

The following lemma describes the map from the section Σ_3 to the section Σ_1, defined in (7.30).

Lemma 7.30. *If the section Σ_3 is chosen sufficiently small, there exists $\varepsilon_0 > 0$ such that the map*

$$\pi_3 : \Sigma_3 \to \Sigma_1, \qquad (f, e) \mapsto (\pi_3^f(f, e, \varepsilon), \pi_3^e(f, e, \varepsilon)), \tag{7.33}$$

is well-defined for $\varepsilon \in [0, \varepsilon_0]$ and smooth for $\varepsilon \in (0, \varepsilon_0]$. The image of Σ_3 is an exponentially thin strip lying exponentially close to $S^1_{a,\varepsilon} \cap \Sigma_1$, i.e., its width in the

f-direction is $\mathcal{O}(\exp(-K/\varepsilon))$ for some $K > 0$. Moreover, $\pi_3(\Sigma_3)$ converges to a segment of $S^a_1 \cap \Sigma_1$ as $\varepsilon \to 0$.

Proof. The basic idea of the proof is based on the map that has been already described in Fig. (7.11) for $\varepsilon = 0$, denoted by π_3^0, and then treat π_3 as an ε-perturbation of π_3^0. If the section Σ_3 is chosen sufficiently small, then the trajectories starting in Σ_3 can be described by the slow flow along the manifold $S^3_{a,\varepsilon}$ combined with the exponential contraction towards the slow manifold until they reach a neighborhood of the jump points on the line ℓ_c. Applying [138, Theorem 1] close to the jump pints, the trajectories switch from the slow dynamics to the fast dynamics, and hence pass the non-hyperbolic line ℓ_c; this transition is well-defined for $\varepsilon \in [0, \varepsilon_1]$, and smooth for $\varepsilon \in (0, \varepsilon_1]$ for some $\varepsilon_1 > 0$. Note that [138, Theorem 1] guarantees that the contraction of the solutions in the e-direction persists during the passage through the fold-line ℓ_c, as is at most algebraically expanding. After that, the solutions follow the fast dynamics ω_2 until they reach a neighborhood of the point p_2, see Fig. 7.11. Next, the solutions follow the slow flow along the manifold $S^6_{a,\varepsilon}$ combined with the exponential contraction towards the slow manifold until they reach a neighborhood of the point q^e. Again applying [138, Theorem 1] close to the jump points, the solutions which are very close to the non-hyperbolic line ℓ^c switch from the slow dynamics to the fast dynamics, and hence pass the non-hyperbolic line ℓ^c, where the corresponding transitions are well-defined for $\varepsilon \in [0, \varepsilon_2]$, and smooth for $\varepsilon \in (0, \varepsilon_2]$ for some $\varepsilon_2 > 0$, and then follow the fast dynamics (ω_4) until they reach a neighborhood of the point q_e. Finally, the solutions follow the slow flow along the manifold $S^1_{a,\varepsilon}$ combined with the exponential contraction towards the slow manifold until they reach the section Σ_1.

Theorem 1 in [138] implies that the map π_3 is at most algebraically expanding in the e-direction, provided that the section Σ_3 is chosen sufficiently small. On the other hand, the slow manifold $S^1_{a,\varepsilon}$ is exponentially contracting in the f-direction (Fenichel theory). Therefore, the image of Σ_3 is a thin strip lying exponentially close to $S^1_{a,\varepsilon} \cap \Sigma_1$. Hence, the statements of the lemma follow. □

Now we are ready to give the proof of the main result.

Proof of Theorem 7.26. Let us define the map $\pi : \Sigma_3 \to \Sigma_3$ as a combination of the maps π_j ($j = 1, 2, 3$), described in Lemmas 7.27, 7.28 and 7.30. More precisely, we define

$$\pi := \pi_2 \circ \pi_1 \circ \pi_3 : \Sigma_3 \to \Sigma_3.$$

If the section Σ_3 is chosen sufficiently small, Lemma 7.30 implies that there exists $\varepsilon_3 > 0$ such that the map π_3 is well-defined for $\varepsilon \in [0, \varepsilon_3]$ and smooth for $\varepsilon \in (0, \varepsilon_3]$, and the image of Σ_3 is a thin strip lying exponentially close to $S^1_{a,\varepsilon} \cap \Sigma_1$, i.e., $\pi_3(\Sigma_3)$ is exponentially contracting with rate $\exp(-K_3/\varepsilon)$, for some $K_3 > 0$, in the

f-direction while it is bounded in the e-direction.

Next, if the entry section Σ_1 is chosen such that $\Sigma_1 \supset \pi_3(\Sigma_3)$, Lemma 7.27 implies that there exists $\varepsilon_1 > 0$ such that the map π_1 is well-defined for any $\varepsilon \in [0, \varepsilon_1]$ and smooth for $\varepsilon \in (0, \varepsilon_1]$, and π_1 is an exponential contraction with rate $\exp(-K_1/\varepsilon)$ for some $K_1 > 0$. Finally, if the entry section Σ_2 is chosen such that $\Sigma_2 \supset \pi_1(\Sigma_1)$, Lemma 7.28 implies that there exists $\varepsilon_2 > 0$ such that the map π_2 is well-defined for any $\varepsilon \in [0, \varepsilon_2]$ and smooth for any $\varepsilon \in (0, \varepsilon_2]$, and further, π_2 is an exponential contraction with rate $\exp(-K_2/\varepsilon)$, for some $K_2 > 0$, such that $\Sigma_3 \supset \pi_2(\Sigma_2)$.

Denoting $\varepsilon_0 := \min\{\varepsilon_1, \varepsilon_2, \varepsilon_3\}$ and $K := \min\{K_1, K_2, K_3\}$, the map $\pi : \Sigma_3 \to \Sigma_3$ is well-defined for any $\varepsilon \in [0, \varepsilon_0]$, and smooth for any $\varepsilon \in (0, \varepsilon_0]$. Further, based on the contracting properties of the maps π_i, $i = 1, 2, 3$, we conclude that $\pi(\Sigma_3) \subset \Sigma_3$ is contraction with rate $\exp(-K/\varepsilon)$. The Banach fixed-point theorem implies the existence of a unique fixed point for the map π, corresponding to the attracting periodic orbit of the system (7.5). Moreover, due to the last assertion of Lemmas 7.27, 7.28 and 7.30, the periodic orbit Γ_ε tends to the singular cycle Γ_0 as $\varepsilon \to 0$. This completes the proof. □

7.4 Blow-up analysis

The slow-fast analysis that we have done in Section 7.3 does not explain the dynamics of system (7.5) close to the non-hyperbolic lines ℓ_1 and ℓ_2. As the segments ω_6 and ω_8 lie on these lines (see Fig. 7.11), we need a detailed analysis close to the non-hyperbolic lines ℓ_1 and ℓ_2, which is carried out in this section via the blow-up method [61, 90, 92]. To apply this, we extend system (7.5) by adding ε as a trivial dynamic variable and obtain

$$\begin{aligned}
\frac{df}{d\tau} &= [\gamma(1-f)(\varepsilon+2f) - 2fe(\varepsilon+1-f)]\, H_2^\varepsilon(c) H_3^\varepsilon(e),\\
\frac{dc}{d\tau} &= [8(1-c)f(\varepsilon+2c) - 4c(\varepsilon+2-2c)]\, H_1^\varepsilon(f) H_3^\varepsilon(e),\\
\frac{de}{d\tau} &= [8(1-e)c(\varepsilon+2e) - 4e(\varepsilon+2-2e)]\, H_1^\varepsilon(f) H_2^\varepsilon(c),\\
\frac{d\varepsilon}{d\tau} &= 0,
\end{aligned} \tag{7.34}$$

where $H_1^\varepsilon(f), H_2^\varepsilon(c)$ and $H_3^\varepsilon(e)$ are defined in (7.3). Note that for the extended system (7.34), the lines $\ell_1 \times \{0\}$ and $\ell_2 \times \{0\}$ are sets of equilibria. Owing to the fact that the linearization of (7.34) around these lines has quadruple zero eigenvalues, system (7.34) is very degenerate close to $\ell_1 \times \{0\}$ and $\ell_2 \times \{0\}$. To resolve these degeneracies, we use the blow-up method, given in next subsections.

7.4.1 Blow-up of the non-hyperbolic line $\ell_1 \times \{0\}$

The blow-up of the non-hyperbolic line $\ell_1 \times \{0\}$ is presented in this subsection. To this end, we transform the non-hyperbolic line of steady states $\ell_1 \times \{0\}$ by

$$f = r\bar{f}, \qquad c = r\bar{c}, \qquad \varepsilon = r\bar{\varepsilon}, \qquad e = \bar{e}, \tag{7.35}$$

where $\bar{f}^2 + \bar{c}^2 + \bar{\varepsilon}^2 = 1$ and $r \geqslant 0$. Note that since $(f, c, e) \in \mathcal{C}$, we may further assume that $\bar{f}, \bar{c} \geqslant 0$ and $\bar{e} \in [0, 1]$. Since all weights are equal to 1 in (7.35), this is a homogeneous blow-up. For fixed $\bar{e}$, each point $(0, 0, \bar{e})$ is blown-up to a sphere $\mathbb{S}^2$, and the line $\ell_1 \times \{0\}$ is blown-up to a cylinder $\mathbb{S}^2 \times [0, 1]$, see Fig. 7.12.

For the analysis of system (7.34) close to the line $\ell_1 \times \{0\}$, we define three charts K_1, K_2 and K_3 by setting $\bar{c} = 1$, $\bar{\varepsilon} = 1$, and $\bar{f} = 1$ in (7.35), respectively:

$$K_1: \quad f = r_1 f_1, \qquad c = r_1, \qquad \varepsilon = r_1\varepsilon_1, \qquad e = e_1, \tag{7.36}$$

$$K_2: \quad f = r_2 f_2, \qquad c = r_2 c_2, \qquad \varepsilon = r_2, \qquad e = e_2, \tag{7.37}$$

$$K_3: \quad f = r_3, \qquad c = r_3 c_3, \qquad \varepsilon = r_3\varepsilon_3, \qquad e = e_3, \tag{7.38}$$

The changes of coordinates from charts K_1 to K_2, and K_2 to K_3 in the blown-up space are given in the following lemma, which can be derived from (7.36), (7.37), and (7.38).

Lemma 7.31. *The changes of coordinates from K_1 to K_2, and from K_2 to K_3 are given by*

$$\kappa_{12}: \quad f_2 = \frac{f_1}{\varepsilon_1}, \qquad c_2 = \frac{1}{\varepsilon_1}, \qquad \varepsilon_2 = r_1\varepsilon_1, \qquad e_2 = e_1, \qquad \varepsilon_1 > 0, \tag{7.39}$$

$$\kappa_{23}: \quad r_3 = r_2 f_2, \qquad c_3 = \frac{c_2}{f_2}, \qquad \varepsilon_3 = \frac{1}{f_2}, \qquad e_3 = e_2, \qquad f_2 > 0. \tag{7.40}$$

The goal of this subsection is to construct the transition map $\pi_1 : \Sigma_1 \to \Sigma_2$, defined in (7.30), and prove Lemma 7.27. Before going into the details, let us briefly describe our approach. We describe the transition map $\pi_1 : \Sigma_1 \to \Sigma_2$ via an equivalent one in the blown-up space. In particular, we define

$$\pi_1 := \Phi \circ \bar{\pi}_1 \circ \Phi^{-1}, \tag{7.41}$$

where

$$\bar{\pi}_1 := \Pi_3 \circ \kappa_{23} \circ \Pi_2 \circ \kappa_{12} \circ \Pi_1, \tag{7.42}$$

and $\Phi : \mathbb{S}^2 \times [0, 1] \times [0, r_0) \to \mathbb{R}^4$ is the cylindrical blow-up defined by (7.35), the maps Π_i are local transitions induced by the blown-up vector fields which are detailed below, and κ_{12} and κ_{23} denote the changes of coordinates, given in Lemma 7.31. $\bar{\pi}_1$ is the transition map in the blown-up space and due to the fact that Φ is

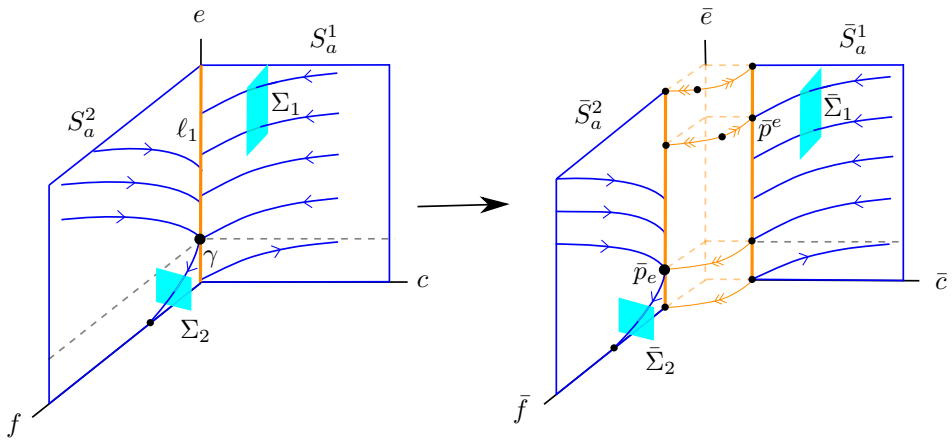

Figure 7.12: The left figure shows the dynamics close to the non-hyperbolic line ℓ_1. The right figure shows the corresponding dynamics in the blown-up space.

a diffeomorphism, it is equivalent to π_1. A schematic of the problem at hand is shown in Figure 7.12.

The left picture in Fig. 7.12 shows the critically manifolds S_a^1 and S_a^2, and the corresponding flows in blue. The non-hyperbolic line ℓ_1 is shown in orange. For $e > \gamma$, the reduced flows on both critically manifolds approach the line ℓ_1. At the point on the line ℓ_1 with $e = \gamma$, a transition from S_a^1 to S_a^2 is possible, as indicated in the figure. The right picture in Fig. 7.12 schematically shows the configuration in the blown-up space. The cylinder, corresponding to $r = 0$, is shown in orange. The part of the phase space corresponding to $\bar{\varepsilon} = 0$ and $r > 0$ are shown outside of the the cylinder. Here we recover the critically manifolds, and the reduced flows in $\bar{S}_a^1$ and $\bar{S}_a^2$. In the blown-up space, the manifolds S_a^1 and S_a^2 are separated and hence gained hyperbolicity, i.e. attractive, as indicated in cylinder. All these assertions will be proven in this section.

Roughly speaking, in chart K_1 we continue the attracting slow manifold $\bar{S}_a^1$ onto the cylinder. Chart K_2 is used to track the flow across the cylinder. The exit of the flow from the cylinder and its transition to $\bar{S}_a^2$ is studied in chart K_3, see Figs. 7.12 and 7.19. The detailed analysis of the maps Π_i introduced in (7.42), is given in the forthcoming subsections.

Analysis in chart K_1

After substituting (7.36) into (7.34), and dividing out all the equations by the common factor r_1, the equations governing the dynamics in chart K_1 are given by

$$\begin{aligned} f_1' &= -4f_1\Gamma_1 G_{11} + [\gamma(1-r_1f_1)(\varepsilon_1+2f_1) - 2f_1e_1(r_1\varepsilon_1+1-r_1f_1)]G_{12},\\ r_1' &= 4r_1\Gamma_1 G_{11},\\ e_1' &= 4r_1[2r_1(1-e_1)(r_1\varepsilon_1+2e_1) - e_1(r_1\varepsilon_1+2-2e_1)]G_{13},\\ \varepsilon_1' &= -4\varepsilon_1[2r_1f_1(1-r_1)(\varepsilon_1+2) - (r_1\varepsilon_1+2-2r_1)]G_{11}, \end{aligned} \tag{7.43}$$

where we denote

$$\begin{aligned} \Gamma_1 &:= [2r_1f_1(1-r_1)(\varepsilon_1+2) - (r_1\varepsilon_1+2-2r_1)],\\ G_{11} &:= (r_1\varepsilon_1+1-r_1f_1)(r_1\varepsilon_1+2-2e_1)(\varepsilon+2f_1)(r_1\varepsilon_1+2e_1),\\ G_{12} &:= (r_1\varepsilon_1+2-2r_1)(r_1\varepsilon_1+2-2e_1)(\varepsilon_1+2)(r_1\varepsilon_1+2e_1),\\ G_{13} &:= (r_1\varepsilon_1+1-r_1f_1)(r_1\varepsilon_1+2-2r_1)(\varepsilon_1+2f_1)(\varepsilon_1+2). \end{aligned}$$

From (7.43) it is clear that the planes $r_1=0$ and $\varepsilon_1=0$ are invariant. Hence, we consider the following cases:

1. $r_1=\varepsilon_1=0$: in this case, the dynamics (7.43) is simplified to

$$\begin{aligned} e_1' &= 0,\\ f_1' &= 32f_1e_1(1-e_1)[2f_1+\gamma-e_1]. \end{aligned} \tag{7.44}$$

   For fixed e, the equilibria of system (7.44) are the attracting point $p_1^a = (f_1,r_1,e_1,\varepsilon_1) = (0,0,e_1,0)$, and the repelling point $p_1^r = (f_1,r_1,e_1,\varepsilon_1) = (\frac{e_1-\gamma}{2},0,e_1,0)$. Note that the two hyperbolic points p_1^a and p_1^r intersect at the non-hyperbolic point $(f_1,r_1,e_1,\varepsilon_1)=(0,0,\gamma,0)$, see Fig. 7.13.

2. $\varepsilon_1=0$ and $r_1\geqslant 0$: in this case, the dynamics (7.43) is represented by

$$\begin{aligned} f_1' &= 32f_1e_1(1-e_1)(1-r_1)(1-r_1f_1)[(\gamma-e_1) - 2f_1(2r_1f_1-1)],\\ r_1' &= 64r_1f_1e_1(1-e_1)(1-r_1)(1-r_1f_1)[2r_1f_1-1],\\ e_1' &= 64r_1f_1e_1(1-e_1)(1-r_1)(1-r_1f_1)[2r_1-1]. \end{aligned} \tag{7.45}$$

   From (7.45), one concludes that the plane $f_1=0$ is the plane of equilibria; this plane when $e\geqslant\gamma$ is denoted by $S^1_{a,1}$, see Fig. 7.13. The non-zero eigenvalue along $S^1_{a,1}$ is $\lambda = 32e_1(1-e_1)(1-r_1)(\gamma-e_1)$, implying that for $0\leqslant r_1<1$ and $e_1>\gamma$, the plane $S^1_{a,1}$ is attracting. The intersection of the e_1-axis with $S^1_{a,1}$ is denoted by ℓ_{e_1}. System (7.45) has also another curve of equilibria, which is defined by $r_1=0$ and $f_1=\frac{e_1-\gamma}{2}$, denoted by $\mathcal{M}_1^r$,

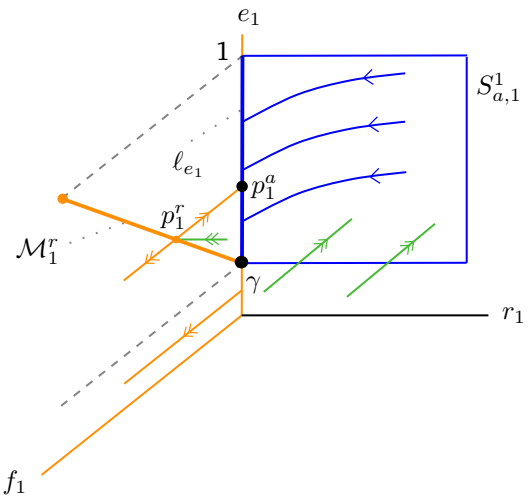

Figure 7.13: Dynamics of system (7.43) in the invariant plane $\varepsilon_1 = 0$.

see Fig. 7.13. This curve of equilibria is of saddle-type with the eigenvalues $\lambda = \pm 32 e_1(e_1-1)(e_1-\gamma)$. Note that here we have recovered the information of case 1 (i.e., $r_1 = \varepsilon_1 = 0$).

3. $r_1 = 0$ and $\varepsilon_1 \geqslant 0$: in this case, the dynamics (7.43) is represented by

$$\begin{aligned} e_1' &= 0, \\ f_1' &= 8e_1(1-e_1)[(\varepsilon_1+2)(\gamma(\varepsilon_1+2f_1)-2f_1e_1)+4f_1(\varepsilon_1+2f_1)], \\ \varepsilon_1' &= 32e_1\varepsilon_1(1-e_1)(\varepsilon_1+2f_1). \end{aligned} \tag{7.46}$$

By setting $\varepsilon_1 = 0$, we again recover the line ℓ_{e_1}, and the curve $\mathcal{M}^r_1$. The Jacobian matrix at any point in ℓ_{e_1} has two eigenvalues: one is zero and the other one is $\lambda = 32e_1(1-e_1)(\gamma - e_1)$, implying that the line ℓ_{e_1} is attracting when $e > \gamma$, see Fig. 7.14. The existence of two zero eigenvalues in this case implies that there exists a two-dimensional center manifold, namely, $\mathcal{C}_{a,1}$.

Remark 7.32. In chart K_1, the most important role is played by the two-dimensional center manifold $\mathcal{C}_{a,1}$, see Lemma 7.34. In fact, this is the continuation of the critical manifold $S^1_{a,1}$.

We summarize the analysis performed in this subsection in the following lemmas.

Lemma 7.33. *System* (7.43) *has the following manifolds of equilibria:*

1. *The plane* $S^1_{1,a}$ *which includes the line* ℓ_{e_1}, *and*

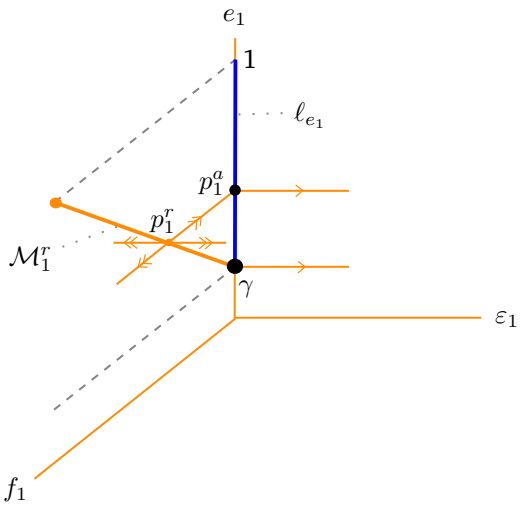

Figure 7.14: Dynamics of system (7.43) in the invariant plane $r_1 = 0$.

2. $\mathcal{M}_1^r = \left\{(f_1, r_1, e_1, \varepsilon_1) \mid f_1 = \frac{e_1-\gamma}{2},\ r_1 = 0,\ e_1 \in [\gamma, 1],\ \varepsilon_1 = 0\right\}$.

Lemma 7.34. *The following properties hold for system* (7.43)*:*

1. *The linearization of* (7.43) *along* $S^1_{1,\varepsilon}$ *has three zero eigenvalues, and the nonzero eigenvalue* $\lambda = 32e_1(1-e_1)(1-r_1)(\gamma - e_1)$*, which for* $r_1 = 0$ *corresponds to the flow in the invariant plane* (f_1, e_1)*.*

2. *There exists a three-dimensional center manifold* $\mathcal{W}^c_{a,1}$ *of the line* ℓ_{e_1} *which contains the plane of equilibria* $S^1_{a,1}$ *and the two-dimensional center manifold* $\mathcal{C}_{a,1}$*. The manifold* $\mathcal{W}^c_{a,1}$ *is attracting, and in the set* D_1*, defined by*

$$D_1 := \{(f_1, r_1, e_1, \varepsilon_1) \mid 0 \leqslant r_1 \leqslant \delta_1,\ ,\ e_1 \in I_1,\ 0 \leqslant \varepsilon_1 \leqslant \alpha_1\},$$

   is given by the graph

$$f_1 = h_{a,1}(r_1, e_1, \varepsilon_1),$$

   where I_1 *is a suitable interval, and* $\alpha_1, \delta_1 > 0$ *are sufficiently small. For the particular point* $p_{a,1} \in \ell_{e_1}$ *where* $e^0 \in I_1$*, the function* $h_{a,1}(r_1, e^0, \varepsilon_1)$ *has the expansion*

$$h_{a,1}(r_1, e^0, \varepsilon_1) = \frac{\gamma}{2(e^0 - \gamma)}\varepsilon_1 + \mathcal{O}(\varepsilon_1^2). \tag{7.47}$$

3. *There exists* $K > 0$ *such that the orbits that are near the center manifold* $\mathcal{W}^c_{a,1}$ *are attracted to* $\mathcal{W}^c_{a,1}$ *by an exponential rate of order* $\mathcal{O}(\exp(-Kt_1))$*.*

Proof. A straightforward calculation shows the first claim. Owing to the fact that the

linearization of (7.43) along $S^1_{1,\varepsilon}$ has three zero eigenvalues, there exists [14, 60] an attracting three-dimensional center manifold $\mathcal{W}^c_{a,1}$ at the point $p_{a,1}$. To derive equation (7.47), we first expand f_1 to the first oder of variables r_1, e_1 and ε_1, and then plug it into (7.43). By comparing the coefficients of r_1, e_1 and ε_1, equation (7.47) is obtained. The last claim is proven by the center manifold theory [14, 60] applied at the point $p_{a,1}$. □

Remark 7.35. The attracting center manifold $\mathcal{W}^c_{a,1}$ recovers parts of the slow manifold $S^1_{a,\varepsilon}$ away form the line $\ell_1 \times \{0\}$, and extends it into an $\mathcal{O}(\varepsilon)$ neighborhood of it. The slow manifold $S^1_{a,\varepsilon}$ is obtained as a section $\varepsilon = constant$ of $\mathcal{W}^c_{a,1}$. In chart K_1, this center manifold is given by the graph (7.47).

Note that our goal in chart K_1 is to understand the dynamics (7.43) close to the center manifold $\mathcal{W}^c_{a,1}$, which corresponds to a sufficiently small neighborhood of the slow manifold $S^1_{a,1}$. Assuming that $\delta_1, \alpha_1, \beta_1 > 0$ are small constants, we define the sections

$$\begin{aligned} \Delta_1^{in} &:= \{(f_1, r_1, e_1, \varepsilon_1) \mid (f_1, r_1, e_1, \varepsilon_1) \in D_1,\ r_1 = \delta_1\}, \\ \Delta_1^{out} &:= \{(f_1, r_1, e_1, \varepsilon_1) \mid (f_1, r_1, e_1, \varepsilon_1) \in D_1,\ \varepsilon_1 = \alpha_1\}, \\ R_1^{in} &:= \{(f_1, r_1, e_1, \varepsilon_1) \mid (f_1, r_1, e_1, \varepsilon_1) \in D_1,\ r_1 = \delta_1, |f_1| \leqslant \beta_1\}. \end{aligned} \tag{7.48}$$

Note that by the way we have defined Δ_1^{in}, we in fact have $\Delta_1^{in} = \bar{\Sigma}_1 := \Phi^{-1}(\Sigma_1 \times \{[0, \rho_1]\})$ for some $\rho_1 > 0$, see Fig. 7.12. Furthermore, the constants $\delta_1, \alpha_1, \beta_1$ are chosen such that $R_1^{in} \subset \Delta_1^{in}$, and the intersection of the center manifold $\mathcal{W}^c_{a,1}$ with Δ_1^{in} lies in R_1^{in}, i.e., $\mathcal{W}^c_{a,1} \cap \Delta_1^{in} \subset R_1^{in}$.

Let us denote Π_1 as the transition map from Δ_1^{in} to Δ_1^{out}, induced by the flow of (7.43). In order to construct the map Π_1, we reduce system (7.43) to the center manifold $\mathcal{W}^c_{a,1}$ and analyze the system based on the the dynamics on $\mathcal{W}^c_{a,1}$. To this end, by substituting (7.47) into (7.43) and rescaling time, the flow of the center manifold is given by

$$\begin{aligned} r_1' &= -r_1, \\ e_1' &= -\frac{1}{2}[\mathcal{O}(r_1) + \mathcal{O}(r_1\varepsilon_1)], \\ \varepsilon_1' &= \varepsilon_1, \end{aligned} \tag{7.49}$$

where the derivative is with respect to the new time scale, namely, t_1. Now let us consider a solution of (7.49), namely, $(r_1(t_1), e_1(t_1), \varepsilon_1(t_1))$ which satisfies the

following conditions:

$$\begin{aligned} r_1(0) &= \delta_1, & r_1(T^{out}) &= r_1^{out}, \\ e_1(0) &= e_1^{in}, & e_1(T^{out}) &= e_1^{out}, \\ \varepsilon_1(0) &= \varepsilon_1^{in}, & \varepsilon_1(T^{out}) &= \alpha_1. \end{aligned} \tag{7.50}$$

From equation $\varepsilon_1' = \varepsilon_1$ with the boundary conditions $\varepsilon_1(0) = \varepsilon_1^{in}$ and $\varepsilon_1(T^{out}) = \alpha_1$, we can calculate the time that $(r_1(t_1), e_1(t_1), \varepsilon_1(t_1))$ needs to travel from Δ_1^{in} to Δ_1^{out}, which is given by

$$T^{out} = \ln \frac{\alpha_1}{\varepsilon_1^{in}}. \tag{7.51}$$

As $e_1' = -\frac{1}{2}[O(r_1)+O(r_1\varepsilon_1)]$ with $e_1(T^{in}) = e_1^{in}$, we can estimate the time evolution of $e_1(t_1)$, which is given by

$$e_1(t_1) = \frac{r_1^{in}}{2}\left[\exp(-t_1) - 1 - t_1\varepsilon_1^{in}\right] + e_1^{in}, \qquad 0 \leqslant t_1 \leqslant T^{out}. \tag{7.52}$$

Hence, in view of (7.51), one has

$$e_1(T^{out}) = e_1^{out} := \frac{r_1^{in}}{2}\left[\frac{\varepsilon_1^{in}}{\alpha_1} - 1 - \varepsilon_1^{in}\ln\frac{\alpha_1}{\varepsilon_1^{in}}\right] + e_1^{in}. \tag{7.53}$$

We summarize the analysis performed in chart K_1 in the following theorem.

Theorem 7.36. *For system* (7.43) *with sufficiently small* $\delta_1, \alpha_1, \beta_1$ *and* $R_1^{in} \subset \Delta_1^{in}$, *the transition map* $\Pi_1 : R_1^{in} \to \Delta_1^{out}$ *is well-defined and has the following properties:*

1. $\Pi_1(R_1^{in}) \subset \Delta_1^{out}$ *is a three-dimensional wedge-like region in* Δ_1^{out}.

2. *The transition map* Π_1 *is given by*

$$\Pi_1\begin{pmatrix} f_1 \\ \delta_1 \\ e_1 \\ \varepsilon_1 \end{pmatrix} = \begin{pmatrix} h_{a,1}(\frac{\delta_1}{\alpha_1}\varepsilon_1, e_1^{out}, \alpha_1) + \Psi(\delta_1, e_1, \varepsilon_1) \\ \frac{\delta_1}{\alpha_1}\varepsilon_1 \\ e_1^{out} \\ \alpha_1 \end{pmatrix},$$

where e_1^{out} *is given in* (7.53), $\Psi(\cdot)$ *is an exponentially small function, and* $h_{a,1}(\cdot)$ *is of order* $\mathcal{O}(\varepsilon_1)$, *due to* (7.47).

We now turn to the analysis in chart K_2.

Analysis in chart K_2

After substituting (7.37) into (7.34), and dividing out all the equations by the common factor r_2, the equations governing the dynamics in chart K_2 are given by

$$\begin{aligned} f_2' &= 8e_2\left[\gamma(1+2f_2)-2f_2e_2\right](1-e_2)(1+2c_2)+\mathcal{O}(\varepsilon),\\ c_2' &= -32c_2e_2(1-e_2)(1+2f_2)+\mathcal{O}(\varepsilon),\\ e_2' &= -16\varepsilon e_2(1-2e_2)(1+2f_2)(1+2c_2)+\mathcal{O}(\varepsilon^2),\\ \varepsilon' &= 0. \end{aligned} \tag{7.54}$$

Due to the fact that $r_2 = \varepsilon$ in chart K_2, we have presented (7.54) in terms of ε. Note that since $r_2' = \varepsilon' = 0$, system (7.54) is a family of three-dimensional vector fields which are parametrized by ε. Moreover, system (7.54) is a slow-fast system in the standard form, i.e., e_2 is the slow variable, and f_2 and c_2 are the fast variables. As the differentiation "prime" in (7.54) is with respect to the fast time variable, namely τ_2, by transforming it to the slow time variable we have $t_2 = \varepsilon\tau_2$, and hence

$$\begin{aligned} \varepsilon\dot{f}_2 &= 8e_2\left[\gamma(1+2f_2)-2f_2e_2\right](1-e_2)(1+2c_2)+\mathcal{O}(\varepsilon),\\ \varepsilon\dot{c}_2 &= -32c_2e_2(1-e_2)(1+2f_2)+\mathcal{O}(\varepsilon),\\ \dot{e}_2 &= -16e_2(1-2e_2)(1+2f_2)(1+2c_2)+\mathcal{O}(\varepsilon), \end{aligned} \tag{7.55}$$

where the "dot" is with respect to t_2. Now by setting $\varepsilon = 0$ in (7.54) we obtain the corresponding layer problem

$$\begin{aligned} f_2' &= 8e_2\left[\gamma(1+2f_2)-2f_2e_2\right](1-e_2)(1+2c_2),\\ c_2' &= -32c_2e_2(1-e_2)(1+2f_2),\\ e_2' &= 0, \end{aligned} \tag{7.56}$$

which has the associated critical manifold $c_2 = 0$ and $f_2 = \frac{\gamma}{2(e_2-\gamma)}$, denoted by N_2^0, see Fig. 7.15. The Jacobian matrix corresponding to (7.56) along N_2^0 has the eigenvalues

$$\lambda_{21} = -16e_2(1-e_2)(e_2-\gamma), \qquad \lambda_{22} = \frac{32e_2^2(e_2-1)}{(e_2-\gamma)}. \tag{7.57}$$

As is clear form (7.57), the critical manifold restricted to $e_2 \in (\gamma, 1)$ is normally hyperbolic, and specially, is fully attracting since both of the eigenvalues are negative. As e_2 approaches γ from above, f_2 develops a singularity along N_2^0. Thus, the behavior of N_2^0 as $e \to \gamma$ has to be studied in chart K_3. Using Fenichel theory and the dynamics in chart K_2 for $\varepsilon = 0$, one is able to describe the dynamics for $0 < \varepsilon \ll 1$ in this chart, i.e., there exists a slow manifold N_2^ε which is the

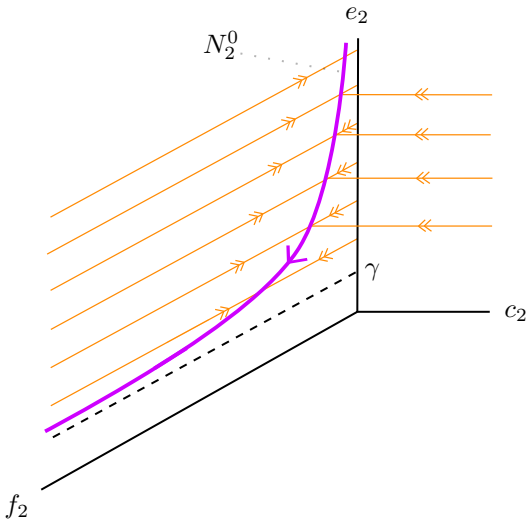

Figure 7.15: Fully attracting critical manifold N_2^0 in purple, and the slow and fast dynamics in chart K_2.

ε-perturbation of N_2^0. We summarize the properties of the critical manifold of chart K_2 in the following lemma.

Lemma 7.37. *The critical manifold*

$$N_2^0 = \left\{ (f_2, c_2, e_2) \mid f_2 = \frac{\gamma}{2(e_2 - \gamma)},\ c_2 = 0,\ e_2 \in I_2^0 \right\}, \tag{7.58}$$

is fully attracting, where I_2^0 is a compact subset of the interval $(\gamma, 1)$. In addition, there exists $\varepsilon_0 > 0$ such that for any $\varepsilon \in (0, \varepsilon_0)$, there exists a smooth locally invariant attracting one-dimensional slow manifold N_2^ε, which is $\mathcal{O}(\varepsilon)$-close to N_2^0, with the slow flow

$$\dot{e}_2 = -4e_2(\varepsilon + 2 - 2e_2)(\varepsilon + 1 - \varepsilon f_2)(\varepsilon + 2)(1 + 2f_2). \tag{7.59}$$

Note that e_2 is decreasing along N_2^ε, see Fig. 7.15. Now, we construct the transition map Π_2. For this, let us define the sections

$$\Delta_2^{in} := \left\{ (f_2, c_2, e_2, \varepsilon) \mid f_2 \in [0, \beta_2],\ c_2 = \frac{1}{\alpha_1},\ e_2 \in I_2,\ \varepsilon \in [0, \alpha_2] \right\},$$
$$\Delta_2^{out} := \left\{ (f_2, c_2, e_2, \varepsilon) \mid f_2 = \beta_2,\ c_2 \in [0, \frac{1}{\alpha_1}],\ e_2 \in I_2,\ \varepsilon \in [0, \alpha_2] \right\}.$$

where $\beta_2 = \frac{\beta_1}{\alpha_1}$, $\alpha_2 = \delta_1 \alpha_1$ with small δ_1, and I_2 is a suitable interval. Note that

$\Delta_2^{in} = \kappa_{12}(\Delta_1^{out})$. Let us define the transition map from Δ_2^{in} to Δ_2^{out} as follows:

$$\Pi_2 : \Delta_2^{in} \to \Delta_2^{out}, \qquad \left(f_2^{in}, \frac{1}{\alpha_1}, e_2^{in}, \varepsilon\right) \mapsto \left(\beta_2, c_2^{out}, e_2^{out}, \varepsilon\right). \tag{7.60}$$

Remark 7.38. In the limit $\varepsilon = 0$, the map Π_2 is defined by first projecting $(f_2, e_2) \in \Delta_2^{in}$ onto N_2^0 along the stable foliation, and then by following the slow flow (7.59).

We summarize the analysis performed in chart K_2 in the following lemma.

Lemma 7.39. *For small $\alpha_1 > 0$, there exists a sufficiently small $\alpha_2 > 0$ such that the transition map Π_2, defined in* (7.60)*, is well-defined. Moreover, for $\varepsilon = constant$, Π_2 is contracting with the contraction rate $\exp(-K/\varepsilon)$ for some $K > 0$.*

Proof. The transition map $\Pi_2 : \Delta_2^{in} \to \Delta_2^{out}$ is described by Fenichel theory, i.e., all orbits starting from Δ_2^{in} are attracted by the slow manifold N_2^ε, with a contraction rate $\exp(-K/\varepsilon)$ for some $K > 0$, and after some time they reach the section Δ_2^{out}. □

Remark 7.40. The slow manifold N_2^ε corresponds to the perturbation of N_2^0 when $\varepsilon = constant$. The family of all such manifolds is denoted by $\mathcal{N}_2$.

Analysis in chart K_3

Solutions in chart K_2 which reach the section Δ_2^{out} must be continued in chart K_3. For this reason, we continue our analysis in chart K_3. After substituting (7.38) into (7.34), and dividing out all the equations by the common factor r_3, we obtain

$$\begin{aligned}
r_3' &= r_3\Gamma_3 G_{31},\\
c_3' &= -c_3\Gamma_3 G_{31} + \left[8r_3(1 - r_3c_3)(\varepsilon_3 + 2c_3) - 4c_3(r_3\varepsilon_3 + 2 - 2r_3c_3)\right] G_{32},\\
e_3' &= r_3\left[8r_3c_3(1 - e_3)(r_3\varepsilon_3 + 2e_3) - 4e_3(r_3\varepsilon_3 + 2 - 2e_3)\right] G_{33},\\
\varepsilon_3' &= -\varepsilon_3\Gamma_3 G_{31},
\end{aligned} \tag{7.61}$$

where we denote

$$\begin{aligned}
\Gamma_3 &:= \left[\gamma(1 - r_3)(\varepsilon_3 + 2) - 2e_3(r_3\varepsilon_3 + 1 - r_3)\right],\\
G_{31} &:= (r_3\varepsilon_3 + 2 - 2r_3c_3)(\varepsilon_3 + 2c_3)(r_3\varepsilon_3 + 2 - 2e_3)(r_3\varepsilon_3 + 2e_3),\\
G_{32} &:= (r_3\varepsilon_3 + 1 - r_3)(\varepsilon_3 + 2)(r_3\varepsilon_3 + 2 - 2e_3)(r_3\varepsilon_3 + 2e_3),\\
G_{33} &:= (r_3\varepsilon_3 + 1 - r_3)(\varepsilon_3 + 2)(r_3\varepsilon_3 + 2 - 2r_3c_3)(\varepsilon_3 + 2c_3).
\end{aligned}$$

System (7.61) has three invariant subspaces, namely, $r_3 = 0$, $\varepsilon_3 = 0$ and their intersection. Recall that by definition $e = e_3$ and hence $e_3 \in [0, 1]$.

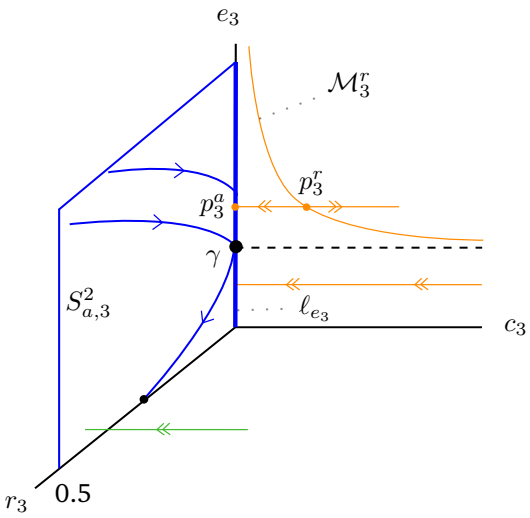

Figure 7.16: Dynamics of system (7.61) in the invariant plane $\varepsilon_3 = 0$.

1. $r_3 = \varepsilon_3 = 0$: in this case the dynamics is given by

$$\begin{aligned} c_3' &= -32c_3e_3(1-e_3)[2+c_3(\gamma-e_3)], \\ e_3' &= 0. \end{aligned} \tag{7.62}$$

For $e_3 > \gamma$, the equilibria of the system are $p_3^a = (r_3, c_3, e_3, \varepsilon_3) = (0, 0, e_3, 0)$ and $p_3^r = (r_3, c_3, e_3, \varepsilon_3) = (0, \frac{2}{e_3-\gamma}, e_3, 0)$. Note that the point p_3^a is attracting for the flow in the plane (c_3, e_3), while the point p_3^r is repelling.

Remark 7.41. When $e_3 \to \gamma$, the point $p_3^r \to \infty$ and is not visible any more in the chart K_3, see Fig. 7.16.

2. $\varepsilon_3 = 0$ and $r_3 \geqslant 0$: in the invariant plane $\varepsilon_3 = 0$, the dynamics is governed by

$$\begin{aligned} r_3' &= r_3c_3\,[\gamma - e_3]\,V(r_3, c_3, e_3), \\ c_3' &= c_3\,[(4r_3 - 2) - c_3(\gamma - e_3)]\,V(r_3, c_3, e_3), \\ e_3' &= 2r_3c_3\,[(2r_3c_3 - 1)]\,V(r_3, c_3, e_3), \end{aligned} \tag{7.63}$$

where $V(r_3, c_3, e_3) := 32e_3(1-r_3)(1-e_3)(1-r_3c_3)$. Recall that $c = r_3c_3$, and hence $V(r_3, c_3, e_3) > 0$. The equilibria of the system are the plane $c_3 = 0$, denoted by S_3^2, and the curve of equilibria given by $c_3 = \frac{2}{e_3-\gamma}$, denoted by $\mathcal{M}_3^r$. The change of stability at the points in S_3^2 occurs at $r_3 = 0.5$, i.e., for $r_3 < 0.5$ these points are attracting, while for $r_3 > 0.5$ are repelling. We

denote the attracting part of S_3^2 by $S_{a,3}^2$. The e_3-axis, which we denote by ℓ_{e_3}, is a boundary of $S_{a,3}^2$, which is a line of equilibria, see Fig. 7.16.

3. $r_3 = 0$ and $\varepsilon_3 \geqslant 0$: In the invariant plane $r_3 = 0$, system (7.61) is represented by

$$\begin{aligned} e_3' &= 0, \\ c_3' &= -8c_3e_3(1-e_3)\left[(\gamma(\varepsilon_3+2)-2e_3)(\varepsilon_3+2c_3)+4(\varepsilon_3+2)\right], \\ \varepsilon_3' &= -8\varepsilon_3e_3(1-e_3)\left[\gamma(\varepsilon_3+2)-2e_3\right](\varepsilon_3+2c_3). \end{aligned} \tag{7.64}$$

The equilibria of the system are the planes $c_3 = 0$, and the line $\varepsilon_3 = \frac{2(e_3-\gamma)}{\gamma}$, denoted by N_3^0. The Jacobian of (7.64) along the curve N_3^0 has the eigenvalues

$$\lambda_{31} = -64e_3(c_3+1)(1-e_3), \qquad \lambda_{32} = -8\gamma\varepsilon_3e_3(1-e_3)(\varepsilon_3+2c_3), \tag{7.65}$$

and hence N_3^0 is fully attracting. In fact, N_3^0 is exactly the critical manifold N_2^0 that we found in chart K_2. In other words, N_3^0 is the image of N_2^0 under the transformation κ_{23}, defined in (7.40).

Remark 7.42. The attracting manifold N_2^0 which is unbounded in chart K_2, is now bounded in chart K_3. So the behavior of the critical manifold that is not visible in chart K_2 when $e \to \gamma$, is now visible in chart K_3. For $e_3 = \gamma$, the critical manifold N_3^0 intersects the line ℓ_{e_3} at the non-hyperbolic point $q_{e_3} = (e_3, c_3, \varepsilon_3) = (\gamma, 0, 0)$.

We summarize the analysis of the invariant planes, performed in this subsection, in the following Lemma.

Lemma 7.43. *The following properties hold for system* (7.61)*:*

1. *The equilibria are the plane $S_{a,3}^2$ which intersects the line ℓ_{e_3}, and the following two one-dimensional manifolds*

$$\begin{aligned} \mathcal{M}_3^r &= \left\{(r_3,c_3,e_3,\varepsilon_3) \mid r_3=\varepsilon_3=0,\ e_3\in(\gamma,1),\ c_3=\frac{2}{e_3-\gamma}\right\}, \\ N_3^0 &= \left\{(r_3,c_3,e_3,\varepsilon_3) \mid r_3=c_3=0,\ e_3\in[\gamma,1),\ \varepsilon_3=\frac{2(e_3-\gamma)}{\gamma}\right\}. \end{aligned}$$

2. *For $e_3 > \gamma$, the equilibria of system* (7.61) *along N_3^0 have*

   (a) *a two-dimensional stable manifold corresponding to the negative eigenvalues given in* (7.65).

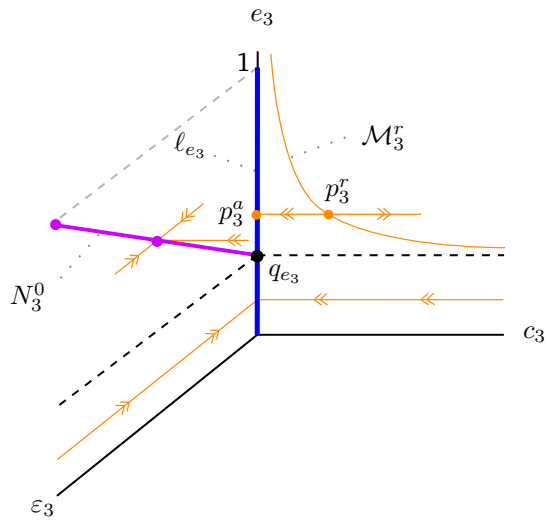

Figure 7.17: Dynamics of system (7.61) in the invariant plane $r_3 = 0$. The slow manifold N_3^0 in purple, the exit point q_{e_3} in black, and the line ℓ_{e_3} of equilibria in blue.

(b) a two-dimensional center manifold corresponding to a double zero eigenvalue.

3. *The linearization of the system in S_3^2 has a triple zero eigenvalue, and the eigenvalue $\lambda = 64e_3(e_3 - 1)(r_3 - 1)(r_3 - 0.5)$ changes its stability at $r_3 = 0.5$.*

4. *The linearization of system* (7.61) *at the steady states in the line ℓ_{e_3} has a stable eigenvalue $\lambda = 64e_3(e_3 - 1)$, and a triple zero eigenvalue. In addition, there exists a three-dimensional center manifold $\mathcal{W}^c_{a,\varepsilon}$ at the point $(r_3, c_3, e_3, \varepsilon_3) = (0, 0, e_3, 0) \in \ell_{e_3}$. In chart K_3 close to the point $e_3 = \gamma$, the center manifold $\mathcal{W}^c_{a,\varepsilon}$ is given by the graph*

$$c_3 = r_3\varepsilon_3(1 + O(r_3\varepsilon_3)). \tag{7.66}$$

Proof. The proof follows the same line of reasoning as the one of Lemma 7.34, and are omitted for brevity. □

The main goal in chart K_3 is to analyze the behavior of the solutions of (7.61) close to the exit point $q_{e_3} \in \ell_{e_3}$. Our analysis in chart K_2 implies that there exists the family of attracting slow manifolds $\mathcal{N}_2$. This in chart K_3 is denoted by $\mathcal{N}_3$ which is the image of $\mathcal{N}_2$ under the transformation κ_{23}, i.e. $\mathcal{N}_3 = \kappa_{23}(\mathcal{N}_2)$. In order to know how $\mathcal{N}_3$ is continued close to the point q_{e_3}, we restrict the dynamics to the

sets

$$D_3^{in} := \{(r_3, c_3, e_3, \varepsilon_3) \mid r_3 \in [0, \alpha_3], e_3 \in (\gamma, 1], \varepsilon_3 \in [0, \beta_3]\},$$
$$D_3^{out} := \{(r_3, c_3, e_3, \varepsilon_3) \mid r_3 \in [0, \alpha_3], e_3 \in [0, \gamma), \varepsilon_3 \in [0, \beta_3]\},$$

where $\alpha_3 = \alpha_2\beta_2$ and $\beta_3 = \frac{1}{\beta_2}$, due to the transformation κ_{23}, defined in (7.40). Now we define the sections as follows

$$\Delta_3^{in} := \{(r_3, c_3, e_3, \varepsilon_3) \in D_3^{in} \mid \varepsilon_3 = \beta_3\},$$
$$\Delta_3^{out} := \{(r_3, c_3, e_3, \varepsilon_3) \in D_3^{out} \mid r_3 = \alpha_3\}.$$

Let us denote Π_3 as the transition map from Δ_3^{in} to Δ_3^{out}, induced by the flow of (7.61). In order to construct the map Π_3, we reduce system (7.61) to its center manifold, namely, $\mathcal{W}^c_{a,3}$ and analyze the system based on the the dynamics on $\mathcal{W}^c_{a,3}$. This is done by substituting (7.66) into system (7.61), and rescaling time by dividing out the common factor

$$\left[r_3\varepsilon_3 + 22r_3^2\varepsilon_3(1 + O(r_3\varepsilon_3)\right]\left[\varepsilon_3 + 2r_3\varepsilon_3(1 + O(r_3\varepsilon_3)\right]. \tag{7.67}$$

In doing so, the flow of the center manifold is represented by

$$\begin{aligned} r_3' &= r_3 G_{34}, \\ e_3' &= r_3(r_3\varepsilon_3 + 1 - r_3)(\varepsilon_3 + 2)G_{35}, \\ \varepsilon_3' &= -\varepsilon_3 G_{34}, \end{aligned} \tag{7.68}$$

where we denote

$$G_{34} := [\gamma(1 - r_3)(\varepsilon_3 + 2) - 2e_3(r_3\varepsilon_3 + 1 - r_3)]\,(r_3\varepsilon_3 + 2 - 2e_3)(r_3\varepsilon_3 + 2e_3),$$
$$G_{35} := \left[8r_3^2\varepsilon_3(1 + O(r_3\varepsilon_3))(1 - e_3)(r_3\varepsilon_3 + 2e_3) - 4e_3(r_3\varepsilon_3 + 2 - 2e_3)\right].$$

As is clear from (7.68), the planes $r_3 = 0$ and $\varepsilon_3 = 0$ are invariant. Setting $r_3 = 0$ in (7.68), one obtains

$$\begin{aligned} e_3' &= 0, \\ \varepsilon_3' &= -4\varepsilon_3 e_3(1 - e_3)[\gamma(\varepsilon_3 + 2) - 2e_3]. \end{aligned} \tag{7.69}$$

The equilibria of (7.68) are again the line ℓ_{e_3} and the manifold N_3^0. The Jacobian of (7.69) along the line ℓ_{e_3} has the eigenvalue $\lambda = 8e_3(1 - e_3)(e_3 - \gamma)$, implying that ℓ_{e_3} is repelling for $e_3 > \gamma$, while attracting for $e_3 < \gamma$. Further, the manifold N_3^0 is attracting for the flow in the plane $r_3 = 0$. The eigenvalue at the point $(r_3, e_3, \varepsilon_3) = (0, \gamma, 0) \in \ell_{e_3}$ is zero and hence this point is *degenerate*, see Fig. 7.18.

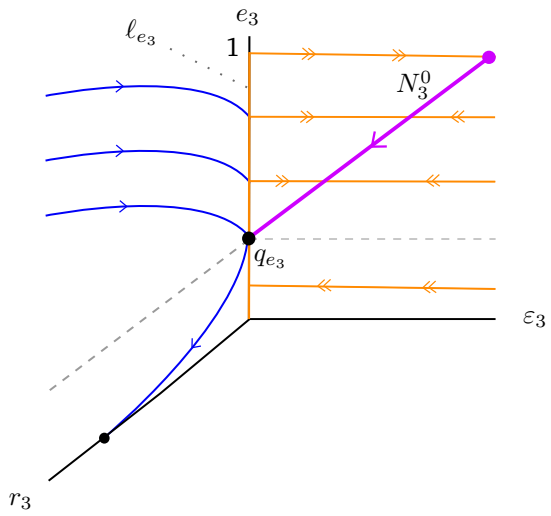

Figure 7.18: Dynamics of system (7.68); the attracting critical manifold N_3^0 in purple, and the nilpotent point q_{e_3} in black.

Setting $\varepsilon_3 = 0$ in system (7.68) results in

$$\begin{aligned} r_3' &= 8r_3e_3(1-e_3)(1-r_3)[\gamma - e_3], \\ e_3' &= -16r_3e_3(1-e_3)(1-r_3). \end{aligned} \tag{7.70}$$

In the plane $\varepsilon_3 = 0$, the line ℓ_{e_3} is attracting for $e_3 > \gamma$ while repelling for $e_3 < \gamma$.

Remark 7.44. The dynamics in the invariant plane $\varepsilon = 0$ corresponds to the reduced flow on S_a^2 in the original system.

Summarizing the analysis, we have the following lemma.

Lemma 7.45. *The following properties hold for system* (7.68)*:*

1. *The curve N_3^0 has a one-dimensional stable manifold, and a two-dimensional center manifold away from the point q_{e_3}.*
2. *The linearization of* (7.68) *at the points in ℓ_{e_3} is given by*

$$\begin{pmatrix} 8e_3(e_3-1)(e_3-\gamma) & 0 & 0 \\ 16e_3(e_3-1) & 0 & 0 \\ 0 & 0 & -8e_3(e_3-1)(e_3-\gamma) \end{pmatrix},$$

3. *The point q_{e_3} is nilpotent.*

As we already mentioned, our goal in chart K_3 is to describe system (7.61) close to the line ℓ_{e_3}, and especially at the point q_{e_3}. To this end, we have defined

the map $\Pi_3 : \Delta_3^{in} \to \Delta_3^{out}$ where Δ_3^{in} is transversal to N_3^0 when $e > \gamma$, while Δ_3^{out} is transversal to the slow manifold in the plane $\varepsilon_3 = 0$ when $e < \gamma$. Lemma 7.45 implies that the point q_{e_3} is nilpotent. Thus, in order to describe the transition map Π_3 we need to blow-up the point q_{e_3}. For such a point, a similar analysis has been carried out in [86], in view of which we have the following lemma.

Lemma 7.46. *Assume that $\hat{R}_3 \subset \Delta_3^{in}$ is a small rectangle centered at the intersection point $N_3^0 \cap \Delta_3^{in}$. For sufficiently small α_3, the transition map $\Pi_3 : \hat{R}_3 \to \Delta_3^{out}$ induced by the flow of* (7.68) *is well-defined and satisfies the following properties:*

1. *The continuation of $\mathcal{N}_3$ by the flow intersects the section Δ_3^{out} in a curve, denoted by σ_3^{out}.*
2. *Restricted to the lines $r_3 = constant$ in $\hat{R}_3$, the map is contracting with the rate $\exp(-K/r_3)$ for some $K > 0$.*
3. *The image $\Pi_3(\hat{R}_3)$ is an exponentially thin wedge-like containing the curve σ_3^{out}.*

The map Π_3 describes the transition from Δ_3^{in} to Δ_3^{out}. If we set $\alpha_3 = \delta_2$ (recall the definition of Σ_2 from (7.29)) we actually have $\Delta_3^{out} = \bar{\Sigma}_2 := \Phi^{-1}(\Sigma_2 \times \{[0, \rho_2]\})$ for some $\rho_2 > 0$, see Fig. 7.12.

Properties of the blow-up of the non-hyperbolic line $\ell_1 \times \{0\}$ and proof of Lemma 7.27

In the above subsections, we have presented the detailed analysis of the blow-up of the non-hyperbolic line $\ell_1 \times \{0\}$ in charts K_1, K_2 and K_3, which has been summarized in Fig. 7.19. A summary of the analysis, carried out in such charts, are as follows.

First of all, the critical manifolds S_a^1 (i.e., $f = 0$) and S_a^2 (i.e., $c = 0$) intersect in the non-hyperbolic line ℓ_1, which is replaced by the orange cylinder, see Figs. 7.12 and 7.19. Note that in Fig. 7.19, the orbits $\bar{\omega}_5$ and $\bar{\omega}_7$ in the blown-up space correspond, respectively, to the orbits ω_5 and ω_7 in the original space. The point at which $\bar{\omega}_5$ reaches the cylinder is denoted by $\bar{q}^e$, and the point at which $\bar{\omega}_7$ starts is denoted by $\bar{q}_e$. Starting from the section $\bar{\Sigma}_1$, the trajectory follows the orbit $\bar{\omega}_5$ on $\bar{f} = 0$ until it reaches the point $\bar{q}^e$. Our analysis in chart K_1 (Lemma 7.34) shows that there exists a three-dimensional attracting center manifold which is the continuation of the family of orbits (indexed by ε) of the attracting slow manifold $S_{a,\varepsilon}^1$. This allows us to connect the family of solutions in $S_{a,\varepsilon}^1$ into the attracting critical manifold N_2^ε in chart K_2 which is inside the cylinder (see the thick orange manifold from $\bar{q}^e$ to $\bar{\mathcal{N}}^0$ in Fig. 7.19). Our analysis in chart K_2 (Lemma 7.58) shows that the slow manifold N_2^ε is normally hyperbolic and stable. Therefore, the family $S_{a,\varepsilon}^1$ is exponentially attracted by the slow manifold N_2^ε. Next, our analysis in chart K_3 (Lemma 7.45, and Fig. 7.18) shows that the unbounded critical

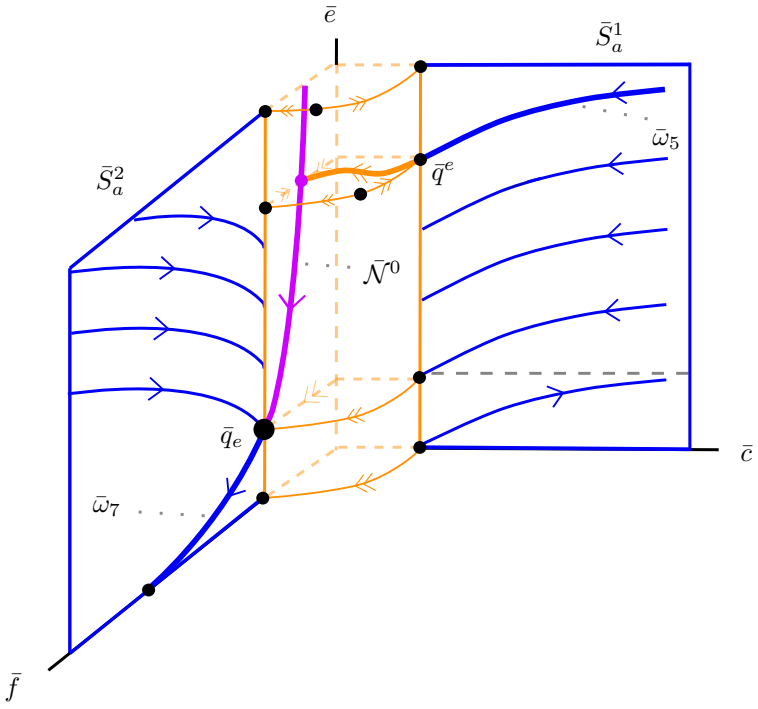

Figure 7.19: Geometry of the blown-up space and the singular cycle close to the non-hyperbolic line $\ell_1 \times \{0\}$, which is blown-up to the orange cylinder. The reduced flows in $\bar{S}_a^1$ and $\bar{S}_a^1$ are illustrated in blue. The thick orange manifold inside the cylinder corresponds to the three-dimensional center manifold in chart K_1. The attracting one-dimensional critical manifold in chart K_2 is shown in purple.

manifold N_2^ε (see Figs. 7.15, 7.18) limits at the point q_{e_3}, which is exactly the point $\bar{q}_e$ in Fig. 7.19. Moreover, we have proven that the point q_{e_3} is degenerate, i.e., the linearization of the dynamics at q_{e_3} has a nonzero (stable) eigenvalue and a triple zero eigenvalue (Lemma 7.45), which allows us to construct a three-dimensional center manifold at the point q_{e_3}. Now, by following the family N_2^ε along such a center manifold, we conclude (Lemma 7.46) that the continuation of N_2^ε for a sufficiently small $\varepsilon > 0$ intersects the section $\bar{\Sigma}_2$ in a point, namely, $(\alpha_3, c_3(\varepsilon_3), e_3(\varepsilon_3), \varepsilon_3) \in \bar{\Sigma}_2$, for some $\varepsilon_3 \in [0, \beta_3]$, which is exponentially close to the slow manifold $S^2_{a,\varepsilon}$. Note that the point $(\alpha_3, c_3(\varepsilon_3), e_3(\varepsilon_3), \varepsilon_3)$ converges to the point $q_2 := \Sigma_2 \cap \omega_7$ as $\varepsilon_3 \to 0$. All these analyses in charts K_1, K_2, and K_3 demonstrate that the transition map $\bar{\pi}_1 : \bar{\Sigma}_1 \to \bar{\Sigma}_2$ is well-defined for $\varepsilon \in [0, \varepsilon_0]$ and is smooth for $\varepsilon \in (0, \varepsilon_0]$, for some $\varepsilon_0 > 0$.

We are now ready to prove Lemma 7.27.

Proof of Lemma 7.27. The proof is carried out by constructing the transition

map $\pi_1 : \Sigma_1 \to \Sigma_2$ for $\varepsilon > 0$ as

$$\pi_1 = \Phi \circ \bar{\pi}_1 \circ \Phi^{-1}, \tag{7.71}$$

where Φ is given by (7.35), Φ^{-1} is the corresponding blown-up transformation, and $\bar{\pi}_1 : \bar{\Sigma}_1 \to \bar{\Sigma}_2$ is a transition map which can equivalently be regarded as

$$\bar{\pi}_1(\bar{\Sigma}_1) = \Pi_3 \circ \kappa_{23} \circ \Pi_2 \circ \kappa_{12} \circ \Pi_1(\bar{\Sigma}_1) \subset \bar{\Sigma}_2 \tag{7.72}$$

The proof is based on the corresponding transition map $\bar{\pi}_1 : \bar{\Sigma}_1 \to \bar{\Sigma}_2$ in the blown-up space and interpreting the result for fixed $\varepsilon \in [0, \varepsilon_0]$, for some $\varepsilon_0 > 0$. Recall that the transition $\bar{\pi}_1 : \bar{\Sigma}_1 \to \bar{\Sigma}_2$ is equivalent to the transition map $\pi_1 : \Sigma_1 \to \Sigma_2$ in the sense that it has the same properties. Furthermore, via the matching maps κ_{ij} defined in Lemma 7.31, we have appropriately identified the relevant sections in each of the charts, allowing us to follow the flow of the blown-up vector field along the three charts.

As summarized above, the transition map $\bar{\pi}_1 : \bar{\Sigma}_1 \to \bar{\Sigma}_2$ is well-defined for $\varepsilon \in [0, \varepsilon_0]$ and is smooth for $\varepsilon \in (0, \varepsilon_0]$, for some $\varepsilon_0 > 0$. It remains to prove that $\bar{\pi}_1$ is a contraction. First of all note that in chart K_1, the map Π_1 is described by an attracting three-dimensional center manifold, which is contracting in the direction of f_1. Next, the map Π_2 is a strong contraction in both directions of (f_2, c_2), as shown in Fig. 7.15; this is due to the existence of a fully attracting one-dimensional slow manifold. This continuation persists (Lemma 7.46) during the passage near the point q_{e_3} in chart K_3 until it reaches the section $\bar{\Sigma}_2$. As the contraction persists from $\bar{\Sigma}_1$ to $\bar{\Sigma}_2$, one concludes that the map $\bar{\pi}_1$ is a contraction. This completes the proof. □

7

7.4.2 Blow-up of the non-hyperbolic line $\ell_2 \times \{0\}$

In this subsection, for the sake of brevity, we summarize the blow-up of the non-hyperbolic line $\ell_2 \times \{0\}$, which is similar to the blow-up of the non-hyperbolic line $\ell_1 \times \{0\}$, and give a sketch of the proof of Lemma 7.28. To this end, we transform the non-hyperbolic line of steady states $\ell_2 \times \{0\}$ by

$$f = \tilde{f}, \qquad c = r\tilde{c}, \qquad \varepsilon = r\tilde{\varepsilon}, \qquad e = r\tilde{e}, \tag{7.73}$$

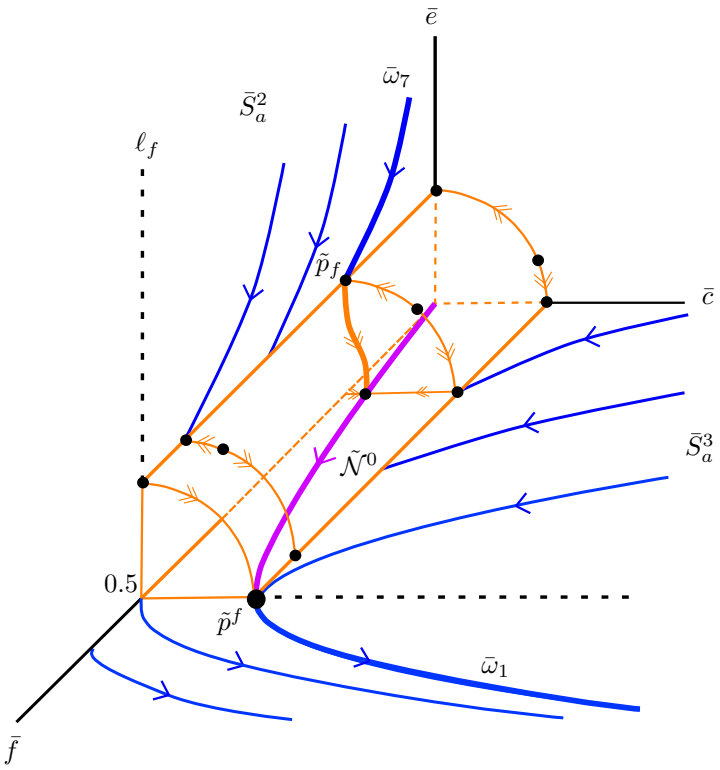

Figure 7.20: Geometry of the blown-up space and the singular cycle close to the non-hyperbolic line $\ell_2 \times \{0\}$, which is blown-up to the orange cylinder. The reduced flows in $\bar{S}_a^2$ and $\bar{S}_a^3$ are shown in blue. The thick orange manifold inside the cylinder corresponds to the three-dimensional center manifold in chart $\tilde{K}_1$. The attracting one-dimensional critical manifold in chart $\tilde{K}_2$ is illustrated in purple.

where $\tilde{c}^2 + \tilde{e}^2 + \tilde{\varepsilon}^2 = 1$, $\bar{f} \in [0, 1]$, and $r \geqslant 0$. Moreover, we define three charts $\tilde{K}_1, \tilde{K}_2$ and $\tilde{K}_3$ as follows:

$$
\begin{aligned}
\tilde{K}_1 &: \quad f = \tilde{f}_1, \quad c = \tilde{r}_1\tilde{c}_1, \quad \varepsilon = \tilde{r}_1\tilde{\varepsilon}_1, \quad e = \tilde{r}_1, \\
\tilde{K}_2 &: \quad f = \tilde{f}_2, \quad c = \tilde{r}_2\tilde{c}_2, \quad \varepsilon = \tilde{r}_2, \quad e = \tilde{r}_2\tilde{e}_2, \\
\tilde{K}_3 &: \quad f = \tilde{f}_3, \quad c = \tilde{r}_3, \quad \varepsilon = \tilde{r}_3\tilde{\varepsilon}_3, \quad e = \tilde{r}_3\tilde{e}_3.
\end{aligned}
$$

Recall that the goal of Lemma 7.28 is to describe the map $\pi_2 : \Sigma_2 \to \Sigma_3$ in the original space. In this subsection, we present a sketch of the proof of Lemma 7.28 by constructing the corresponding map $\bar{\pi}_2 : \bar{\Sigma}_2 \to \bar{\Sigma}_3$ in the blown-up space. We have summarized the analysis of the blow-up of the non-hyperbolic line $\ell_2 \times \{0\}$ in Fig. 7.20.

First of all, note that the non-hyperbolic line ℓ_2, which is the intersection of the critical manifolds S_a^2 (i.e., $c = 0$) and S_a^3 (i.e., $e = 0$), has been blown-up to the orange cylinder. We have illustrated the slow flows in the planes $c = 0$ and $e = 0$ in blue. The orbits $\bar{\omega}_7$ and $\bar{\omega}_1$ which are in the blown-up space correspond, respectively, to the orbits ω_7 and ω_1 in the original space, compare Figs. 7.20 and 7.11. As is shown in Fig. 7.20, the intersection of the cylinder with $\bar{\omega}_7$ and $\bar{\omega}_1$ is denoted by $\tilde{p}_f$ and $\tilde{p}^f$, respectively.

An analysis in chart $\tilde{K}_1$ proves that there exists a three-dimensional attracting center manifold at the point $\tilde{p}_f$, which is the continuation of the family of the attracting slow manifold $S_{a,\varepsilon}^2$. In view of such a center manifold, the family of the slow manifold $S_{a,\varepsilon}^2$ enters the chart $\tilde{K}_2$. In chart $\tilde{K}_2$ it is proven that there exists a one-dimensional slow manifold $\tilde{\mathcal{N}}^0$, which fully attracts the interior of the cylinder. An analysis in chart $\tilde{K}_3$ shows that the critical manifold $\tilde{\mathcal{N}}^0$ limits at the point $\tilde{p}^f$, see Fig. 7.20. It is proven that $\tilde{p}^f$ is a *degenerate* point, and hence, we can construct a three-dimensional attracting center manifold. Thus, $\tilde{\mathcal{N}}^0$ follows this center manifold and then intersects the section Σ_3 in a point $(f(\varepsilon), \delta_3, e(\varepsilon))$, for some $\varepsilon, \delta_3 > 0$ (see section Σ_3, defined in (7.29)), which is exponentially close to the slow manifold $S_{a,\varepsilon}^3$ and converges to the point $q_3 := \Sigma_3 \cap \omega_1$ as $\varepsilon \to 0$. This proves that the transition map $\bar{\pi}_2 : \bar{\Sigma}_2 \to \bar{\Sigma}_3$ and hence $\pi_2 : \Sigma_2 \to \Sigma_3$ are well-defined for $\varepsilon \in [0, \varepsilon_0]$ and smooth for $\varepsilon \in (0, \varepsilon_0]$, for some $\varepsilon_0 > 0$. The proof of contraction of the transition map π_2 follows the same line of reasoning as that of the map π_1.

7.5 Range of parameter γ in Theorem 7.26

Although in our simulations in Figs. 7.1 and 7.2 we have fixed the parameter $\gamma = 0.08$, and based on this parameter value we have constructed the singular cycle Γ_0, illustrated in Fig. 7.11, in this section we show that the behavior of the singular cycle Γ_0 will remain qualitatively the same in a neighborhood of $\gamma = 0.08$, and hence Theorem 7.26 holds for these values as well.

As is shown in Fig. 7.11, ω_2 and ω_4 are described by the layer problem (7.8), whose behavior highly depends on the parameter γ. If the layer problem starts from a point in $S_a^3 \cap \ell_e$, namely $p_\gamma := (f_\gamma, \frac{1}{2}, 0) \in \ell_e$ when $\frac{1}{2} < f_\gamma < 1$, the parameter γ can influence the fast dynamics to arrive at a point either in S_a^1, S_a^2, S_a^3, S_a^4, S_a^5 or S_a^6. Moreover, if the layer problem starts from a point in $S_a^6 \cap \ell^e$, namely $p^\gamma := (f^\gamma, \frac{1}{2}, 1) \in \ell^e$ when $0 < f^\gamma < \frac{1}{2}$, the parameter γ can influence the fast dynamics to arrive at a point either in S_a^1 or S_a^2. In this section, our aim is to find a certain range for γ such that the qualitative behavior of the fast dynamics remains the same as ω_2 and ω_4, shown in Fig. 7.11, i.e., the fast dynamics moves *directly* from p_γ to a point in S_a^6, and from p^γ to a point in S_a^1, while does not intersect with

the other planes.

In view of equations (7.25), it is shown that the slow flow, started from the point $p^f = (\frac{1}{2}, 0, 0)$, arrives at the point $p_1 = (\frac{1+\sqrt{\gamma}}{2}, \frac{1}{2}, 0)$. In order to find a certain range for γ, as the layer problem (7.8) is linear, we can find the closed form of solutions. In view of the boundary conditions in S_a^3 and S_a^6, we get a system of transcendental equations, whose solution is a point at which ω_2 intersects with S_a^6. However, due to the fact that it is impossible to solve such a system of equations analytically, we have used numerical methods to calculate the solution of the transcendental equations. Computed numerically, for any $\gamma \in \mathcal{R}_1 \approx (0.0561,\ 0.1177)$, the qualitative behavior of the fast dynamics is the same as ω_2, illustrated in Fig. 7.11. Moreover, for any $\gamma \in \mathcal{R}_1$, the qualitative behavior of the fast dynamics is the same as ω_4 as well, illustrated in Fig. 7.11. All these imply that Theorem 7.26 is valid for all $\gamma \in \mathcal{R}_1$. Analogously, one can find a range for the case that γ is close to 1, see Remark 7.3.

7.6 Conclusions

Numerical simulations show that the Frz system, introduced in [73], has oscillatory behavior in certain parameter regimes, and in particular, when Michaelis-Menten constants of the system are sufficiently small. After unifying such constants by a parameter ε, we have analyzed the dynamics of this biochemical oscillator in the limit of ε, and analytically proven that for sufficiently small ε, there exists a strongly attracting limit cycle.

Our approach has been based on the geometric singular perturbation analysis and the blow-up method. Geometric singular perturbation theory and geometric desingularization by several blow-ups allow us to fully understand the structure of the limit cycle of the Frz as well as the time scales along it, for sufficiently small ε. From the multiple-time-scale nature of the problem, it turns out that the Frz system is indeed a relaxation oscillator, although a global separation into slow and fast variables is not explicitly given in the model. We emphasize that the approach and tools presented in this chapter, i.e. geometric singular perturbation theory and the blow-up method, are not limited to the analysis of system (7.1); these tools can be applied to similar systems, such as [94] whose parameters have the property of zero-order ultrasensitivity.

8

Conclusions and future research

The thesis has been concerned with modeling, analysis, and control of biological oscillators. Chapter 1 has presented a brief background on the problems that have been studied in this book. Chapter 2 has reviewed some concepts and tools, used in next chapters. The main results have been presented in Chapters 3 - 7. The present chapter reflects on such results, and points out some potential directions for future research.

8.1 Conclusions

GENERALLY, the main aim of this thesis has been to show that mathematical models along with tools from dynamical systems and control theory are useful for investigating a large number of topics in biological sciences. A mathematical model, which is built based on the underlying biology, is a nice platform for *in silico* experimentation. In addition, such a model can help us to better understand the regulatory processes between one biological component and another one, and also how variation in one component affects the variation in another. Further, it can reveal some aspects of the corresponding biological system that might not be observable experimentally.

Part I of this thesis has been devoted to modeling, analysis, and control of endocrine systems, and Part II has been allocated to the mathematical analysis of a biochemical oscillator model. Here we summarize the results, presented in Chapters 3 - 7.

8.1.1 Conclusions of Part I

Chapters 3, 4, and 5 have studied three mathematical models of endocrine regulation. Although such second- and third-order models cannot "fully" describe the real process of endocrine regulation, these models are still insightful for understanding the basic control mechanisms underlying endocrine regulation; such models can be used in biomedical engineering, e.g., to develop optimal therapies of endocrine dysfunctions. Conclusions of each chapter are given as follows.

In Chapter 3, we have developed a second-order impulsive differential equation model of cortisol's diurnal patterns by taking the release of cortisol as a part of an impulsive control feedback system. Further, by maintaining the blood cortisol levels within a specific circadian range, we have established an analytical approach along with an algorithm to identify the number, timing, and amplitude of secretory events. Employing our approach to various examples, we have shown that the obtained cortisol levels are in line with the known physiology of cortisol secretion.

Inspired by the intermittent controller proposed in Chapter 3, one can design such controllers to improve the battery life of the brain implant in brain-machine interface design, and reduce the number of surgeries required for changing the battery of the implant controller [34]. In addition, this type of bio-inspired pulse controller can potentially be used to control major depression, addiction, and post-traumatic stress disorder. We emphasize that the potential applications of the intermittent controllers go beyond the neuroendocrine and mental disorders presented here, and potentially can be used for some other disorders which arise in neuroscience.

In Chapter 4, we have studied a new model of endocrine regulation, derived from the classical Goodwin's oscillator yet has an additional nonlinear negative feedback. In this model, the two feedback loops can be described by different nonlinearities, i.e., they are not restricted to be Hill functions. In contrast to the existing works that are mainly confined to numerical analysis or presenting local stability properties and Hopf bifurcation analysis, we have established both local and global properties of the proposed model such as the oscillatory behavior of almost all its solutions. It should be noticed that the potential applications of the model introduced in Chapter 4 are not limited to endocrine regulation; similar models with multiple feedback loops have been reported to describe the dynamics of some metabolic pathways [43, 107, 126].

In Chapter 5, we have extended the recently proposed impulsive Goodwin's model by introducing an additional affine feedback. In contrast to the model studied in [15], the dynamics between two consecutive pulses is described by a non-Metzler matrix, and hence the system may leave the positive orthant and produce infeasible solutions. Nevertheless, we show that, under some conditions on the parameters of the affine feedback, the results of [15] still hold, i.e., there

exists a positive and unique 1-cycle solution to the extended system.

8.1.2 Conclusions of Part II

Part II of this thesis has been concerned with the analysis of a biochemical oscillator model (the Frz system), describing the developmental stage of myxobacteria. This biochemical oscillator is proposed in [73] as the control mechanism of motion reversals of myxobacteria, a type of soil bacteria. In Chapters 6 and 7, we have given a rigorous and detailed analysis of the claims made in [73], and of our observations from numerical simulations. Our approach in Chapters 6 and 7 has been based on regular perturbation theory and geometric singular perturbation theory, respectively. The conclusions of each chapter are given as follows.

In Chapter 6, We have studied the Frz system from a regular-perturbation perspective. With the results of this chapter, we have formalized and refined the claims made in [73]. Particularly, after unifying all the Michaels-Menten constants of the model by a parameter ε, we have given an estimate of such a parameter for which almost all trajectories of the biochemical oscillator indeed converge to a finite number of periodic solutions.

Although the coexistence among stable limit cycles has been reported for a number of models for cellular oscillatory processes (see e.g. [19]), such a coexistence among multiple stable rhythms has not yet been observed *experimentally*[1] in a biological context. Nevertheless, having a mathematical model, the convergence of solutions to a finite number of periodic solutions can be investigated by tools from dynamical systems theory, and in particular, bifurcation theory. Thus, we conclude that mathematical models along with tools from dynamical systems indeed complement experiments. We emphasize that the presented approach in Chapter 6 is not confined to the specific oscillator that is studied there, and that the ideas provided there can be applied to many other oscillatory systems, such as [88, 94].

In Chapter 7, we have analyzed the dynamics of the Frz system in the limit of ε, corresponding to the small Michaels-Menten constants of the model. We have proven that for sufficiently small $\varepsilon > 0$, there exists a strongly attracting limit cycle for the system. Our approach has been based on a detailed geometric analysis of an auxiliary system, being the polynomial form of the original system. To prove the main result, we have used geometric singular perturbation theory and the blow-up method. One conclusion of this chapter is that geometric singular perturbation theory along with the blow-up method is a powerful tool for the analysis of multiple-time-scale oscillators, even for those systems which are not in the standard from.

[1] The author would like to thank Prof. Albert Goldbeter (Université Libre de Bruxelles) for motivating this part.

8.2 Directions for future research

The following subsections provides some directions for further research of the problems that have been studied in Parts I and II.

8.2.1 Potential research directions for Part I

The second-order mathematical model proposed in Chapter 3 is a minimal model, describing the pituitary-adrenal system. A more complete model should also include the interactions from the hypothalamus as well as the effects of the exogenous factors such as sleep, stress, and meals [7].

In Chapter 3, we have assumed that the infusion and clearance rates are constant. However, these parameters can be considered such that they change after every jump. In other words, it might be the case that after every jump either the infusion rate changes while the clearance rate does not change or vice versa, or both of them change simultaneously. In all such cases, the problem can be formulated as a switched linear system, and hence investigated by the tools and theories developed for switched systems.

The model presented in Chapter 4 is the first step in modeling as the transport delays among hormones, discontinuities and stochastic noises are not taken into account. A more complete model of endocrine regulation with several negative feedback loops should consider such effects.

As we discussed in Chapter 4, the slop restriction on the additional nonlinear feedback is only a sufficient condition for the convergence of solutions to periodic orbits. One may relax such a restriction, and derive necessary and sufficient conditions for the solutions' convergence to periodic orbits. Moreover, our observations from numerical solutions show that (almost) all solutions of both the Goodwin's model and its extension converge to a unique limit cycle, which is another open problem that can be investigated.

In Chapter 5, the additional feedback is described by an affine function. As discussed in [35], such a feedback can be described by a quadratic or cubic function; note that in these two cases the dynamics between two consecutive pulses is not linear anymore, posing some mathematical challenges. Another possibility to improve the model, presented in Chapter 5, is to take into account the transport delays among hormones.

8.2.2 Potential research directions for Part II

As discussed in Chapter 6, when a cell collides with other cells, a C-signal is produced which influences the coordination of motion of such a cell. In the model studied in Part II, the C-signal is assumed to be constant, i.e. $k_{\mathrm{a}}^{\max} \equiv constant$.

A more interesting and complicated case that can be investigated is that such an input signal is not constant but a square pulse such as [73]

$$k_{\mathrm{a}}^{\max} = k_1 + k_2 \left(H(t - t_0) - H(t - t_0 - \Delta t) \right),$$

where k_1 and k_2 are suitable constants, $H(t)$ is a Heaviside function creating a square pulse of unit amplitude, t_0 is the beginning of the signaling pulse, and Δt is its duration.

In Chapter 7, we have proven that the limit cycle is locally unique. The geometric method could be pushed to analyze the "global" uniqueness of the limit cycle which is clearly of great interest from both the mathematical and biological point of view. This requires a more global analysis of the singular flows, and in particular, connecting orbits between the critical manifolds S^i $(i = 1, 2, ..., 6)$, by orbits of the layer problem.

Bibliography

[1] F. Allgöwer and F. Doyle. Introduction to the special issue on systems biology. *Automatica*, 47:1095–1096, 2011.

[2] M. Arcak and E.D. Sontag. Diagonal stability of a class of cyclic systems and its connection with the secant criterion. *Automatica*, 42:1531–1537, 2006.

[3] C.J. Bagatell, K.D. Dahl, and W.J. Bremner. The direct pituitary effect of testosterone to inhibit gonadotropin secretion in men is partially mediated by aromatization to estradiol. *J. Andrology*, 15(1):15–21, 1994.

[4] N. Bairagi, S. Chatterjee, and J. Chattopadhyay. Variability in the secretion of corticotropin-releasing hormone, adrenocorticotropic hormone and cortisol and understandability of the hypothalamic-pituitary-adrenal axis dynamics: a mathematical study based on clinical evidence. *Mathematical Medicine and Biology*, 25:37–63, 2008.

[5] L.E. Baylis. *Living control systems*. Freeman, 1966.

[6] C. Bernard. *Introduction à l'étude de la médecine expérimentale*. Paris, 1859.

[7] E.N. Brown, P.M. Meehan, and A.P. Dempster. A stochastic differential equation model of diurnal cortisol patterns. *American Journal of Physiology-Endocrinology And Metabolism*, 280(3):E450–E461, 2001.

[8] E.J. Candes, M.B. Wakin, and S.P. Boyd. Enhancing sparsity by reweighted ℓ_1 minimization. *Journal of Fourier analysis and applications*, 14(5):877–905, 2008.

[9] W.B. Cannon. Organization for physiological homeostasis. *Physiological reviews*, 9(3):399–431, 1929.

[10] C. Carmen. Ordinary differential equations with applications. *Texts in Applied Mathematics*, 34, 2006.

[11] M. Cartwright and M. Husain. A model for the control of testosterone secretion. *J. Theor. Biol.*, 123(2):239–250, 1986.

[12] B. Chance, A.K. Ghosh, and E.K. Pye. *Biological and biochemical oscillators*. Academic Press, 2014.

[13] C. Chicone. *Ordinary differential equations with applications*. Springer Science & Business Media, 2006.

[14] S.-N. Chow, C. Li, and D. Wang. *Normal forms and bifurcation of planar vector fields*. Cambridge University Press, 1994.

[15] A. Churilov, A. Medvedev, and A. Shepeljavyi. Mathematical model of non-basal testosterone regulation in the male by pulse modulated feedback. *Automatica*, 45(1):78–85, 2009.

[16] A. Churilov, A. Medvedev, and P. Mattsson. Periodical solutions in a pulse-modulated model of endocrine regulation with time-delay. *IEEE Trans. Autom. Control*, 59(3):728–733, 2014.

[17] J. Cronin. The Danziger-Elmergreen theory of periodic catatonic schizophrenia. *Bull. Math. Biol.*, 35:689–707, 1973.

[18] P. Das, A.B. Roy, and A Das. Stability and oscillations of a negative feedback delay model for the control of testosterone secretion. *Biosystems*, 32(1): 61–69, 1994.

[19] O. Decroly and A. Goldbeter. Birhythmicity, chaos, and other patterns of temporal self-organization in a multiply regulated biochemical system. *Proceedings of the National Academy of Sciences*, 79(22):6917–6921, 1982.

[20] M. Desroches, B. Krauskopf, and H.M. Osinga. The geometry of mixed-mode oscillations in the olsen model for the peroxidase-oxidase reaction. *Discrete and Continuous Dynamical Systems: Series S*, 2(4):807, 2009.

[21] A. Dhooge, W. Govaerts, and Y.A. Kuznetsov. Matcont: a matlab package for numerical bifurcation analysis of odes. *ACM Transactions on Mathematical Software (TOMS)*, 29(2):141–164, 2003.

[22] F. Dumortier and R.H. Roussarie. *Canard cycles and center manifolds*, volume 577. American Mathematical Soc., 1996.

[23] F. Dumortier and R.H. Roussarie. Geometric singular perturbation theory beyond normal hyperbolicity. In *Multiple-time-scale dynamical systems*, pages 29–63. Springer, 2001.

[24] M. Dworkin. Recent advances in the social and developmental biology of the myxobacteria. *Microbiological reviews*, 60(1):70, 1996.

[25] A.S. Elkhader. A result on a feedback system of ordinary differential equations. *J. Dynam. Diff. Equations*, 4(3):399–418, 1992.

[26] G. Enciso and E.D. Sontag. On the stability of a model of testosterone dynamics. *J. Math. Biol.*, 49(6):627–634, 2004.

[27] G.A. Enciso, H.L. Smith, and E.D. Sontag. Nonmonotone systems decomposable into monotone systems with negative feedback. *J. Diff. Equations*, 224: 205–227, 2006.

[28] I.R. Epstein and J.A. Pojman. *An introduction to nonlinear chemical dynamics: oscillations, waves, patterns, and chaos*. Oxford University Press, 1998.

[29] W.S. Evans, L.S. Farhy, and M.L. Johnson. Biomathematical modeling of pulsatile hormone secretion: a historical perspective. *Methods in enzymology*, 454:345–366, 2009.

[30] R.T. Faghih. *System identification of cortisol secretion: Characterizing pulsatile dynamics*. PhD thesis, Massachusetts Institute of Technology, 2014.

[31] R.T. Faghih. From physiological signals to pulsatile dynamics: A sparse system identification approach. In *Dynamic Neuroscience*, pages 239–265. Springer, 2018.

[32] R.T. Faghih, M.A. Dahleh, G.K. Adler, E.B. Klerman, and E.N. Brown. Deconvolution of serum cortisol levels by using compressed sensing. *PloS one*, 9 (1):e85204, 2014.

[33] R.T. Faghih, M.A. Dahleh, G.K. Adler, E.B. Klerman, and E.N. Brown. Quantifying pituitary-adrenal dynamics and deconvolution of concurrent cortisol and adrenocorticotropic hormone data by compressed sensing. *IEEE Transactions on Biomedical Engineering*, 62(10):2379–2388, 2015.

[34] R.T. Faghih, M.A. Dahleh, and E.N. Brown. An optimization formulation for characterization of pulsatile cortisol secretion. *Frontiers in neuroscience*, 9, 2015.

[35] L.S. Farhy. Modeling of oscillations of endocrine networks with feedback. *Methods in Enzymology*, 384:54–81, 2004.

[36] M. Fazel. *Matrix rank minimization with applications*. PhD thesis, Stanford University, 2002.

[37] N. Fenichel. Geometric singular perturbation theory for ordinary differential equations. *Journal of Differential Equations*, 31(1):53–98, 1979.

[38] G. Fink, D.W. Pfaff, and J.E. Levine. *Handbook of neuroendocrinology*. Academic Press, 2012.

[39] H.P. Fischer. Mathematical modeling of complex biological systems: from parts lists to understanding systems behavior. *Alcohol Research & Health*, 31 (1):49, 2008.

[40] C.R. Fox, L.S. Farhy, W.S. Evans, and M.L. Johnson. Measuring the coupling of hormone concentration time series using polynomial transfer functions. *Methods in enzymology*, 384:82–94, 2004.

[41] A.K. Gelig and A.N. Churilov. Stability and oscillations of pulse-modulated nonlinear systems, 1998.

[42] A.K. Gelig and A.N. Churilov. *Stability and oscillations of nonlinear pulse-modulated systems*. Springer Science & Business Media, 2012.

[43] P.G. Ghomsi, F.M.M. Kakmeni, T.C. Kofane, and C. Tchawoua. Synchronization dynamics of chemically coupled cells with activator-inhibitor pathways. *Phys. Lett. A*, 378:2813–2823, 2014.

[44] L. Glass and M.C. Mackey. *From clocks to chaos: the rhythms of life*. Princeton University Press, 1988.

[45] A. Goldbeter. A minimal cascade model for the mitotic oscillator involving cyclin and cdc2 kinase. *Proceedings of the National Academy of Sciences*, 88 (20):9107–9111, 1991.

[46] A. Goldbeter. *Biochemical oscillations and cellular rhythms: the molecular bases of periodic and chaotic behaviour*. Cambridge university press, 1997.

[47] A. Goldbeter. Dissipative structures and biological rhythms. *Chaos: An Interdisciplinary Journal of Nonlinear Science*, 27(10):104612, 2017.

[48] A. Goldbeter and D.E. Koshland. Ultrasensitivity in biochemical systems controlled by covalent modification. interplay between zero-order and multistep effects. *Journal of Biological Chemistry*, 259(23):14441–14447, 1984.

[49] M. Golubitsky and V. Guillemin. *Stable mappings and their singularities*, volume 14. Springer Science & Business Media, 2012.

[50] M. Golubitsky and D. Schaeffer. A theory for imperfect bifurcation via singularity theory. *Communications on Pure and Applied Mathematics*, 32(1): 21–98, 1979.

[51] D. Gonze and W. Abou-Jaoudé. The Goodwin model: Behind the Hill function. *PLoS One*, 8(8):e69573, 2013.

[52] B.C. Goodwin. Oscillatory behaviour in enzymatic control processes. *Advances in Enzyme Regulation*, 3:425–438, 1965.

[53] W. Govaerts. Numerical bifurcation analysis for odes. *Journal of Computational and Applied Mathematics*, 125(1):57–68, 2000.

[54] J.R. Graef, J. Henderson, and A. Ouahab. *Impulsive differential inclusions: a fixed point approach*, volume 20. Walter de Gruyter, 2013.

[55] D. Greenhalgh and Q.J.A. Khan. A delay differential equation mathematical model for the control of the hormonal system of the hypothalamus, the pituitary and the testis in man. *Nonlinear Analysis: Theory, Methods & Applications*, 71(12):e925–e935, 2009.

[56] G.M. Greuel, G. Pfister, H. Schönemann, O. Bachmann, W. Decker, C. Gorzel, H. Grassmann, A. Heydtmann, K. Krueger, M. Lamm, et al. A computer algebra system for polynomial computations. *Centre for Computer Algebra. University of Kaiserslautern (< http://www. singular. uni-kl. de>)*, 2016.

[57] J.S. Griffith. Mathematics of cellular control processes. negative feedback to one gene. *J. Theor. Biol.*, 20:202–208, 1968.

[58] F.S. Grodins. *Control theory and biological systems*. Columbia University Press, 1963.

[59] F.S. Grodins, J.S. Gray, K.R. Schroeder, A.L. Norins, and R.W. Jones. Respiratory responses to co_2 inhalation. a theoretical study of a nonlinear biological regulator. *Journal of applied physiology*, 7(3):283–308, 1954.

[60] J. Guckenheimer and P. Holmes. *Nonlinear oscillations, dynamical systems, and bifurcations of vector fields*, volume 42. Springer Science & Business Media, 2013.

[61] I. Gucwa and P. Szmolyan. Geometric singular perturbation analysis of an autocatalator model. *Discrete and Continuous Dynamical Systems: Series S*, 2:783–806, 2009.

[62] W.M. Haddad, V. Chellaboina, and S.G. Nersesov. Impulsive and hybrid dynamical systems. *Princeton Series in Applied Mathematics*, 2006.

[63] G.H. Hardy, J.E. Littlewood, and G. Pólya. *Inequalities*. Cambridge university press, 1952.

[64] S. Hastings, J. Tyson, and D. Webster. Existence of periodic solutions for negative feedback cellular control systems. *J. Differential Equations*, 25: 39–64, 1977.

[65] A.L. Hodgkin and A.F. Huxley. A quantitative description of membrane current and its application to conduction and excitation in nerve. *The Journal of physiology*, 117(4):500–544, 1952.

[66] F.C. Hoppensteadt and E.M. Izhikevich. *Weakly connected neural networks*, volume 126. Springer Science & Business Media, 2012.

[67] Y. Hori, T.-H. Kim, and S. Hara. Existence criteria of periodic oscillations in cyclic gene regulatory networks. *Automatica*, 47:1203–1209, 2011.

[68] Y. Hori, M. Takada, and S. Hara. Biochemical oscillations in delayed negative cyclic feedback: Existence and profiles. *Automatica*, 49(9):2581–2590, 2013.

[69] S.-B. Hsu and J. Shi. Relaxation oscillator profile of limit cycle in predator-prey system. *Disc. Cont. Dyna. Syst.-B*, 11:893–911, 2009.

[70] C. Huang and J. Cao. Hopf bifurcation in an n-dimensional Goodwin model via multiple delays feedback. *Nonlinear Dynamics*, 79:2541–2552, 2015.

[71] A. Huber and P. Szmolyan. Geometric singular perturbation analysis of the yamada model. *SIAM Journal on Applied Dynamical Systems*, 4(3):607–648, 2005.

[72] P.A. Iglesias and B.P. Ingalls. *Control theory and systems biology*. MIT Press, 2010.

[73] O.A. Igoshin, A. Goldbeter, D. Kaiser, and G. Oster. A biochemical oscillator explains several aspects of myxococcus xanthus behavior during development. *Proceedings of the National Academy of Sciences of the United States of America*, 101(44):15760–15765, 2004.

[74] E.M. Izhikevich. *Dynamical systems in neuroscience*. MIT press, 2007.

[75] T.D. Johnson. Bayesian deconvolution analysis of pulsatile hormone concentration profiles. *Biometrics*, 59(3):650–660, 2003.

[76] C.K.R.T. Jones. Geometric singular perturbation theory. In *Dynamical systems*, pages 44–118. Springer, 1995.

[77] D. Kaiser. Coupling cell movement to multicellular development in myxobacteria. *Nature Reviews Microbiology*, 1(1):45–54, 2003.

[78] H. Kalmus et al. *Regulation and control in living systems*. Wiley, 1966.

[79] D.M. Keenan and J.D. Veldhuis. Stochastic model of admixed basal and pulsatile hormone secretion as modulated by a deterministic oscillator. *Amer. J. Physiol. - Regulatory, Integrative and Comparative Physiology*, 273(3): R1182–R1192, 1997.

[80] D.M. Keenan and J.D. Veldhuis. A biomathematical model of time-delayed feedback in the human male hypothalamic-pituitary-leydig cell axis. *Amer. J. Physiol.– Endocrinology And Metabolism*, 275(1):E157–E176, 1998.

[81] D.M. Keenan, W. Sun, and J.D. Veldhuis. A stochastic biomathematical model of the male reproductive hormone system. *SIAM J. Appl. Math.*, 61 (3):934–965, 2000.

[82] D.M. Keenan, J.D. Veldhuis, and W. Sun. A stochastic biomathematical model of the male reproductive hormone system. *SIAM Journal on Applied Mathematics*, 61(3):934–965, 2000.

[83] D.M. Keenan, S. Chattopadhyay, and J.D. Veldhuis. Composite model of time-varying appearance and disappearance of neurohormone pulse signals in blood. *Journal of theoretical biology*, 236(3):242–255, 2005.

[84] A. Khovanskii. *Topological Galois Theory: Solvability and Unsolvability of Equations in Finite Terms*. Springer Monographs in Mathematics, Springer-Verlag, 2013.

[85] T.-H. Kim, Y. Hori, and S. Hara. Robust stability analysis of gene-protein regulatory networks with cyclic activation repression interconnections. *Syst. Control Lett.*, 60(6):373–382, 2011.

[86] I. Kosiuk. *Relaxation oscillations in slow-fast systems beyond the standard form*. PhD thesis, Leipzig University, 2012.

[87] I. Kosiuk and P. Szmolyan. Scaling in singular perturbation problems: blowing up a relaxation oscillator. *SIAM Journal on Applied Dynamical Systems*, 10(4):1307–1343, 2011.

[88] I. Kosiuk and P. Szmolyan. Geometric analysis of the Goldbeter minimal model for the embryonic cell cycle. *Journal of Mathematical Biology*, 72(5): 1337–1368, 2016.

[89] L.Z. Krsmanović, S.S. Stojilković, F. Merelli, S.M. Dufour, M.A. Virmani, and K.J. Catt. Calcium signaling and episodic secretion of gonadotropin-releasing hormone in hypothalamic neurons. *Proceedings of the National Academy of Sciences*, 89(18):8462–8466, 1992.

[90] M. Krupa and P. Szmolyan. Extending geometric singular perturbation theory to nonhyperbolic points—fold and canard points in two dimensions. *SIAM journal on mathematical analysis*, 33(2):286–314, 2001.

[91] M. Krupa and P. Szmolyan. Relaxation oscillation and canard explosion. *Journal of Differential Equations*, 174(2):312–368, 2001.

[92] C. Kuehn. *Multiple time scale dynamics*, volume 191. Springer, 2015.

[93] C. Kuehn and P. Szmolyan. Multiscale geometry of the olsen model and non-classical relaxation oscillations. *Journal of Nonlinear Science*, 25(3): 583–629, 2015.

[94] C. Kut, V. Golkhou, and J.S. Bader. Analytical approximations for the amplitude and period of a relaxation oscillator. *BMC systems biology*, 3(1):6, 2009.

[95] Y.A. Kuznetsov. *Elements of applied bifurcation theory*, volume 112. Springer Science & Business Media, 2013.

[96] V. Lakshmikantham, P.S. Simeonov, et al. *Theory of impulsive differential equations*, volume 6. World scientific, 1989.

[97] M. Lee, N. Bakh, G. Bisker, E.N. Brown, and M.S. Strano. A pharmacokinetic model of a tissue implantable cortisol sensor. *Advanced healthcare materials*, 5(23):3004–3015, 2016.

[98] R. Leproult, G. Copinschi, O. Buxton, and E. Van Cauter. Sleep loss results in an elevation of cortisol levels the next evening. *Sleep*, 20(10):865–870, 1997.

[99] B.-Z. Liu and G.M. Deng. An improved mathematical model of hormone secretion in the hypothalamo-pituitary-gonadal axis in man. *J. Theor. Biol.*, 150(1):51–58, 1991.

[100] D.J. MacGregor and G. Leng. Modelling the hypothalamic control of growth hormone secretion. *Journal of neuroendocrinology*, 17(12):788–803, 2005.

[101] J. Mallet-Paret and G.R. Sell. The Poincaré–Bendixson theorem for monotone cyclic feedback systems with delay. *Journal of Differential Equations*, 125(2): 441–489, 1996.

[102] J. Mallet-Paret and G.R. Sell. Systems of differential delay equations: Floquet multipliers and discrete Lyapunov functions. *Journal of Differential Equations*, 125(2):385–440, 1996.

[103] J. Mallet-Paret and H.L. Smith. The poincaré-bendixson theorem for monotone cyclic feedback systems. *Journal of Dynamics and Differential Equations*, 2(4):367–421, 1990.

[104] P. Mattsson and A. Medvedev. Modeling of testosterone regulation by pulse-modulated feedback: an experimental data study. In *AIP Conference Proceedings*, volume 1559, pages 333–342. AIP, 2013.

[105] P. Mattsson and A. Medvedev. Modeling of testosterone regulation by pulse-modulated feedback. In *Signal and Image Analysis for Biomedical and Life Sciences*, pages 23–40. Springer, 2015.

[106] D. McMillen, N. Kopell, J. Hasty, and J.J. Collins. Synchronizing genetic relaxation oscillators by intercell signaling. *Proceedings of the National Academy of Sciences*, 99(2):679–684, 2002.

[107] A.I. Mees and P. E. Rapp. Periodic metabolic systems: Oscillations in multiple-loop negative feedback biochemical control networks. *J. Math. Biol.*, 5: 99–114, 1978.

[108] H.T. Milhorn. *Application of control theory to physiological systems*. WB Saunders, 1966.

[109] A. Milik and P. Szmolyan. Multiple time scales and canards in a chemical oscillator. In *Multiple-time-scale dynamical systems*, pages 117–140. Springer, 2001.

[110] E.F. Mishchenko and N.K. Rozov. Rozov. *Differential Equations with Small Parameters and Relaxation Oscillations (translated from Russian)*. *Plenum Press*, 1980.

[111] C. Morris and H. Lecar. Voltage oscillations in the barnacle giant muscle fiber. *Biophysical journal*, 35(1):193–213, 1981.

[112] J. Muñoz-Dorado, F.J. Marcos-Torres, E. García-Bravo, A. Moraleda-Muñoz, and J. Pérez. Myxobacteria: moving, killing, feeding, and surviving together. *Frontiers in microbiology*, 7:781, 2016.

[113] J.D. Murray. *Mathematical Biology I: An introduction*. 3rd ed. Springer, New York, 2002.

[114] H.F. Nijhout, J.A. Best, and M.C. Reed. Using mathematical models to understand metabolism, genes, and disease. *BMC biology*, 13(1):79, 2015.

[115] B. Novák and J.J. Tyson. Design principles of biochemical oscillators. *Nature reviews Molecular cell biology*, 9(12):981–991, 2008.

[116] R. Pasquali, D. Biscotti, G. Spinucci, V. Vicennati, A.D. Genazzani, L. Sgarbi, and F. Casimirri. Pulsatile secretion of acth and cortisol in premenopausal women: effect of obesity and body fat distribution. *Clinical endocrinology*, 48(5):603–612, 1998.

[117] A. Pogromsky, T. Glad, and H. Nijmeijer. On diffusion driven oscillations in coupled dynamical systems. *Int. J. Bifurcation and Chaos*, 9(04):629–644, 1999.

[118] A.B. Poore. On the theory and application of the Hopf-Friedrichs bifurcation theory. *Archive Rational Mech. Anal.*, 60(4):371–393, 1976.

[119] N. Popović. A geometric analysis of logarithmic switchback phenomena. In *Journal of Physics: Conference Series*, volume 22, page 164. IOP Publishing, 2005.

[120] S.S. Rhee and E.N. Pearce. The endocrine system and the heart: a review. *Revista Española de Cardiología (English Edition)*, 64(3):220–231, 2011.

[121] F. Roelfsema, P. Aoun, and J.D. Veldhuis. Pulsatile cortisol feedback on acth secretion is mediated by the glucocorticoid receptor and modulated by gender. *The Journal of Clinical Endocrinology & Metabolism*, 101(11): 4094–4102, 2016.

[122] S. Roston. Mathematical representation of some endocrinological systems. *Bull. Math. Biophys.*, 21:271–282, 1959.

[123] T. Samad, A. Annaswamy, et al. The impact of control technology: Overview, success stories, and research challenges. *IEEE Control Systems Society*, 2011.

[124] L.S. Satin, P.C. Butler, J. Ha, and A.S. Sherman. Pulsatile insulin secretion, impaired glucose tolerance and type 2 diabetes. *Molecular aspects of medicine*, 42:61–77, 2015.

[125] S.P. Sethi and G.L. Thompson. *Optimal control theory: applications to management science and economics*. Springer Science & Business Media, 2006.

[126] S. Sinha and R. Ramaswamy. On the dynamics of controlled metabolic network and cellular behavior. *BioSystems*, 20:341–354, 1987.

[127] H.L. Smith and H.R. Thieme. *Dynamical systems and population persistence*, volume 118. American Mathematical Society Providence, RI, 2011.

[128] W.R. Smith. Hypothalamic regulation of pituitary secretion of luteinizing hormone. II. feedback control of gonadotropin secretion. *Bull. Math. Biol.*, 42(1):57–78, 1980.

[129] W.R. Smith. Qualitative mathematical models of endocrine systems. *Amer. J. Physiol. - Regulatory, Integrative and Comparative Physiology*, 245(4): R473–R477, 1983.

[130] K. Spiegel, R. Leproult, and E. Van Cauter. Impact of sleep debt on metabolic and endocrine function. *The lancet*, 354(9188):1435–1439, 1999.

[131] K. Sriram, M. Rodriguez-Fernandez, and F.J. Doyle III. Modeling cortisol dynamics in the neuro-endocrine axis distinguishes normal, depression, and post-traumatic stress disorder (PTSD) in humans. *PLoS Computational Biology*, 8(2):e1002379, 2012.

[132] D.A. Stavreva, M. Wiench, S. John, B.L. Conway-Campbell, M.A. McKenna, J.R. Pooley, T.A. Johnson, T.C. Voss, S.L. Lightman, and G.L. Hager. Ultradian hormone stimulation induces glucocorticoid receptor-mediated pulses of gene transcription. *Nature cell biology*, 11(9):1093–1102, 2009.

[133] E.B. Stear. Application of control theory to endocrine regulation and control. *Annals of biomedical engineering*, 3(4):439–455, 1975.

[134] S. Strogatz. *Sync: The emerging science of spontaneous order*. Penguin UK, 2004.

[135] S. Strogatz. *Nonlinear dynamics and chaos: with applications to physics, biology, chemistry, and engineering*. Hachette UK, 2014.

[136] X. Sun, R. Yuan, and J. Cao. Bifurcations for Goodwin model with three delays. *Nonlin. Dynamics*, 84:1093–1105, 2016.

[137] P. Szmolyan and M. Wechselberger. Canards in $\mathbb{R}^3$. *Journal of Differential Equations*, 177(2):419–453, 2001.

[138] P. Szmolyan and M. Wechselberger. Relaxation oscillations in $\mathbb{R}^3$. *Journal of Differential Equations*, 200(1):69–104, 2004.

[139] H. Taghvafard, A.V. Proskurnikov, and M. Cao. Stability properties of the Goodwin-Smith oscillator model with additional feedback. *IFAC-PapersOnLine*, 49(14):131–136, 2016.

[140] H. Taghvafard, A.V. Proskurnikov, and M. Cao. An impulsive model of endocrine regulation with two negative feedback loops. *IFAC-PapersOnLine*, 50(1):14717–14722, 2017.

[141] H. Taghvafard, M. Cao, Y. Kawano, and R.T. Faghih. Design of intermittent control for cortisol secretion under time-varying demand and holding cost constraints. Submitted, 2018.

[142] H. Taghvafard, H. Jardón-Kojakhmetov, and M. Cao. Parameter-robustness analysis for a biochemical oscillator model describing the social-behaviour transition phase of myxobacteria. *Proceedings of the Royal Society A – Mathematical, Physical and Engineering Sciences*, 474(2209):20170499, 2018.

[143] H. Taghvafard, H. Jardón-Kojakhmetov, P. Szmolyan, and M. Cao. Geometric analysis of oscillations in the Frzilator. in preparation, 2018.

[144] H. Taghvafard, A. Medvedev, A.V. Proskurnikov, and M. Cao. Impulsive model of endocrine regulation with a local continuous feedback. in preparation, 2018.

[145] H. Taghvafard, A.V. Proskurnikov, and M. Cao. Local and global analysis of endocrine regulation as a non-cyclic feedback system. *Automatica*, 91: 190–196, 2018.

[146] T. Tanutpanit, P. Pongsumpun, and I. M. Tang. A model for the testosterone regulation taking into account the presence of two types of testosterone hormones. *Journal of Biological Systems*, 23(2):259–273, 2015.

[147] S. Ten, M. New, and N. Maclaren. AddisonâĂŹs disease 2001. *The Journal of Clinical Endocrinology & Metabolism*, 86(7):2909–2922, 2001.

[148] D. Terman and D. Wang. Global competition and local cooperation in a network of neural oscillators. *Physica D: Nonlinear Phenomena*, 81(1-2): 148–176, 1995.

[149] R. Thaxter. Contributions from the cryptogamic laboratory of Harvard University. XVI-II. on the Myxobacteriaceae, a new order of Schizomycetes. *Botanical Gazette*, 14:389–406, 1892.

[150] C.D. Thron. The secant condition for instability in biochemical feedback control. I. the role of cooperativity and saturability. *Bull. Math. Biol.*, 53(3): 383–401, 1991.

[151] E.A. Tomberg and V.A. Yakubovich. Conditions for auto-oscillations in nonlinear systems. *Siberian Math. J.*, 30(4):641–653, 1989.

[152] B. van der Pol and J. van der Mark. LXXII. the heartbeat considered as a relaxation oscillation, and an electrical model of the heart. *The London, Edinburgh, and Dublin Philosophical Magazine and Journal of Science*, 6(38): 763–775, 1928.

[153] M.L. Vance, D.L. Kaiser, W.S. Evans, R. Furlanetto, W. Vale, J. Rivier, and M.O. Thorner. Pulsatile growth hormone secretion in normal man during a continuous 24-hour infusion of human growth hormone releasing factor (1-40). evidence for intermittent somatostatin secretion. *Journal of Clinical Investigation*, 75(5):1584, 1985.

[154] J.D. Veldhuis. Recent insights into neuroendocrine mechanisms of aging of the human male hypothalamic-pituitary-gonadal axis. *J. Andrology*, 20(1): 1–18, 1999.

[155] J.D. Veldhuis. Pulsatile hormone secretion: mechanisms, significance and evaluation. In *Ultradian Rhythms from Molecules to Mind*, pages 229–248. Springer, 2008.

[156] J.D. Veldhuis, A. Iranmanesh, G. Lizarralde, and M.L. Johnson. Amplitude modulation of a burstlike mode of cortisol secretion subserves the circadian glucocorticoid rhythm. *American Journal of Physiology-Endocrinology And Metabolism*, 257(1):E6–E14, 1989.

[157] J.D. Veldhuis, D.M. Keenan, and S.M. Pincus. Motivations and methods for analyzing pulsatile hormone secretion. *Endocrine reviews*, 29(7):823–864, 2008.

[158] J.D. Veldhuis, D.M. Keenan, P.Y. Liu, A. Iranmanesh, P.Y. Takahashi, and A.X. Nehra. The aging male hypothalamic–pituitary–gonadal axis: Pulsatility and feedback. *Molecular and Cellular Endocrinology*, 299(1):14–22, 2009.

[159] G.J. Velicer and M. Vos. Sociobiology of the myxobacteria. *Annual review of microbiology*, 63:599–623, 2009.

[160] A. Vidal, Q. Zhang, C. Médigue, S. Fabre, and F. Clément. Dynpeak: An algorithm for pulse detection and frequency analysis in hormonal time series. *PloS one*, 7(7):e39001, 2012.

[161] F. Vinther, M. Andersen, and J.T. Ottesen. The minimal model of the hypothalamic–pituitary–adrenal axis. *Journal of mathematical biology*, 63 (4):663–690, 2011.

[162] D.J. Vis, J.A. Westerhuis, H.C.J. Hoefsloot, H. Pijl, F. Roelfsema, J. van der Greef, and A.K. Smilde. Endocrine pulse identification using penalized

methods and a minimum set of assumptions. *American Journal of Physiology-Endocrinology And Metabolism*, 298(2):E146–E155, 2009.

[163] J.J. Walker, J.R. Terry, and S.L. Lightman. Origin of ultradian pulsatility in the hypothalamic–pituitary–adrenal axis. *Proceedings of the Royal Society of London B: Biological Sciences*, 277(1688):1627–1633, 2010.

[164] J.J. Walker, J.R. Terry, K. Tsaneva-Atanasova, S.P. Armstrong, C.A. McArdle, and S.L. Lightman. Encoding and decoding mechanisms of pulsatile hormone secretion. *Journal of neuroendocrinology*, 22(12):1226–1238, 2010.

[165] J.J. Walker, F. Spiga, E. Waite, Z. Zhao, Y. Kershaw, J.R. Terry, and S.L. Lightman. The origin of glucocorticoid hormone oscillations. *PLoS biology*, 10(6):e1001341, 2012.

[166] N. Wiener. *Cybernetics: Control and communication in the animal and the machine*. Wiley New York, 1948.

[167] S. Wiggins. *Introduction to applied nonlinear dynamical systems and chaos*, volume 2. Springer Science & Business Media, 2003.

[168] A.T. Winfree. Biological rhythms and the behavior of populations of coupled oscillators. *Journal of Theoretical Biology*, 16(1):15–42, 1967.

[169] A.T. Winfree. *The Geometry of Biological Time*, volume 12. Springer Science & Business Media, 2001.

[170] V.A. Yakubovich. Frequency-domain criteria for oscillation in nonlinear systems with one stationary nonlinear component. *Siberian Math. J.*, 14(5): 768–788, 1973.

[171] E.A. Young, J. Abelson, and S.L. L.ightman. Cortisol pulsatility and its role in stress regulation and health. *Frontiers in neuroendocrinology*, 25(2):69–76, 2004.

[172] E.A. Young, S.C. Ribeiro, and W. Ye. Sex differences in acth pulsatility following metyrapone blockade in patients with major depression. *Psychoneuroendocrinology*, 32(5):503–507, 2007.

[173] Z.T. Zhusubaliyev and E. Mosekilde. *Bifurcations And Chaos In Piecewise-Smooth Dynamical Systems: Applications to Power Converters, Relay and Pulse-Width Modulated Control Systems, and Human Decision-Making Behavior*, volume 44. World Scientific, 2003.

Summary

This book is devoted to the study of rhythms, so-called "oscillators". In particular, it is concerned with modeling, analysis, and control of biological oscillators. It is divided into two parts, where Part I is devoted to the application of control theory to endocrinology, and Part II is allocated to the application of dynamical systems to microbiology.

Part I develops three mathematical models of endocrine regulation. The first model, which is a second-order impulsive differential equation, describes the cortisol's diurnal patterns. Through an analytical approach, we design an impulsive controller to identify the timing and amplitude of secretory events, while the blood cortisol levels are restricted to a specific circadian range. By proposing an algorithm and employing it into various examples, we show that the achieved cortisol levels lead to the circadian and ultradian rhythms, which are in line with the known physiology of cortisol secretion.

The second model, which is a third-order ordinary differential equation, generally describes the control mechanisms in the hypothalamic-pituitary axes, controlled by the brain. For this model, which is an extension of the conventional Goodwin's oscillator with an additional nonlinear feedback, we establish the relationship between its local behavior at the equilibrium point and its global behavior, i.e., the convergence of solutions to periodic orbits.

The last model, which is a third-order impulsive differential equation, describes the pulsatile secretion of the hypothalamic-pituitary axes. This model, obtained from an impulsive version of the Goodwin's oscillator, has an additional affine feedback. For this model, we present conditions for the existence, uniqueness, and positivity of a type of periodic solution.

Part II studies a biochemical oscillator model (known as "Frzilator"), which describes the social-behavior transition phase of *myxobacteria*, a kind of soil bacteria. This part studies the Frzilator from two different perspectives, namely, regular perturbation, and geometric singular perturbation, respectively. Using regular

perturbation theory, we investigate parameter-robustness analysis of the Frzilator. In particular, after identifying and unifying some small parameters of the system, we establish the relation between its local and global behavior at the equilibrium point. Moreover, we explicitly give certain parameter regimes in which solutions of the system converge to a finite number of periodic orbits.

Using geometric singular perturbation theory and the blow-up method, we analyze the dynamics of the Frzilator in the limit of small parameters of the system. We prove that, within certain parameter regimes, there exists a strongly attracting periodic orbit for the system. Moreover, we give the detailed description of the structure of such an orbit as well as the timescales along it. The existence of multiple time scales along the orbit demonstrates that the Frzilator is a relaxation oscillator.

Samenvatting

Dit boek is toegewijd aan de studie van ritmes, zogenaamde “oscillatoren”. In het bijzonder richt dit proefschrift zich op het modeleren, analyseren en reguleren van biologische oscillatoren. Er zijn twee delen: het Deel I richt zich op het toeppassen van regeltechniek op endocrinologie en Deel II focust op het toepassen van dynamische systemen op microbiologie.

In Deel I worden drie wiskundige modellen van de endocriene regulering ontwikkeld. Het eerste model is een tweede orde impulsieve differentiaalvergelijking die de dagelijkse patronen van cortisol beschrijft. Met een analytische methode wordt een impulsieve regelaar ontworpen voor de tijdsbepaling en amplitude van hormoonafscheidingen waarbij de cortisol gehaltes in het bloed binnen een specifiek circadiaans bereik worden gehouden. Door het voorgestelde algoritme toe te passen op verschillende voorbeelden tonen we aan dat de door het model gegenereerde cortisol gehaltes in het bloed circadiaanse en ultradiaanse ritmes vertonen die in lijn zijn met de bekende fysiologie van cortisol afscheiding in het lichaam.

Het tweede model is een derde orde gewone differentiaalvergelijking dat, door de toevoeging van een extra niet-lineaire terugkoppeling een uitbreiding is van de conventionele Goodwin oscillator. Het model beschrijft in het algemeen de regelmechanismen in de hypothalamus-hypofyse-bijnier as die wordt aangestuurd door het menselijke brein. We bepalen de relatie tussen de lokale dynamica rondom het evenwichtspunt en het globale dynamische gedrag, i.e., de convergentie van de oplossingen naar een periodieke baan.

Het laatste model is een derde orde impulsieve differentiaalvergelijking die de pulserende hormoonafgiftes van de hypothalamus-hypofyse-bijnier-as beschrijft. Dit model, dat is afgeleid van een impulsieve versie van een Goodwin’s oscillator, heeft een additionele lineaire terugkoppeling. Voor dit model presenteren we condities voor existentie, uniciteit en positiviteit van een type periodieke oplossing.

Deel II bestudeert een biochemische oscillator model (bekend als “Frzilator”), die transitie fases in het sociale gedrag van myxobacteriën, een soort bodem-

bacteriën, beschrijft. Dit deel bestudeert de Frzilator vanuit twee perspectieven: reguliere perturbatietheorie en geometrische singuliere perturbatie. Door gebruik te maken van reguliere perturbatie theorie bestuderen we de robuustheid van de parameters in de Frzilator. In het bijzonder, na het identificeren en verenigen van kleine parameters in het systeem, beschrijven we de relatie tussen het lokale en globale gedrag bij het evenwichtstoestand. Bovendien geven we een expliciete bereik van parameter waarden waarvoor de oplossingen van het systeem convergeren naar een eindig aantal periodieke banen.

Door gebruik te maken van singuliere perturbatie theorie en de blow-up methode analyseren we de dynamica van het Frzilator model in de limiet van kleine parameter waarden in het systeem. We bewijzen dat, voor bepaalde parameter waarden, er een sterk aantrekkende periodieke baan bestaat voor het systeem. Bovendien geven we een gedetailleerde beschrijving van de structuur van een dergelijke baan en de tijdschalen erlangs. Het bestaan van meerdere tijdschalen langs de baan van de oplossingen demonstreert dat de Frzilator een relaxatie-oscillator is.